

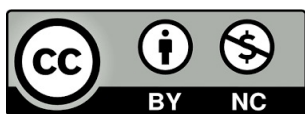
Ana Piqueras Lorente

Comparative Analysis of Human  
Body Model and Post Mortem  
Human Subjects in Oblique  
Impact: Evaluating Chest  
Deformation and Personalization  
Techniques

Director/es

López Valdés, Francisco José

<http://zaguan.unizar.es/collection/Tesis>



Universidad de Zaragoza  
Servicio de Publicaciones

ISSN 2254-7606



**Universidad**  
Zaragoza

Tesis Doctoral

COMPARATIVE ANALYSIS OF HUMAN BODY  
MODEL AND POST MORTEM HUMAN SUBJECTS  
IN OBLIQUE IMPACT: EVALUATING CHEST  
DEFORMATION AND PERSONALIZATION  
TECHNIQUES

Autor

Ana Piqueras Lorente

Director/es

López Valdés, Francisco José

**UNIVERSIDAD DE ZARAGOZA**  
**Escuela de Doctorado**

Programa de Doctorado en Ingeniería Mecánica

2024





**Universidad**  
Zaragoza

## Tesis Doctoral

Comparative Analysis of Human Body Model  
and Post Mortem Human Subjects in Oblique  
Impact: Evaluating Chest Deformation and  
Personalization Techniques

Autor

Ana Piqueras Lorente

Director

Francisco José López Valdés

Tutor

Mario Vicente Maza Frechín

Escuela de Ingeniería y Arquitectura  
2024

---

**Comparative Analysis of Human Body Model and Post Mortem  
Human Subjects in Oblique Impact: Evaluating Chest Deformation  
and Personalization Techniques**

---

*PhD thesis by:*

Ana Piqueras Lorente

*Supervisor:*

Dr. Francisco J. López Valdés

*Doctoral advisor:*

Dr. Mario Maza Frechín

***PhD Programme in Mechanical Engineering***

Escuela de Ingeniería y Arquitectura (EINA)  
Universidad de Zaragoza





## Acknowledgements

I would like to express my deepest gratitude to Francisco José López-Valdés, the director of this thesis, for his unwavering dedication to my work and constant guidance on all aspects related to this research. His support has been invaluable, shaping the trajectory of this endeavour. I extend my appreciation to Mario Maza Frechín, my thesis tutor, for providing me with the opportunity to work at the Impact Laboratory and pursue this doctoral thesis.

Special thanks go to Bengt Pipkorn and Johan Iraeus, the supervisors of my stays in Sweden and co-authors of my publications. Their collaboration and contributions stemming from their outstanding professional backgrounds have significantly enriched both the publications and the research stays. I am grateful to international experts Raúl Aranda and Andre Eggers, whose insightful reviews of the thesis provided fundamental feedback, undoubtedly elevating the quality of the work.

To my colleagues at the Impact Laboratory, with whom I worked hand in hand across various research lines, they transformed the laboratory into what it is today, thank you. I would also like to acknowledge my colleagues at Warak Consulting, whose support and encouragement sustained me throughout the past two and a half years of work. Your camaraderie has been a source of strength.

My heartfelt thanks go to my friends, who have been a constant source of support in both good and challenging times, always ready to create memorable moments. A special mention to Óscar, my steadfast companion in work and joy, whose contagious determination has been a driving force throughout this process.

To my mother and sister, whose unconditional support has been my anchor in every aspect of life. And, of course, to my nieces Alba and Lucas, my favourite people, whose genuine smiles are the direct cause of my own.

For those who are, were, and will be, thank you.



## Abstract

The aim of this dissertation is to evaluate how Human Body Models (HBM) can be improved to accurately predict the chest deflection in oblique impact configurations and how the different personalization techniques influence the prediction. HBM, which can be modified to individual characteristics, are instrumental in study of the biomechanics. Accurately measuring chest deflection is crucial for evaluating thoracic biomechanics and injury risk. Therefore, this study aims to compare HBM predictions of chest deformation with real-world data to better understand how subject-specific factors impact chest motion and, consequently, safety systems.

To achieve these goals, the study conducted three sled tests in a nearside oblique impact scenario at the University of Zaragoza's Impact Laboratory. It used the SAFER HBM v8 model based on the THUMS v3 model as a reference point for assessing personalization techniques. Various versions of the model were employed, including the unmodified base model, and modified models with aligned spine curvature, mass and anthropometry adjustments to mimic individual post-mortem human subjects (PMHS). The research used the CORA rating to quantify the correlation between predicted responses and sled test results.

The subsequent chapters built upon these findings, each with a specific focus. Chapter 3 quantified the impact of personalization techniques on spinal kinematics during oblique impacts. The study compared predicted displacements from HBM simulations with actual spinal displacements recorded during physical tests. It identified factors contributing to disparities between predictions and measurements, including modelling limitations or age-related variations in body composition among others.

Chapter 4 centred on analysing the six degrees of freedom (6DOF) motion of the human spine during crash events. The study explored how personalization techniques influenced predictions of spinal bone rotations using HBM. The Finite Helical Axis (FHA) was used to model dynamic motion, with a focus on precision in motion descriptions. The study compared results from various HBM versions assessing their significance with statistical tests.

In Chapter 5, the research conducted an evaluation of chest deformation prediction capability of the models. It assessed how personalization techniques influenced the prediction. The study presents a sensitivity analysis of the chest deflection of the HBM in relation to the personalization techniques.

In summary, this dissertation's primary objective is to enhance the understanding in biomechanical responses during oblique automotive impacts, particularly in the thoracic and spinal regions. These oblique impacts are known to cause more significant chest deformations, making them crucial for injury prevention and safety standards. The research quantitatively assesses the influence of personalization techniques on spinal kinematics and chest deformation using HBM. It contributes to the understanding of these biomechanical responses and identifies areas for refinement in predictive modelling to enhance automotive safety.

## Resumen

El propósito de esta tesis doctoral es mejorar los Modelos de Cuerpo Humano (HBM, por sus siglas en inglés) para predecir con precisión las deformaciones en pecho en impactos oblicuos y analizar cómo diferentes técnicas de personalización afectan estas predicciones. Los HBM, son modelos computacionales adaptables a características individuales, son fundamentales en la biomecánica. Medir con precisión la deflexión del pecho es esencial para evaluar la biomecánica torácica y el riesgo de lesiones. Por lo tanto, este estudio busca comparar las predicciones de deformación del pecho de HBM con datos reales para entender cómo factores específicos del sujeto influyen en el movimiento del pecho.

Para lograrlo, se realizaron tres pruebas con cadáveres humanos (PMHS) en un escenario de impacto oblicuo en el Laboratorio de Impacto de la Universidad de Zaragoza. Se usó el modelo SAFER HBM v8 basado en THUMS v3 como referencia para evaluar las técnicas de personalización. Se emplearon varias versiones del modelo, incluyendo el modelo base sin modificaciones y modelos con ajustes de columna vertebral, masa y antropometría para emular características de los PMHS. La correlación entre las predicciones y los resultados de las pruebas se midió con un análisis CORA.

Los siguientes capítulos se basaron en estos hallazgos, cada uno con un enfoque específico. El Capítulo 3 cuantificó el impacto de las técnicas de personalización en la cinemática de la columna vertebral durante impactos oblicuos, comparando predicciones de HBM con mediciones experimentales. Se identificaron factores que contribuyeron a las diferencias, como limitaciones en la modelización y variaciones relacionadas con la edad.

El Capítulo 4 analizó el movimiento de la columna vertebral en seis grados de libertad durante el impacto, explorando cómo las técnicas de personalización afectaron las predicciones de las rotaciones de la columna utilizando HBM. Se utilizó el Eje Finito Helicoidal (FHA) para modelar el movimiento dinámico y se compararon resultados de diferentes versiones de HBM evaluando su significancia estadística.

En el Capítulo 5, la investigación evaluó la capacidad de predicción de deformación del pecho de los modelos. Se evaluó cómo las técnicas de personalización influyen en esta predicción. El estudio presenta un análisis de la sensibilidad de la deflexión del pecho del HBM frente a las distintas técnicas de personalización.

En resumen, esta tesis doctoral busca mejorar la comprensión de las respuestas biomecánicas en impactos oblicuos, especialmente en el pecho y la columna vertebral. Estos impactos son críticos para la prevención de lesiones y la seguridad automovilística. La investigación cuantifica la influencia de las técnicas de personalización en la cinemática de la columna vertebral y la deformación del pecho con HBM, contribuyendo al entendimiento de estas respuestas biomecánicas y señalando áreas para mejorar en la modelización predictiva.

## **Thesis by compendium of publications**

This thesis is a compendium of the following published articles in peer-reviewed research journals:

Piqueras A, Iraeus J, Lorente AI, López-Valdés FJ, Juste-Lorente Ó, Maza-Frechín M, Pipkorn B. Kinematic assessment of subject personification of human body models (THUMS). In: Proceedings of IRCOBI Conference 2018.; 2018:191–206.

Piqueras A, Pipkorn B, Iraeus J, Lorente AI, Juste-Lorente Ó, Maza M, López-Valdés FJ. Analysis of the spinal 3D motion of postmortem human surrogates in nearside oblique impacts. *Traffic Inj. Prev.* 2023;24(1):69–74. (Q3)

Piqueras A, Pipkorn B, Iraeus J, Maza-Frechín M, Lopez-Valdes FJ. Assessment of in situ chest deflection of post mortem human subjects (PMHS) and personalized human body models (HBM) in nearside oblique impacts. *Traffic Inj Prev.* 2022;0(0):1–6 (Q3)

Piqueras A, Iraeus J, Pipkorn B, López-Valdés FJ. Assessment of the sensitivity of thoracic injury criteria to subject-specific characteristics using human body models. *Front Bioeng Biotechnol.* 2023;11(February):1–10. (Q1)



# Content

Acknowledgements .....	II
Abstract .....	IV
Resumen .....	V
Thesis by compendium of publications.....	VI
Index of Figures .....	X
Index of Tables.....	XI
Nomenclature and Abbreviations.....	XII
<b>1. INTRODUCTION.....</b>	<b>1</b>
1.1. Background .....	1
1.2. The Study of Impact Biomechanics .....	2
1.2.1. Volunteer testing .....	2
1.2.2. Post Mortem Human Surrogates testing.....	3
1.2.3. Anthropometric Tests Devices testing .....	3
1.2.4. In-silico testing.....	4
1.2.5. Injury criteria and severity classification .....	6
1.3. Oblique impacts and chest injuries.....	7
1.3.1. Chest deflection measurement on experimental testing .....	8
1.3.2. Chest injury assessment using ATD.....	10
1.3.3. Chest injury assessment using Human Body Model .....	11
1.4. Objectives.....	13
References .....	14
<b>2. MATERIALS AND METHODS .....</b>	<b>18</b>
2.1. Experimental Testing .....	18
2.1.1. PMHS information.....	18
2.1.2. Testing set-up .....	19
2.1.3. Instrumentation .....	20
2.1.4. Post-test analysis and injury outcome .....	21
2.2. Simulation .....	21
2.2.1. Finite Element Human Body Model .....	21
2.2.2. Personalization of the HBM.....	22
2.2.3. Simulation Test Matrix.....	24
2.3. Bones kinematics acquisition and comparison.....	25
References .....	28
<b>3. HBM PREDICTION OF SPINAL TRAJECTORIES .....</b>	<b>29</b>
3.1. Introduction .....	29
3.2. Methods.....	30
3.2.1. Bone Trajectories Comparison.....	30
3.2.2. Quantitative Assessment of the Kinematic Response .....	30
3.2.3. Statistical analysis .....	31
3.3. Results .....	32
3.3.1. Summary of Paper A.....	32
3.3.2. Influence of the personalization techniques .....	33
3.4. Discussion .....	34
References .....	36

4. HBM PREDICTION OF SPINAL ROTATIONS .....	37
4.1. Introduction .....	37
4.2. Methods .....	37
4.2.1. Rotation representation .....	37
4.2.2. Quantitative assessment .....	39
4.2.3. Statistical analysis .....	39
4.3. Results .....	40
4.3.1. Summary of Paper B .....	40
4.3.2. Bone Rotations Comparison.....	41
4.3.3. CORA analysis.....	46
4.3.4. Influence of the personalization techniques .....	49
4.4. Discussion .....	50
References .....	53
5. CHEST DEFLECTION ANALYSIS .....	55
5.1. Introduction .....	55
5.2. Methods .....	55
5.2.1. Chest deflection measurement .....	55
5.2.2. Quantitative assessment .....	57
5.2.3. Statistical analysis .....	58
5.3. Results .....	58
5.3.1. Summary of Paper C .....	58
5.3.2. Summary of Paper D.....	59
5.3.3. Analysis of the influence of the personification techniques.....	60
5.4. Discussion .....	61
References .....	62
6. DISCUSSION AND CONCLUSIONS .....	63
6.1. Discussion .....	63
6.1.1. Relationship between the spinal motion and the chest deflection .....	63
6.1.2. Reasons of the discrepancies between chest deflection in the HBM and PMHS.....	67
6.1. Limitations .....	74
6.2. Contributions of the study to the field.....	75
6.3. Conclusions .....	76
6.4. Conclusions (in Spanish).....	79
6.5. Future Work .....	82
References .....	84
Paper A .....	86
Paper B .....	96
Paper C .....	104
Paper D .....	112
Appendices .....	123
Appendix A: Ethical Approval.....	124
Appendix B: Methods Extended .....	125
Appendix C: Model Versions Mesh Quality Analysis.....	127
Appendix D: MatLab Code for FHA Calculation .....	128
Appendix E: Chest deflection plots.....	131



## Index of Figures:

Figure 1-1: Distribution of deaths by road user type (Source: Global status report on road safety 2018. Geneva: World Health Organization; 2018. License: CC BY- NC-SA 3.0 IGO) .....	1
Figure 1-2: Frontal impact configurations. ....	7
Figure 2-1: PMHS sled test fixture and configuration.....	20
Figure 2-2: PMHS's anterior chest landmarks. ....	21
Figure 2-3: Visualization of the different model versions. Models 3 and 4 corresponding to the mass scaled versions share the same external geometry with models 1 and 2 (Baseline and postured model versions). ....	24
Figure 2-4: Top view schema of the structure and calculation matrices. ....	26
Figure 2-5: Bone-plate sub-structure CT scan.....	26
Figure 3-1: Values of CORA Total rating for the different model versions including both restraint system versions. ....	33
Figure 4-1: Components of the unit vector of the FHA of the head calculated every 8° for the PMHS (black lines) and the SAFER HBM model (coloured lines). ....	42
Figure 4-2: Components of the unit vector of the FHA of the T1 vertebra (T4 for PMHS C) calculated every 8° for the PMHS (black lines) and the SAFER HBM model (coloured lines). ....	43
Figure 4-3: Components of the unit vector of the FHA of the T8 vertebra (T7 for PMHS C) calculated every 8° for the PMHS (black lines) and the SAFER HBM model (coloured lines). ....	44
Figure 4-4: Components of the unit vector of the FHA of the L2 vertebra (L1 for PMHS C) calculated every 8° for the PMHS (black lines) and the SAFER HBM model (coloured lines). ....	45
Figure 4-5: Values of CORA Total rating for both restraint system versions. ....	50
Figure 4-6: Model body parts that which mass were adjusted for the mass-scaled version. ....	51
Figure 4-7: Effect of the mass distribution on the rotation around the vertical axis. ....	51
Figure 5-1: PMHS's anterior chest landmarks. ....	56
Figure 5-2: Chest deflection representation along one rib level. The slashed line represents the undeformed rib profile. ....	56
Figure 6-1: Values of Cmax for the different model versions including both restraint system versions (x=average value, circle = median value).....	64
Figure 6-2: Values of PC Score for the different model versions including both restraint system versions (x=average value, circle = median value).....	64
Figure 6-3: Values of trajectories CORA Total rating for the different model versions including both restraint system versions (x=average value, circle = median value). ....	65
Figure 6-4: Values of trajectories CORA rating at middle spine for the different model versions including both restraint system versions (x=average value, circle = median value). ....	66
Figure 6-5: Values of rotations CORA Total rating for the different model versions including both restraint system versions (x=average value, circle = median value). ....	66
Figure 6-6: Values of rotations CORA rating at middle spine for the different model versions including both restraint system versions (x=average value, circle = median value). ....	67
Figure 6-7: Costal cartilage calcifications for subject A (left, frontal plane) and C (right, coronal plane) 71	
Figure 6-8: Clavicle strain results for all model versions belonging to RSv1. ....	72
Figure 6-9: Clavicle strain results for all model versions belonging to RSv2. ....	72

## Index of Tables:

Table 1-1: Relative merits of human surrogates for injury biomechanics (Crandall et al. 2011) .....	6
Table 2-1: PMHS information and test set-up .....	19
Table 2-2: Test matrix and personalization technique applied to each model version. ....	25
Table 3-1: Model versions groups for the analysis of the influence of the three personalization techniques. .....	31
Table 3-2: p-value for each comparison (bold=statistical significance). ....	34
Table 3-3: Effect size r for each comparison (bold = statistical significance) including the sign of $\Delta m$ between brackets only where negative values were obtained. ....	34
Table 4-1: CORA score for the selected landmarks rotation in RSv1. The highest values obtained for the selected landmarks have been highlighted. ....	46
Table 4-2: CORA score for the selected landmarks rotation in RSv2. The highest values obtained for the selected landmarks have been highlighted. ....	47
Table 4-3: p-value for each comparison (bolded=statistical significance) .....	49
Table 4-4: Effect size r for each comparison (bold = large effect) including the sign of $\Delta m$ between brackets only where negative values were obtained. ....	49
Table 5-2: p-value for each comparison (bolded=statistical significance). ....	60
Table 5-3: Effect size r of Cmax and PC Score discretized by personalization technique and injury metric (large effect >0.5) including the sign of $\Delta m$ between brackets only where negative values were obtained. ....	60
Table 6-1: Geometrical measurements for the PMHSs and all six corresponding model versions. ....	68

## **Nomenclature and Abbreviations:**

3D	3 Dimensions
AIS	Abbreviated Injury Scale
ATD	Anthropomorphic Test Device
CEICA	Ethical Commission for Clinical Research of Aragón
CT	Computed Tomography
DOF	Degrees of Freedom
FE	Finite Element
FHA	Finite Helical Axis
GCS	Global Coordinate System
GHBMC	Global Human Body Model Consortium
GS	Gold Standard
HBM	Human Body Model
L	Lumbar vertebra (L1 and L2)
LCS	Local Coordinate System
MBS	Multi-Body System
NFR	Number of Fractured Ribs
PMHS	Post-Mortem Human Surrogate
R4L	Fourth left rib
R4R	Fourth right rib
R8L	Eight left rib
R8R	Eight right rib
RSv	Restraint System version (RSv1 and RSv2)
T	Thoracic vertebra (T1, T4, T7 and T8)
THUMS	Total Human Model for Safety



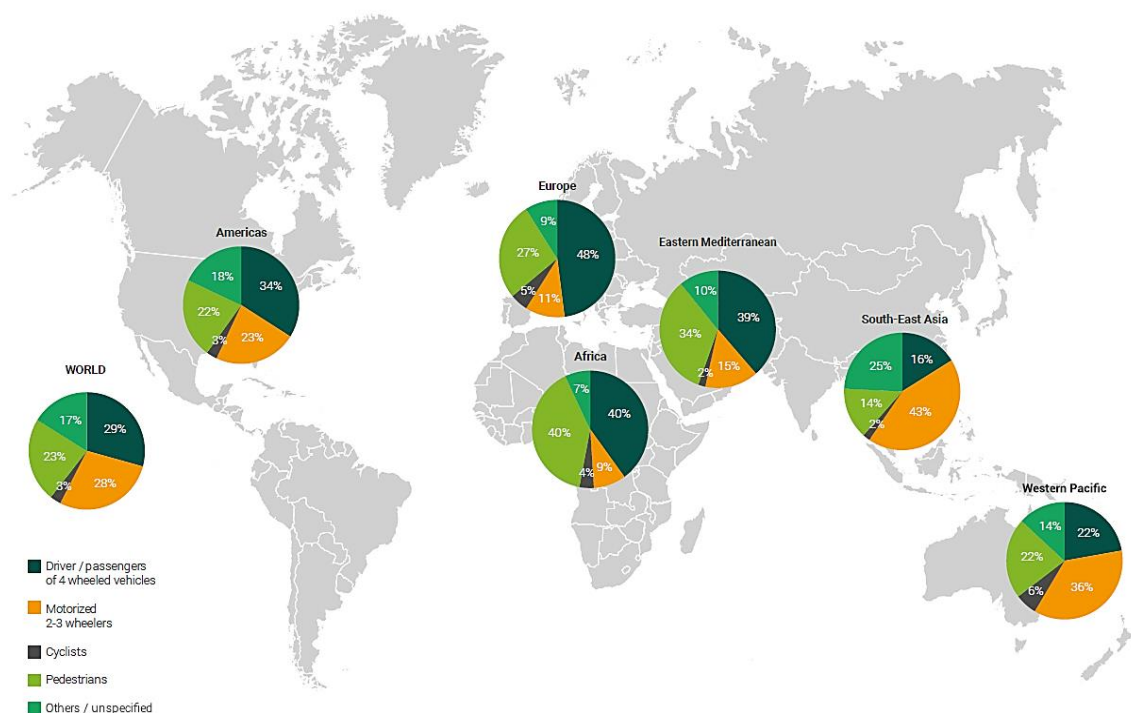
## INTRODUCTION

### 1.1. Background

Over the past few decades, significant progress has been made in improving road occupant safety through advancements in vehicle crashworthiness and restraint systems. However, according to the World Health Organization, 1.35 million people die each year on the world's roads, and 20 to 50 million people sustain non-fatal injuries from collisions, making them a major cause of morbidity (Global Status Report On Road Safety 2018).

In the European region, over 85 000 people were killed in 2018, making road-traffic injuries a leading cause of death for those aged 5–14 years (Passmore et al. 2019). Traffic injuries sustained by drivers or passengers of four-wheeled vehicles account for 48% (see Figure 1-1) of road fatalities in Europe.

Figure 1-1: Distribution of deaths by road user type (Source: Global status report on road safety 2018. Geneva: World Health Organization; 2018. License: CC BY- NC-SA 3.0 IGO)



In 2010, the World Health Organization, published an action plan for the decade, predicting 2.4 million deaths each year unless “*immediate and effective action is taken*” (Global plan for the Decade of Action for Road Safety 2011–2020 2010). Thanks to the development on traffic safety, the number of deaths per year has remained stable but not

decreased, and further effort is needed to reduce the number of accidents, not only through active safety measures to prevent crashes, but also through passive safety measures that mitigate the impact of a crash.

Regarding passive safety, restraint systems such as seatbelts, airbags or child restraint systems have largely proven their effectiveness. According to the National Highway Traffic Safety Administration (NHTSA) of the United States, in 2017, 87% of passenger vehicle occupants who survived a car crash were restrained at the time of the crashworthiness (National Highway Traffic Safety Administration 2017). Nevertheless, the document was also reported that the 53% of the people who died in a traffic accident in the US were anyhow restrained.

This highlights the fact that passive safety systems can be improved to cover a wider range of injury mechanisms and their severity through the study of impact biomechanics.

## **1.2. The Study of Impact Biomechanics**

Biomechanics is a multidisciplinary field of study that examines the mechanical principles of biological structures in motion. This science has been applied to traffic safety during the past decades and has led to significant advancements in vehicle crashworthiness and occupant safety.

The ultimate goal of this discipline is to know how the human body behaves during an impact, in order to prevent the mechanisms that lead to injury to define injury tolerances at which tissues fail to recover. One of the pioneers in this field was Colonel John Paul Stapp, who became known as “the fastest man on earth”, and who tried to assess the limits of acceleration that a human body can withstand without injury, with himself as the test subject (Stapp et al. 1957). Since then, important advances have been made in the development of human surrogates, focusing on creating biofidelic substitutes of the human lived body. In this field of research, four main types of surrogates are employed: Human volunteers, Post Mortem Human Surrogates (PMHS), anthropometric tests devices (ATDs) and computational human body models (HBM).

### **1.2.1. Volunteer testing**

Human volunteers are a useful experimental model for studying the response of living humans since they are identical to the population of interest. However, there are practical limitations to both laboratory and epidemiological studies of human response. Field or epidemiology studies of actual car crashes are retrospective and cannot directly assess the injury mechanisms or tolerances. The primary utility of these types of studies is in identifying injury trends and assessing the efficacy of countermeasures such as seatbelts or airbags. However, they have limited utility for defining the relationship between applied loads and injury risk since too little is known about the nature of the loading (Kent and Baas 2012).

Laboratory studies are carried out within an ethical agreement and using non-injurious methods with the foremost priority being the safety of the volunteer. The experiments enable the study of the body's reaction, considering the muscular activation against low stimuli. This field is not designed to directly evaluate the injury mechanism or tolerance of the human body; its primary purpose is to improve the understanding of human response with variations in the levels of muscle activation using non-invasive instrumentation (Crandall et al. 2011). Volunteer testing is crucial for the development of human body models that can accurately represent the human body and its motion during a crash.

### **1.2.2. Post Mortem Human Surrogates testing**

In order to evaluate the human body's motion and reaction under injurious levels of stimuli, PMHS (Post Mortem Human Surrogates) testing offers the advantage of being an exact representation of the human anatomy and anthropometry. One weakness of this method is the study of the mechanism for some injuries such as traumatic hemothorax, pneumothorax or aortic rupture, related to the functioning of the circulatory and respiratory systems. However, some researchers pressurize the circulatory systems with blood simulants before testing to recreate a nominal *in vivo* level of pressure immediately prior to testing (Eichberger et al. 2000; Michaelson et al. 2008; Shaw et al. 2002). In the case of Michaelson et al. 2008, among others (Forman et al. 2006; Lopez-Valdes et al. 2018) air lung inflation was also recreated with on-board pressure systems, particularly in the study of thoracic response.

Another challenge in PMHS testing is the absence of muscular activation. Muscular tension leads to discrepancies in occupant kinematics and dynamics, even among different age ranges (Lopez-Valdes et al. 2016), and may potentially influence the risk of injury. Some efforts have been made on this issue using external hardware such as springs, to approach the influence of muscular tone but this technique still has limitations (Kang et al. 2018).

Nevertheless, the grater handicap of the PMHS testing is subject availability. Depending on the country or region body donation protocols can vary and the social acceptance of cadaver use in injury biomechanics research is fundamental to facilitate this type of testing. It has been estimated that more than 60 lives are saved and countless injuries are prevented for each cadaver test (King et al. 1995).

### **1.2.3. Anthropometric Tests Devices testing**

Anthropometric Test Devices (ATDs), also known as crash test dummies, have been developed as alternatives to other surrogates. ATDs are mechanical devices designed to have an anthropometric shape based on population percentiles and are validated through the previous testing types. ATDs are largely used in transportation safety, providing a

highly repeatable and cost-effective testing method compared to the previous testing methods. ATDs are designed to represent the human body with the highest internal biofidelity (accelerations, deformations, energy absorption, rigidity, articulations of the body regions, etc.) and external biofidelity (i.e. shape, size and interaction with the environment). The more they resemble human characteristics, the more accurately they represent the human body's response to external stimuli.

Instrumented with sensors to measure accelerations, forces, moments, and deformations, ATDs allow for the analysis of protection offered by restraint systems during impacts. Years of development have made the dummies complex devices composed of advanced materials with dozens of channels of instrumentation increasing their cost of production. Due to this degree of complexity, some ATD have been simplified and specifically designed according to the use for which they are intended. Some examples are the HIII and THOR, which were designed for the study of the human body under frontal impact conditions. Some others such as RID3D and BioRID dummies, which are used for rear impacts or SID (Side Impact Dummy), BIOSID or WorldSID, designed for side impact conditions. Frequently, only parts of the body are represented, this is the case of the lower limbs, for the development of pedestrian protections (used on Euro NCAP, JNCAP or KNCAP), or headforms in the field of helmet homologation testing, according to regulations such as ECE/ONU R22.06.

Dummies are the main tool in compliance and regulatory testing, and therefore, a high level of biofidelity is necessary for these devices. However, the requirements for durability and repetitive testing lead to specifications that are contradictory to those desirable for biofidelity (Crandall et al. 2011). Furthermore, they are mechanically limited, in terms of anatomy and anthropometry, to a number of sizes and shapes and this leads to a decrease of the biofidelity in the task of representing a significant portion of the worldwide population.

Several studies have highlighted differences in the response of ATDs compared with PMHS (Forman et al. 2006; Lopez-Valdes et al. 2010a; Pipkorn, López-Valdés, et al. 2016; Shaw et al. 2002). When lateral bending and axial torsion of the spine are induced by the asymmetric load of the three-point seatbelt, these limitations in ATDs can lead not only to unrealistic spine and neck loads, but also to errors in the estimation of the chest deflections that are evaluated with respect to the spine (Shaw et al. 2013).

#### **1.2.4. In-silico testing**

Due to advancements in computing capabilities over the past few decades, several computational human body models have been developed to predict the response of the human body during blunt impacts. The most complex impact scenarios require the model to interact with the environment, and two main types of models are widely used: the multibody human models (Multi-Body Systems or MBS) and Finite Element Human Body Models (FE-HBM). The MBS models are a reasonable approximation to the human



anatomy and consist of a set of rigid parts representing human structures and mass distribution, connected by various types of joints. On the other hand, FE-HBM models analyse the human body as an assembly of deformable solids, accurately representing the human anatomy (bones, skin, ligaments, muscles, etc.). These last models represent tissue level response using governing equations based on continuum mechanics.

The primary advantage of a full human body FE model is its capability to predict injuries based on local values of deformation, providing a considerable advantage over simpler multi-body models or dummies. The distribution of stress and strain produced by a stimulus can be assessed using this method, thereby identifying the mechanisms that cause certain injuries during a crash. Unlike ATDs, FE models use to be fully modifiable in terms of material properties, such as bone density, muscular tone or ligaments rigidity, and geometry. This leads to subject-specific models allowing the study of diverse groups of population including elderly, overweight, underweight and different percentiles.

However, the accuracy of any computational model for assessing injury risk depends inherently on the quality of the model in terms of model geometry and material properties. An improvement in model quality leads, not only to a more biofidelic model, but also to higher computational requirements incrementing costs. Therefore, the biofidelity of the human FE model must be evaluated across different loading conditions to better predict the life human behaviour on the development of the occupant safety.

Two commercially available full-body finite element models are widely used due to their level of detail and range of validation. The Global Human Body Model Consortium (GHBMC) model developed by Elemance is composed of 2.3 million of elements in its detailed 50<sup>th</sup> percentile version (Gayzik et al. 2011). So far, four anthropometries have been developed for the model: 95<sup>th</sup> percentile male, 50<sup>th</sup> percentile male, 5<sup>th</sup> percentile female and the 6 year-old child version. All of them are available in both detailed and simplified versions and in standing and seating positions, although the child model is only available in a standing simplified version.

The direct competitor of the GHBMC model is the one developed by Toyota Motor Company and Toyota Central R&D (Iwamoto and et al. 2002). The THUMS (Total Human Model for Safety) model contains about 80.000 elements allowing a faster computation compared to GHBMC. It is also available for the 95<sup>th</sup> percentile male, 50<sup>th</sup> male and 5<sup>th</sup> female in standing and seating position. In this case, three child models are available: 3, 6 and 10 years-old versions in standing and seating position.

Other models have also been developed, such as HUMOS, one of the first FE-HBM which has been surpassed by the aforementioned models, and ViVA (Virtual Vehicle Safety Assessment) created to promote the gender diversity in the study of the impact biomechanics and focused on the cervical spine response in rear end impacts applying muscular activation.

A summary with the main advantages of the mentioned approaches is given in Table 1-1.

Table 1-1: Relative merits of human surrogates for injury biomechanics (Crandall et al. 2011)

	Volunteers	ATD	HBM	PMHS
Human Anthropometry	Yes	Yes	Yes	Yes
Human Anatomy	Yes	Partial	Yes	Yes
Physiologic Response	Yes	No	Potential	No
Testing To Injurious Levels	No	Yes	Yes	Yes
Direct Observation on Injury	No	No	Potential	Yes

### 1.2.5. Injury criteria and severity classification

An injury criterion is the evaluation of a measurable physical property (injury metric), or a combination of them, that demonstrates a correlation with certain type of injury. Due to the variability of the human body and impact conditions, it is not possible to define an exact value of safety. Thus, the measurable parameters that define the injury criterion, or injury metrics, are related with a probability of injury by means of injury risk functions and because of that are called probabilistic methods.

The development of injury criteria depends on the type of injury being assessed and the injury risk function must be established experimentally as the correlation between the injury metric and the severity of the injury outcome.

To cite some examples, the Combined Deflection (Dc) was developed by Song et al. (2011) to assess certain number of fractured ribs using FE-HBM. The Dc is a chest deformation-based injury criterion that considers the sternal deflection and the asymmetrical deformations of the ribcage. The HUMOS2LAB human body model were adapted and used to reproduce diverse PMHS sled tests available in literature. A strain threshold was established as an indicator of rib fractures and the deformation was correlated with a certain number of fractured ribs. However, the authors highlight that the formulation is model-dependent, thus, to be applied to other HBM or even ATD the established thresholds and parameters of the formulation must be adapted. In the same line and as proposed by Song et al., (2011), the DcTHOR was developed by Davidsson et al. (2014) to be applied for the THOR dummy. For the development of the DcTHOR, 59 PMHS tests with a known injury outcome were conducted and reproduced with ATD. In this study, the chest deformation of the ATD and the strain generated on the ribs were computed and related to the number of rib fractures to develop the corresponding injury risk functions for the mentioned injury metrics.

However, the degree of injury severity, as well as the definition of the term “severe”, must be established to develop consistent injury risk functions for comparison between subjects and injury criteria. In this regard, the most commonly used method in medicine and engineering to categorize the severity of an injury is the Abbreviated Injury Scale

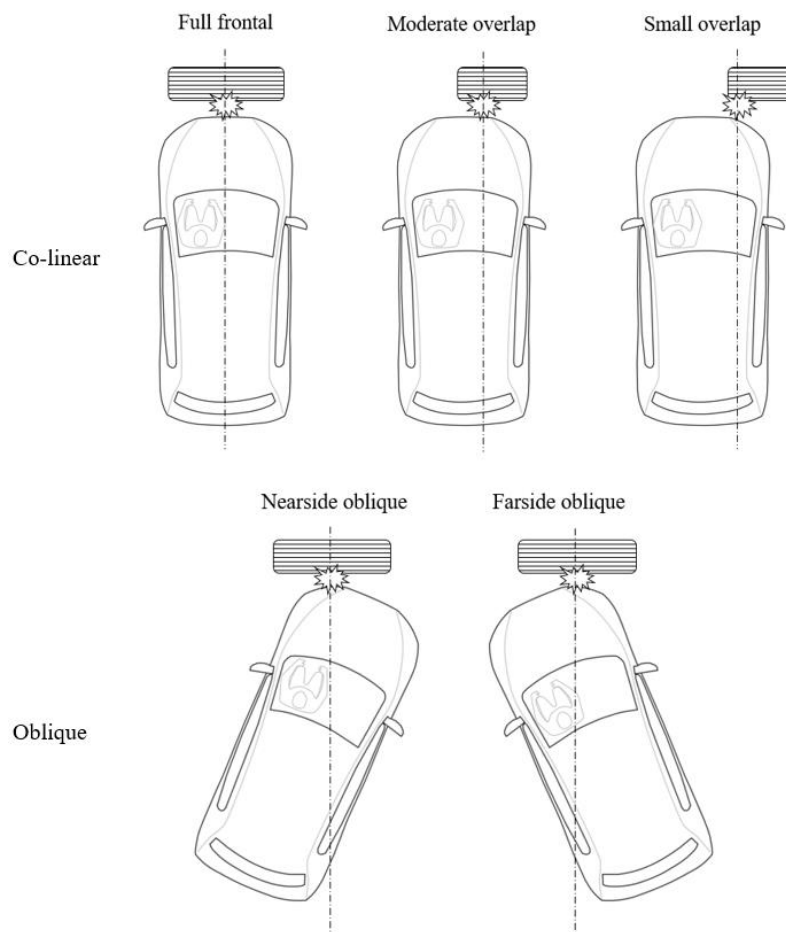
(AIS) (AAAM 1971). This scale was designed to classify injuries by body region and severity in terms of hospitalization duration and mortality, among others. This scale has been updated on several occasions, until the last update AIS2018 (AAAM 2015) which has up to 15 digits defining each category of injury and its severity. The last digit consists of a scale from 0 (AIS0), meaning 100% probability of survival, to 6 (AIS6), corresponding to less than 20% survival probability. When a subject sustains more than one type of injury, the Maximum AIS (MAIS) is commonly used, corresponding to the maximum AIS scale among the injury outcomes.

This consensus allows for the evaluation of various injury metrics associated with a specific injury for probabilistic methods.

### 1.3. Oblique impacts and chest injuries

After severe frontal crashes, oblique and small overlap crashes (see Figure 1-2) are the second most common crash type leading to fatal injuries (Bean et al. 2009). These configurations, differently from the full-frontal impact, cause the occupant to move in a forward-lateral direction, which may not be optimal for the existing belt and airbag restraint system.

Figure 1-2: Frontal impact configurations.



The National Highway Traffic Safety Administration (NHTSA) conducted an assessment program and found that drivers in oblique crashes experienced more MAIS 3+ injuries to various body regions compared to drivers in co-linear crashes. The chest was identified as the most frequently injured body region in both co-linear and oblique impacts, followed by the lower and upper extremities (NHTSA 2015). Contemporary research, analysing the NASS CDS database for the last 15 years, has pointed out that oblique impacts were still the most prevalent collision configuration leading to fatal injuries and MAIS 3+ thoracic injuries occurred with a higher frequency than injuries in other body regions (Suarez-del Fueyo et al. 2021).

Several studies have concluded that the rib fractures are the most common thoracic injuries in frontal impacts (Carroll et al. 2010; Crandall et al. 2000; Eigen et al. 2007; Kent et al. 2003) being a major source of morbidity and mortality (Nirula and Pintar 2008). Diagonal belt load and side structure impact have been found as main injury mechanisms for thoracic injuries under oblique impacts (Iraeus et al. 2013). Despite the overall improvement in traffic safety during the past decades, rib fractures are still prevalent in road crashes, especially in elderly occupants (Forman et al. 2019; Kent et al. 2005; Suarez-del Fueyo et al. 2021).

To enhance occupant protection, the Insurance Institute for Highway Safety (IIHS 2012) introduced the small overlap load case in their consumer rating portfolio, using the Hybrid III dummy in the driver position and limiting the chest deflection to 50 mm, but considering also a maximum value for the acceleration ( $a_{3ms} < 60$  g), the viscous criterion ( $VC < 0.8$  m/s) and the deflection rate ( $< 6.6$  m/s). The Euro NCAP/ANCAP MPDB (Moving Progressive Deformable Barrier) frontal impact consists of a 50% overlap frontal test at 50 km/h against a moving barrier with the THOR 50<sup>th</sup> percentile in the driver position (ANCAP 2020). The maximum score for the thorax region requires that the maximum resultant deflection of the thorax of the dummy  $R_{max}$  is below the 35 mm threshold. In 2015, the NHTSA released a request for comment pertaining to including a new oblique test using a moving deformable barrier (OMDB) impacting a stationary vehicle at 90 km/h at a 15-degree angle (NHTSA 2015).

The differences in these procedures highlight a lack of agreement on which injury criterion or criteria should be used to assess thoracic injuries in oblique impacts. This reflects the scarcity of detailed in situ experimental data that could support the development of a thoracic injury criterion for oblique impacts.

### **1.3.1. Chest deflection measurement on experimental testing**

For the thoracic injury assessment, the 3D measurement of the chest deflection is considered to be the best predictor of thoracic injury risk (Davidsson et al. 2014; Kemper et al. 2011; Poplin et al. 2017). Several injury criteria have been developed to assess the injury risk of an occupant under certain loading conditions. Thus, as mentioned in section 1.2.5, independently on the methods used for the development of any injury criteria, the

injury risk curves have to be established experimentally, thus, accurate measurement of chest deflection is crucial for evaluating the complex deformation patterns of the chest during impact or loading events. Various methods can be employed to measure chest motion, each offering distinct advantages and disadvantages.

High-speed imaging, often using high-speed cameras, offers visual assessment of chest deflection and deformation, allowing for qualitative analysis of the global behaviour of the chest during an impact. It provides valuable insights into the dynamic response of the chest. However, challenges may arise in obtaining quantitative measurements without additional analysis techniques, and this method is limited to surface measurements, unable to capture internal deformations.

X-ray imaging techniques, such as radiography or computed tomography (CT) scans, have proven to be valuable in the measurement of chest deflection. X-ray imaging enables the assessment of internal deformations and the identification of potential rib fractures, providing detailed visualization of the chest's anatomical structures. For example, Ali et al. (2005) used CT imaging to track rib deformation under anterior loading as a function of chest deflection, obtaining full-thoracic CT scans at each level of deflection. However, it is important to note that X-ray imaging techniques do not provide real-time or dynamic information, and they are limited to static images.

One commonly used method for chest deflection measurement is the utilization of chest bands. These elastic bands equipped with strain gauges or other sensors directly measure the displacement and deformation of the chest. Albert et al. (2018) employed two 59-channel chest bands to obtain the chest deformation in 20 full frontal PMHS sled tests, obtaining external chest deformation data for comparison with Hybrid III and THOR-M ATDs. Poulard et al. (2014) selected 40 nodes on an HBM chest contour to assess model chest deflection and compare with PMHS sled tests available in the literature (Lessley et al. 2010; Shaw et al. 2014). While chest bands provide continuous data during the event and can be employed in various impact scenarios, they measure outward deflection and may lack information about internal rib behaviour. Additionally, the measurement of chest and spine landmarks in the vertical axis is limited with this method, impeding a comprehensive assessment of chest deformation.

Stereophotogrammetry has been typically used for spine kinematics acquisition, allowing the assessment of the 6-DOF motion of spinal motion (Forman et al. 2015; Lopez-Valdes et al. 2010b; Shaw et al. 2014). However, some authors have employed this method for capturing chest deflection in three dimensions (Acosta et al., 2016; Salzar et al., 2013; Shaw et al., 2009, 2013). By utilizing multiple cameras to capture images of the chest from different angles, stereophotogrammetry enables the tracking of specific chest and spine landmarks and subsequent measurement and analysis of their movement with respect to a specific spine landmark. It provides detailed spatial information the motion, allowing for the evaluation of complex deformation patterns (Acosta et al. 2016; Salzar et al. 2013; Shaw et al. 2009, 2013). However, careful calibration and

synchronization of multiple cameras are required, and the method can be sensitive to markers occlusions.

In the context of PMHS tests, accurate measurement of chest deflection is crucial for understanding thoracic biomechanics and assessing injury risk. The 3D measurement of chest landmarks and the establishment of a reference point on the spine, play a vital role in defining chest deflection. This motion analysis enables the determination of rib deformation in the three dimensions and, consequently, the assessment of fracture probabilities.

### **1.3.2. Chest injury assessment using ATD.**

Several metrics based on the measurement of the 3D deformation of the chest have been proposed in the development of a reliable injury criterion. These metrics have been associated with a function that relates the deformation values obtained to the probability (P) of a certain number of fractures.

Saunders et al. (2015) proposed a method to calculate the probability of AIS3+ occurrence ( $P(\text{AIS}3+)$ ), defined as any occurrence of three or more fractured ribs (AAAM 2015) based on the maximum compression of the chest. The peak resultant chest deflection measured at any of four rib deflection measurement locations ( $C_{\text{max}}$ ) was used as a metric in THOR ATD frontal offset oblique impacts. In the mentioned study, all nearside conditions showed a higher risk of chest injury compared to the far-side conditions. Using the same metric based on chord deflection as discriminator, Shaw et al. (2010) compared PMHS and THOR torso deformation and found that the ATD failed to capture the “bulge-out” observed on the lower chest during the PMHS tests and addressed the need to develop a deformation metric that better reflects injury potential.

Davidsson et al. (2014) developed the DcTHOR, a multi-point combined deflection criterion based on a set of 59 PHMS test under diverse loading conditions. The experimental tests were reproduced using the THORAX demonstrator fitted with instrumentation that measures 3D chest deformation (IR-TRACCS) and the combined deflection formulation was proposed. The results were compared with fundamental chest deflection components and a strain-based injury criterion, Number of Fractured Ribs (NFR). DcTHOR criterion showed good injury risk quality index and, while NFR was identified as a potentially useful injury criterion, it had a lower quality index compared to displacement-based criteria.

In line with the design of the multi point chest deformation injury criteria Poplin et al. (2017) proposed the total and differential chest deformations (PC Score) and the  $C_{\text{max}}$  as reliable discriminators of probability of injury. Considering a set of 45 PMHS tests under 13 different tests conditions, those were reproduced with the THOR Anthropometric Test Device (ATD). The mentioned study suggested an injury risk function to relate the proposed discriminators to the probability of AIS 3+. The authors observed that the predicted probability of AIS 3+ (three or more fractured ribs (AAAM

2015)) thoracic injuries obtained by either injury criteria was very similar. The same observation was reported in Lopez-Valdes et al. (2018), which used both injury criteria with the THOR dummy to predict the thoracic injuries of three elderly male PMHS in sled frontal impacts. This study also highlighted that both criteria had underestimated the actual risk of thoracic injury observed in the PMHS tests.

Studies focusing on oblique impacts have suggested that oblique loading can cause larger chest deformations than frontal loading (Acosta et al. 2016; Piqueras et al. 2022). However, current ATD were developed for evaluation of either frontal impacts (Hybrid III, THOR) or side impacts (EuroSID, WorlSID) and, thus, the response under oblique impact may not be biofidelic.

### **1.3.3. Chest injury assessment using Human Body Model**

FE-HBMs allow for geometrical modification for the study of injury assessment in different populations. These modifications, or personalization techniques, enable the representation of subject-specific characteristics and the reproduction of injury-causing conditions, making them a crucial tool for injury mechanism research and the development of biofidelic injury criteria. Kent et al. (2005) suggested that using more biofidelic thoracic models can improve the injury risk assessment. Some authors have developed parametric models to reproduce the subject-specific characteristics to accurately represent the injury risk of a specific population group (Hwang et al. 2016; Larsson et al. 2019; Shi et al. 2014). Poulard et al. (2015) found that the HBM pre-impact posture altered the predicted kinematics and rib fracture risk in frontal impacts, although it had a limited effect, suggesting that anthropometry can play a more relevant role in the outputs provided by HBM. Despite the fact that the modification of the anthropometry and pre-impact posture of the HBM demonstrated to improve the HBM predictions of external occupant kinematics, the rib deformation patterns do not accurately represent the PMHS ribcage behaviour and the chest deflection was underpredicted (Larsson et al. 2019).

The FE-HBM description of the material properties of the tissue allows, at least theoretically, the calculation of injury risk to be based on strain measurements, a magnitude that is more likely to be related to the actual mechanisms causing the tissue to fail. Accordingly, several studies have proposed injury criteria for HBM based on strain (Forman et al. 2012; Iraeus et al. 2020; Laituri et al. 2005). Two main groups can be distinguished: deterministic and probabilistic criteria.

In the deterministic criteria, the strain predicted by the FE-HBM is compared to a previously accepted injury threshold, if the strain exceeds the threshold, an injury is predicted. The number of fractured ribs (NFR) can be evaluated based on those elements that have reached certain strain value.

In the probabilistic criteria, the predicted strain is transformed into the probability of sustaining such strain given the known distribution of strain in the population (that

needs to be known/estimated before). The probability of obtaining a stated number of fractures is based on the strain results of the entire ribcage, such as in the case of the deformation-based criteria applied for ATD.

Forman et al., (2012) was the first study developing a probabilistic injury criteria approach for FE-HBM and Pipkorn et al. (2019) showed that this method was capable of predicting the number of fractured ribs observed in PMHS sled tests. However, to succeed on the injury risk prediction, the HBM had to be developed to predict accurately the actual strain of the tissue. Therefore, the injury risk functions are dependent on model characteristics such as mesh size of each HBM and have to be developed and validated for each loading scenario (Forman et al. 2022), which is not always feasible.

However, the strain-based methods showed poor correlation with the number of fractures and have been found to be less sensitive to the restraint conditions than the deformation-based criteria (Davidsson et al. 2014; Larsson et al. 2019; Song et al. 2011).

Thus, in parallel to strain based thoracic injury criteria, several studies have used HBM chest deformations as a potential predictor of thoracic injuries, similarly to what it is done with ATD. For instance, Song et al. (2011) proposed the Dc criterion a chest deformation-based injury criterion that considers the sternal deflection (Ds) and the differential deformation produced on the lower ribcage aspects (dD) using the HUMOS2LAB HBM. A strain threshold was established as an indicator of rib fractures by means of validation against PMHS sled tests and the deformation was correlated with a certain number of fractured ribs.

Mendoza-Vazquez et al. (2015) developed a set of thoracic injury risk curves for AIS2+ using diverse deformation-based criteria such as Dmax, Cmax, VCmax among others and included the DcTHOR, a multi-point chest deflection measurement proposed by Davidsson et al. (2014) that considers differential deformations of the measured rib points, but adapted to be used for the THUMS HBM. This study was conducted using a detailed Finite Element ribcage model and concluded that the curve for DcTHOR obtained the best confidence interval results and those metrics based on multi-point measurements (DcTHOR and Dc) were less sensitive to variations in material properties.

Current studies show multiple examples of the application of deformation based criteria to the prediction of chest injuries using FE-HBM such as Brodin and Wass (2016), which used DcTHOR and Dmax metrics with the THUMS model for the assessment of the injury protection provided by a safety-vest in equestrian riders, or Grébonval et al. (2021), which used the Cmax and PC Score to compare the thoracic injury risk predicted by the GHBMC HBM and the THOR ATD in frontal impacts in reclined occupant positions.

Due to the foregoing, whether HBM are used either to benchmark the biofidelity of chest deformation measured under specific restraint and loading configurations or to propose an injury threshold related to chest deformation, HBM must show a reliable



prediction of the human chest deformation in 3D and becomes essential to evaluate how personification techniques can influence the prediction of rib fractures.

#### **1.4. Objectives**

The previous paragraphs highlight the high frequency and severity of thoracic injuries in oblique impact configurations. Therefore, the study of occupant kinematics and the injury mechanisms that lead to rib fractures becomes essential for occupant protection. Human body models have been utilized in the development of more biofidelic injury criteria and restraint system design to enhance the occupant protection, as these models can be modified or personalized to represent the subject-specific characteristics of an occupant or a population group.

Due to the foregoing, the aim of this work is to evaluate how HBMs can be improved to accurately predict the chest kinematics in oblique impact configurations and how the different personalization techniques can influence the chest deformation. To accomplish this main objective, the chest deformation of the HBM has to be compared with experimental data to assess how the subject-specific characteristics may influence the chest kinematics. However, the chest deflection measurement requires a reference point on the spine, thus the biofidelity of this spinal kinematics has to be evaluated first.

In this regard, to achieve the goal of this study, the following questions must be answered:

1. Are the HBM capable of mimicking occupant kinematics in terms of spinal bone trajectories?
2. Are the HBM capable of mimicking occupant kinematics in terms of spinal bone rotations?
3. Are the HBM capable of mimicking occupant chest deformation during oblique impacts?
4. How does the chest deflection of the HBM respond to the different personalization techniques?

To analyse the behaviour of the human body in a nearside oblique impact, the kinematics of three PMHS sled tests carried out at the Impact Laboratory-I3A (University of Zaragoza-Spain) were investigated. Translational and rotational motion as well as chest deflection of the PMHS were analysed and compared with the results obtained from a FE-HBM to assess the prediction capability for both spine kinematics and chest deformation. The HBM was personalized to represent the anthropometry and posture of the PMHS before the impact to evaluate the influence of personification techniques on the HBM's prediction capability.

The following chapters will present the methodology and results derived from evaluating the previous questions and finally achieve the main objective.

## References:

- AAAM. Rating the Severity of Tissue Damage – The Abbreviated Injury Scale.; 1971.
- AAAM. The abbreviated injury scale 2015, update 2018. Des Plaines, IL; 2015.
- Acosta SM, Ash JH, Lessley DJ, Shaw CG, Heltzel SB, Crandall JR. Comparison of whole body response in oblique and full frontal sled tests. 2016 IRCOBI Conference Proceedings - International Research Council on the Biomechanics of Injury. 2016;(Table I):740–754.
- Albert DL, Beeman SM, Kemper AR. Assessment of Thoracic Response and Injury Risk Using the Hybrid III, THOR-M, and Post-Mortem Human Surrogates under Various Restraint Conditions in Full-Scale Frontal Sled Tests. SAE Technical Papers. 2018;2019-November:1–65.
- Ali T, Kent RW, Murakami D, Kobayashi S. Tracking Rib deformation under anterior loads using computed tomography imaging. SAE Technical Papers. 2005;2005(724).
- ANCAP. ANCAP Test Protocol. Mobile Progressive Deformable Barrier.; 2020.
- Bean JD, Kahane CJ, Mynatt M, Rudd RW, Rush CJ, Wiacek C. Fatalities in Frontal Crashes Despite Seat Belts and Air Bags. National Highway Traffic Safety Administration. 2009;(September):88.
- Carroll J, Adolph T, Chauvel C, Labrousse M, Trosseille X, Pastor C, Eggers A, Smith S, Hynd D. Overview of serious thorax injuries in European frontal car crash accidents and implications for crash test dummy development. International Research Council on the Biomechanics of Injury - 2010 International IRCOBI Conference on the Biomechanics of Injury, Proceedings. 2010;(September):217–234.
- Crandall J, Kent R, Patrie J, Fertile J, Martin P. Rib fracture patterns and radiologic detection-a restraint-based comparison. Annual proceedings / Association for the Advancement of Automotive Medicine. Association for the Advancement of Automotive Medicine. 2000;44(1989):235–259.
- Crandall JR, Bose D, Forman J, Untaroiu CD, Arregui-Dalmases C, Shaw CG, Kerrigan JR. Human surrogates for injury biomechanics research. Clinical Anatomy. 2011;24(3):362–371.
- Davidsson J, Carroll J, Hynd D, Lecuyer E, Song E, Trosseille X, Eggers A, Sunnevang C, Praxl N, Martinez L, Lemmen P, Been B. Development of injury risk functions for use with the THORAX Demonstrator; an updated THOR. In: Proceedings of IRCOBI Conference 2014.; 2014a:359–376.
- Davidsson J, Carroll J, Hynd D, Lecuyer E, Song E, Trosseille X, Eggers A, Sunnevang C, Praxl N, Martinez L, Lemmen P, Been B. Development of injury risk functions for use with the THORAX Demonstrator; an updated THOR. In: Proceedings of IRCOBI Conference 2014.; 2014b:359–376.
- Eichberger A, Darok M, Steffan H, Leinzinger PE, Boström O, Svensson MY. Pressure measurements in the spinal canal of post-mortem human subjects during rear-end impact and correlation of results to the neck injury criterion. Accid Anal Prev. 2000;32(2):251–260.
- Eigen AM, Benteil SA, Smith DL. The crash problem for advanced restraints. International Technical Conference on the Enhanced Safety of Vehicles, June 18-21. 2007;1:1–13.
- Forman J, Lessley D, Shaw G, Evans J, Kent R. Thoracic Response of Belted PMHS, the Hybrid III, and the THOR-NT Mid-Sized Male Surrogates in Low Speed, Frontal Crashes. Stapp Car Crash Journal. 2006;50:191–215.
- Forman J, Perry B, Henderson K, Gjolaj JP, Heltzel S, Lessley D, Riley P, Salzar R, Walilko T. Blunt impacts to the back: Biomechanical response for model development. 2015;48(12).

- Forman J, Poplin GS, Shaw CG, McMurry TL, Schmidt K, Ash J, Sunnevang C. Automobile injury trends in the contemporary fleet: Belted occupants in frontal collisions. *Traffic Inj Prev.* 2019;20(6):607–612.
- Gayzik FS, Moreno DP, Vavalle NA, Rhyne AC, Stitzel JD. Development of the Global Human Body Models Consortium mid-sized male full body model. *Injury Biomechanics Research.* 2011:39–12.
- Global plan for the Decade of Action for Road Safety 2011–2020. World Health Organization. 2010:25.
- Hwang E, Hallman J, Klein K, Rupp J, Reed M, Hu J. Rapid Development of Diverse Human Body Models for Crash Simulations through Mesh Morphing. *SAE Technical Papers.* 2016;2016-April.
- IIHS. Small Overlap Frontal Crashworthiness Evaluation Crash Test Protocol (Version I); 2012:25.
- Iraeus J, Lindquist M, Wistrand S, Sibgård E, Pipkorn B. Evaluation of chest injury mechanisms in nearside oblique frontal impacts. *Annals of Advances in Automotive Medicine.* 2013;57(August 2018):183–195.
- Iwamoto M, et al. Development of a Finite Element Model of the Total Human Model for Safety (THUMS) and Application to Injury Reconstruction. *Ircobi.* 2002;1(2).
- Kang YS, Stammen J, Moorhouse K, Bolte J. Head and neck responses of post mortem human subjects in frontal, oblique, side and twist scenarios. *Conference proceedings International Research Council on the Biomechanics of Injury, IRCOBI.* 2018;2018-Sept:130–149.
- Kent R, Baas C. Experimentación con animales (Experimentation with animals). In: Dalmases CA, Luzón Narro BJ, López-Valdés FJ, Del Pozo De Dios E, Seguí-Gómez M, eds. *Fundamentos de Biomecánica en las Lesiones por Accidente de Tráfico (Fundamentals of Biomechanics and Road Traffic Injuries).* 1st ed. Madrid: ETRASA-Editorial Tráfico Vial S.L.; 2012:p 151–177.
- Kent R, Lee SH, Darvish K, Wang S, Poster CS, Lange AW, Brede C, Lange D, Matsuoka F. Structural and Material Changes in the Aging Thorax and Their Role in Crash Protection for Older Occupants. *Stapp Car Crash Journal.* 2005;2005-November:231–249.
- Kent R, Sherwood C, Lessley D, Overby B, Matsuoka F. Age-Related Changes in the Effective Stiffness of the Human Thorax Using Four Loading Conditions. *IRCOBI Conference Proceedings.* 2003:249–264.
- King A, Viano DC, Mizeres N, States JD. Humanitarian Benefits of Cadaver Research on Injury Prevention. *The Journal of Trauma: Injury, Infection, and Critical Care.* 1995;38(4):564–569.
- Larsson KJ, Pipkorn B, Iraeus J, Bolte JH, Agnew AM, Hu J, Reed MP, Sunnevang C. Evaluation of the benefits of parametric human body model morphing for prediction of injury to elderly occupants in side impact. In: *Conference proceedings International Research Council on the Biomechanics of Injury, IRCOBI.* Florence, Italy; 2019:150–174.
- Lessley D, Shaw G, Parent D, Arregui-Dalmases C, Kindig M, Riley P, Purtsezov S, Sochor M, Gochenour T, Bolton J, Subit D, Crandall J, Takayama S, Ono K, Kamiji K, Yasuki T. Whole-Body Response to Pure Lateral Impact. *SAE Technical Papers.* 2010;54(November):289–336.
- Lopez-Valdes F, Juste-Lorente O, Lorente A, Piqueras-Lorente, A Danauskienė A, Muehlbauer J, S S, Symeonidis, Maza-Frechin M, Peldschus S. Kinematics and dynamic responses of young and elderly occupants in low-speed frontal tests. 2016.
- Lopez-Valdes FJ, Lau A, Lamp J, Riley P, Lessley DJ, Damon A, Kindig M, Kent R, Balasubramanian S, Seacrist T, Maltese MR, Arbogast KB, Higuchi K, Tanji H. Analysis

- of spinal motion and loads during frontal impacts. Comparison between PMHS and ATD. *Annals of Advances in Automotive Medicine - 54th Annual Scientific Conference*. 2010a:61–77.
- Lopez-Valdes FJ, Lau A, Lamp J, Riley P, Lessley DJ, Damon A, Kindig M, Kent R, Balasubramanian S, Seacrist T, Maltese MR, Arbogast KB, Higuchi K, Tanji H. Analysis of spinal motion and loads during frontal impacts. Comparison between PMHS and ATD. In: *Annals of Advances in Automotive Medicine - 54th Annual Scientific Conference*.; 2010b:61–77.
- Mendoza-Vazquez M, Davidsson J, Brodin K. Construction and evaluation of thoracic injury risk curves for a finite element human body model in frontal car crashes. *Accid Anal Prev*. 2015;85:73–82.
- Michaelson J, Forman J, Kent R, Kuppa S. Rear Seat Occupant Safety: Kinematics and Injury of PMHS Restrained by a Standard 3-Point Belt in Frontal Crashes. *SAE Technical Papers*. 2008;2008-November:295–325.
- National Highway Traffic Safety Administration. 2017 Data: Occupant Protection in Passenger Vehicles.; 2017.
- NHTSA. New Car Assessment Program.; 2015:56928–56935.
- Nirula R, Pintar FA. Identification of vehicle components associated with severe thoracic injury in motor vehicle crashes: A CIREN and NASS analysis. *Accid Anal Prev*. 2008;40(1):137–141.
- Passmore J, Yon Y, Mikkelsen B. Progress in reducing road-traffic injuries in the WHO European region. *Lancet Public Health*. 2019;4(6):e272–e273.
- Pipkorn B, López-Valdés FJ, Juste-Lorente O, Insausti R, Lundgren C, Sunnevång C. Assessment of an innovative seat belt with independent control of the shoulder and lap portions using THOR tests, the THUMS model, and PMHS tests. *Traffic Inj Prev*. 2016;17(September):124–130.
- Poplin GS, McMurphy TL, Forman JL, Ash J, Parent DP, Craig MJ, Song E, Kent R, Shaw G, Crandall J. Development of thoracic injury risk functions for the THOR ATD. *Accid Anal Prev*. 2017;106(December 2015):122–130.
- Poulard D, Subit D, Donlon J-P, Lessley DJ, Kim T, Park G, Kent RW. The Contribution of Pre-impact Spine Posture on Human Body Model Response in Whole-body Side Impact. *Stapp Car Crash J*. 2014;58(November):385–422.
- Poulard D, Subit D, Nie B, Donlon JP, Kent RW. The Contribution of Pre-impact Posture on Restrained Occupant Finite Element Model Response in Frontal Impact. *Traffic Inj Prev*. 2015;16(September 2016):87–95.
- Salzar RS, Lau SH, Lessley DJ, Sochor MR, Shaw CG, Kent RW, Crandall JR. Thoracic Response to Shoulder Belt Loading: Comparison of Tabletop and Frontal Sled Tests with PMHS. *Traffic Inj Prev*. 2013;14(2):159–167.
- Saunders J, Parent D, Ames E. NHTSA oblique crash test results: vehicle performance and occupant injury risk assessment in vehicles with small overlap countermeasures. In: *Proceedings of the 24th ESV Conference*. Gothenburg, Sweden; 2015:1–23.
- Shaw G, Crandall J, Butcher J. Biofidelity Evaluation of the THOR Advanced Frontal Crash Test Dummy. *International Journal of Crashworthiness*. 2002;7(3):239–254.
- Shaw G, Lessley D, Ash J, Crandall J, Parent D. Response Comparison for the Hybrid III, THOR Mod Kit with SD-3 Shoulder, and PMHS in a Simulated Frontal Crash. In: *23rd ESV Conference*.; 2013:1–19.
- Shaw G, Lessley DJ, Ash JL, Sochor MR, Crandall JR, Luzon-Narro J, Arregui-Dalmases C. Side

- Impact PMHS Thoracic Response With Large-Volume Air Bag. *Traffic Inj Prev.* 2014;15(1):40–47.
- Shaw G, Parent D, Purtsezov S, Lessley D, Crandall J, Kent R, Guillemot H, Ridella S a, Takhounts E, Martin P. Impact response of restrained PMHS in frontal sled tests: skeletal deformation patterns under seat belt loading. *Stapp Car Crash J.* 2009;53(November):1–48.
- Shaw G, Parent D, Purtsezov S, Lessley D, Crandall J, Törnvall F. Torso deformation in frontal sled tests: Comparison between THOR NT, THOR NT with the chalmers SD-1 shoulder, and PMHS. *International Research Council on the Biomechanics of Injury - 2010 International IRCOBI Conference on the Biomechanics of Injury, Proceedings.* 2010;1(September):247–263.
- Shi X, Cao L, Reed MP, Rupp JD, Hoff CN, Hu J. A statistical human rib cage geometry model accounting for variations by age, sex, stature and body mass index. *J Biomech.* 2014;47(10):2277–2285.
- Song E, Lecuyer E, Trosseille X. Development of injury criteria for frontal impact using a human body FE model. In: *International Technical Conference on the Enhanced Safety of Vehicles.* Washington, D.C.; 2011:1–15.
- Stapp JP, Air H, Base F. Human Tolerance to Deceleration. *The American Journal of Surgery.* 1957;93(4).
- Suarez-del Fueyo R, Junge M, Lopez-Valdes F, Gabler HC, Woerner L, Hiermaier S. Cluster analysis of seriously injured occupants in motor vehicle crashes. *Accid Anal Prev.* 2021;151:1–12.
- World Health Organization. *Global Status Report On Road Safety 2018.* Geneva; 2018.

## **MATERIALS AND METHODS**

---

This section provides a general overview of the materials and methods used in the dissertation to achieve the objectives outlined in 1.4 Objectives. Specific methods are described in greater detail in their corresponding chapter section.

### **2.1. Experimental Testing**

The present study aims to assess the HBM injury and kinematic prediction capabilities. Therefore, it is necessary to compare the results obtained from simulations with experimental results. In this regard, three PMHS sled tests were carried out at the Impact Laboratory of the University of Zaragoza in a 30 ° nearside oblique impact configuration (López-Valdés et al. 2016).

All procedures related to the PMHS tests, including recruitment, informed consent, and methods, were reviewed and approved by the Ethical Commission for Clinical Research of Aragón (CEICA). CEICA is the official body responsible for assessing all research projects involving human subjects in the region of Aragón. The commission also supervised the procurement and handling of the human donors according to the established procedures of the Impact Laboratory (I3A) at the University of Zaragoza. The approval certificate N° 16/2015 was approved by the Ethics Committee for Research of Aragón (CEICA) on October 14th, 2015, as part of the initial ethics assessment of the project. The letter of approval is included in Appendix A.

The protocol included safety measures such as blood analysis for the donors and personal protective equipment for the operators to ensure their health and safety.

#### **2.1.1. PMHS information**

The three PMHS were selected from the Donor Program established in the Impact Laboratory (I3A) at the University of Zaragoza. To preserve tissue properties and the structural conditions, the subjects were frozen no more than 48 hours after decease, avoiding other techniques of preservation, such as formalin. Otherwise, degradation or chemical products, especially soft tissues (muscles, ligaments, internal organs, etc), could have affected the mechanical properties of the tissues.

Age at the time of death, physical condition, and cause of death play an important role in the tissue material properties and can compromise the expected results. Therefore, these variables were carefully considered.

Table 2-1 summarizes the PMHS information, while the complete anthropometries of the subjects measured before the tests are given in Appendix B. Computed Tomography (CT) scans were performed on each subject before the tests to rule out potential injuries such as bone fractures that could affect the behaviour and compromise the results. If any relevant fracture or injury was encountered, the subject was discarded.

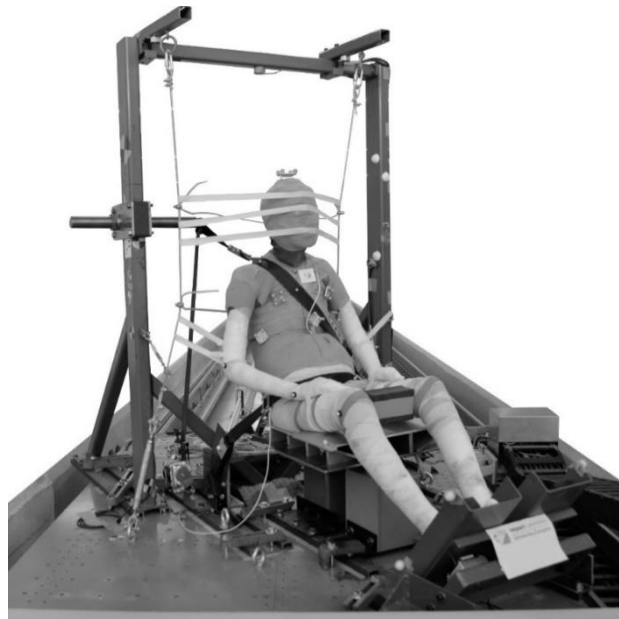
Table 2-1: PMHS information and test set-up

PMHS	Restraint system v1		Restraint system v2
	PMHS A	PMHS B	PMHS C
Impact angle (deg)		30	
Velocity (km/h)		35	
Seatbelt		3-point	
Pretensioner		Shoulder (2kN) Lap belt 3.5 kN	Lap belt 3.5 kN
Force Limiter		Shoulder belt 4.5 kN	
Configuration		Passenger	
Age	66	68	60
Sex	Male	Male	Male
Stature (cm)	175	169	170.5
Weight (kg)	47	53	57
Cause of death	Pancreatic cancer	Lung cancer	Lung cancer
Fractured ribs (total number of fractures)	15 (22)	5 (7)	10 (11)

### 2.1.2. Testing set-up

The three PMHS tests consisted in a nearside oblique (30°) impact configuration of an occupant restrained with a three-point seatbelt in a passenger position, as described by López-Valdés et al. (2016). The physical tests were carried out using a modified version of the Gold Standard fixture (GS), which was initially developed in 2009 to investigate a thoracic injury criterion (Shaw et al. 2009). The GS fixture consisted of a rigid metallic frame supporting a cable seat back, which approximated the seating position of a car occupant, allowing for visual access to the subject and its instrumentation (see Figure 2-1).

Figure 2-1: PMHS sled test fixture and configuration.



The fixture included a pelvic support and footrest to preserve the occupant's posture and was designed so that the interaction of the occupant with the seat was comparable to that of an occupant in a production vehicle seat. The occupants were restrained with two different versions of passenger side three-point seatbelt. In restraint system version 1 (RSv1), the shoulder belt was pretensioned at 2 kN and force-limited to 4.5 kN, while the lap belt was equipped with a 3.5 kN outboard pretensioner. The shoulder belt pretensioner was fired at 10 ms after the trigger, and lap belt pretensioner was fired at 18 ms after the trigger. In RSv2, the same restraint system was used, but the shoulder pretensioner was not activated. The three PMHS were subjected to a trapezoidal 15g deceleration pulse.

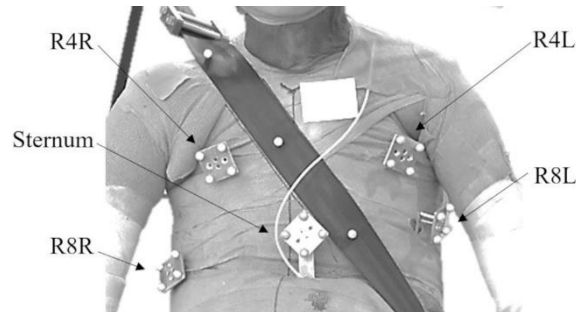
### 2.1.3. Instrumentation

The three-dimensional motion of each subject was collected at 1 kHz using an optoelectronic stereo photogrammetric system consisting of 10 Vicon TS™ cameras that tracked the position of retro-reflective spherical markers throughout a calibrated 3D space during the impact event. Single markers were attached to selected locations on the sled fixture, seatbelt and occupant. In order to obtain the 6 degree-of-freedom of the selected anatomical landmarks (Head, first thoracic vertebra (T1), eighth thoracic vertebra (T8) and second lumbar vertebra (L2)), marker clusters were rigidly attached to the corresponding bone following the method described by Shaw et al. (2009). Additionally, clusters of markers were attached to five anterior chest locations: the body of the sternum, to the 4<sup>th</sup> (R4) and 8<sup>th</sup> (R8) ribs bilaterally (L: left; R: right) of each PMHS (see Figure 2-2). A photogrammetric algorithm within the Vicon Nexus software package (Nexus® 1.8.5, Vicon®, Oxford, UK) reconstructed the 3D position of each target for each video



sample increment from the multiple 2D camera images. Sensor data were low pass filtered according to the Society of Automotive Engineers (SAE 1998).

Figure 2-2: PMHS's anterior chest landmarks.



The seatbelt-occupant interaction was recorded using four force transducers installed in the upper and lower shoulder belt and the inner and outer lap belt band. Two high-speed cameras recorded the occupant behaviour in the sagittal and frontal anatomical planes at 1 kHz providing useful information to understand the motion of the occupants.

#### 2.1.4. Post-test analysis and injury outcome

After the tests, another CT scan was conducted to identify potential injuries resulting from the impact and damages to the instrumentation hardware. Autopsies were also performed to confirm the results of the CT scan and find injuries on soft tissues.

All three subjects presented rib fractures. In RSv1, PMHS A was diagnosed with a total of 22 fractures during the autopsy, with 15 of them located on the right side. Additionally, a pelvic fracture and bilateral transverse process fracture at L3 were detected through CT scan analysis. PMHS B presented 7 rib fractures, with 6 of them located on the right side. An additional right clavicle fracture was also detected. Neither subject showed injuries or lacerations on soft tissues.

Concerning to the RSv2, a total of 11 fractures were observed in PMHS C, bilaterally distributed with 5 on the right side and 6 on the left. In addition, a right clavicle and 2 sternum fractures were detected. During the CT scan, 4 vertebra fractures were identified (T1, T2, T3 and T4) that could not be identified by the autopsy due to visual access limitations. Consistent with RSv1, no other injury related to the impact was found.

## 2.2. Simulation

### 2.2.1. Finite Element Human Body Model

In term of licensing and availability, by virtue of the collaboration established with SAFER (Chalmers University, Gothenburg), SAFER HBM v8 model was used. The SAFER HBM v8 was based on the commercial THUMS v3, but includes some important

modifications for this study, such as a remodelled ribcage as mentioned on Larsson et al. (2019) and an updated lumbar spine (Afewerki 2016). The model had been previously validated for frontal and side loading (Pipkorn et al. 2008; Pipkorn and Mroz 2008). After the version 3 of the THUMS model in which the SAFER HBM v8 was based, subsequent versions of THUMS were released. However, these newer versions were developed to focus on muscular activation. Since muscular activation is not relevant for the present study, as the comparison is done with PMHS, all model versions that include this functionality have been discarded.

All simulations were prepared using LS-PrePost v4.3 and carried out using the LS-DYNA® software solver.

### **2.2.2. Personalization of the HBM**

The process of personalizing the HBM involved three steps, each increasing in complexity. First, the overall mass of the HBM was adjusted to match that of the PMHS for the relevant sled test. Second, the THUMS model was morphed to reflect the individual anthropometry of each PMHS. Third, the posture of the THUMS model was adjusted to the actual positions of the PMHS. These modifications resulted in six versions of the THUMS model for each crash scenario: the baseline model and five modified models with varying levels of personalization (see Figure 2-3):

#### **1. *Baseline:***

The first level used the unmodified HBM as it is. The THUMS v3 model represents an occupant with a stature of about 177cm and a body mass of about 77kg in a standard seating position in terms of spine alignment and limbs position (see Figure 2-3). This model served as reference for the evaluation of the personalization techniques.

#### **2. *Baseline postured:***

To analyse the influence of initial posture, according to the findings of some authors (Poulard et al. 2014, 2015), the baseline model was modified by aligning the spine curvature of the model to match the actual spine curvature of the PMHSs at  $t=0$ ms. This was performed using an independent pre-simulation where a prescribed motion was applied to the head CoG, T1, T8 and L2 to finally conform to the positions measured in the PMHSs.

#### **3. *Scaled mass:***

In the second version, the overall mass of the model was adjusted to represent the individual PMHS (specified on

Table 2-1 and Appendix B by changing the material density of the outer flesh properties maintaining the external shape and size of the baseline model. The flesh parts were selected, and their density was modified to personalize the targeted mass. To maintain the structural integrity of the model, no other material properties were modified; therefore, variables such as osteoporosis or muscle tone have not been considered.

**4. Scaled mass postured:**

In this version of the model, the same procedure described on the previous paragraph was applied to the mass scaled version, modifying both mass and posture to resemble the weight and posture of the occupant while keeping the body size of the baseline model.

**5. Morphed:**

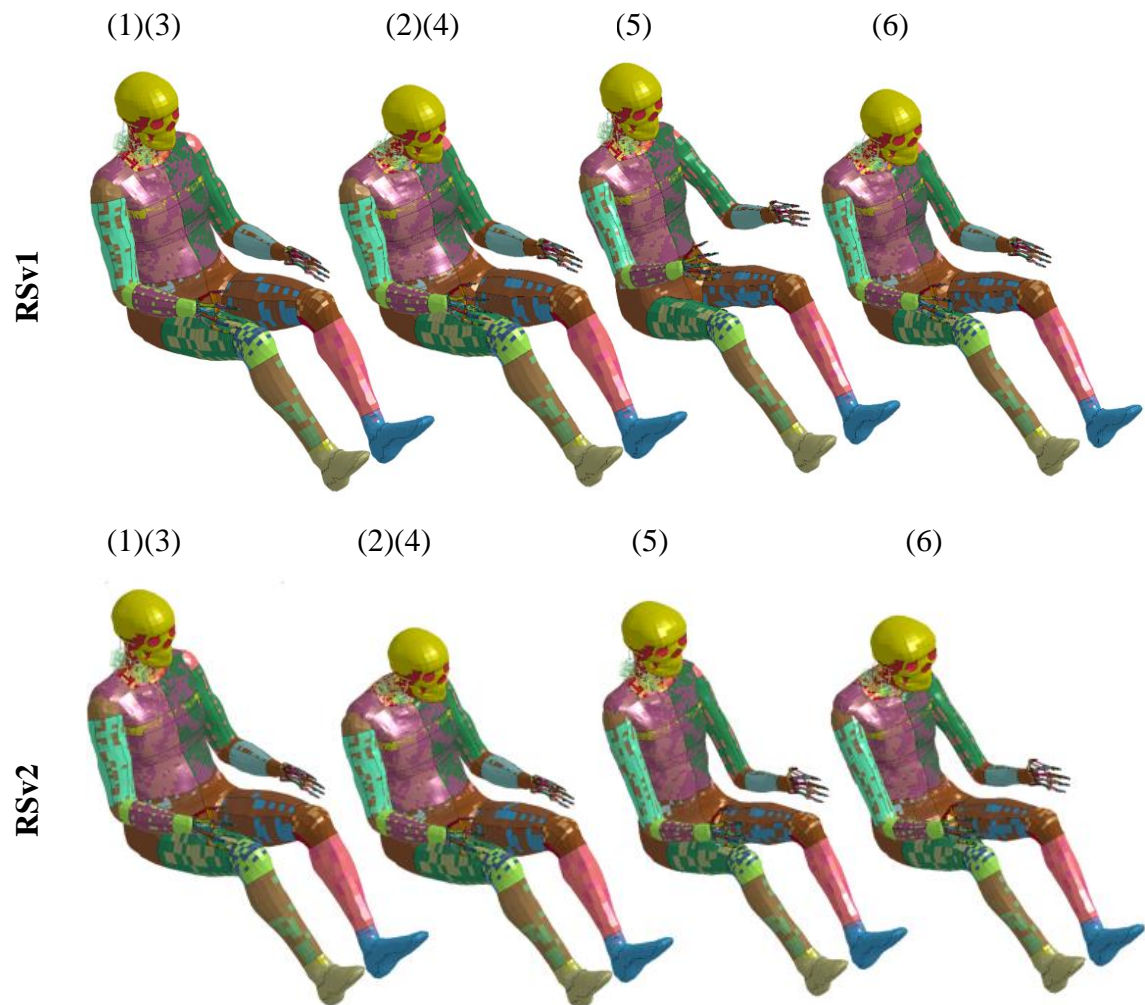
The HBM model was morphed to reflect the individual anthropometry and body mass of each PMHS measured before each test using PIPER® v1.0 software. The THUMS model was prepared to be processed by means of a metadata file in which all FE parts were identified and classified as bone, flesh (including muscles, fat, ligaments, etc.), organs and skin parts and divided into six main areas: head, trunk, upper limbs and lower limbs. In order to perform the morphing, lengths and contours had to be identified. Lengths was defined as the distance between two landmarks. For this purpose, two nodes of the model had to be identified in the metadata and used as landmarks. The PIPER software created auxiliary control points semi-automatically to define the body contours. The anthropometric dimensions (lengths and contours) in seated position used as input values for each subject were extracted from the seated anthropometry measurements Appendix B and from the captures of the VICON® markers before the tests. However, more data was required in order to morph the model accurately and, because of that, the PIPER database tool was used.

**6. Morphed postured:**

The spine posture of the morphed version (3) was adapted with the procedure followed for the model versions 4 and 5. This version involves all personalization techniques, and the contribution of each approach to the global kinematics and the injury prediction capabilities can be assessed by analysing the previous versions compared with the baseline model (1).

All model versions that involved a mesh modification, those where posture and anthropometry were adjusted, were studied in terms of mesh quality analysis. The result of this analysis is available on Appendix C.

Figure 2-3: Visualization of the different model versions. Models 3 and 4 corresponding to the mass scaled versions share the same external geometry with models 1 and 2 (Baseline and postured model versions).



### 2.2.3. Simulation Test Matrix

The targeted mass, anthropometry and spine alignment have been calculated based on the tested subjects for each RSv. The anthropometry of PMHS A and PMHS B was averaged to develop a single personalized HBM. This was decided due to the similarities in anthropometry and initial posture (Appendix B) of the two subjects that would have resulted in minimal differences in the corresponding HBMs. PMHS C data was used to develop the HBM versions for the RSv2. A total of 12 simulations were performed, corresponding to six versions for each of the two RSv, as shown in Table 2-2. The table indicates the test matrix and personalization techniques applied to each model version for both RSv1 and RSv2.

Table 2-2: Test matrix and personalization technique applied to each model version.

	Model Number	Model Name	Mass scaling	Morphing	Posturing
RSv1	(1)	Baseline			
	(2)	Baseline postured			Yes
	(3)	Scaled mass	Yes		
	(4)	Scaled mass postured	Yes		Yes
	(5)	Morphed	Yes	Yes	
	(6)	Morphed postured	Yes	Yes	Yes
RSv2	(1)	Baseline			
	(2)	Baseline postured			Yes
	(3)	Scaled mass	Yes		
	(4)	Scaled mass postured	Yes		Yes
	(5)	Morphed	Yes	Yes	
	(6)	Morphed postured	Yes	Yes	Yes

### 2.3. Bones kinematics acquisition and comparison

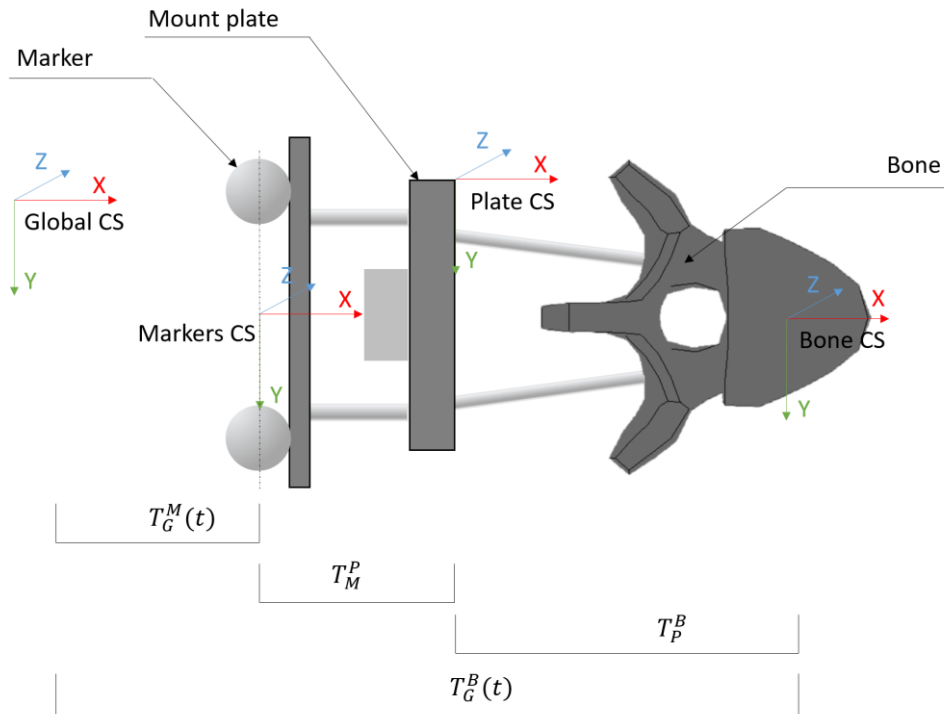
The study reports the 6 degrees-of-freedom (6-dof) motion of anatomical locations recorded by the Vicon system. The methodology used in the study is based on the work described by Kinzel et al. (1972) and discussed extensively by Shaw et al. (2009). The 3D rigid body motion is characterized using the transformation matrix (T), which is composed of the rotation matrix ( $R_{3 \times 3}$ ) and the position vector ( $P_{3 \times 1}$ ) of a point of the rigid body with respect to a chosen reference coordinate system (1). In this study, the transformation matrix was calculated for each anatomical location (Bone coordinate system) and expressed with respect to a common coordinate system valid for the three tested PMHS (Global coordinate system).

$$T_G^B(t) = \begin{bmatrix} R_{3 \times 3} & P_{3 \times 1} \\ 0_{1 \times 3} & 1 \end{bmatrix} = \begin{bmatrix} R_{11} & R_{12} & R_{13} & Px \\ R_{21} & R_{22} & R_{23} & Py \\ R_{31} & R_{32} & R_{33} & Pz \\ 0 & 0 & 0 & 1 \end{bmatrix} \begin{matrix} Bone \\ \\ \\ Global \end{matrix} \quad (1)$$

During the cadaver preparation, before the tests, the mount plate is rigidly attached to the bone, and once the PMHS is on the seated position during the test set-up preparation, the marker cluster is located over the mount plate to avoid potential damages on the assembly during the PMHS transportation. Thus, the transformation matrix associated with the motion of a particular bone with respect to the global coordinate system cannot be measured directly since the bone is not visible nor accessible for

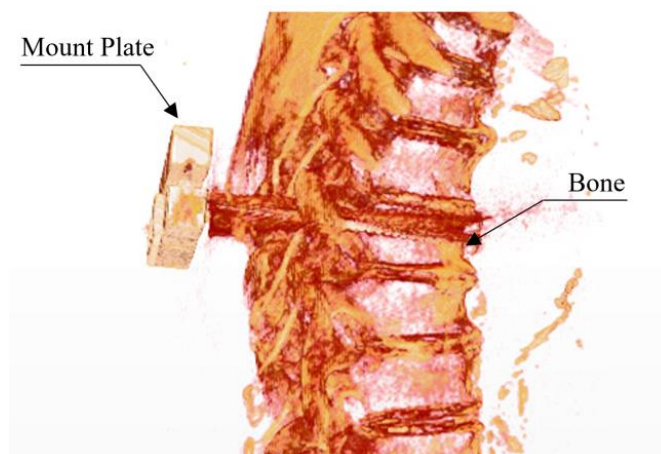
measurements. It needs to be obtained by means of the assembly sub-structures (see Figure 2-4).

Figure 2-4: Top view schema of the structure and calculation matrices.



First, CT scan of the subject was performed and segmented to obtain the geometry of the bone-plate sub-structure (see Figure 2-5) to calculate the  $T_P^B$  matrix of the bone (B) relative to the mount plate coordinate system (P).

Figure 2-5: Bone-plate sub-structure CT scan.



Second, after the test, the cluster-plate had to be measured to obtain the matrix  $T_M^P$  representing the plate (P) orientation and position with respect to the markers coordinate system (M).

Third, the transformation matrix  $T_G^M$  of the markers (M) with respect to the global coordinate system (G) was extracted from the data acquired with the Vicon system. Finally, the desired matrix  $T_G^B(t)$  was calculated by multiplying the previous matrices according to the equation (2).

$$T_G^B(t) = T_G^M(t) \times T_M^P \times T_P^B \quad (2)$$

This procedure was followed to extract the transformation matrix for the head, the instrumented vertebrae, and five anterior chest locations, including the sternum and four rib locations. (Shaw et al., 2009)

To compare the results of the experimental testing with the predictions obtained with the different versions of the SAFER HBM v8, homologous points were selected for the spinal and thoracic landmarks. Following the same procedure to that used for the PMHS, the head LCS origin was located in the midpoint between the two External Auditory Meati nodal points. The vertebrae LCS origin was placed at a node on the midpoint of the superior and inferior endplate's centre. In both cases and for the Global Coordinate System (GCS) was used as a reference for the calculations, where the X-axis pointed forward, the Y-axis pointed to the right, and the Z-axis pointed inferiorly, following the SAE J211 recommendations (Society of Automotive Engineers 2014).

The rigid bodies rotations were extracted from the rbdout output file on the previously defined coordinate system, while the nodal locations were obtained from the nodout file referred to the GCS. The relative distances of the marker clusters from the sternum along each rib were used to select analogous points on the different versions of the SAFER HBM. Thus, the analysed chest landmark for each PMHS were compared to homologous points in the corresponding simulation.

The comparison between experimental testing and predictions from the SAFER HBM v8 using homologous points and a standardized coordinate system allows for a reliable method for evaluating the accuracy of the simulation model.

## References

- Afewerki H. Biofidelity Evaluation of Thoracolumbar Spine Model in THUMS. 2016.
- Iwamoto M, Nakahira Y, Kimpara H. Development and Validation of the Total HUMAN Model for Safety (THUMS) Toward Further Understanding of Occupant Injury Mechanisms in Precrash and During Crash. *Traffic Inj. Prev.* 2015;16(June):S36–S48.
- Kinzel GL, Hall AS, Hillberry BM. Measurement of the total motion between two body segments-I. Analytical development. *J. Biomech.* 1972;5(1):93–105.
- Larsson KJ, Pipkorn B, Iraeus J, Bolte JH, Agnew AM, Hu J, Reed MP, Sunnevång C. Evaluation of the benefits of parametric human body model morphing for prediction of injury to elderly occupants in side impact. In: Conference proceedings International Research Council on the Biomechanics of Injury, IRCOBI. Florence, Italy; 2019:150–174.
- López-Valdés FJ, Juste-Lorente Ó, Maza-Frechin M, Pipkorn B, Sunnevang C, Lorente A, Asó-Vizan A, Davidsson J. Analysis of occupant kinematics and dynamics in nearside oblique impacts. *Traffic Inj. Prev.* 2016;17(September):86–92.
- Pipkorn B, Halldin P, Jakobsson L, Iraeus J, Backlund M, Mroz K, Lanner D, Holmqvist K, Kleiven S. Mathematical human body models in side impacts- A validation study with particular emphasis on the torso and shoulder and their influence on head and neck motion. *Int. Res. Counc. Biomech. Inj. - 2008 Int. IRCOBI Conf. Biomech. Inj. Proc.* 2008;(September):99–114.
- Pipkorn B, Mroz K. Validation of a human body model for frontal crash and its use for chest injury prediction. *SAE Tech. Pap.* 2008;1(1).
- Poulard D, Subit D, Donlon J-P, Lessley DJ, Kim T, Park G, Kent RW. The Contribution of Pre-impact Spine Posture on Human Body Model Response in Whole-body Side Impact. *Stapp Car Crash J.* 2014;58(November):385–422.
- Poulard D, Subit D, Nie B, Donlon JP, Kent RW. The Contribution of Pre-impact Posture on Restrained Occupant Finite Element Model Response in Frontal Impact. *Traffic Inj. Prev.* 2015;16(September 2016):87–95.
- Shaw G, Parent D, Purtsezov S, Lessley D, Crandall J, Kent R, Guillemot H, Ridella S a, Takhounts E, Martin P. Impact response of restrained PMHS in frontal sled tests: skeletal deformation patterns under seat belt loading. *Stapp Car Crash J.* 2009;53(November):1–48.



## **HBM PREDICTION OF SPINAL TRAJECTORIES**

---

### **3.1. Introduction**

This chapter is focused on the prediction of spinal trajectories using HBMs and addresses the first research question presented in the introduction. The primary objective is to investigate the capability of HBMs to predict spinal displacement during oblique impacts and quantify the influence of subject-specific characteristics on the HBM's kinematic response.

The biomechanical response of the human body to an impact is a complex process that involves the interaction between the body and the environment. The kinematics of the occupant will determine the potential contact of the body parts with the internal structures of the vehicle during a crash event and the interaction of the occupant with the restraint system.

Spinal kinematics is a crucial factor in the understanding of the chest deflection in both PMHS and HBM. Thus, it describes the motion of the thoracic and lumbar vertebrae and the distribution of loads across the thorax and the resulting injury patterns. Therefore, a detailed analysis of spinal trajectories in response to impact is necessary for the accurate prediction of chest deflection and injury risk.

The importance of spinal trajectory analysis for understanding chest deflection has been highlighted in previous research studies. Poulard et al. (2014, 2015) found that the spinal trajectory can affect the magnitude and distribution of loads across the thorax, which in turn influences the likelihood of chest injury. Similarly, Katagiri et al. (2016) demonstrated that the spinal trajectory is a critical factor in the development of accurate thoracic injury criteria, which are essential for the evaluation and improvement of restraint systems.

Moreover, spinal kinematics during impact can vary significantly between individuals due to differences in body size, shape, and posture. As a result, subject-specific characteristics, such as gender, age, and body mass, can affect the spinal trajectory and the resulting injury patterns (Hu et al. 2017; Hwang, Hu, et al. 2016; Larsson et al. 2019; Piqueras et al. 2018). Therefore, it is essential to account for these individual differences in HBM to ensure that they accurately reflect the spinal kinematics and injury risk for a given population.

The study presented here builds upon the findings of Paper A (Piqueras et al. 2018), which quantitatively assessed the agreement between the predicted displacements obtained from HBM simulations and the spinal displacements measured in physical tests.

This chapter aims to quantify the influence of the diverse personalization techniques applied to the HBM on the predicted spinal kinematics.

## **3.2. Methods**

### **3.2.1. Bone Trajectories Comparison**

To obtain the bone trajectories, Vicon markers were attached to the PMHS and used to record their movement during testing. The markers were placed at specific locations on the head and the spine, to allow for accurate reconstruction of the motion. The Vicon Nexus software was used to collect the marker data to reconstruct the motion of the body segments. This allowed for the generation of three-dimensional trajectories of the bones.

Three PMHS were exposed to a nearside oblique impact using two different restraint systems which differed on the use of shoulder belt pretensioner. PMHS A and B belonging to the RSv1 were equipped with a shoulder belt pretensioner, while in RSv2 (PMHS C) the pretensioner was not activated.

The trajectories of the spinal bones of the PMHS were obtained through the reconstruction of the trajectories of Vicon markers rigidly attached to the bones using the transformation matrix. The spinal bones trajectories of the PMHS were then compared with the trajectories obtained from the simulations. The time-history location of the CoG for each spinal landmark (Head, T1, T8 and L2 for RSv1 and Head T1, T7 and L1 for RSv2) was extracted according to the methods described in Chapter 2. For this section the H-point was used as reference for the spinal position and was calculated as the average position of two markers located bilaterally and attached externally to the position of the greater trochanter. The head LCS origin was located at the midpoint between the two External Auditory Meatii nodal points and the vertebrae LCS origin was placed in a node on the mid-point of the superior and inferior endplate's centre.

The same procedure was applied to the baseline HBM and all personalized model versions listed in section 2.2.2 Personalization of the HBM. The obtained trajectories were used to compare the performance of all HBM version for each RSv.

### **3.2.2. Quantitative Assessment of the Kinematic Response**

In Paper A, the correlation between the predicted response and the sled test results was quantified using CORA v 4.0.4 (Gehre et al. 2009). CORA rating is a method to evaluate time-history signals by comparing the reference curve (physical test) with the predicted response (simulation) ranging from 0 to 1, with a score of 1 representing perfect agreement between the two curves. The CORA scores for the individual landmarks are weighted to obtain a total CORA rating for each model. Paper A used the magnitude of the landmark displacement to weight the landmarks signals accordingly.

According to the rating stipulated in ISO/TR 18571, the resulting CORA scores are classified into four categories: values above 0.94 are considered excellent, values between 0.94 and 0.8 are good, values between 0.8 and 0.58 are considered as fair correlation, and values below 0.58 are treated as poor correlation.

### 3.2.3. Statistical analysis

Additionally, to the quantitative assessment carried out in Paper A, a further assessment of the influence of the diverse personalization techniques were conducted in this dissertation.

In this chapter, the main objective was to compare a baseline model with three modified versions that used different personalization techniques, including mass scaling, morphing, and posturing, to analyse their influence on the CORA Score. The simulation results were divided into two groups for each personalization technique: a reference group that did not include the monitored personalization technique and a second group that included the modified models with the technique. The grouping for the analysis of each modification is shown in Table 3-1.

*Table 3-1: Model versions groups for the analysis of the influence of the three personalization techniques.*

Personalization technique	Group 1	Group 2
Mass scaling	(1) Baseline	(3) Scaled mass
	(2) Baseline postured	(4) Scaled mass postured (5) Morphed (6) Morphed postured
Morphing	(1) Baseline	(5) Morphed
	(2) Baseline postured (3) Scaled mass (4) Scaled mass postured	(6) Morphed postured
Posturing	(1) Baseline	(2) Baseline postured
	(3) Scaled mass (5) Morphed	(4) Scaled mass postured (6) Morphed postured

The significance of the differences between the groups was evaluated using the Mann-Whitney non-parametric test, which is a statistical test used to compare the medians of two independent groups. The p-value obtained from this test represents the probability of obtaining the observed difference between the groups by chance alone, assuming that there is no real difference between them. The statistical significance level of the tests was set at  $p\text{-value} < 0.05$ . In addition to the p-value, the effect size  $r$  was also analysed to determine the magnitude of the differences between the groups. The effect size  $r$  is a measure that indicates the strength of the relationship between two variables,

independent of sample size. Cohen's guidelines were used to interpret the effect size  $r$  values, where an effect size of  $r = 0.10$  is considered small,  $r = 0.30$  is considered moderate, and  $r = 0.50$  is considered large. For example, an effect size of  $r = 0.5$  suggests that 25% of the variance in one variable can be explained by the other variable (Cohen 1988). However, it is important to note that this method of calculating effect size uses absolute values, which means that the resulting  $r$  value does not indicate whether the effect is positive or negative. In other words, this method does not provide information on whether the results represent an improvement or deterioration compared to the baseline. To address this aspect, it is necessary to consider the differences in medians ( $\Delta m$ ) between the two groups (positive or negative) to determine whether the results are superior or inferior to the baseline. In example, if the difference in medians between the non-postured and postured models is positive, means that the second group represent an improvement compared to the baseline ( $\Delta m = \text{medians of the second group} - \text{medians of the reference group}$ ).

By analysing the effect size  $r$  in addition to the  $p$ -value, this study provides a more comprehensive assessment of the impact of the personalization techniques on the modified models compared to the baseline model.

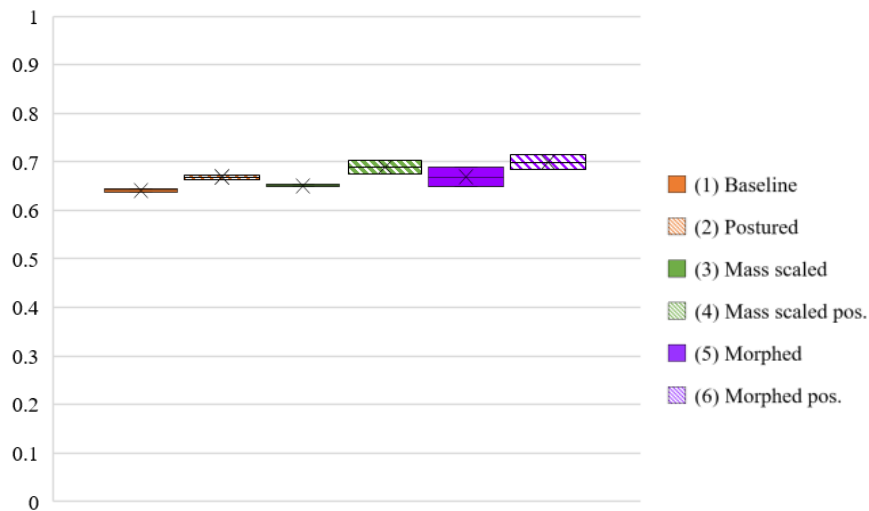
### **3.3. Results**

#### **3.3.1. Summary of Paper A**

As previously mentioned, this chapter builds upon the work presented in Paper A. The paper aimed to assess whether personalizing the SAFER HBM v8 using the personalization techniques detailed in section 1.2.2 could increase the agreement between the predicted and measured kinematic responses of the HBM. The study employed as reference four PMHS sled tests: The three nearside oblique tests described in section 2.1 and an additional full-frontal sled test.

The results showed that the more personalized the HBM was to the anthropometry and posture of the PMHS, the greater the agreement between the predicted and measured kinematics as shown in Figure 3-1.

Figure 3-1: Values of CORA Total rating for the different model versions including both restraint system versions.



Each personalization technique improved the predicted kinematics of the model to varying degrees, depending on the specific landmark and reference axis being evaluated. The morphed postured model achieved the highest CORA score, with the head showing better agreement than T1, T8, and pelvis. The influence of personification techniques was particularly pronounced when subject characteristics differed significantly from the baseline THUMS model.

However, the study identified some factors that could contribute to the observed differences between the predicted and measured trajectories, including modelling limitations, potential underestimation of seat friction, and HBM buttock flesh modelling. Age-related changes in body composition could also play a role in the observed discrepancies, although this was not considered in the study. Thus, more efforts should be made to address these limitations and validate the model further.

The lateral kinematics were not sensitive to the studied personification strategies and the lower spine kinematics were not being correctly predicted by the HBM. Therefore, more work is needed to address this limitation and improve the model's validation.

In conclusion, this study demonstrates that subject personification techniques can improve the accuracy of predicting the kinematics of PMHSs in frontal and nearside oblique impacts. However, the sensitivity of the HBM to the defined personalization techniques remains unclear, thus the following sections aim to clarify the individual influence of each personification technique.

### 3.3.2. Influence of the personalization techniques

Table 3-2 presents the p-values obtained from the Mann-Whitney non-parametric test for each comparison between the baseline model and the modified models using different personalization techniques. A p-value less than 0.05, as mentioned before, is

considered statistically significant, indicating a difference between the groups. According to Table 3-2, the posturing technique had a statistically significant difference compared to the baseline model in the total rating (p-value=0.02597). The mass scaling technique had a statistically significant difference in the head region (p-value=0.04848), as well as the morphing technique which shows a p-value= 0.00808. No other statistically significant differences were found in the other body regions.

Table 3-2: p-value for each comparison (bold=statistical significance).

PERSONALIZATION TECHNIQUE	MASS SCALING	POSTURING	MORPHING
<i>Total rating</i>	0.10909	<b>0.02597</b>	0.15354
<i>Head</i>	<b>0.04848</b>	0.39394	<b>0.00808</b>
<i>Upper Spine</i>	0.68283	0.48485	0.93333
<i>Middle Spine</i>	0.39394	0.81818	0.93333
<i>H-Point</i>	0.21414	0.93723	0.28283

Table 3-3 presents the effect size  $r$  for each comparison including the sign of  $\Delta m$  between brackets only when it is negative (-) to facilitate the table visualization. The effect size indicates the magnitude of the difference between the groups, independent of sample size. The effect size is categorized into small ( $r=0.10$ ), moderate ( $r=0.30$ ), and large ( $r=0.50$ ). According to Table 3-3, the posturing technique had a large effect size in the total rating ( $r=0.62404$ ), however had a small effect in the body regions individually. The mass scaling technique had a large effect size in the head ( $r=0.56383$ ) and a moderate effect size in the total rating and the H-Point. Similarly, to the mass scaling technique, the morphing technique had a large effect size in the Head trajectory ( $r=0.71092$ ) and a moderate effect size in the total rating and the H-Point.

Table 3-3: Effect size  $r$  for each comparison (bold = statistical significance) including the sign of  $\Delta m$  between brackets only where negative values were obtained.

PERSONALIZATION TECHNIQUE	MASS SCALING	POSTURING	MORPHING
<i>Total rating</i>	0.46578	<b>0.62404</b>	0.41675
<i>Head</i>	<b>0.56383</b>	0.25424	<b>0.71092</b>
<i>Upper Spine</i>	0.09823	0.20838	0.00000
<i>Middle Spine</i>	0.25424	(-) 0.06934	(-) 0.02451
<i>H-Point</i>	0.36772	(-) 0.02311	0.31869

### 3.4. Discussion

The present study aimed to evaluate the impact of three different personalization techniques, namely mass scaling, morphing and posturing, on the CORA score. The analysis of the results revealed that the effect of these techniques varied across the different components of the CORA score.

The highest effect size was observed for the morphing technique on the head trajectories, with a value of 0.71092. This suggests that the head motion is sensitive to the model geometry. Similarly, the posturing technique showed a significant effect on the total CORA rating, with an effect size of 0.62404. This suggests that the trajectories were highly influenced by these two modifications and can explain why the highest CORA score was obtained for the morphed postured model (Paper A).

In contrast, the analysis did not reveal significant differences in the upper, middle, and lower spine body regions for any of the three personalization techniques. This suggests that the impact of the personalization techniques may be limited to certain body regions and that more focused modifications may be required to improve the model's performance in these regions.

Overall, the results of this study suggest that the use of personalization techniques can improve the prediction of the spinal trajectories. Further research can be conducted to investigate the impact of other personalization techniques on the CORA score and to develop new techniques that may have a greater impact.

## References

- Cohen J. The Significance of a Product Moment  $r$ . In: *Statistical Power Analysis for the Behavioral Sciences*. Second Edi. London: Academic Press; 1988;p 75-109.
- Gehre C, Gades H, Wernicke P. Objective rating of signals using test and simulation responses. In: *21st International Technical Conference on the Enhanced Safety of Vehicles ESV 2009*.; 2009:15–18.
- Hu J, Zhang KS, Fanta A, Hwang E, Reed MP. Effects of Male Stature and Body Shape on Thoracic Impact Response Using Parametric Finite Element Human Modeling. In: *25th ESV Conference*.; 2017:1–11.
- Hwang E, Hu J, Chen C, Klein KF, Miller CS, Reed MP, Rupp JD, Hallman JJ. Development, Evaluation, and Sensitivity Analysis of Parametric Finite Element Whole-Body Human Models in Side Impacts. *Stapp Car Crash J*. 2016;60(November):473–508.
- Katagiri M, Zhao J, Kerrigan J, Kent R, Forman J. Comparison of Whole-Body Kinematic Behaviour of the GHBMOC Occupant Model. In: *IRCOBI Conference*.; 2016:679–693.
- Larsson KJ, Pipkorn B, Iraeus J, Bolte JH, Agnew AM, Hu J, Reed MP, Sunnevång C. Evaluation of the benefits of parametric human body model morphing for prediction of injury to elderly occupants in side impact. In: *Conference proceedings International Research Council on the Biomechanics of Injury, IRCOBI*. Florence, Italy; 2019:150–174.
- Piqueras A, Iraeus J, Lorente AI, López-Valdés FJ, Juste-Lorente Ó, Maza-Frechín M, Pipkorn B. Kinematic assessment of subject personification of human body models (THUMS). In: *Proceedings of IRCOBI Conference 2018*.; 2018:191–206.
- Poulard D, Subit D, Donlon J-P, Lessley DJ, Kim T, Park G, Kent RW. The Contribution of Pre-impact Spine Posture on Human Body Model Response in Whole-body Side Impact. *Stapp Car Crash J*. 2014;58(November):385–422.
- Poulard D, Subit D, Nie B, Donlon JP, Kent RW. The Contribution of Pre-impact Posture on Restrained Occupant Finite Element Model Response in Frontal Impact. *Traffic Inj. Prev*. 2015;16(September 2016):87–95.



## **HBM PREDICTION OF SPINAL ROTATIONS**

---

### **4.1. Introduction**

Experimentally, the spinal kinematics of the occupant during a crash has been frequently analysed as the 2D trajectories of selected vertebrae both in the sagittal and transverse planes (López-Valdés et al. 2016; Piqueras et al. 2018; Poulard et al. 2015). However, trajectories only compound 3 of the 6 degrees-of-freedom (DOF) of a rigid body motion and the 3D rigid body rotation of vertebrae has rarely been addressed in experimental studies. Therefore, the validation of the capabilities of Anthropometric Test Devices (ATD) and Finite Element Human Body Models (HBM) to describe 3D spinal rotations is very limited.

Previous studies have shown that ATD have limited capabilities to predict the spinal kinematics compared with Post Mortem Human Surrogate (PMHS) sled tests even in frontal impacts (Lopez-Valdes et al. 2010a; Pipkorn, Lopez-Valdes, et al. 2016). When lateral bending and axial torsion of the spine are induced by the asymmetric load of the three-point seatbelt, these ATD limitations can lead not only to unrealistic spine and neck loads but also to errors in the estimation of chest deflections that are evaluated with respect to the spine (Shaw et al. 2013). Therefore, Hwang et al. (2020) suggested the use of Finite Element Human Body Models (HBM) for a detailed assessment of human response in lateral loading.

Paper B presents an analysis of the six degrees of freedom (6DOF) motion of the human spine during a crash event, using the PMHS test. This chapter aims to present the results of the analysis and compare them with those obtained from various versions of a HBM that have been modified to represent subject-specific characteristics through personalization techniques. Furthermore, the following sections seek to evaluate the influence of the three personalization techniques on the prediction of spinal bone rotations. Ultimately, the objective of this chapter is to address the second research question proposed in the introduction of this dissertation.

### **4.2. Methods**

#### **4.2.1. Rotation representation**

The proper method to represent the 3D rotation of rigid anatomical structures has been discussed extensively in the literature (Kinzel et al. 1972; Medendorp et al. 1998;

Woltring 1994). Some authors have pointed the disadvantages of the use of formulations such as Eulerian/Cardanic angles. This formulation can lead to results ambiguity caused by the angle sequence dependence (Anderst and Aucie 2017; Kettler et al. 2004; Medendorp et al. 1998; Woltring 1991). An additional difficulty associated to the Euler angles when there are 3D rotations is that successive rotations are calculated with respect to local coordinate systems (LCS) which are oriented based on the magnitude of the previous rotations. These LCS are different from subject to subject and, therefore, the comparison across different subjects is not straightforward. As an alternative, the Finite Helical Axis (FHA) describes an axis that characterizes the 3D motion of a rigid body between two instants of time as a rotation about and a translation along its unit vector. It approximates the definition of the instantaneous helical axis (Woltring 1994) and allows the report of the actual axis of rotation in a global coordinate system, which is comparable across different subjects (Kettler et al. 2004).

The methodology used to obtain the transformation matrix characterizing the motion of the bone referred to the defined GCS has been detailed in Chapter 2. Once the transformation matrix  $T_{B/G}(t)$  (Eq. (3)) is obtained with respect to the GCS, the FHA can be calculated according to the equations proposed by Spoor and Veldpaus, (1980).

$$T_G^B(t) = \begin{bmatrix} R_{3x3} & P_{3x1} \\ 0_{1x3} & 1 \end{bmatrix} = \begin{bmatrix} R_{11} & R_{12} & R_{13} & Px \\ R_{21} & R_{22} & R_{23} & Py \\ R_{31} & R_{32} & R_{33} & Pz \\ 0 & 0 & 0 & 1 \end{bmatrix}_G^B \quad (3)$$

If  $R$  is the rotation matrix within the calculated  $T_{B/G}(t)$  of one of the selected bones with elements  $R_{ij}$  ( $i, j = 1, 2, 3$ ), the angle rotated about the FHA ( $\varphi$ ) can be calculated from Eq. (4):

$$\sin(\varphi) = \frac{1}{2} \sqrt{(R_{21} - R_{12})^2 + (R_{32} - R_{23})^2 + (R_{13} - R_{31})^2} \quad (4)$$

The components of the unit vector  $\bar{u}$  are given by Eq. (5):

$$\bar{u} = \begin{bmatrix} ux \\ uy \\ uz \end{bmatrix} = \frac{1}{2 \sin(\varphi)} \begin{bmatrix} R_{32} - R_{23} \\ R_{13} - R_{31} \\ R_{21} - R_{12} \end{bmatrix} \quad (5)$$

When the rotation of the rigid body is aligned with a coordinate axis, the corresponding FHA component will be either 1 or -1 and the sign of the component indicates the direction of around the positive or the negative axis following the right-hand rule. For instance, if the head rotates around the Y-axis in flexion (towards the chest)

between two instants of time, the X, Y and Z components of the FHA would be equal to 0, -1 and 0 respectively, according to the SAE J211 convention.

The FHA is used to model the motion between two successive positions, and the closer these two positions are, the more accurate the motion description given by the FHA is. However, small values of rotation ( $\varphi$ ) can produce indeterminate results (Eq. 5) (Medendorp et al. 1998; Woltring 1994). To overcome this difficulty, the transformation matrix was calculated for positions (p) separated by a predefined  $\varphi$  interval rotation ( $T_{B(p)/B(p-\varphi^\circ)}$ ) (Eq. 6).

$$T_{B(p)/B(p-\varphi^\circ)} = [T_{B(p-\varphi^\circ)/G}]^{-1} \cdot T_{B(p)/G} \quad (6)$$

The components of the unit vector of the FHA every  $\varphi$  can be obtained directly from Eq. 6. The calculation of the FHA from the bone transformation matrix ( $T_{B/G}(t)$ ) was carried out using Matlab and the scripts used for this calculation are available on Appendix D.

#### 4.2.2. Quantitative assessment

Paper B was only focused on the PMHS's spinal bones rotations; thus, this chapter includes the results of the model versions detailed in section 1.1.2 "Personalization of the HBM". The assessment of the SAFER HBM v8 and the personalized models was conducted by comparing the predicted time-history rotations in the X, Y and Z axis of the selected anatomical landmarks with those of the three PMHS. The agreement between the predicted response and the sled test results was quantified using CORA v 4.0.4 (Gehre et al. 2009) similarly to the trajectories comparison the in previous chapter. According to the rating defined in ISO/TR 18571, CORA scores are classified into four categories: excellent (above 0.94), good (between 0.94 and 0.8), fair (between 0.8 and 0.58), and poor (below 0.58) correlation.

In contrast to the displacements analysed in the previous chapter, the FHA components for rotational analysis are limited to values between -1 and 1. Therefore, no weighting factor was applied to the total score in this case. The parameters used for the analysis, including corridor width and transition coefficients, were based on the study published by Poulard et al., (2015).

#### 4.2.3. Statistical analysis

This chapter aims to assess the influence of the three personalization techniques on the HBM, thus, similarly to the previous chapter, the baseline model and modified versions using different personalization techniques were compared. To evaluate the statistical significance of the differences between the groups, the Mann-Whitney non-parametric test for non-paired samples was utilized, as in the case of the trajectory

analysis. The simulation results were then sorted similarly to the trajectory results. The statistical significance level of the tests was set at  $p\text{-value} < 0.05$ . In addition, the effect size  $r$  was calculated and categorized into small, moderate, and large effects, corresponding to values of  $r$  equal to 0.10, 0.3, and 0.5, respectively (Cohen 1988). To determine whether the results are superior or inferior to the baseline, the difference between the medians of the compared groups were calculated ( $\Delta m$ ) and expressed as positive or negative sign.

### **4.3. Results**

#### **4.3.1. Summary of Paper B**

Paper B analysed the motion of the spine in the three PMHS during sled tests using the FHA to provide new experimental data for HBM and ATD benchmarking. The sled tests were conducted with two different restraint system versions and corresponded to a 30 nearside oblique impact at 35 km/h. The FHA method was used to describe the rotational behaviour of the bones, allowing inter-subject comparisons of the rotations with respect to the same coordinate system. The FHA components were calculated based on a pre-defined interval of  $\varphi = 8^\circ$  of rotation. The reason for using this interval is that the FHA is used to model the motion between two positions, and the closer these two positions are, the more accurate the motion description given by the FHA is. However, small values of the rotation angle  $\varphi$  can produce indeterminate results, as per previous studies. For the tests within this study diverse intervals were considered, and the  $8^\circ$  interval has been found to be long enough to avoid indeterminate results without losing information about variations attributed to physical events.

The analysis of the FHA components showed that the three PMHS exhibited flexion movement of the whole body and torsion to the right side of the occupant. The seatbelt acted as a fulcrum of the rotational movement of the bony landmarks, and the interaction of the PMHS with the retention system was noted by analysing the time in which the head and the upper spine initiated the rotation and the sudden changes of rotational direction of the three PMHS's head.

The study found that the rotational movement observed for the PMHS under nearside oblique impacts was comparable with the motion exhibited under full-frontal impacts (Lopez-Valdes et al. 2010b). When the trajectories and the rotations were analysed, some oscillations observed on the rotational analysis and attributed to physical events such as the belt interaction and the arm contact with the head had not been identified on the trajectory analysis. This means that some experimental events acquired with the 3D analysis can remain unnoticed by means of the 2D analysis (Piqueras et al. 2023).

The results of Paper B highlight the importance of analysing the 6 DOF motion of the spine during impact events and contribute to the understanding of the motion of the spine during impact events and can be used to develop injury criteria for oblique impacts. However, the study did not explore the capability of HBM to predict the spinal rotations.

#### **4.3.2. Bone Rotations Comparison**

In this section, the results obtained from PAPER B will be compared with the different versions of the SAFER HBM v8 to assess the influence of the diverse personalization techniques.

The FHA components of the selected landmarks on the simulations were computed using the same method as for the PMHS. The corresponding results for 3D rotations of the head, T1, T8 and L2 (head, T4, T7 and L1 for RSv2) for each simulation are shown in Figure 4-1 to Figure 4-4 represented by coloured lines.

As observed in the PMHS tests, in the simulations, all four landmarks exhibited X-positive rotation values until the rebound around 80-100 ms (depending on the spinal level), which indicates that the whole body tends to tilt towards the right side of the occupant.

For both RS versions, the FHA component corresponding to the Y-axis for the head and upper spine (T1 for RSV1 and T4 for RSv2) exhibited values near -1, implying a flexion movement towards the chest. The other bones rotated around an axis that cannot be considered aligned with any of the axes of the GCS for most of the duration of the tests, as in the PMHS tests. However, the instabilities observed in the PMHS's head rotational time-histories were not present in the simulations since the interaction between the head and the right arm did not occur in the simulations.

Similarly to the PMHS sled tests, the unit vector traces in the RSv1 began between 47-49 ms depending on the model version, while in the RSv2, it started between 59-63 ms. This delay was attributed to the earlier interaction of the seatbelt with the occupant because of the shoulder pretensioner involved in the RSv1. Nevertheless, this very first 8° rotation began, in general, earlier during the PMHS tests for all the bones observed. Furthermore, the sensitivity of T1 and T8 (T4 and T7 for RSv2) to the pretensioner exhibited for the PMHS tests at the beginning of the tests, was not noticeable in the HBM results.

Figure 4-1: Components of the unit vector of the FHA of the head calculated every 8° for the PMHS (black lines) and the SAFER HBM model (coloured lines).

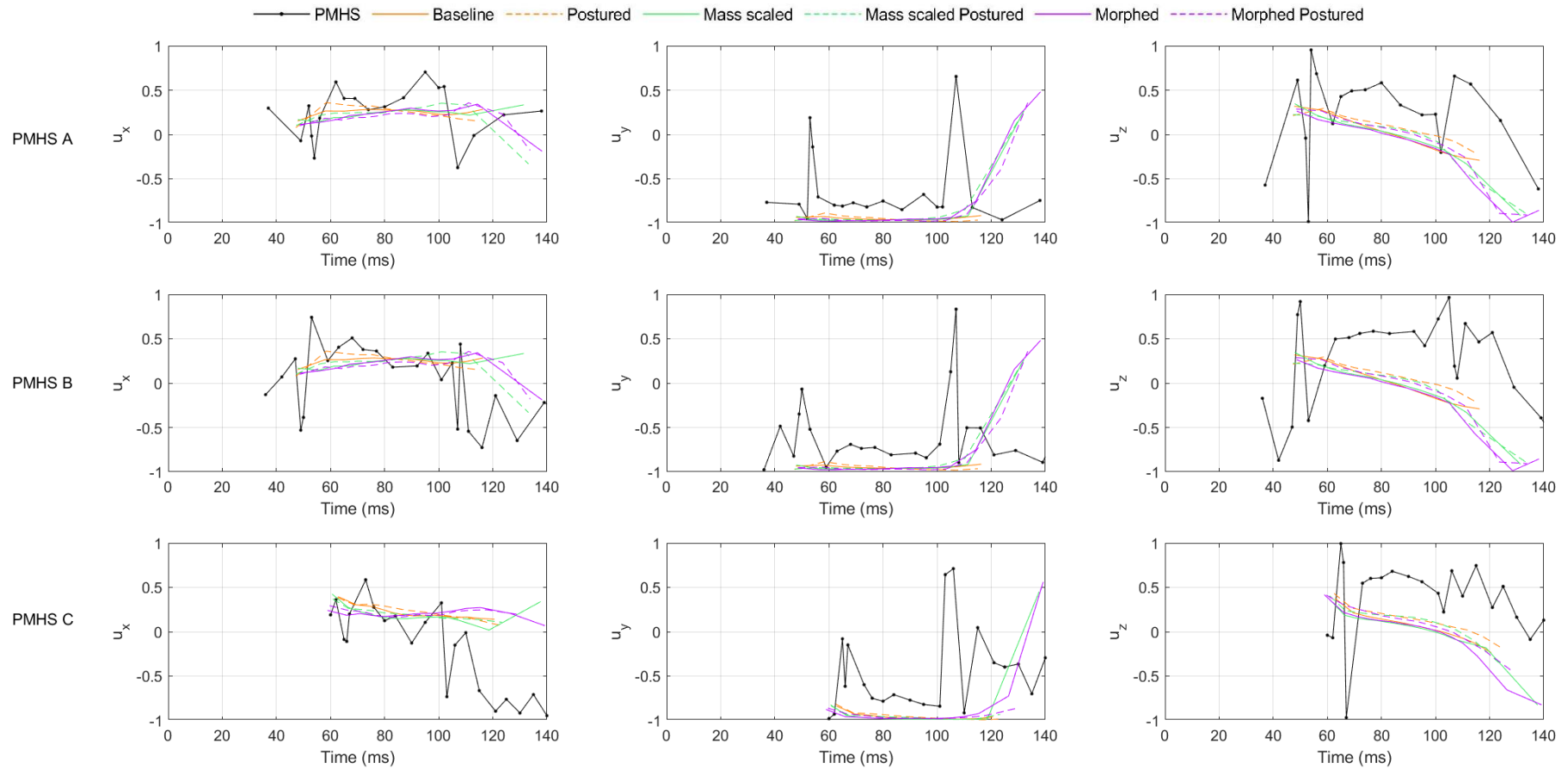


Figure 4-2: Components of the unit vector of the FHA of the T1 vertebra (T4 for PMHS C) calculated every 8° for the PMHS (black lines) and the SAFER HBM model (coloured lines).

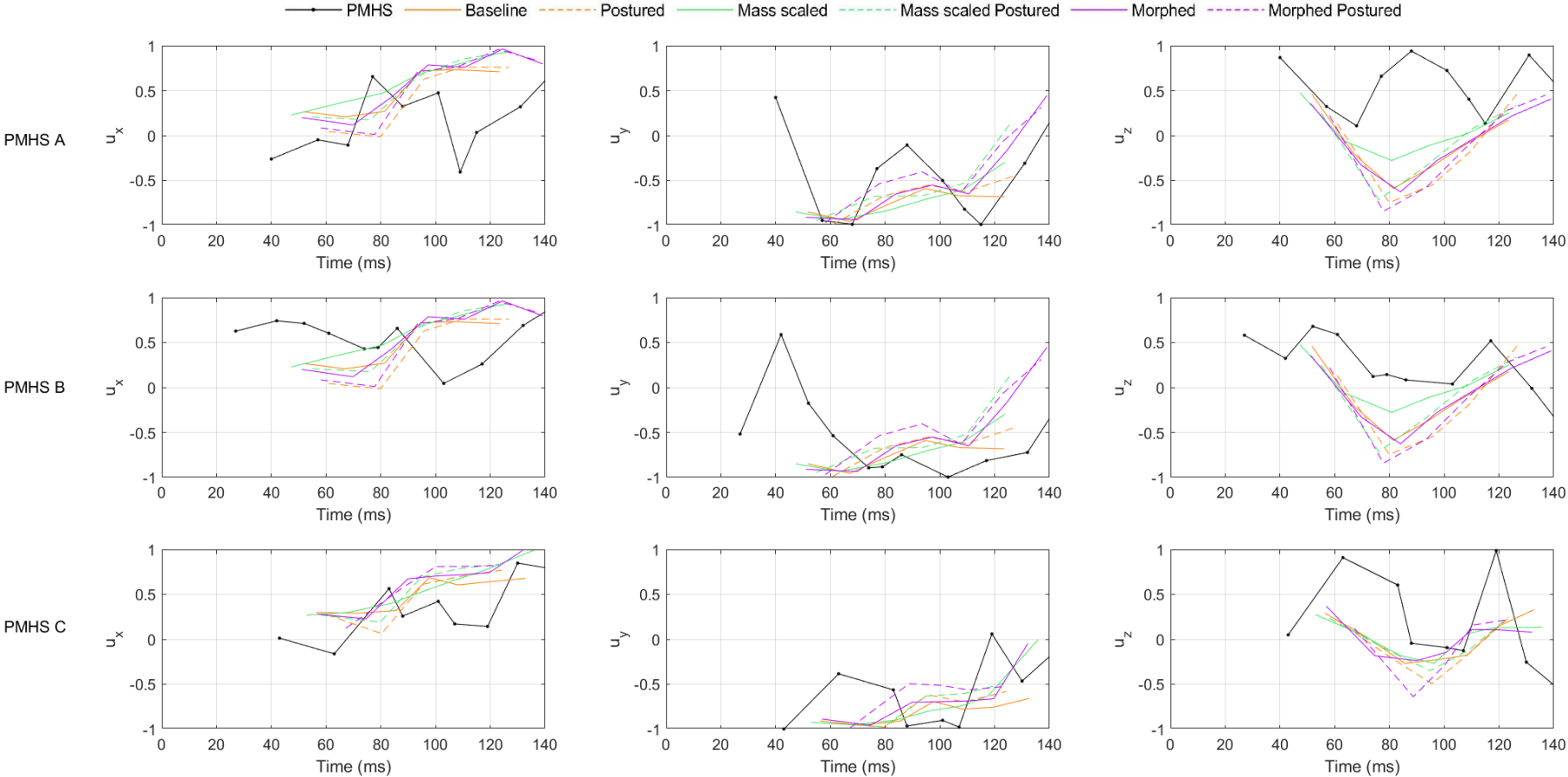


Figure 4-3: Components of the unit vector of the FHA of the T8 vertebra (T7 for PMHS C) calculated every 8° for the PMHS (black lines) and the SAFER HBM model (coloured lines).

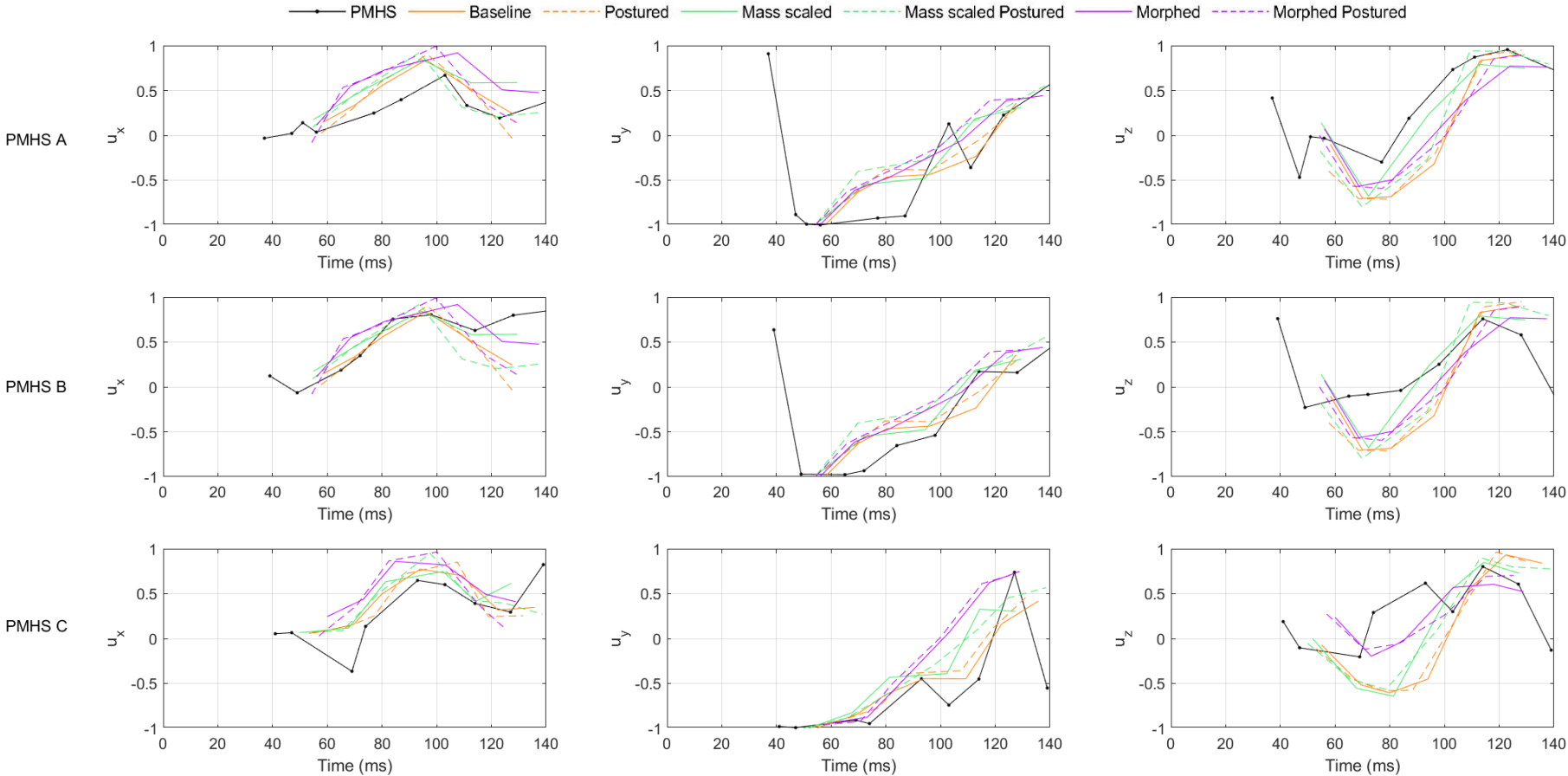
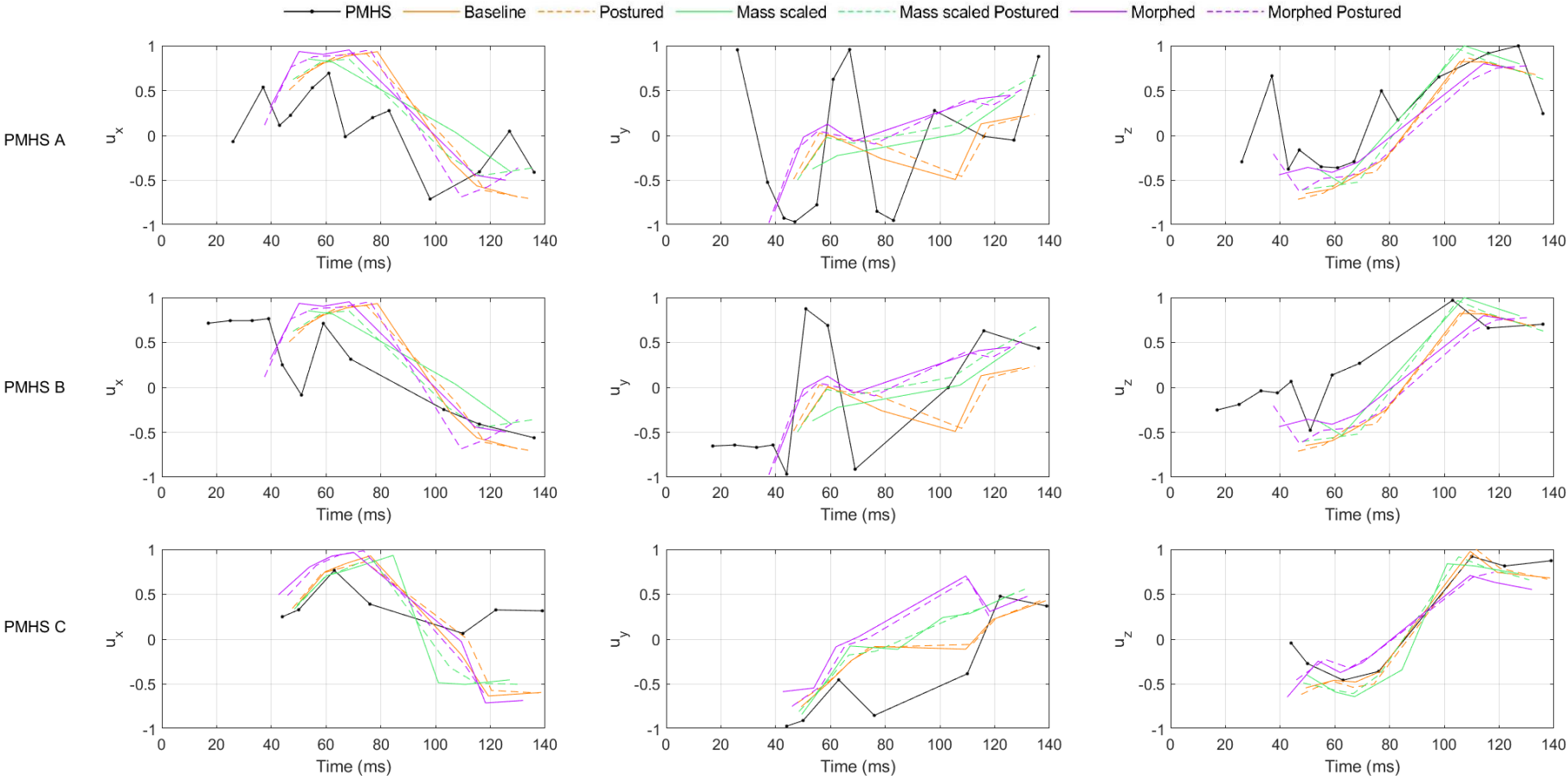




Figure 4-4: Components of the unit vector of the FHA of the L2 vertebra (L1 for PMHS C) calculated every 8° for the PMHS (black lines) and the SAFER HBM model (coloured lines).



### 4.3.3. CORA analysis

The results of the CORA analysis are shown in Table 4-1 and Table 4-2. The diverse personification techniques applied to the SAFER HBM v8 did not substantially modified the results, obtaining slight differences in the global correlation from the baseline model (SD=0.018 for RSv1 and SD=0.027 for RSv2). The HBM exhibited fair correlation ( $0.58 < \text{rating} \leq 0.8$ ) with the experimental tests in both RS versions. However, correlation values varied depending on the landmark and the axis regarded, such as for the displacements.

Table 4-1: CORA score for the selected landmarks rotation in RSv1. The highest values obtained for the selected landmarks have been highlighted.

MODEL VERSION	Baseline	Mass scaled	Postured	Mass scaled postured	Morphed	Morphed postured
<i>Total rating</i>	0.641	<b>0.674</b>	0.634	0.634	0.646	0.621
<i>Head</i>	0.62	0.591	<b>0.675</b>	0.618	0.592	0.596
X	0.695	0.653	0.755	0.688	0.658	0.628
Y	0.779	0.744	0.781	0.755	0.748	0.743
Z	0.387	0.375	0.488	0.41	0.371	0.417
<i>Upper spine</i>	0.613	<b>0.615</b>	0.515	0.55	0.582	0.512
X	0.568	0.545	0.4	0.517	0.509	0.432
Y	0.912	0.798	0.891	0.783	0.874	0.829
Z	0.36	0.502	0.254	0.349	0.363	0.274
<i>Middle Spine</i>	0.747	<b>0.856</b>	0.781	0.745	0.783	0.774
X	0.928	0.88	0.934	0.843	0.862	0.852
Y	0.773	0.881	0.849	0.768	0.82	0.815
Z	0.54	0.805	0.56	0.624	0.666	0.665
<i>Lower spine</i>	0.582	<b>0.634</b>	0.566	0.622	0.628	0.604
X	0.523	0.58	0.54	0.629	0.552	0.546
Y	0.552	0.527	0.501	0.526	0.617	0.65
Z	0.67	0.796	0.657	0.712	0.714	0.617

Table 4-2: CORA score for the selected landmarks rotation in RSv2. The highest values obtained for the selected landmarks have been highlighted.

MODEL VERSION	Baseline	Mass scaled	Postured	Mass scaled postured	Morphed	Morphed postured
<i>Total rating</i>	0.623	0.588	<b>0.647</b>	0.604	0.58	0.578
<i>Head</i>	0.517	0.54	<b>0.582</b>	0.559	0.527	0.552
X	0.581	0.589	0.589	0.594	0.586	0.588
Y	0.563	0.604	0.57	0.601	0.617	0.614
Z	0.409	0.427	0.588	0.483	0.337	0.455
<i>Upper spine</i>	0.548	<b>0.569</b>	0.53	0.531	0.504	0.504
X	0.511	0.529	0.464	0.449	0.426	0.429
Y	0.736	0.796	0.725	0.732	0.756	0.724
Z	0.398	0.382	0.4	0.412	0.331	0.36
<i>Middle Spine</i>	0.691	0.652	<b>0.697</b>	0.667	0.654	0.621
X	0.764	0.745	0.81	0.771	0.638	0.613
Y	0.954	0.784	0.911	0.796	0.612	0.611
Z	0.355	0.428	0.37	0.434	0.712	0.638
<i>Lower spine</i>	0.736	0.589	<b>0.781</b>	0.657	0.634	0.636
X	0.687	0.492	0.803	0.648	0.763	0.761
Y	0.547	0.35	0.586	0.384	0.285	0.277
Z	0.972	0.926	0.954	0.94	0.852	0.87

### *Analysis by spinal landmark*

#### *Head:*

For all three subjects (RSv1 and RSv2), the rotation of the HBM's head around the Z-axis was positive at the beginning of the simulation (see Figure 4-1). After 84 milliseconds in RSv1 and 102 milliseconds in RSv2, the head started to rotate in a negative Z-rotation, while the PMHS' head exhibited positive Z-rotation during this period leading to poor correlations in the analysis of this axis. The analysis of the head CORA scores revealed that the X and Y components of the FHA showed higher CORA values than the Z component in both RSv1 and RSv2, with the Z component showing poor correlation with the experimental tests (<0.58). Concerning to the X axis, a sudden fluctuation can be seen around 100 ms on the PMHS traces corresponding to the contact of the arm with the head during the experimental testing. This contact did not occur for any of the simulations and can influence the CORA score after that time.

***Upper spine:***

For the upper spinal level, all model versions in both RSv, the Y component of the FHA showed values ranging from 0.724 to 0.912 while the X and Z axis presented poor correlation. Looking at Figure 4-2 corresponding to the mentioned spinal level, it can be seen that the Z component showed the opposite sign of rotation, which is more evident for PMHS A.

***Middle spine:***

In the RSv1, the middle spinal level exhibited the highest correlation compared to the other landmarks. In this RSv the X and Y components showed a good correlation with the experiments being the mass scaled the version of the HBM that showed the highest values (0.856). The Z component score was improved from poor to good correlation by this personification technique, increasing the landmark CORA score in 0.109 from the baseline model. In RSv2, similar trends were found, with the postured model obtaining the highest CORA score for this spinal level. Additionally, all model versions had lower correlation values than those exhibited in RSv1.

***Lower spine:***

The Z component of this spinal level showed, in general, higher scores than the X and Y components, reaching excellent correlation values in RSv2 (0.852 to 0.972). However, in the RSv1 the Z component CORA scores did not differ substantially from the X and Y components. Under this loading conditions the correlation values for the lower spine demonstrated to be lower than those in RSv2, being the mass-scaled model the one with a higher correlation (0.634). Contradictorily to the RSv2, in RSv1 the postured model showed a poor correlation with the experimental testing worsening the CORA results compared to the baseline model.

***Analysis by FHA component***

When the three axes were analysed individually, in both RS versions the rotation around the Y-axis, in general, presented higher correlations with the PMHS results compared with the X and Z FHA components, except for the lower spine.

In RSv1, the average of the Y-axis results computing all bony landmarks presented a good correlation of 0.825, followed by the X-axis (0.721) and the Z-axis (0.484) components. In RSv2, also the rotation around the Y-axis obtained the greatest average CORA score (0.712), while X and Z-axis revealed poor correlation with the experimental results (0.566 and 0.569, respectively).

The poor CORA scores ( $\leq 0.58$ ) obtained when the X axis was analysed in RSv2, were due to differences in the curves' shape between the PMHS and simulations, while the signs of rotation (tilting to the right or left side of the occupant) were, in general, captured by the HBM simulations (see Figures 4-1 to 4-4). However, poor correlations regarding to the rotation around the Z-axis in the upper and medium spine for both RS were related to the sign of this FHA component. For instance, the HBM predicted a Z

negative rotation (left side of the occupant) while the PMHS' upper and medium spine rotation values were near zero (no rotation) or positive (right side of the occupant) as can be seen in Figures 4-2 and 4-3.

#### 4.3.4. Influence of the personalization techniques

##### *Statistical analysis*

In Table 4-3, the p-values resulting from the Mann-Whitney non-parametric test for each comparison between the baseline model and the modified models utilizing different personalization techniques are presented. The results indicate that none of the personalization techniques exhibited statistical significance on the prediction of spinal rotations.

Table 4-3: p-value for each comparison (bolded=statistical significance)

PERSONALIZATION TECHNIQUE	MASS SCALING	POSTURING	MORPHING
<i>Total rating</i>	0.21414	0.69913	0.21414
<i>Head</i>	0.56970	0.30952	0.68283
<i>Upper Spine</i>	0.93333	0.06494	0.10909
<i>Middle Spine</i>	0.68283	0.81818	0.80808
<i>Lower Spine</i>	0.93333	0.81818	0.93333

Table 4-4 displays the effect size  $r$  for each comparison including the sign of  $\Delta m$  between brackets only when it is negative (-) to facilitate the table visualization. The results show that only posturing had a large effect on the rotational prediction of the upper spine ( $r=-0.5937$ ), and morphing exhibited a moderate effect ( $r=-0.46659$ ). However, both of these personalization techniques resulted in negative influences (negative  $\Delta m$ ), indicating a decline in the prediction of spinal rotation. In contrast, only mass scaling and posturing displayed positive effects on the prediction for the upper spine and the head, respectively. Nonetheless, with the exception of the upper spine when posturing was used, the effect size  $r$  for all instances was determined to be moderate or small.

Table 4-4: Effect size  $r$  for each comparison (bold = large effect) including the sign of  $\Delta m$  between brackets only where negative values were obtained.

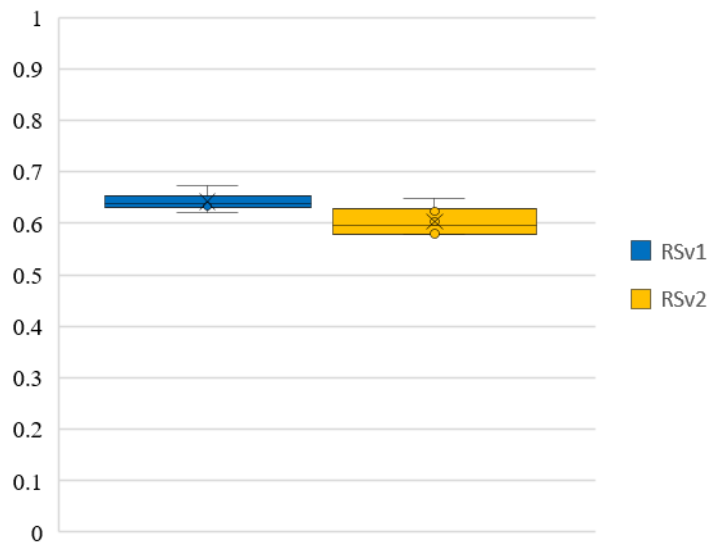
PERSONALIZATION TECHNIQUE	MASS SCALING	POSTURING	MORPHING
<i>Total rating</i>	(-) 0.34380	(-) 0.11577	(-) 0.36836
<i>Head</i>	(-) 0.17160	0.30046	(-) 0.12257
<i>Upper Spine</i>	0.02456	(-) <b>0.50937</b>	(-) 0.46659
<i>Middle Spine</i>	(-) 0.12257	0.06934	(-) 0.07354
<i>Lower Spine</i>	(-) 0.02456	(-) 0.06946	0.00000

## 4.4. Discussion

### *Comparison of HBM and PMHS Results*

According to the results, the rotation of the spinal landmarks was better predicted for RSv1 than for RSv2. This can be seen in Figure 4-5 that represents the distribution of the CORA total rating for each RSv. The range of values reveals a low variability (height of the box plots) which means that the CORA total rating was not sensitive to the model modifications as was found with the statistical analysis.

Figure 4-5: Values of CORA Total rating for both restraint system versions.



In general, the rotation about the Y-axis showed higher correlations than the other FHA components, followed by the X-axis, while the Z-axis demonstrated poor or fair correlations in both RS (see Table 4-1 and Table 4-2). Two exceptions were observed in the results. For RSv1, the X-component of the middle spine vertebra exhibited a higher correlation than the Y-component with the PMHS tests (Table 4-1), while in RSv2, the Z-component of the lower spine surpassed the Y-component correlation (Table 4-2).

During the analysis of the FHA components, a poor correlation was found regarding the rotation around the Z-axis in the upper and middle spine in relation to the sign of rotation. This was particularly evident for the upper spine of the PMHS A, which exhibited a positive rotation around the vertical axis (Z), while the HBM model versions predicted a negative rotation. PMHS A had the lowest mass (47 kg), followed by PMHS B and PMHS C (53 and 57 kg respectively). At this point, it is important to note that the mass scaled version (3) significantly improved the CORA rating and the rotation around the Z-axis were closer predicted by this model version. Regarding to the RSv2, the morphed model showed a similar behaviour improving the CORA score in Z axis for the middle spine. This can suggest that the rotation of the upper spine may be related to the mass distribution of the occupant.

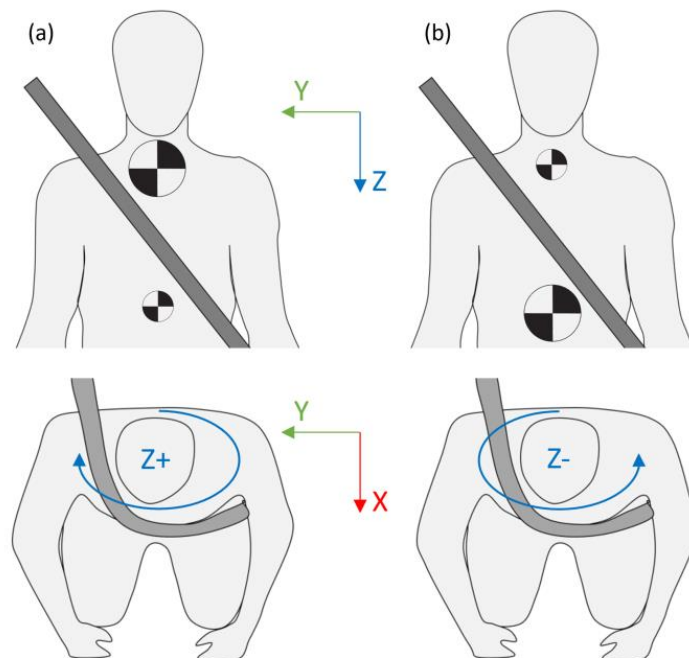
Figure 4-6 shows the body parts that were modified for the mass-scaled version and the position of the seatbelt in the view in which the occupant faced the impact (30° nearside oblique). In this position at  $t=0\text{ms}$ , those parts located over the seatbelt summed 4.28 kg, while the lower part between the two belt bands compound 10.13 kg. This means that the lower part of the body suffered a higher reduction of mass than the upper part.

Figure 4-6: Model body parts that which mass were adjusted for the mass-scaled version.



During an impact, the seatbelt acts as a fulcrum, and the inertial effect of the body parts that are over and under the shoulder belt can determine the sign of rotation around the vertical axis (see Figure 4-7).

Figure 4-7: Effect of the mass distribution on the rotation around the vertical axis.



Therefore, the improvement achieved in the Z rotation of the upper spine for the mass-scaled version can be attributed to the mass distribution variation from the baseline model to the mass scaled or morphed model (more similar to Figure 4-7a).

Although the mass scaled (3) and morphed version (5) improved the prediction of the Z-rotation, had a detrimental effect on the rotation around the Y-axis in both cases and this can be the reason why the statistical analysis did not reveal any significant impact on the prediction of rotation. According to the statistical analysis, the posturing had a large negative effect on the rotation of the upper spine (size  $r = -0.50937$ ). Posturing leads to a lower height of the torso increasing the volume of body parts under the shoulder belt portion (similar to the Figure 4-7b mass distribution) and leading to negative Z rotations. This effect can be seen in Figure 4-2 were the dashed lines representing the postured models reached values closer to -1.

Regarding to the middle spine, all model versions that involved mass scaling (versions 3 to 6) improved the rotation around the Z-axis (see Figure 4-3 and Table 4-1 and 4-2). However, as occurred at the upper spine, these modifications had a detrimental effect, in this case, on the prediction of the rotation around the X-axis.

According to the statistical analysis, none of the personification techniques revealed statistically significant impact on the prediction of rotation, which suggests that the combined use of personification techniques does not result in linear trends due to the different effects of each technique on each bone and axis.

One possible contributing factor to the discrepancies between HBM and PMHS results is the material properties of the intervertebral discs, ligaments, and spinal muscles in the HBM. Studies have demonstrated that modifications to these properties can have a significant impact on spinal kinetics and kinematics (Afewerki 2016; Chawla et al. 2005). Paas et al. (2015) and Wu et al. (2017) found that the HBM spine was stiffer than the PMHS spine in lateral bending, which could explain the signal stability of the simulations in comparison to the PMHS, as well as the lack of contact between the head and the arm during the simulations.

Previous validation studies have suggested the modification of the intervertebral gap, articulating processes, and ligament material properties, among others, to improve the biofidelity of the HBM. Although the SAFER HBM v8 incorporates some of these updates for the lumbar spine, they were not included for the cervical and thoracic spine. Therefore, there is still scope for enhancing the biofidelity of the HBM in future studies.



## References

- Afewerki H. Biofidelity Evaluation of Thoracolumbar Spine Model in THUMS. 2016.
- Anderst WJ, Aucie Y. Three-dimensional intervertebral range of motion in the cervical spine: Does the method of calculation matter? *Med. Eng. Phys.* 2017;41:109–115.
- Chawla A, Mukherjee S, Mohan D, Jain S. Validation of the Cervical Spine Model in Thums. *Proc. 19th Int. Tech. Conf. Enhanc. Saf. Veh.* 2005:1–11.
- Cohen J. The Significance of a Product Moment  $r$ . In: *Statistical Power Analysis for the Behavioral Sciences*. Second Edi. London: Academic Press; 1988:p 75-109.
- Gehre C, Gades H, Wernicke P. Objective rating of signals using test and simulation responses. In: *21st International Technical Conference on the Enhanced Safety of Vehicles ESV 2009.*; 2009:15–18.
- Hwang E, Hu J, Reed MP. Validating diverse human body models against side impact tests with post-mortem human subjects. *J. Biomech.* 2020;98:109444.
- Kettler A, Marin F, Sattelmayer G, Mohr M, Mannel H, Dürselen L, Claes L, Wilke HJ. Finite helical axes of motion are a useful tool to describe the three-dimensional in vitro kinematics of the intact, injured and stabilised spine. *Eur. Spine J.* 2004;13(6):553–559.
- Kinzel GL, Hall AS, Hillberry BM. Measurement of the total motion between two body segments- I. Analytical development. *J. Biomech.* 1972;5(1):93–105.
- López-Valdés FJ, Juste-Lorente Ó, Maza-Frechín M, Pipkorn B, Sunnevang C, Lorente A, Aso-Vizan A, Davidsson J. Analysis of occupant kinematics and dynamics in nearside oblique impacts. *Traffic Inj. Prev.* 2016;17(September):86–92.
- Lopez-Valdes FJ, Lau A, Lamp J, Riley P, Lessley DJ, Damon A, Kindig M, Kent R, Balasubramanian S, Seacrist T, Maltese MR, Arbogast KB, Higuchi K, Tanji H. Analysis of spinal motion and loads during frontal impacts. Comparison between PMHS and ATD. *Ann. Adv. Automot. Med. - 54th Annu. Sci. Conf.* 2010a:61–77.
- Lopez-Valdes FJ, Lau A, Lamp J, Riley P, Lessley DJ, Damon A, Kindig M, Kent R, Balasubramanian S, Seacrist T, Maltese MR, Arbogast KB, Higuchi K, Tanji H. Analysis of spinal motion and loads during frontal impacts. Comparison between PMHS and ATD. In: *Annals of Advances in Automotive Medicine - 54th Annual Scientific Conference.*; 2010b:61–77.
- Medendorp WP, Melis BJM, Gielen CCAM, Van Gisbergen JAM. Off-centric rotation axes in natural head movements: Implications for vestibular reafference and kinematic redundancy. *J. Neurophysiol.* 1998;79(4):2025–2039.
- Paas R, Davidsson J, Brodin K. Head Kinematics and Shoulder Biomechanics in Shoulder Impacts Similar to Pedestrian Crashes—A THUMS Study. *Traffic Inj. Prev.* 2015;16(5):498–506.
- Pipkorn B, Lopez-Valdes FJ, Juste-Lorente O, Maza M, Sunnevang C. Study of the kinematics of the THOR dummy in nearside oblique impacts. In: *Proceedings of IRCOBI Conference 2016.*; 2016:637–648.
- Piqueras A, Iraeus J, Lorente AI, López-Valdés FJ, Juste-Lorente Ó, Maza-Frechín M, Pipkorn B. Kinematic assessment of subject personification of human body models (THUMS). In: *Proceedings of IRCOBI Conference 2018.*; 2018:191–206.
- Piqueras A, Pipkorn B, Iraeus J, Lorente AI, Juste-Lorente Ó, Maza M, López-Valdés FJ. Analysis of the spinal 3D motion of postmortem human surrogates in nearside oblique impacts. *Traffic Inj. Prev.* 2023;24(1):69–74.
- Poulard D, Subit D, Nie B, Donlon JP, Kent RW. The Contribution of Pre-impact Posture on Restrained Occupant Finite Element Model Response in Frontal Impact. *Traffic Inj. Prev.*

2015;16(September 2016):87–95.

Shaw G, Lessley D, Ash J, Crandall J, Parent D. Response Comparison for the Hybrid III, THOR Mod Kit with SD-3 Shoulder, and PMHS in a Simulated Frontal Crash. In: 23rd ESV Conference.; 2013:1–19.

Spoor CW, Veldpaus FE. Rigid body motion calculated from spatial co-ordinates of markers. *J. Biomech.* 1980;13(4):391–393.

Woltring HJ. Representation and calculation of 3-D joint movement. *Hum. Mov. Sci.* 1991;10(5):603–616.

Woltring HJ. 3-D attitude representation of human joints: A standardization proposal. *J. Biomech.* 1994;27(12):1399–1414.

Wu T, Kim T, Bollapragada V, Poulard D, Chen H, Panzer MB, Forman JL, Crandall JR, Pipkorn B. Evaluation of biofidelity of THUMS pedestrian model under a whole-body impact conditions with a generic sedan buck. *Traffic Inj. Prev.* 2017;18(S1):S148–S154.

## **CHEST DEFLECTION ANALYSIS**

---

### **5.1. Introduction**

This chapter is focused on the prediction of chest deflection using HBM and aims to address the final two research questions: 3) Are HBMs capable of mimicking the occupant chest deformation? and 4) How does the chest deflection of the HBM respond to the different personalization techniques?

Oblique impacts have been found to cause larger chest deformations than frontal loading (Acosta et al. 2016). During a crash event, the interaction between the body and the vehicle environment leads to complex biomechanical responses. Chest deflection is a crucial factor in understanding the injury risk associated with oblique impacts (Davidsson et al. 2014; Kemper et al. 2011; Poplin et al. 2017).

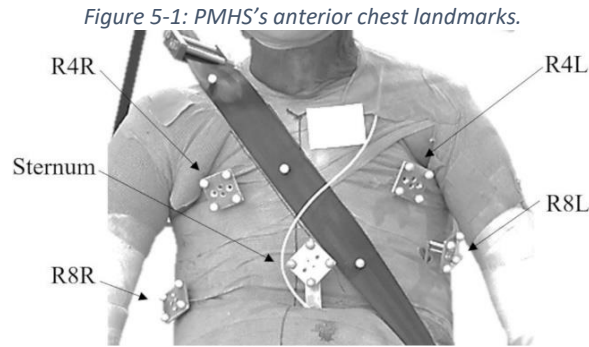
HBMs have been widely used to predict the biomechanical response of the human body to an impact. However, it remains unclear whether they are capable of accurately mimicking the occupant chest deformation.

Building upon the work published in Papers C and D, this chapter aims to investigate the ability of HBMs to accurately predict chest deflection during an oblique impact. In Paper C, the baseline HBM was compared with the morphed postured model, the most personalized HBM, and PMHS chest deflection data was analysed to assess the effectiveness of personalization techniques. Furthermore, Paper D used a single-point (Cmax) and a multi-point (PC Score) chest deformation indicators to quantify the effect of personalization techniques as well as the equivalence on the use of these two types of chest deflection measurement. In this chapter, the results of Paper C and Paper D will be summarized and the influence of the personification techniques on these predictors will be examined.

### **5.2. Methods**

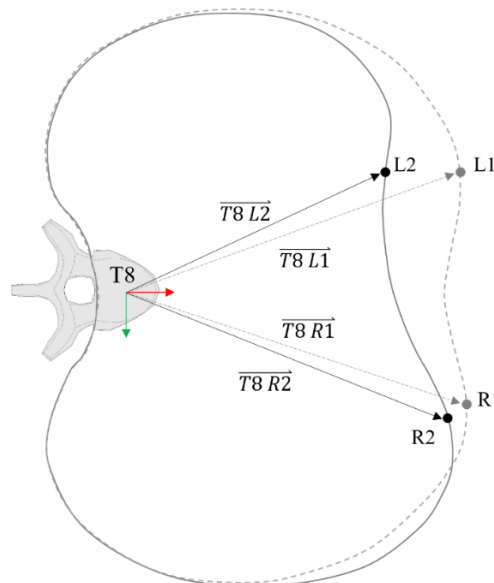
#### **5.2.1. Chest deflection measurement**

To compute the chest deflection of the PMHS presented in Paper C, Vicon marker kinematics for the sternum and the 4th and 8th ribs bilaterally (R4L, R4R, R8L and R8R) were used (see Figure 5-1). Bone motion was reconstructed based on the Vicon recordings using the method by Shaw et al. (2009) as detailed in Chapter 2.



The chest deflection was calculated by measuring the change in length of a vector joining the location of a marker cluster that was used to define a local coordinate system (LCS) rigidly attached to the rib points mentioned above and the origin of a LCS attached to the eighth thoracic vertebra (T8). Figure 5-2 illustrates the calculation process. L1 and R1 denote two points on the anterior ribcage on the left and right lateral aspects, respectively, while L2 and R2 represent the corresponding points on the ribcage after deformation. The chest deformation is then calculated as the difference between the lengths of the vectors joining the origin T8 and the marker clusters defining the rib points before and after deformation ( $|\overline{T8 L1}| - |\overline{T8 L2}|$ ).

Figure 5-2: Chest deflection representation along one rib level. The slashed line represents the undeformed rib profile.



A similar procedure was followed for calculating the chest deflection for the human body models. The relative distances of the marker clusters from the sternum along each rib, were used to select analogous points on the different versions of the SAFER HBM. Thus, the analysed chest landmark for each PMHS were compared to homologous points in the corresponding simulation.

### 5.2.2. Quantitative assessment

In order to accomplish a comprehensive sensitivity analysis of the influence of the personalization techniques on the HBM chest deflection prediction one or more defined and comparable parameters are required. Paper C reported the complex deformation patterns occurred on the chest and the asymmetry on the chest deformation, thus, the differential deformation must be considered in the sensitivity analysis. As suggested by Song et al. (2011) and following the steps of Davidsson et al. (2014) and (Mendoza-Vazquez et al. 2015), a model-specific criterion should be developed to be applied for the SAFER HBM v8, however, only three PMHS tests are available for the development.

To simplify the assessment of differences in the diverse HBM predictions and considering that the objective is to perform a sensitivity analysis rather than to predict a probability of injury, it was decided to use already-developed chest deformation indicators based on the displacement of the chest landmarks measured during the PMHS tests. To do so, it was proposed to use Cmax and DcTHOR as chest deflection indicators for the HBM chest deflection predictors as described by Mendoza-Vazquez et al., (2015). DcTHOR considers differential deformations, however, similarly to the Dc injury criterion (Song et al., 2011), its formulation contains conditional thresholds for these differential deformations proposed by Davidsson et al., (2014) for a THOR ATD. Values of less than 20mm are considered as 0 differential deformations, leading to discontinuous functions which are not suitable for the sensitivity analysis, and, thus, DcTHOR was discarded for the analysis. Therefore, instead of the DcTHOR it was decided to use the PC Score proposed by Poplin et al. (2017), which considers combined deformation (maximum and differential) and is, up to the date of writing this dissertation, the only one which results in a continuous function for the entire domain of deformations.

Consequently, in order to accomplish the sensitivity analysis of the influence of the personalization techniques on the HBM chest deflection prediction, two main predictors based on chest deformation measurements were used: Cmax and PC Score. Cmax calculates the maximum posterior resultant displacement of any studied rib point of the chest, irrespective of the displacement of the rest of the rib points. For instance, as shown in Figure 5-2, Cmax will calculate the deflection of the left point (L), regardless of the right point (R) deflection. PC Score calculates the sum of the maximum deformation measured at the upper and lower chest (UPtot and LOWtot) and the maximum differential deformation of the upper and lower rib measurement points (UPdif and LOWdif) (Poplin et al. 2017). Referring to the example, PC Score will calculate not only the maximum deformation that occurred at L and R points, but also the differential deformation between these two points for the upper and lower chest. Using these chest deformation indicators together enables the analysis of differences on HBM versions' response.

In utilizing PC Score on HBMs, it is crucial to note that this indicator was originally developed for ATDs. However, its application in this study serves the specific purpose of facilitating a consistent comparison between different HBM model versions considering

asymmetrical deformations, allowing to assess the sensitivity of these models to various personalization techniques.

### 5.2.3. Statistical analysis

In accordance with the previous chapters, the statistical analysis of the current study aimed to evaluate the sensitivity of the results to the personalization techniques proposed in this work. To this end, the Mann-Whitney non-parametric test for non-paired samples was utilized, as in the case of the trajectory and rotational analyses, to evaluate the statistical significance of the differences between the groups. In order to determine the statistical significance level of the tests, a p-value threshold of  $<0.05$  was selected. Moreover, the effect size  $r$  was calculated, in accordance with Cohen (1988), and classified into small, moderate, and large effects, corresponding to values of  $r$  equal to 0.10, 0.3, and 0.5, respectively. To determine whether the results are superior or inferior to the baseline, the difference between the medians of the compared groups were calculated ( $\Delta m$ ) and expressed as positive or negative sign.

## 5.3. Results

### 5.3.1. Summary of Paper C

This section presents the findings of the analysis conducted in Paper C, which examined the 3D chest deflection of the three PMHS sled tests described in Chapter 2, following the procedure outlined in section 5.2.1. The objective was to evaluate the 3D in situ chest deformation under nearside oblique impacts and the ability of the baseline SAFER HBM v8 to predict the chest deformation. Additionally, the morphed postured model, the most personalized version, was also compared to assess whether this model modification could improve the prediction of the chest deformation.

The experiments showed that the response of the chest deflection was sensitive to the restraint system used. For occupants A and B (RSv1), the sternum exhibited compression from the beginning of the test, while for occupant C (RSv2), all five chest locations exhibited expansion at the beginning of the test. For the latter subject, after 45 ms, rib landmarks continued moving forward while the sternum was being compressed. The forward movement of the sternum at the beginning of this last test was not predicted by any of the HBM versions.

For all three subjects, the lower right chest (R8R) consistently exhibited positive deformation (forward motion), in line with previous literature (Rouhana et al. 2003; Shaw et al. 2009), but reaching higher values, which can be attributed to the oblique impact configuration. Both baseline and morphed postured versions, correctly predicted the forward motion of the lower right chest, however, the deflection values were

underpredicted. The potential causes of this underprediction were extensively discussed in Paper C.

Regarding the lateral displacement of the five chest landmarks, in the upper chest, R4L moved to the right, while R4R moved to the left, indicating that both lateral aspects of the upper chest displaced towards the medial ribcage, thereby increasing the local deformation of the upper chest. However, none of the HBM version predicted the leftward displacement of R4R.

Both model versions underpredicted the ribcage deformation. As seen in previous chapters, the use of the personalization techniques in combination does not necessarily lead to superimposed effects. Therefore, the results of all model versions need to be analysed separately to assess the effect of the personalization techniques on the chest injury prediction.

### 5.3.2. Summary of Paper D

Continuing with the work of Paper C, the aim of Paper D was to evaluate the sensitivity of the HBM of the diverse personalization techniques described in Chapter 2. To achieve this, the values of AIS3+ calculated based on chest deformation parameters Cmax and PC Score were evaluated.

The results in Paper D revealed that the mass scaling and morphing of the HBM significantly influenced the prediction of chest deformation while the posturing did not show statistically significant differences in the results, regardless of the injury metric used. However, also indicated that the postured version showed the highest values of the calculated parameters and resulted in predictions that more closely resembled the observed injury outcome in the reference PMHS tests, which included 15, 5, and 10 fractured ribs, respectively.

However, the mass scaled postured (4) and morphed postured (6) versions did not improved the results of the corresponding non-postured models (3 and 5 respectively). This finding suggests that the use of personalization techniques in combination does not necessarily lead to superimposed effects for the chest deflection behaviour.

Moreover, the models in which the posturing was performed successfully predicted that the lower right chest landmark (R8R) exhibited the maximum deformation among the rib locations (without considering the sternum), consistent with the PMHS tests.

At this point, it was proposed to additionally compare the differences in the use of both indicators. To ensure a consistent comparison of the results obtained from both injury criteria, the probability of sustaining an AIS3+ injury to the chest (AAAM 2015) was calculated according to the injury risk functions developed by Poplin et al. (2017). An additional finding of this study was that the PC Score-based prediction exhibited higher values of  $p(\text{AIS3+})$  than the Cmax-based prediction for the oblique loading conditions and personalization techniques analysed, contrary to previous literature

focused solely on frontal impacts (Lopez-Valdes et al. 2018; Poplin et al. 2017) in which both metrics predicted similar values of p(AIS3+).

The results were compared also with a previous study of the THOR ATD injury prediction capability based on Cmax, which used the same PMHS sled as reference (Pipkorn, Lopez-Valdes, et al. 2016). The calculations based on the ATD thorax deformations were lower than the prediction obtained with the baseline HBM using the same deformation metric (Cmax), suggesting that the use of HBM may be more suitable for omnidirectional impacts.

### 5.3.3. Analysis of the influence of the personification techniques

In Table 5-5, the p-values from the Mann-Whitney non-parametric test for each comparison between the baseline model and the modified models utilizing different personalization techniques are presented. This analysis revealed that the mass scaling and morphing of the HBM significantly influenced the prediction of chest deformation while the posturing did not show statistically significant differences in the results, consistently with the results of Paper D.

Table 5-5: p-value for each comparison (bolded=statistical significance).

PERSONALIZATION TECHNIQUE	MASS SCALING	POSTURING	MORPHING
<i>Cmax</i>	<b>0.013</b>	0.545	<b>0.002</b>
<i>PC Score</i>	<b>0.0002</b>	0.730	<b>0,004</b>

In addition to the p-value calculation conducted in Paper D, which focused solely on assessing the statistical significance of incorporating different personalization techniques, the present chapter aims to evaluate the impact of these personalization techniques on the results of Cmax and PC Score by determining the effect size  $r$ .

Table 5-6 displays the effect size  $r$  values, discretized by injury metric and personalization technique, where a large effect size is defined as greater than 0.5.

Table 5-6: Effect size  $r$  of Cmax and PC Score discretized by personalization technique and injury metric (large effect >0.5) including the sign of  $\Delta m$  between brackets only where negative values were obtained.

PERSONALIZATION TECHNIQUE	MASS SCALING	POSTURING	MORPHING
<i>Cmax</i>	(-) <b>0.56</b>	(-) 0.14	(-) <b>0.67</b>
<i>PC Score</i>	(-) <b>0.76</b>	(-) 0.08	(-) <b>0.63</b>

The results in Table 5-6 indicate that all three personalization techniques produced a negative influence on the Cmax and PC Score, as evidenced by the negative sign of  $\Delta m$ . Specifically, the mass scaling and morphing techniques had the largest negative effect size values, with effect sizes of -0.56 and -0.67 for Cmax, and -0.76 and -0.63 for PC Score, respectively. The posturing technique also had a negative effect size for both injury metrics, although with a smaller magnitude (-0.14 for Cmax and -0.08 for PC Score).



As depicted in Table 5-6, the personalization techniques that showed a large effect size were consistent with those that exhibited statistical significance. However, none of the three personalization techniques improved the prediction of the baseline model, as indicated by their negative sign of  $\Delta m$ .

#### **5.4. Discussion**

The results included in this chapter indicate that the personalization techniques evaluated in the study did not show statistically significant improvement on the injury prediction capability of the baseline model. This is supported by the negative effect sizes obtained for all three personalization techniques (mass scaling, posturing, and morphing) for both injury metrics (Cmax and PC Score). The effect sizes were calculated using the size  $r$  value, which measures the magnitude of the difference between the means of two groups relative to the standard deviation of the data. These findings are consistent with the statistical significance results presented in Paper D, which showed that none of the personalization techniques had a significant effect on the p(AIS3+) calculation based on Cmax and PC Score as chest deformation indicators.

It is important to note that the negative effect sizes do not necessarily imply that the personalization techniques had a detrimental effect on the injury prediction capability of the baseline model. Since the postured model showed an improvement in predicting chest deflection compared to the baseline model, instead, the results suggest that the incorporation of these personalization techniques in combination does not necessarily lead to linear trends as occurred with the spinal rotation prediction. Further research may be necessary to explore alternative personalization techniques that may enhance the injury prediction capability of the baseline model.

## References

- AAAM. The abbreviated injury scale 2008, update 2015. Des Plaines, IL; 2015.
- Acosta SM, Ash JH, Lessley DJ, Shaw CG, Heltzel SB, Crandall JR. Comparison of whole body response in oblique and full frontal sled tests. 2016 IRCOBI Conf. Proc. - Int. Res. Council. Biomech. Inj. 2016;(Table I):740–754.
- Davidsson J, Carroll J, Hynd D, Lecuyer E, Song E, Trosseille X, Eggers A, Sunnevang C, Praxl N, Martinez L, Lemmen P, Been B. Development of injury risk functions for use with the THORAX Demonstrator; an updated THOR. In: Proceedings of IRCOBI Conference 2014.; 2014:359–376.
- Kemper AR, Kennedy EA, McNally C, Manoogian SJ, Stitzel JD, Duma SM. Reducing chest injuries in automobile collisions: Rib fracture timing and implications for thoracic injury criteria. *Ann. Biomed. Eng.* 2011;39(8):2141–2151.
- Lopez-Valdes FJ, Mroz K, Eggers A, Pipkorn B, Muehlbauer J, Schick S, Peldschus S. Chest injuries of elderly postmortem human surrogates (PMHSs) under seat belt and airbag loading in frontal sled impacts: Comparison to matching THOR tests. *Traffic Inj. Prev.* 2018;19(sup2):S55–S63.
- Mendoza-Vazquez, M., Davidsson, J., & Brodin, K. (2015). Construction and evaluation of thoracic injury risk curves for a finite element human body model in frontal car crashes. *Accident Analysis and Prevention*, 85, 73–82.
- Pipkorn B, Lopez-Valdes FJ, Juste-Lorente O, Maza M, Sunnevang C. Study of the kinematics of the THOR dummy in nearside oblique impacts. In: Proceedings of IRCOBI Conference 2016.; 2016:637–648.
- Poplin GS, McMurry TL, Forman JL, Ash J, Parent DP, Craig MJ, Song E, Kent R, Shaw G, Crandall J. Development of thoracic injury risk functions for the THOR ATD. *Accid. Anal. Prev.* 2017;106(December 2015):122–130.
- Rouhana SW, Kankanala S V., Prasad P, Rupp JD, Jeffreys TA, Schneider LW. Biomechanics of 4-Point Seat Belt Systems in Frontal Impacts. *SAE Tech. Pap.* 2003;47:367–399.
- Shaw G, Parent D, Purtsezov S, Lessley D, Crandall J, Kent R, Guillemot H, Ridella S a, Takhounts E, Martin P. Impact response of restrained PMHS in frontal sled tests: skeletal deformation patterns under seat belt loading. *Stapp Car Crash J.* 2009;53(November):1–48.

## **DISCUSSION AND CONCLUSIONS**

---

### **6.1. Discussion**

The present dissertation aimed to investigate the biomechanical response of the human body during oblique automotive impact events, with a particular focus on the thorax and spine. Through a combination of experimental tests and computational simulations, a comprehensive analysis of the kinematics associated with different oblique impact scenarios was conducted. It is worth noting that oblique impacts have been shown to produce larger chest deformations than frontal impacts, making them a critical aspect to consider in terms of injury prevention and safety standards. The results of this study provide insights into the complex interplay between the occupant's anatomy, impact loading conditions and injury outcomes.

In this discussion chapter, the main findings of the study and their implications will be examined. Specifically, the key factors that influence the biomechanical response of the thorax and spine will be discussed. Additionally, the limitations of the current study will be presented, and future research directions aimed at further improving our understanding of the biomechanics of oblique automotive impacts will be suggested.

#### **6.1.1. Relationship between the spinal motion and the chest deflection**

The current study aimed to examine the complex interplay between the spinal bone trajectories and rotations, and the chest deflection results during automotive impact events. Chest deflection has been measured referred to the eight thoracic vertebrae, thus, the kinematics of the spine can influence the chest deflection measurements and, therefore, the ability of the HBM to effectively estimate chest deformation. Consequently, the purpose of this section is to investigate the relationship between spinal motion and chest deformation prediction, as well as to explore the potential influence of the diverse personalization techniques on this relationship.

Figure 6-1 and Figure 6-2 presents the range of C<sub>max</sub> and PC Score values respectively used as indicators of chest deflection prediction for each model version. The postured model (2) achieved the highest average values (×) for both parameters, indicating better alignment with experimental data.

Regarding to the C<sub>max</sub> average values, in addition to the postured version, the mass scaled version (3) can improve the results with higher values compared with the baseline. However, the high variability of the results in this model version (box height) reached

values under the baseline prediction. All other model versions showed lower Cmax values indicating a worse chest deflection prediction compared to the baseline prediction.

Figure 6-1: Values of Cmax for the different model versions including both restraint system versions (x=average value, circle = median value).

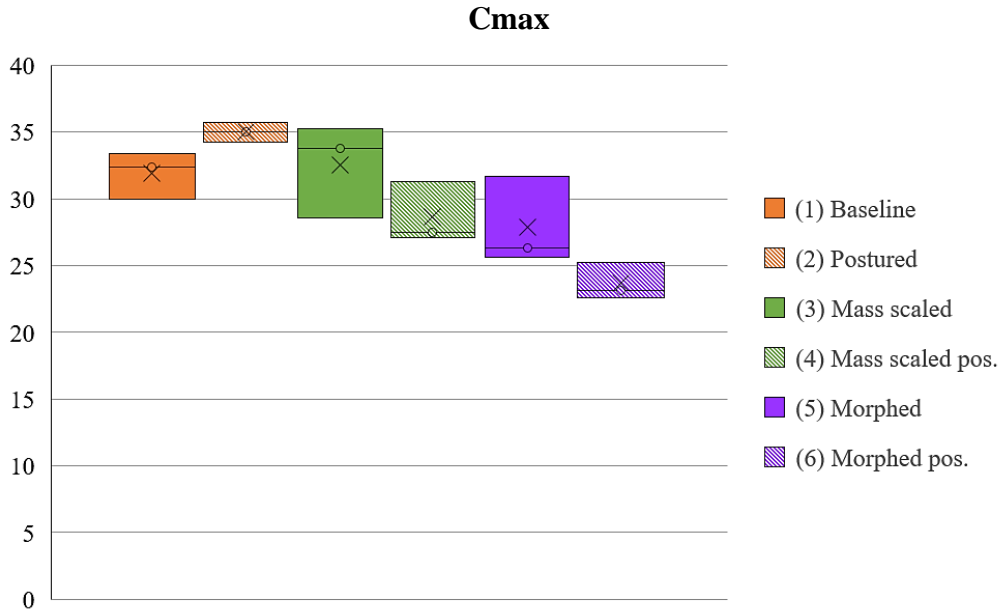
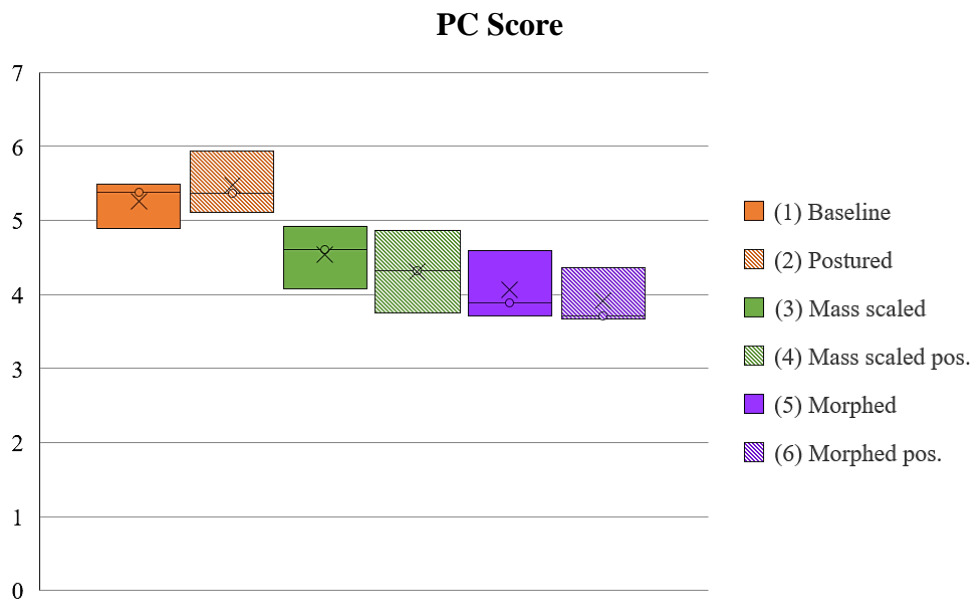


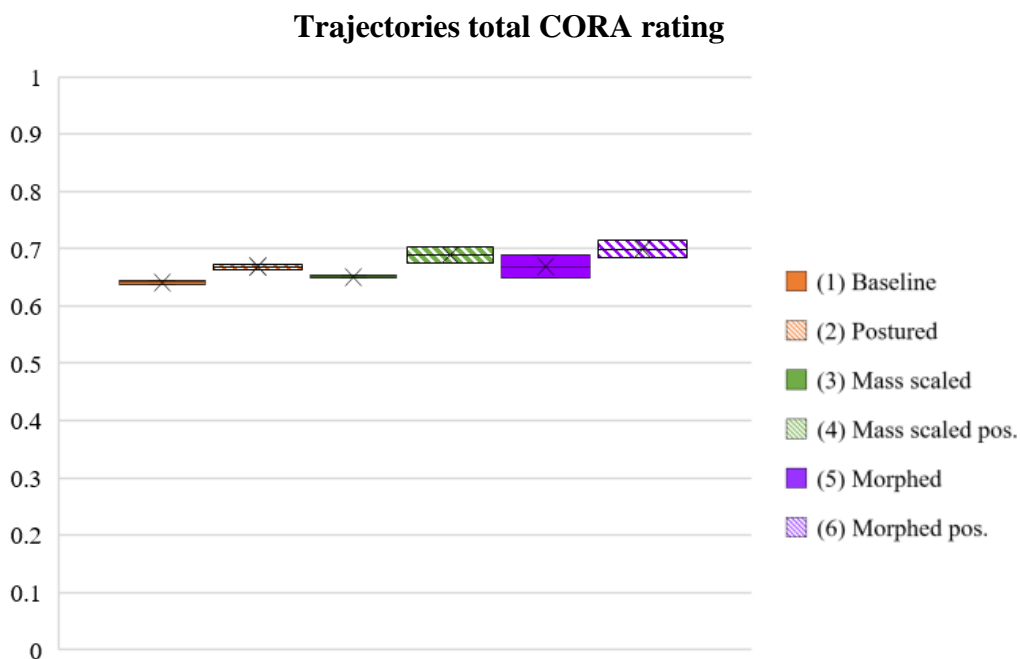
Figure 6-2 shows that except for the postured version (2), all other versions obtained lower values of PC Score than the baseline. The morphed postured model which involved all the personalization techniques, showed the lowest values of PC Score as occurred with the Cmax values and consistently with the findings described in Paper C, in which peak deflection for the five anterior chest landmarks were reported, and Paper D.

Figure 6-2: Values of PC Score for the different model versions including both restraint system versions (x=average value, circle = median value).



Regarding trajectories, the results reported in Chapter 3 demonstrated that personalization techniques improved the prediction of the spine kinematics, being the morphed postured model (version 6) the one that obtained the highest CORA values (see Figure 6-3). However, despite the improvements in trajectory rating achieved by the model versions 3 to 6, it was observed that these enhancements did not consistently translate into improved predictions of thoracic deformation, independently on the parameter used as reference, peak deflection (Paper C), Cmax or PC Score.

Figure 6-3: Values of trajectories CORA Total rating for the different model versions including both restraint system versions (x=average value, circle = median value).

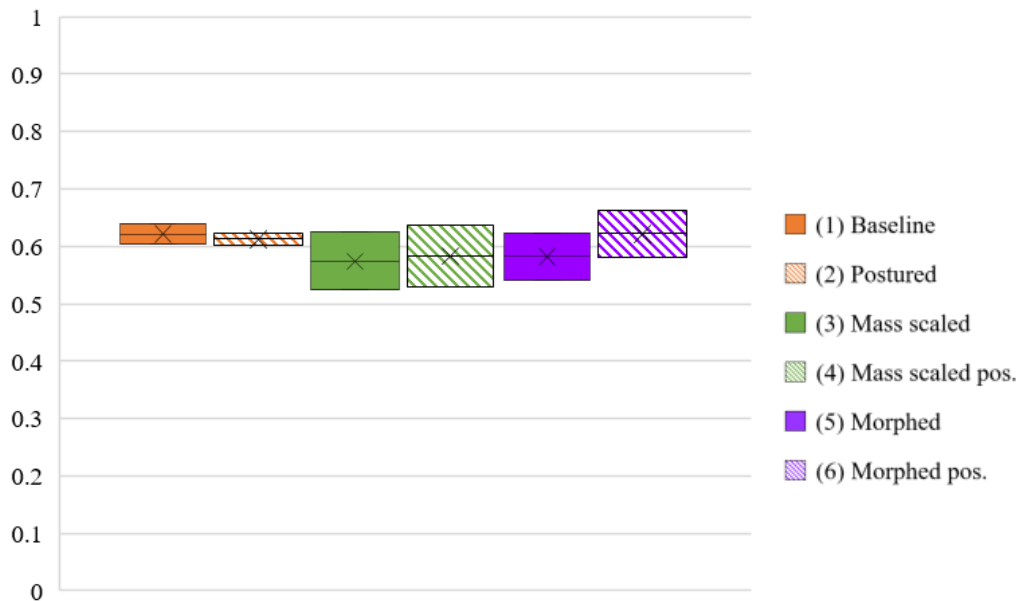


This can suggest that the improvement on the global spine trajectories prediction do not necessarily lead to improvements in chest deformation prediction.

However, the chest deflection was measured using the middle spine as reference, thus the response of the middle spine can influence the chest deflection prediction. Figure 6-4 shows the CORA rating of the middle spine for all model versions. According to the median and average values, only the morphed postured model version showed a slightly improvement on the landmark biofidelity compared to the baseline model. Contrary to the total rating tendency, the statistical analysis revealed that none of the personalization techniques significantly varied the prediction of the middle spine trajectories. This suggest that the variations on the chest deflection predictions were not directly related with the middle spine displacements.

Figure 6-4: Values of trajectories CORA rating at middle spine for the different model versions including both restraint system versions ( $x$ =average value, circle = median value).

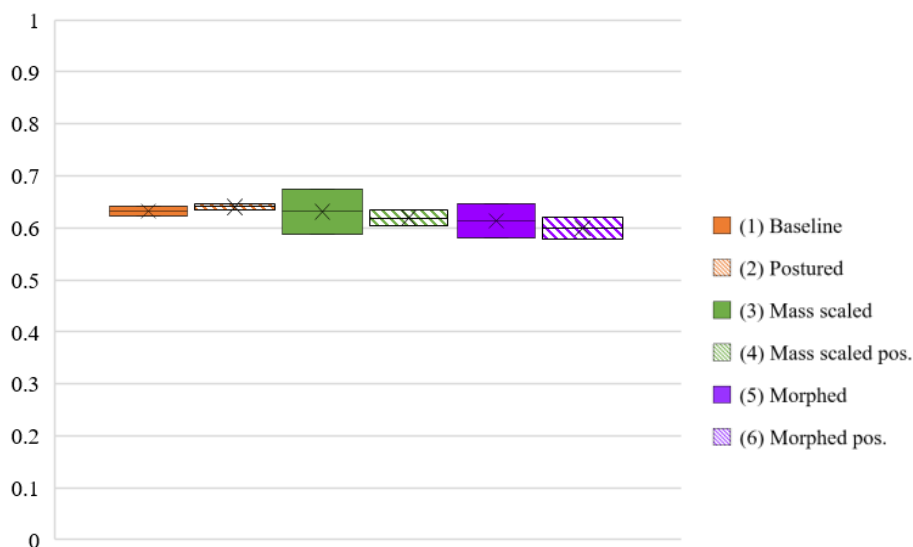
### Middle spine trajectories CORA rating



In terms of rotations, the statistical analysis conducted in Chapter 4 revealed that none of the personalization techniques significantly influenced the rotations prediction. However, despite the low variations on the median values of the model versions prediction (0.632, 0.641, 0.631, 0.619, 0.613 and 0.6 for versions 1 to 6 respectively), Figure 6-5 shows similar patterns in the rotations total CORA rating than those obtained in Figure 6-1 and Figure 6-2 for the Cmax and PC Score chest deformation indicators where only the postured and mass scaled model versions improved the injury prediction.

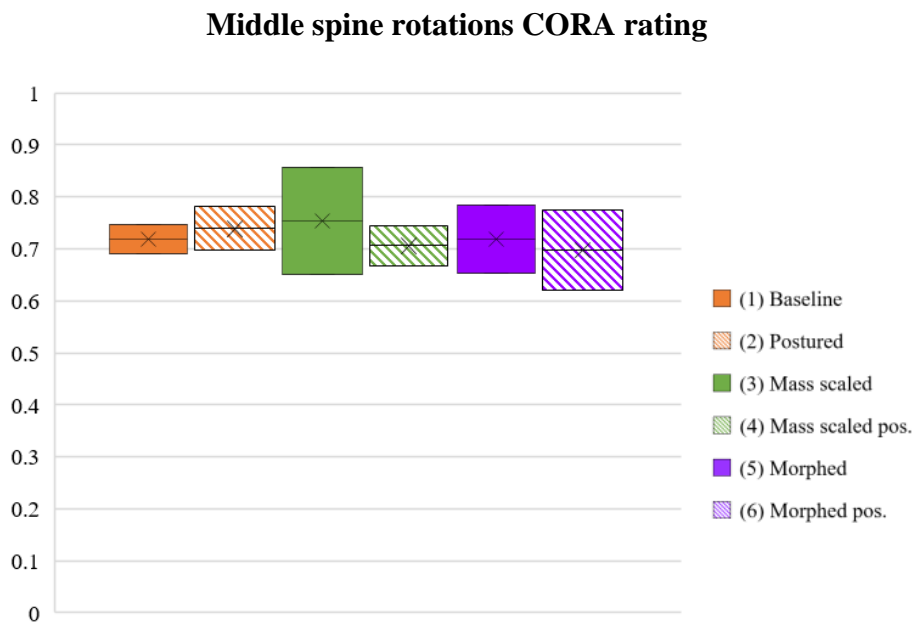
Figure 6-5: Values of rotations CORA Total rating for the different model versions including both restraint system versions ( $x$ =average value, circle = median value).

### Rotations total CORA rating



Regarding to the predictions of rotation at the middle spine (see Figure 6-6), the results showed that the mass scaled version (3) can improve the prediction of the bone rotation as occurred for RSv1, where the CORA rating increased from 0.747 (baseline) to 0.856 (mass scaled). However, for the RSv2, the improvement of this model version on the rotation around the Z-axis (+0.073) did not compensate the detrimental effect on the other two axis (-0.019 on X-axis and -0.170 on Y-axis) obtaining lower CORA score than the baseline model at the upper spinal level.

Figure 6-6: Values of rotations CORA rating at middle spine for the different model versions including both restraint system versions ( $x$ =average value, circle = median value).



Due to the similarities on the model versions median and average values and the variation on the range of results, the statistical analysis did not reveal significant differences on the use of any of the personalization techniques for the middle spine.

The results suggest similarities on the improvement of the spinal rotations prediction and the prediction of the chest deformation. However, the improvements on the spinal rotations observed for the total CORA score or the middle spine CORA score, were not sufficient to explain the variation on the results of chest deflection prediction. Thus, this means that the chest deflection does not depend solely on the spine kinematics and was influenced by other factors.

### 6.1.2. Reasons of the discrepancies between chest deflection in the HBM and PMHS

Results showed in Chapter 5 revealed that the chest deformation prediction based on PC Score obtained higher values compared with the Cmax based calculation. However, all model versions underpredicted the chest deformation. In Paper C some factors that could contribute to the differences between the chest deflection observed for

the PMHS and the predicted by the HBM were discussed. This section expands that discussion adding other explored factors.

### *Geometrical factors*

Among the factors influencing the dissimilarities in results, one significant aspect is the internal geometry of the model. While the anthropometry, mass and posture of the HBM were modified to mimic the external shape of the PMHSs, certain aspects such as rib angle with respect to the spine and the distribution of cortical and trabecular areas remained unchanged. These unmodified internal geometrical factors may have implications in the deviations observed in the results.

Some authors pointed out that the rib angle measured in the sagittal plane increases with age, becoming more perpendicular to the spine, due to kyphosis of the thoracic spine or pulmonary pathologies (Kent et al., 2005; and Gayzik et al., 2008 and Shi et al., 2014). This increment has been associated with a change in the ribcage depth and width introducing changes on its structural behaviour resulting in differences on the injury outcome. However, the angle referred to the corresponding vertebra was measured and PMHSs presented lower angles compared with baseline THUMS versions, obtaining a difference of -6.54, -4.24 and -9.03 degrees for PMHS A, B and C respectively (see Table 6-1). This can be due to stronger correlations were found by Kent et al., 2005 between BMI and rib angle. Following the linear regression proposed on the mentioned study, PMHSs should present  $-5.35^{\circ} \pm 1.68$  of rib angle compared with the baseline model which is consistent with the obtained results. In the view of the foregoing, the fragility of the PMHSs was not supposed to be increased due to the change on the rib angle.

Table 6-1: Geometrical measurements for the PMHSs and all six corresponding model versions.

	PMHS A	Baseline	Mass scaled	Postured	Postured scaled	Morphed	Morphed postured
cort. Area (mm)	--	23,74	23,74	23,74	23,74	22,03	22,03
Area (mm)	358,05	301,92	301,92	301,92	301,92	238,42	238,42
Izz (mm <sup>4</sup> )	284	165	165	165	165	89	89
Ixx (mm <sup>4</sup> )	1576	1344	1344	1344	1344	965	965
Rib Angle (°)	59,27	65,81	65,81	67,93	67,93	69,00	64,62

	PMHS B	Baseline	Mass scaled	Postured	Postured scaled	Morphed	Morphed postured
cort. Area (mm)	--	23,84	23,84	23,84	23,84	21,83	21,83
Area (mm)	280,28	279,65	279,65	279,65	279,65	235,25	235,25
Izz (mm <sup>4</sup> )	140	127	127	127	127	83	83
Ixx (mm <sup>4</sup> )	1131	1302	1302	1302	1302	946	946
Rib Angle (°)	61,57	65,81	65,81	67,93	67,93	69,00	64,62



	PMHS C	Baseline	Mass scaled	Postured	Postured scaled	Morphed	Morphed postured
cort. Area (mm)	--	23,65	23,65	23,65	23,65	21,78	21,78
Area(mm)	307,48	269,24	269,24	269,24	269,24	227,95	227,95
Izz (mm <sup>4</sup> )	221	111	111	111	111	76	76
Ixx (mm <sup>4</sup> )	1032	1274	1274	1274	1274	940	940
Rib Angle (°)	56,50	65,81	65,81	64,40	64,40	66,11	66,64

Another factor discussed in the literature is the decrease of the rib cross-sectional area and the cortical thickness with age. It has been investigated as a critical factor of fracture generation (Agnew et al., 2015; Kemper et al., 2007; Kent et al., 2005; Shi et al., 2014 and Stein and Granik, 1976). Martynenko et al., 2017 suggested that the rib external geometry contributed more to stiffness and chest compression than the ribs tissue material properties. Nevertheless, the THUMS v3 ribcage accurately represents the rib geometry proposed by Shi et al. (2014). In order to identify potential differences on the cross-sectional areas, the rib points in which the marker clusters were located on the PMHSs were analysed in terms of internal geometry. Then, homologous rib points were measured on all HBM versions. Measurements are available on Table 6-1 showing that the three PMHSs presented higher or similar values than the computational versions due to the THUMS's cross-sectional area was based on subjects with an average age of 71 years old (Iraeus and Pipkorn 2019).

Due to the lack of resolution of the computed thermography scans of the PMHS (0.5 and 1mm pixels) was similar to the expected value, subject's cortical thickness was not measured. Notwithstanding, the cortical bone consists of a shell element part with a prescribed thickness of 0.7 mm, based on the 71 years old average mentioned before and consistently with Kemper et al., 2007 and Stein and Granik, 1976.

Some studies have demonstrated the cortical thickness variation across rib region and level (Cormier et al. 2005; Kemper et al. 2005, 2007) suggesting that the use of the average value could affect to the strain and stress outcome in those areas in which the value differs the most with the average (Agnew et al. 2015; Katzenberger et al. 2020).

However, Kent et al., 2005 found stronger correlations between age-related change on material properties and the number of fractures than other factors such as rib angle or cortical thickness. Therefore, internal geometrical values were not found to be a critical source of the results discrepancy for this dissertation.

### ***Tissue material properties***

After a review of the geometrical factors, another crucial factor that can be influencing the results is the definition of the material properties assigned to the tissues of the HBM. Some studies have addressed the decrease in Young's modulus, ultimate

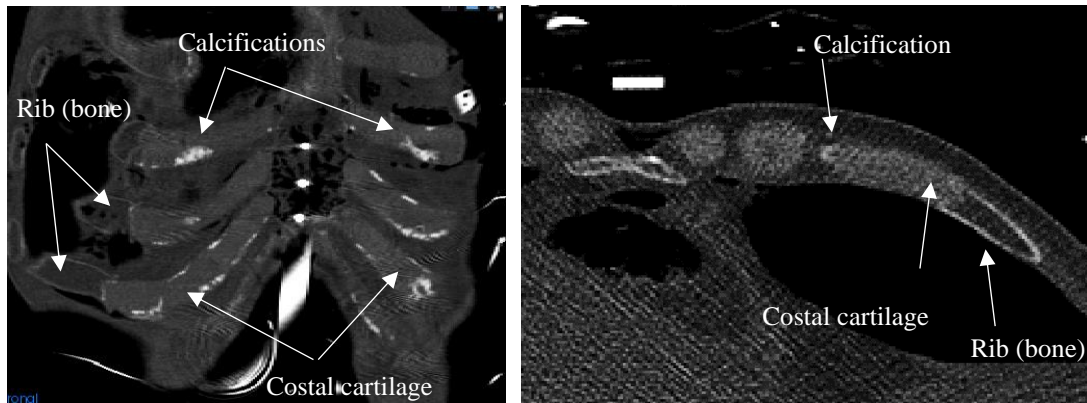
strength and yield stress with age (Katzenberger et al. 2020; Zioupos and Currey 1998). However, these studies were carried out using long bones coupon testing. McCalden et al. (1993) theorized existing differences between long bone and thoracic bone composition due to the external solicitations of these bones. Kemper et al. (2007) found that rib material properties have no significant variation regarding to rib level or region. On the contrary, the results of three-point bending tests showed significant variations on Young's modulus, stiffness and peak strain for the same variables, consistently with Martynenko et al. (2017). Kent et al. (2005) carried out a parametric study in order to evaluate the influence of age-related changes on material properties and geometrical parameters. This author found the material properties to have a stronger correlation with the number of fractures than the geometrical factors. However, material properties of the present THUMS version were based on literature for 18-81 age group (Kemper et al. 2005, 2007) being a reasonable representation of the subjects within this study ( $64 \pm 4$  y.o.).

The relative volume of bone and porous space have been demonstrated to have decrease in magnitude with the bone material properties (Kang et al. 2017; McCalden et al. 1993). Unfortunately, CT scans resolution and methodology used on this study did not allow these measurements.

The costal cartilage, which connects the ribs to the sternum, acts as a coupling component between the ribs and the sternum. Therefore, the costal cartilage plays a significant role in transmitting the applied forces between the sternum and ribs during the loading process. The costal cartilage is a hyaline cartilage surrounded by a perichondrium layer around the mid-substance. Most of the FE models rely solely on the mid-substance material properties for the costal cartilage characterization, while perichondrium has demonstrated to play an important role on the thoracic stiffness (Forman et al. 2010). Additionally, FE models consider the costal cartilage as an isotropic elastic material, and this can affect to the strain and stress distribution varying the fracture outcome (Murakami et al. 2006). Lau et al. (2008) indicates that there was not significant degradation of the costal cartilage material with age. Nevertheless, the presence of perichondral calcifications can be associated with the increasing of the structural stiffness of the ribcage and an increment of the number of rib fractures (Forman and Kent 2011).

By means of the CT scans observation, several calcification areas were identified for subject A that could explain the larger number of fractures sustained by this PMHS (15 fractured ribs). For the subjects B and C, calcifications were also observed, but, in these cases, the areas were smaller and were isolated (see Figure 6-7). Calcification can modify the strain patterns disturbing the predictions of strain-based probability of AIS3+.

Figure 6-7: Costal cartilage calcifications for subject A (left, frontal plane) and C (right, coronal plane)



### *Structural factors*

Finally, the previous factors can contribute to the third category, referred to differences on the chest deflection behaviour as structure. During the physical tests, PMHS exhibited higher chest deflection and probability of AIS3+ values than the predicted by simulations. Unfortunately, the rib strain was not measured during the physical tests preventing from the analysis of the time of fractures but it is known that rib fractures may occur before the first 35% chest compression (Duma et al. 2006, 2011; Kemper et al. 2011). Thus, the large amount of fractures sustained by PMHSs, can compromise the structural behaviour of the ribcage influencing the maximum deformation and, consequently, the deformation-based prediction of AIS3+ occurrence. All three PMHSs presented right clavicle fractures, which could have an influence on the chest loading conditions when compare with the simulations. Due to the absence of strain gages on the clavicle, there was no possibility to identify the fracture timing during the sled tests, thus a strain time-history analysis was done to the simulation results. Fourteen elements on the anterior surface of the right clavicle were selected to analyse the strain from the most proximal point of the clavicle body to the most distal location for both RSv (Figure 6-8 and Figure 6-9).

Figure 6-8: Clavicle strain results for all model versions belonging to RSv1.

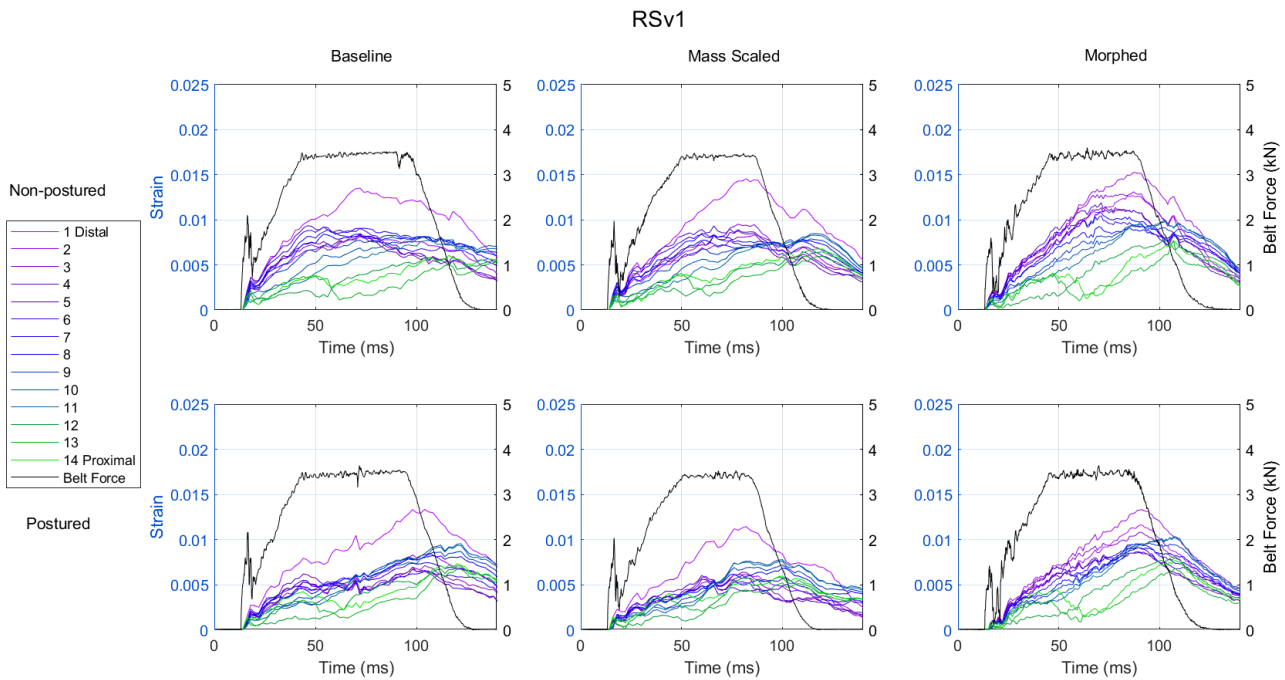
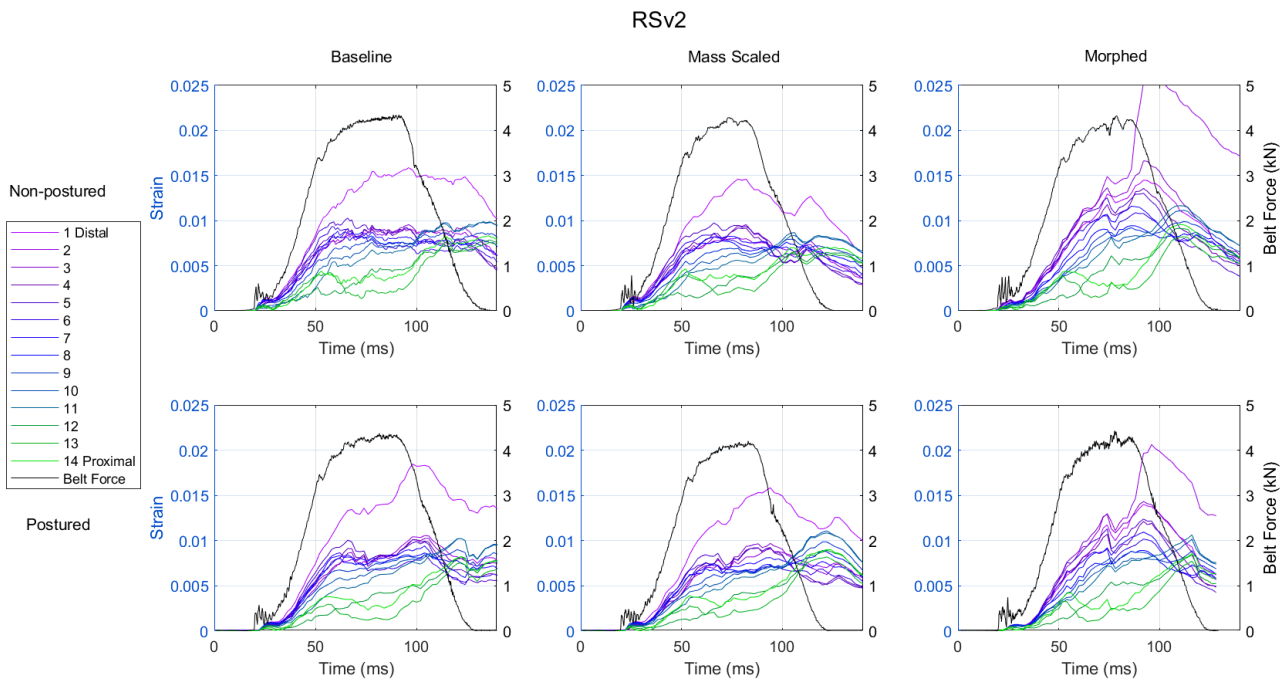


Figure 6-9: Clavicle strain results for all model versions belonging to RSv2.



This analysis shown that, establishing the limits proposed by Kemper et al. (2009), the critical strain value of 0.015 was reached on the proximal third of the clavicle after 75 milliseconds for the morphed model and for all the postured models for RSv2. The predicted location was consistent with the location of the fracture for the three subjects and the time is consistent with previous studies (Poulard et al. 2015) which found clavicle fractures after 80 milliseconds. This critical instant coincides with the moment in which

the proximal and distal ends of the clavicle were displaced forward because of the body and right arm inertias, while the clavicle was retained by the shoulder belt, resulting in clavicle bending. For the PMHS C (RSv2), an instantaneous force drop was visible on the load cell located on the upper shoulder belt that could confirm the time of the clavicle fracture, but no timing evidence was found for the other two subjects. Since the clavicle fracture seems to take place after the time in which fractures occur, it has been discarded such a potential source of discrepancies on the p (AIS3+) calculations. Additionally, despite of the fact that presented the higher amount of rib fractures, subject A sustained a monocortical posterior clavicle fracture that did not affect the clavicle integrity.

The analysis of the PMHSs chest kinematics reveals a positive deflection on the lower right chest that was confirmed by the high-speed videos. This phenomenon was reported by Rouhana et al. (2003) who proposed two potential mechanisms. The extension of the spine leading to an expansion of the thorax and the inertial effect of the internal organs pushing the anterior chest forward. Shaw et al. (2009) confirmed this so-called “bulge-out” suggesting that the internal organs and ribs inertia under the effect of the asymmetric loading can produce the positive displacement of the unrestricted chest areas. (Larsson et al. 2019) demonstrated that modifying the torso flesh materials to a softer viscoelastic response, the HBM predicted higher chest deflection magnitudes compared with the reference model.

Within this study, PMHSs presented larger bulge-out values than those obtained by Shaw et al. (2009). This can be due to the impact configuration as a 30° oblique impact, facing the inertial effects to the right aspect of the ribcage. The simulation results revealed that all HBM versions exhibited a positive X-deflection (bulge-out) at the lower right aspect of the ribcage, while this positive relative displacement was not found either when similar tests carried out with THOR, H3 dummies, cadaveric table top tests nor including airbag set up (Duma et al. 2011; Shaw et al. 2013). However, the computational models only predicted 7% to 45% of the PMHS deflection values across the different model versions and restraint system versions. This underprediction of the chest deformation can affect the injury prediction calculated based on deformation injury metrics such as those used in Chapter 5. For instance, Cmax only considers the maximum posterior resultant displacement of any studied rib point of the chest, independently of the displacement of the rest of the rib points. Thus, Cmax can underestimate the asymmetry produced by this phenomenon being the reason why the PC Score based calculations of probability of injury showed higher values than those based on Cmax.

## 6.1. Limitations

This section acknowledges the limitations of the study as they can influence generalizability and accuracy of the findings.

### *Sample Size and Statistical Analysis:*

Firstly, the study only evaluated the effect of subject personification on the accuracy of predicted kinematics for three post-mortem human subject sled tests. As a result, the generalizability of the findings to other crash scenarios and populations is limited. Additionally, the study only evaluated the effect of three personification techniques, and other techniques may have a greater or lesser effect on the accuracy of predicted kinematics.

Regarding the statistical analysis, the number of samples may also influence the results of the study. Using only three PMHS tests divided into two restraint system versions may lead difficulties in identifying potential outlier results.

Concerning to the spine rotation analysis, which used an 8-degree rotational interval to avoid indeterminate results and signal oscillations not attributed to physical events. However, the CORA analysis could be sensitive to the interval of measurement.

Another limitation is related to the chest deflection sensitivity analysis. Despite the utility of PC Score in facilitating a comparative analysis of diverse HBM versions considering differential deformations in the ribcage, it is essential to acknowledge certain limitations associated with its application. PC Score indicator was developed to be used with THOR ATD and, in order to use it for any other application, whether for other ATD or HBM, the formulation must be adapted for that specific use. Consequently, caution should be exercised in generalizing findings, and additional research is warranted to explore specialized indicators tailored specifically for HBMs.

### *Personalization Techniques:*

The morphing personification technique was implemented attending to the external anthropometry, thus internal subject-specific geometry was not personalized, and soft and hard tissues material properties remained unmodified from the SAFER HBM. Another limitation is related to the use of the Anthropometric Survey of U.S. Army Personnel (ANSUR) anthropometric database, which was used to perform the regression for the morphing technique. This database includes younger subjects who are probably more fit than the occupants of the experiments, which may result in non-accurate morphing of the skeleton due to different muscle/fat/bone volume proportions.

### *Experimental limitations:*

Finally, the measurement of thoracic and belt markers also has some limitations. Some of the markers were covered by the PMHS body during the motion of the occupant, limiting the visibility of the markers and therefore the calculation of the chest deformation

at those instants. This lack of visibility also limited the reconstruction of the belt path avoiding the evaluation of the belt as a fulcrum of the whole body motion. The attachment of the marker cluster to the vertebrae required the perforation of the vertebrae pedicle, compromising the integrity of the bone. Similarly, the attachment of the rib markers to the ribs required the perforation of the pleura, which is an invasive procedure. Nevertheless, this methodology, initially proposed in Shaw et al. (2009), is, to the authors' knowledge, the only available method to measure the in situ 3D kinematics of the spine during an impact.

## **6.2. Contributions of the study to the field**

Firstly, it has provided new experimental data for the development of HBM and ATD benchmarking. These data can be used to validate and improve human body models and anthropometric test devices and develop injury criteria for oblique impacts.

Moreover, this study has made a contribution to the quantitative assessment of the influence of personalization techniques on the predicted spinal kinematics and chest deformation in HBMs. These findings are essential in improving the accuracy of HBMs used in various applications, such as automotive safety, and can guide future research in developing more advanced and accurate HBMs.

Another contribution of this study is to highlight the potential of the FHA to predict spinal motion during oblique impacts. The research has also provided new experimental data framework for future studies to investigate the effect of different impact conditions on spinal motion. This is important for the analysis of body kinematics during oblique impacts, which can improve the accuracy of injury prediction and injury prevention.

Furthermore, this study has evaluated the sensitivity of the chest deformation to several personalization techniques of HBM in nearside oblique sled tests. The study found that the HBM underpredicted the chest deflection of the PMHS sled tests. Additionally, any of the personalization techniques explored within this dissertation significantly improved the chest deflection prediction. The results suggest that the incorporation of these personalization techniques in combination does not necessarily lead to superimposed effects.. These findings provide insights into the limitations of using FE-HBM to predict thoracic injury risk and the need for further research to improve the accuracy of injury risk predictions.

Finally, this research has contributed to the development of general guidelines for the integral evaluation of the HBM biofidelity. These guidelines can be used by researchers to evaluate the biofidelity of different human body models, and to improve the accuracy of injury prediction and injury prevention.

### 6.3. Conclusions

The main objective of this dissertation was the evaluation of the influence of the personalization techniques on the prediction of chest deformation in oblique impact configurations. To accomplish this main objective four research questions were set to carry out an integral evaluation of the influence of the personalization techniques explored in this work. Each research question resulted on relevant conclusions that are summarised in this section.

*1. Are the HBM capable of mimicking occupant kinematics in terms of spinal bone trajectories?*

Regarding the first research question, the PhD study found that HBM could accurately mimic occupant kinematics in terms of spinal bone trajectories. The predicted trajectories showed similarity in shape and magnitude across all scenarios and landmarks, indicating the models' capability to accurately predict spinal motion (CORA total rating average = 0.669 and SD = 0.024). The study found that all personalization techniques improved the predicted kinematics of the model to some extent, but the degree of improvement varied depending on the personalization techniques used and the landmark being analysed.

The study showed that subject personalization techniques significantly influenced the predicted spinal displacement on HBM and improved the accuracy of predicting the kinematics of post-mortem human subjects in nearside oblique impacts. The more similar the HBM was to the anthropometry and posture of the sled tested PHMS, the more similar the predictions were to the measured responses of the PMHS, resulting in a higher CORA score. Thus, the morphed postured model produced the highest CORA score compared to the other model versions.

The accuracy of spinal trajectory predictions varied depending on the specific landmark being analysed. The morphing technique on the head trajectories showed the highest effect size ( $r = 0.71092$ ), followed by the posturing on the total CORA rating ( $r = 0.62404$ ). Additionally, the CORA score for the head was generally higher than for the upper, middle, and lower spine. This may be because the human body model in previous validation efforts was primarily correlated and validated for head displacement, and there is less PMHS validation data available for the observed spinal levels than for the head. Therefore, for all model versions, poor agreement between predicted and measured lower spine displacement (lowest CORA score) was obtained.



2. *Are the HBM capable of mimicking occupant kinematics in terms of spinal bone rotations?*

Regarding the second research question, the PhD study revealed that HBM are capable of mimicking occupant kinematics in terms of spinal bone rotations, with an average CORA total rating of 0.6225 and a standard deviation of 0.0297. However, the accuracy of these predictions is influenced by the personalization techniques used and the specific landmark being analysed.

The study found that the HBM models performed better in predicting the trajectories of the head and upper spine, resulting in higher CORA scores. On the contrary, rotations were better predicted for the middle and lower spine. The study identified that the rotation of the upper and middle spine around the Z-axis can be related to the mass distribution of the occupant. Contrary to the trajectory's predictions, the combined use of personification techniques on rotations prediction did not lead to additional improvements due to the varying effects of each technique on different bones and axes. Therefore, statistical analysis revealed that none of the personification techniques had a statistically significant influence on rotation predictions.

In terms of rotational components, the study showed that rotation about the Y-axis exhibited higher correlations compared to the X and Z components, with some exceptions, across both RS versions. Discrepancies between the HBM and PMHS could be attributed to the material properties of intervertebral discs, ligaments, and spinal muscles within the HBM, as these factors play a crucial role in spinal kinetics and kinematics.

The PhD study highlighted the importance of analysing the 6-DOF motion of the spine during impact events. It demonstrated the effectiveness of the FHA in analysing spine motion during sled tests. Notably, the rotational analyses were found to be more sensitive to experimental events than trajectory analyses in the conducted physical tests. By examining the timing of head and upper spine rotations and the abrupt changes in rotational direction, the study successfully identified the interaction of PMHS with the retention system.

3. *Are the HBM capable of mimicking occupant chest deformation during oblique impacts?*

Regarding the third research question, the PhD revealed that the baseline HBM and the personalized versions can reflect the complex deformation patterns of the chest under oblique impacts to some extent. However, all model versions underestimated the chest deformation experienced by the PMHS and the HBM demonstrated to have some limitations.

The response of chest deflection was found to be sensitive to the restraint system used. In the case of occupants A and B (RSv1), the sternum exhibited compression from the beginning of the test. However, for occupant C (RSv2), all five chest locations initially showed expansion. Nevertheless, none of the HBM versions accurately predicted the forward movement of the sternum at the beginning of this last test.

Across all three subjects, the lower right chest (R8R) displayed forward motion. While all model versions correctly predicted the forward motion of the lower right chest, they underpredicted the deflection values. This underprediction could be attributed to differences in material properties between the PMHS and HBM, which remained unmodified in the present investigation.

Regarding the lateral displacement of the five chest landmarks, in the upper chest region, R4L moved to the right, while R4R moved to the left, indicating that both lateral aspects of the upper chest shifted toward the medial ribcage, thereby increasing local deformation. However, neither HBM version predicted the leftward displacement of R4R.

*4. How does the chest deflection of the HBM respond to the different personalization techniques?*

Lastly, the PhD addresses the fourth research question regarding the influence of personalization techniques on the HBM chest deformation. Both the baseline HBM and the personalized model versions demonstrated better prediction of the probability of the chest deflection compared to the ATD, although some limitations remained.

All model versions underpredicted the probability of injury, as they also underestimated the chest deflection values. Among the HBM versions, the postured model showed the better alignment with the experimental results.

The mass-scaling and morphing techniques resulted in statistically significant differences in the chest deflection prediction for both deformation indicators (Cmax and PC Score). However, they yielded lower values compared to the baseline and postured versions. The negative effect sizes (size  $r$ ) obtained do not necessarily indicate that the personalization techniques had a detrimental effect on the chest deformation prediction capability of the baseline model. Instead, the results suggest that the incorporation of these personalization techniques in combination does not lead to superimposed effects, similar to what was observed in spinal rotation predictions. This indicates that chest deflection depends not only on the external geometry of the occupant but also on other variables.

Additionally, the study reported on Paper D found that predicting chest deflection based on the PC Score resulted in higher values than predictions based on Cmax for the loading conditions and personalization techniques analysed in this study. Thus, the study demonstrates the importance of considering differential deformation to estimate the risk of thoracic injuries under oblique loading conditions.

## 6.4. Conclusions (in Spanish)

El objetivo principal de esta disertación ha sido evaluar la influencia de las técnicas de personalización en la predicción de deformación del pecho en configuraciones de impacto oblicuo. Para lograr este objetivo principal y para llevar a cabo una evaluación integral de la influencia de las técnicas de personalización exploradas en este trabajo, se plantearon cuatro preguntas de investigación. Cada pregunta de investigación resultó en conclusiones relevantes que se resumen en esta sección.

1. *¿Son los HBM capaces de reproducir la cinemática del ocupante en términos de trayectorias de los huesos de la columna vertebral?*

En cuanto a la primera pregunta de investigación, el estudio encontró que los HBM podían reproducir con precisión la cinemática del ocupante en términos de trayectorias de la columna vertebral. Las trayectorias predichas mostraron similitud en tanto en comportamiento como en magnitud para todos los escenarios, lo que indica la capacidad de los modelos para predecir con precisión el movimiento de la columna vertebral (promedio de puntuación total CORA = 0,669 y desviación estándar = 0,024). El estudio encontró que todas las técnicas de personalización mejoraron la cinemática predicha del modelo, pero el grado de mejora varía según las técnicas de personalización utilizadas y el punto de referencia analizado.

El estudio muestra que las técnicas de personalización aplicadas influenciaron significativamente en la predicción de desplazamientos y mejoraron la precisión en la predicción de la cinemática de PMHS. Cuanto más similar era el HBM a la antropometría y postura de los PMHS, más precisas eran las predicciones, lo que resulta en una puntuación CORA más alta. Por lo tanto, el modelo con antropometría y postura modificadas (versión 6) produjo la puntuación CORA más alta en comparación con las otras versiones del modelo.

La precisión de las predicciones de trayectorias de la columna varía según el punto de referencia específico analizado. La técnica de modificación de antropometría en las trayectorias de la cabeza mostró el mayor valor de tamaño del efecto ( $r = 0,71092$ ), seguida de la modificación de postura en la puntuación CORA total ( $r = 0,62404$ ). Además, la puntuación CORA para la cabeza fue, en general, más alta que para la parte superior, media e inferior de la columna vertebral. Esto puede deberse a que el modelo del cuerpo humano haya sido validado principalmente para el desplazamiento de la cabeza, y hay menos datos de validación disponibles para los niveles espinales observados que para la cabeza. Por lo tanto, para todas las versiones del modelo, se obtuvo una baja correlación entre el desplazamiento espinal predicho y medido (puntuación CORA más baja) en la parte inferior de la columna vertebral.

2. *¿Son capaces los HBM de reproducir la cinemática del ocupante en términos de rotaciones de los huesos de la columna vertebral?*

En cuanto a la segunda pregunta de investigación, el estudio demuestra que los HBM son capaces de imitar la cinemática del ocupante en términos de rotaciones, con una puntuación total promedio de CORA de 0,6225 y una desviación estándar de 0,0297. Sin embargo, la precisión de estas predicciones está influenciada por las técnicas de personalización utilizadas y el punto de referencia específico analizado.

El estudio encontró que los modelos HBM obtuvieron una mejor correlación en la predicción de las trayectorias de la cabeza y la parte superior de la columna vertebral, lo que resultó en puntuaciones CORA más altas. Por el contrario, las rotaciones se predijeron mejor para la parte media e inferior de la columna vertebral. El estudio identificó que la rotación de la parte superior y media de la columna vertebral alrededor del eje Z puede estar relacionada con la distribución de masa del ocupante. Al contrario que en las predicciones de trayectorias, el uso combinado de técnicas de personalización en la predicción de rotaciones no condujo a mejoras adicionales debido a los efectos variables de cada técnica en diferentes huesos y ejes. Por ello, el análisis estadístico reveló que ninguna de las técnicas de personalización tuvo una influencia estadísticamente significativa en las predicciones de rotación.

En cuanto a los componentes de rotación, el estudio mostró que la rotación alrededor del eje Y exhibió correlaciones más altas en comparación con los componentes X y Z, con algunas excepciones, en ambas versiones de los HBM. Las discrepancias entre los HBM y los PMHS pueden atribuirse a las propiedades del material de los discos intervertebrales, ligamentos y músculos espinales dentro de los HBM, ya que estos factores desempeñan un papel crucial en la cinética y cinemática espinal.

El estudio resaltó la importancia de analizar el movimiento de 6 grados de libertad (6-DOF) de la columna vertebral durante los eventos de impacto. Demostró la eficacia del análisis de movimiento de la columna vertebral en los experimentos. Específicamente, los análisis de rotación resultaron ser más sensibles a los eventos experimentales que los análisis de trayectorias en las pruebas físicas realizadas. Al examinar el momento de inicio de la rotación de la cabeza y la parte superior de la columna vertebral y los cambios bruscos en la dirección de rotación, el estudio identificó con éxito la interacción de los PMHS con el sistema de retención.

3. *¿Son capaces los HBM de reproducir la deformación del pecho del ocupante durante impactos oblicuos?*

En cuanto a la tercera pregunta de investigación, el estudio revela que el HBM de referencia y las versiones personalizadas pueden reflejar en cierta medida los patrones complejos de deformación del pecho en impactos oblicuos. Sin embargo, todas las

versiones del modelo subestimaron la deformación del pecho experimentada por los sujetos, y el HBM demostró tener algunas limitaciones.

Se encontró que la respuesta del pecho era sensible al sistema de retención utilizado. En el caso de los ocupantes A y B (RSv1), el esternón mostró compresión desde el inicio del ensayo. Sin embargo, para el ocupante C (RSv2), las cinco ubicaciones del pecho mostraron expansión al inicio del ensayo. No obstante, ninguna de las versiones del HBM predijo con precisión el movimiento hacia adelante del esternón al comienzo de esta última prueba.

En los tres sujetos, la parte inferior derecha del pecho (R8R) mostró movimiento hacia adelante. Si bien todas las versiones del modelo predijeron correctamente este movimiento, subestimaron los valores de deflexión. Esta subestimación podría atribuirse a diferencias en las propiedades de los materiales entre los PMHS y el HBM, que no se modificaron en la presente investigación.

En cuanto al desplazamiento lateral de los cinco puntos de referencia del pecho, en la región del pecho superior, R4L se desplazó hacia la derecha, mientras que R4R se desplazó hacia la izquierda, lo que indica que ambos aspectos laterales del tórax superior se desplazaron hacia la zona medial, aumentando así la deformación local. Sin embargo, ninguna de las versiones del HBM predijo el desplazamiento hacia la izquierda de R4R.

#### *4. ¿Cómo responde la deflexión del pecho del HBM a las distintas técnicas de personalización?*

Por último, el doctorado aborda la cuarta pregunta de investigación sobre la influencia de las técnicas de personalización en la capacidad del HBM para predecir deformaciones en el pecho. Tanto el HBM de referencia como las versiones personalizadas demostraron una mejor predicción de deformaciones en comparación con los ATD (dummy antropomórfico), aunque con algunas limitaciones.

Todas las versiones del modelo subestimaron los valores de deflexión del pecho. Entre las versiones del HBM, el modelo con postura modificada (versión 2) mostró la mayor probabilidad de lesión y predicciones que se asemejaban estrechamente a los resultados de lesiones observados en las pruebas de referencia con PMHS.

Las técnicas de escalado de masa y modificación de antropometría resultaron en diferencias estadísticamente significativas en los cálculos de deformación del pecho para ambos indicadores (Cmax y PC Score). Sin embargo, produjeron valores más bajos en comparación con las versiones de referencia y con postura modificada. Los tamaños efecto ( $r$ ) negativos obtenidos no indican necesariamente que las técnicas de personalización tuvieran un efecto perjudicial en la capacidad de predicción de deformaciones del modelo de referencia. Por el contrario, sugieren que la incorporación de estas técnicas de personalización en combinación no conduce a efectos de superposición, similar a lo observado en las predicciones de rotación. Esto indica que la

deflexión del pecho depende no solo de la geometría externa del ocupante, sino también de otras variables.

Además, el estudio del Paper D, encontró que las predicciones basadas en el PC Score resultaron en valores más altos que las basadas en Cmax para las condiciones de impacto y las técnicas de personalización estudiadas en esta disertación. Por lo tanto, el estudio demuestra la importancia de considerar la deformación diferencial entre las distintas partes del pecho para estudiar el riesgo de lesiones torácicas bajo condiciones de impacto oblicuo.

En resumen, la disertación concluye que los modelos de cuerpo humano (HBM) pueden reproducir en cierta medida la cinemática del ocupante y la deformación del pecho durante impactos oblicuos. Las técnicas de personalización utilizadas en el HBM pueden mejorar la precisión de las predicciones, especialmente en términos de trayectorias y rotaciones de los huesos de la columna vertebral. Sin embargo, persisten desafíos en la predicción de la deformación del pecho y la probabilidad de lesiones, y se requiere una investigación adicional para mejorar la capacidad del HBM en este aspecto.

## **6.5. Future Work**

Based on the findings and conclusions of this dissertation, several areas for future work are suggested to further advance the field of human body modelling and improve the accuracy of injury risk predictions. Addressing these areas of future work will contribute to the advancement of human body modelling, enhance injury risk predictions, and further validate the findings of this study in various crash scenarios and population groups.

### ***Sample Size and Statistical Analysis:***

- Increasing the sample size to enhance the statistical power of the study: Including a larger number of subjects and tests can improve the statistical robustness of the findings and increase confidence in the results.

### ***Personalization Techniques and Model Validation:***

- Exploring other personalization techniques that may have greater impact on the kinematical and chest deflection prediction: The study evaluated three personification techniques, but future research should consider exploring other techniques. Incorporating additional personalization strategies, such as subject-specific internal geometry, can improve the representation of the human body and enhance the accuracy of the models.

- Modifying the material properties of the spine in the HBM: Investigating the impact of different material properties for intervertebral discs, ligaments, and spinal muscles can lead to improved predictions of spinal kinematics and provide a more realistic representation of the human body behaviour under oblique impacts.

- Modifying the material properties of soft and hard tissues in the thorax of the HBM: Future studies should focus on considering the modification of the diverse body parts, including internal organs and costal cartilage, to enhance the accuracy of the human body model.

***Evaluation of Different Crash Scenarios:***

- Investigating the effect of different impact speeds and angles on spine kinematics: Exploring a wider range of impact conditions can provide insights into the impact response of the spine and help develop more comprehensive models.

- Extending the study to other types of impacts: Examining the effects of different impact scenarios and exploring alternative personalization techniques can broaden the applicability of the findings and improve injury risk predictions for various crash scenarios and populations.

***Chest deformation indicators***

- Exploring alternative chest deformation parameters that may provide different results: Investigating different indicators can offer additional perspectives and insights into the evaluation of HBM chest deflection prediction capabilities.

## References

- Agnew AM, Schafman M, Moorhouse K, White SE, Kang YS. The effect of age on the structural properties of human ribs. *J. Mech. Behav. Biomed. Mater.* 2015;41:302–314.
- Cormier JM, Stitzel JD, Duma SM, Matsuoka F. Regional variation in the structural response and geometrical properties of human ribs. *Annu. Proc. - Assoc. Adv. Automot. Med.* 2005;(January):153–170.
- Duma SM, Kemper AR, Stitzel JD, McNally C, Kennedy EA, Matsuoka F. Rib fracture timing in dynamic belt tests with human cadavers. *Clin. Anat.* 2011;24(3):327–338.
- Duma SM, Stitzel JD, Kemper AR, McNally C, Kennedy EA, Matsuoka F. A Method to Acquire Non-censored Rib Fracture Data During Dynamic Belt Loading Tests. In: *INJURY BIOMECHANICS RESEARCH.*; 2006:103–116.
- Forman JL, Kent RW. Modeling costal cartilage using local material properties with consideration for gross heterogeneities. *J. Biomech.* 2011;44(5):910–916.
- Forman JL, Del Pozo De Dios E, Dalmases CA, Kent RW. The contribution of the perichondrium to the structural mechanical behavior of the costal-cartilage. *J. Biomech. Eng.* 2010;132(9).
- Gayzik FS, Yu MM, Danelson KA, Slice DE, Stitzel JD. Quantification of age-related shape change of the human rib cage through geometric morphometrics. *J. Biomech.* 2008;41(7):1545–1554.
- Iraeus J, Pipkorn B. Development and validation of a generic finite element ribcage to be used for strain-based fracture prediction. In: *Proceedings of IRCOBI Conference 2019.*; 2019:193–210.
- Kang YS, Agnew AM, Hong CB, Icke K, Bolte JH. Elderly PMHS thoracic responses and injuries in frontal impacts. In: *Proceedings of IRCOBI Conference 2017.*; 2017:539–557.
- Katzenberger MJ, Albert DL, Agnew AM, Kemper AR. Effects of sex, age, and two loading rates on the tensile material properties of human rib cortical bone. *J. Mech. Behav. Biomed. Mater.* 2020;102(August 2019):103410.
- Kemper AR, Kennedy EA, McNally C, Manoogian SJ, Stitzel JD, Duma SM. Reducing chest injuries in automobile collisions: Rib fracture timing and implications for thoracic injury criteria. *Ann. Biomed. Eng.* 2011;39(8):2141–2151.
- Kemper AR, McNally C, Clayton AP, Freeman LJ, Duma SM, Rouhana SW. The biomechanics of Human Ribs: Material and Structural Properties from Dynamic Tension and Bending Tests. *Stapp Car Crash Journal.* 2007;51:235–273.
- Kemper AR, McNally C, Kennedy EA, Manoogian SJ, Rath AL, Ng TP, Stitzel JD, Smith EP, Duma SM, Matsuoka F. Material Properties of Human Rib Cortical Bone from Dynamic Tension Coupon Testing. *SAE Tech. Pap.* 2005;2005-November:199–230.
- Kemper AR, Stitzel JD, McNally C, Gabler HC, Duma SM. Biomechanical response of the human clavicle: The effects of loading direction on bending properties. *J. Appl. Biomech.* 2009;25(2):165–174.
- Kent R, Lee SH, Darvish K, Wang S, Poster CS, Lange AW, Brede C, Lange D, Matsuoka F. Structural and Material Changes in the Aging Thorax and Their Role in Crash Protection for Older Occupants. *Stapp Car Crash Journal.* 2005;2005-November:231–249.
- Larsson KJ, Pipkorn B, Iraeus J, Bolte JH, Agnew AM, Hu J, Reed MP, Sunnevång C. Evaluation of the benefits of parametric human body model morphing for prediction of injury to elderly occupants in side impact. In: *Conference proceedings International Research Council on the Biomechanics of Injury, IRCOBI. Florence, Italy; 2019:150–174.*
- Lau A, Oyen ML, Kent RW, Murakami D, Torigaki T. Indentation stiffness of aging human costal



- cartilage. *Acta Biomater.* 2008;4(1):97–103.
- Martynenko O, Kleinbach C, Hammer M, Haeufle DFB, Mayer C, Schmitt S. A Comparison of Rib Structural and Material Properties from Matched Whole Rib Bending and Tension Coupon Tests. *IRCOBI Conf. Proc.* 2017;44(0):679–680.
- McCalden RW, McGeough JA, Barker MB, Court-Brown CM. Age Related Changes in the Tensile Properties of Cortical Bone. *J. Bone Jt. Surg.* 1993;75-A(8):1193–1205.
- Murakami D, Kobayashi S, Torigaki T, Kent R. Finite Element Analysis of Hard and Soft Tissue Contributions to Thoracic Response: Sensitivity Analysis of Fluctuations in Boundary Conditions. *SAE Tech. Pap.* 2006;2006-November.
- Poulard D, Subit D, Nie B, Donlon JP, Kent RW. The Contribution of Pre-impact Posture on Restrained Occupant Finite Element Model Response in Frontal Impact. *Traffic Inj. Prev.* 2015;16(September 2016):87–95.
- Rouhana SW, Kankanala S V., Prasad P, Rupp JD, Jeffreys TA, Schneider LW. Biomechanics of 4-Point Seat Belt Systems in Frontal Impacts. *SAE Tech. Pap.* 2003;47:367–399.
- Shaw G, Lessley D, Ash J, Crandall J, Parent D. Response Comparison for the Hybrid III, THOR Mod Kit with SD-3 Shoulder, and PMHS in a Simulated Frontal Crash. In: *23rd ESV Conference.*; 2013:1–19.
- Shaw G, Parent D, Purtsezov S, Lessley D, Crandall J, Kent R, Guillemot H, Ridella S a, Takhounts E, Martin P. Impact response of restrained PMHS in frontal sled tests: skeletal deformation patterns under seat belt loading. *Stapp Car Crash J.* 2009;53(November):1–48.
- Shi X, Cao L, Reed MP, Rupp JD, Hoff CN, Hu J. A statistical human rib cage geometry model accounting for variations by age, sex, stature and body mass index. *J. Biomech.* 2014;47(10):2277–2285.
- Stein ID, Granik G. Rib Structure and Bending Strength: An Autopsy Study. *Calcif. Tissue Res.* 1976;1:61–73.
- Zioupos P, Currey JD. Changes in the stiffness, strength, and toughness of human cortical bone with age. *Bone.* 1998;22(1):57–66.

**PAPER A**

**Kinematic Assessment of Subject Personification of Human Body  
Models (THUMS)**

### Kinematic Assessment of Subject Personification of Human Body Models (THUMS).

Ana Piqueras-Lorente, Johan Iraeus, Ana I. Lorente, Francisco J. López-Valdés, Óscar Juste-Lorente,  
Mario Maza-Frechín, Bengt Pipkorn

**Abstract** The goal of this study was to quantify the effect of improving the geometry of a human body model on the accuracy of the predicted kinematics for 4 post-mortem human subject sled tests. Three modifications to the computational human body model THUMS were carried out to evaluate if subject personification can increase the agreement between predicted and measured kinematics of post-mortem human subjects in full frontal and nearside oblique impacts. The modifications consisted of: adjusting the human body model mass to the actual subject mass, morphing it to the actual anthropometry of each subject and finally adjustment of the model initial position to the measured position in selected post-mortem human subject tests.

A quantitative assessment of the agreement between predicted and measured response was carried out by means of CORA analysis by comparing the displacement of selected anatomical landmarks (head CoG, T1 and T8 vertebrae and H-Point).

For all three scenarios, the more similar the human body model was to the anthropometry and posture of the sled tested post-mortem human subject, the more similar the predictions were to the measured responses of the post-mortem human subject, resulting in higher CORA score.

**Keywords** biomechanics, biofidelity, simulation, subject personification, THUMS

#### I. INTRODUCTION

Several Finite Element Human Body Models (FE-HBM) have been developed to predict the response of the human body under blunt impacts. However, the commercially available models such as THUMS, from Toyota Motor Corporation and Toyota Central R&D [1] and GHBMC from the Global Human Body Model Consortium [2] represent a limited number of anthropometric sizes (95<sup>th</sup> percentile male, 50<sup>th</sup> percentile male and 5<sup>th</sup> percentile female are the most common sizes) and they are only available in a standard seated position for the vehicle occupant or standing posture for the pedestrian [3]. Due to the anthropometric and pre-impact posture variability of real humans, to mimic the impact response of specific subjects, it is suggested that human body models should be *personalised*. The personification of human body models can for example be done by modifying the mass or the geometry (both external and internal). For HBMs based on the FE method, this could be carried out by modifying material properties or nodal coordinates through morphing. Previous work has been done by [4]-[7] with such modifications in frontal and side impacts.

The morphing was carried out by means of Kriging interpolation. The module was included in the PIPER v1.0.0 software [8] PIPER EU project, "piper-project.org" [<http://www.piper-project.org/>], 2017/11/10 [2018/01/11]. The PIPER software can estimate the missing dimensions based on a selected database (ANSUR; SNYDER or CCTANTHRO) using certain known anthropometry values as input variables. The ANSUR database includes adult anthropometry values measured in supine and seated position.

The aim of this study is to evaluate if model modifications using subject personification techniques increases the similarity between the predicted kinematic responses of a human body model (HBM) and the measured response from post-mortem human subjects (PMHSs) in frontal and nearside oblique impacts using contemporary restraints. The agreement between the predicted and the measured response was quantified using CORA (correlation and analysis) rating [9].

Ana Piqueras (+34 635 38 94 61, [apiquera@unizar.es](mailto:apiquera@unizar.es)), Ana I. Lorente and Óscar Juste-Lorente are PhD students and Mario Maza-Frechín is Associate Professor at the Impact Laboratory (I3A) at University of Zaragoza, Spain. Johan Iraeus is PhD at the Mechanics and Maritime Sciences department at Chalmers University of Technology in Gothenburg, Sweden. Francisco J. López-Valdés is Assistant Professor and Research Associate, Instituto de Investigación Tecnológica (IIT), ICAI, Universidad Pontificia de Comillas, Madrid, Spain. Bengt Pipkorn is Director of Simulation and Active structures at Autoliv Research, Vårgårda, Sweden and Adjunct Professor at Chalmers University of Technology in Gothenburg, Sweden.

## II. METHODS

A modified version of THUMS v3 model [10] was used in this study. Modifications included remodelling of the ribcage [11] and recalibration of the lumbar spine properties [12]. To evaluate the kinematic response of this HBM, four PMHS sled tests in frontal and frontal oblique load cases were carried out [13]-[14].

The sled test fixture (Gold Standard) consisted of a rigid metallic frame allowing complete visual access to the occupant while preserving the basic geometry of a standard seat of a passenger car. This test fixture was developed as a reasonable approximation to the passenger posture in the development of thoracic injury criteria [15]-[16]. In these tests, the knee bar that was used in the references provided was removed from the fixture. The seat for scenarios 1 and 2 was composed of inclined steel plates designed to restrain the pelvis motion to mimic pelvis kinematics observed in tests with real vehicle seats. In the Scenario 3 the seat consisted on a single horizontal steel plate.

PMHS information and sled test fixtures for the three studied scenarios is shown in Table I.

TABLE I  
PMHS INFORMATION AND TEST SET-UP

	SCENARIO 1		SCENARIO 2	SCENARIO 3
<i>PMHS</i>	A	B	C	D
<i>Test</i>	1	2	3	4
<i>Nominal velocity (km/h)</i>	34.1	34.3	34.3	35
<i>Restraint system</i>	3-point seatbelt. Shoulder PT (2kN). Lap PT (3.5kN) and FL (4.5kN)	3-point seatbelt. Shoulder PT (2kN). Lap PT (3.5kN) and FL (4.5kN)	3-point seatbelt. Lap PT (3.5kN) and FL (4.5kN)	2B seatbelt. Shoulder PT (2kN), lap PT (3.5kN) and FL (6kN)
<i>Seat</i>	Inclined steel plates	Inclined steel plates	Inclined steel plates	Horizontal steel plate
<i>Impact angle (°)</i>	30	30	30	0
<i>Age</i>	66	68	60	39
<i>Gender</i>	Male	Male	Male	Male
<i>Stature (cm)</i>	175	169	170.5	181
<i>Seated height (cm)</i>	96.3	103.8	101.4	97
<i>Weight (kg)</i>	47	53	57	62
<i>Cause of death</i>	Pancreatic cancer	Lung cancer	Lung cancer	Cardiac arrest

### Instrumentation

The kinematic responses of the subjects from Scenarios 1 and 2 (Table I) were collected at 1 kHz using a 3D motion capture system (Vicon, TS series, Oxford, UK). Retroreflective markers were attached to selected locations of the subject, sled fixture and restraint system. In order to accurately acquire the response of the selected bones and its initial positions, the markers were attached directly to the skull and vertebrae by means of plates screwed directly to the bones. With the geometry of each screwed plate and the corresponding bone morphology (obtained from a computed tomography (CT) scan) the movement of each bone was reconstructed [17] after defining their own Local Coordinates System [18].

For the full-frontal impact configuration, corresponding to the Scenario 3, the kinematic behaviour of the left head external auditory meatus (EAM), left acromion and left tibial condyle in the sagittal plane were tracked from the high speed video recorded at 1,000 fps.

In all three scenarios, four force transducers were installed in the upper and lower shoulder belt and the inner and outer lap belt band, recording the belt forces.

### Boundary Conditions

All simulations were carried out in the same conditions for each scenario. Sled acceleration pulses, obtained from the physical tests, were applied to the sled fixture in order to obtain the same loading scenarios. The parameters of the restraint system were adjusted to accurately represent the interaction between the seatbelt and the occupant, taking the belt forces from the real tests as reference.

### HBM Personification

The HBM was personalised in three steps. In each step, the level of complexity was increased. First, the overall mass of the HBM was adjusted to the one of the Post Mortem Human Subject (PMHS) of the relevant sled test. Second, the THUMS model was morphed to reflect the individual anthropometry of each PMHS. Third, the postures of the original, mass-scaled and morphed THUMS models were adjusted to the actual positions of the PMHS. These modifications resulted in a total of six versions of the THUMS model for each crash scenario, the baseline model and five modified models with different levels of personification:

1. *Baseline*: The first level was to use the unmodified HBM as it is. The THUMS v3 model represents an occupant with a stature of about 177cm and a body mass of about 77kg.
2. *Scaled mass*: In the second model, the overall mass was adjusted to represent the individual PMHS (Table I) by scaling the density of the outer flesh properties.
3. *Morphed*: The HBM model was morphed to reflect the individual anthropometry and body mass of each PMHS measured before each test. The THUMS model was prepared to be processed by means of a metadata file in which all FE parts were identified and classified as bone, flesh (including muscles, fat, ligaments, etc.), organs and skin parts and divided into six main areas: head, trunk, upper limbs and lower limbs (as shown in Fig. 1). In order to perform the morphing, lengths and contours had to be identified. Lengths was defined as the distance between two landmarks. For this purpose, two nodes of the model had to be identified in the metadata and used as landmarks. The PIPER software created auxiliary control points semi-automatically to define the body contours. The anthropometric dimensions (lengths and contours) in seated position used as input values for each subject were extracted from the seated anthropometry measurements (Table VIII(A), Appendix) and from the captures of the VICON markers before the tests. However, more data was required in order to morph the model accurately especially in Scenario 3, where the seated anthropometry was not available. Values shown on Table VII(A) and Table VIII(A) were entered as input variables and, after the regression analysis, the PIPER software calculated the missing target dimensions.

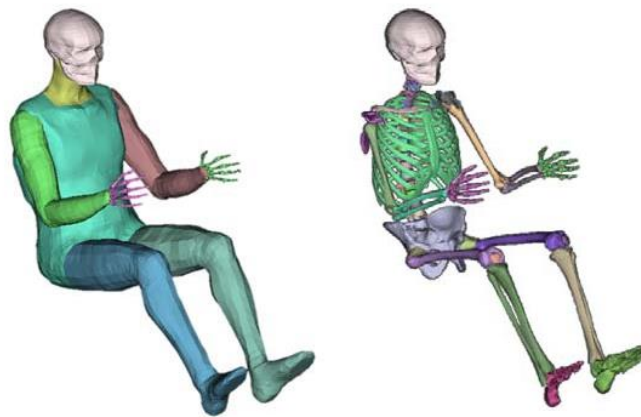


**Fig. 1: Visualization of the entities used for the morphing process**

4. *Baseline postured*: To analyse the influence of initial posture, the baseline model was modified by aligning the spine curvature of the model to the actual spine curvature of the PMHSs at t=0ms. This was done using a pre-simulation where the displacements of the head CoG, T1, T8 and H-Point were prescribed, to finally conform to the positions measured in the PMHSs.
5. *Scaled mass postured*: In this version of the model, both mass and posture were modified to resemble the weight and posture of the occupant.
6. *Morphed postured*: The posture of the morphed version (3) was adapted with the procedure followed for the model versions 4 and 5.

TABLE II  
ANGLE FORMED WITH THE VERTICAL OF  
THE SELECTED LANDMARKS IN THE SPINE WITH RESPECT TO THE PREVIOUS

SUBJECT	THUMS	PMHS A	PMHS B	PMHS C		PMHS D
Test	---	1	2	3		4
$\alpha_{\text{Head-T1}}$	-20	-16	-12	-9	$\alpha_{\text{Head-T1}}$	-14
$\alpha_{\text{T1-T8}}$	-25	-30	-25	-28	$\alpha_{\text{T1-H-Point}}$	26
$\alpha_{\text{T8-L2}}$	38	44	39	40		
$\alpha_{\text{L2-H-Point}}$	51	60	38	41		

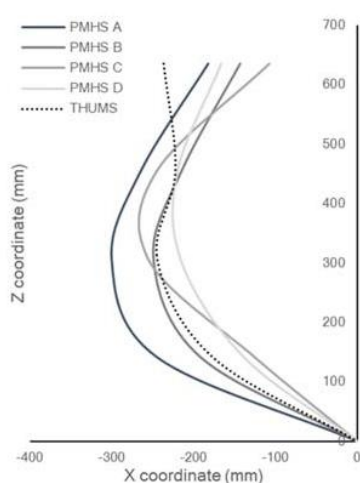


Fig. 2: Pre-impact spline alignment of the PMHSs compared with the spine alignment of the baseline THUMS model. The origin of the graph represents the H-Point and the endpoint of each curve represents the head of the subjects.

### Quantitative Assessment of the Kinematic Response

The assessment of the different versions of the HBM was done by comparing the trajectories in X, Y and Z-axis of selected anatomical landmarks: head CoG, T1 and T8 vertebrae and H-Point for Scenarios 1 and 2 and left EAM, left shoulder and left knee for Scenario 3. The agreement between the predicted response and the sled test results was quantified using CORA v 4.0.4 [9]. CORA rating is a method to evaluate the time-history signals, the reference curve (physical test) and the predicted response (simulation). CORA uses two methods to calculate the signals correlation taking the physical tests as the reference: The corridor method calculates the deviation of the signal between two curves automatically created by the CORA software and the cross-correlation method evaluates some specific characteristics of the signal such as phase shift, size and shape. The total CORA score is calculated by adding the weighted ratings obtained from both methods and expressed in a scale from 0 to 1, where 1 represents a perfect correlation and 0 represents no correlation. According to the rating stipulated in ISO/TR 18571 the resultants of the CORA score are classified into four categories: Values above 0.94 are considered excellent, values between 0.94 and 0.8 are good, values between 0.8 and 0.58 are considered as a fair correlation and values below 0.58 are treated as a poor correlation.

The standard CORA implementation uses equal weighting for all the signals analysed for a load case. However, as the displacement of the analysed body landmarks differs substantially in magnitude (see Table IV(A), Table V(A) and Table VI(A)), i.e., the head displacement during the test was between five and ten times larger than the H-Point displacement, it was considered reasonable to weight the signals accordingly. Therefore, in this study it was chosen to weight the landmarks signals based on the magnitude of the landmark displacement (available in Table IV(A), Table V(A) and Table VI(A)) in the CORA analysis. The CORA scores for the individual landmarks and the total

score using the modified weighting factors can be seen in Table I(A), Table II(A) and Table III(A). The weighting factors can be seen in TABLE III.

TABLE III  
WEIGHTING FACTORS FOR THE SELECTED LANDMARKS OF EACH CRASH SCENARIO

	SCENARIO 1	SCENARIO 2	SCENARIO 3		
<i>Head</i>	0.483	0.409	<i>Head</i>	0.483	
<i>T1</i>	0.261	0.272	<i>Shoulder</i>	0.459	
<i>T8</i>	0.203	0.235	<i>Knee</i>	0.058	
<i>H-Point</i>	0.053	0.084	<i>Total</i>	1	
<i>Total</i>	1	1			

### III. RESULTS

Displacement plots in transverse and sagittal plane for all simulations are shown in Fig. 1(A), Fig. 2(A) and Fig. 3(A) (see Appendix) and compared with the corresponding physical tests for each crash scenario.

The results of the CORA analysis for all the model versions are shown in Table IV. Quantitatively, the morphed postured version has the highest CORA score in all three scenarios and each personification strategy leads to an improvement in the overall kinematic response compared to the sled tests. The CORA score for the X-axis, Y-axis and Z-axis landmarks displacement is provided in Table I(A), Table II(A) and Table III(A) (see Appendix).

TABLE IV  
CORA SCORES FOR THE THREE CRASH SCENARIOS

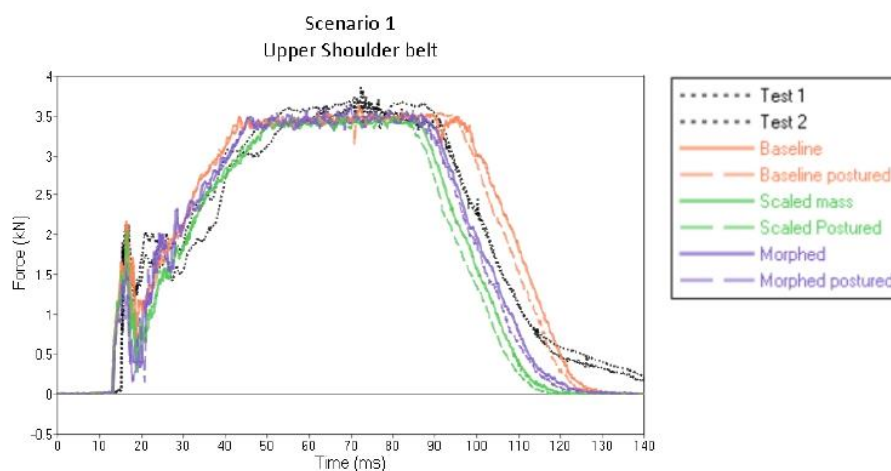
MODEL VERSION	BASELINE	SCALED MASS	MORPHED	BASELINE POSTURED	SCALED MASS POSTURED	MORPHED POSTURED
<i>Scenario 1</i>	0.644	0.648	0.650	0.664	0.675	0.684
<i>Scenario 2</i>	0.638	0.653	0.688	0.673	0.704	0.715
<i>Scenario 3</i>	0.565	0.637	0.684	0.654	0.679	0.713

#### Seatbelt forces

The elements selected for the force measurement during the simulation were selected in accordance with the location of the force transducers during the physical tests.

The belt forces recorded during the tests were used to adjust the parameters of the restrain system on the simulations. Peak values due to the pretensioner and the force limiter were established and the load curves were modified to resemble the physical tests for each scenario. The upper shoulder belt forces from the tests and simulations can be observed in Fig. 3.

During the rebound phase, the duration of the force limit value differs depending on the model version. For all three scenarios a longer duration was observed for the baseline and baseline postured versions than the versions in which the mass of the occupant was adjusted, not only during the rebound phase, but also during the loading phase in those cases in which a pretensioner was installed (scenarios 1 and 3).



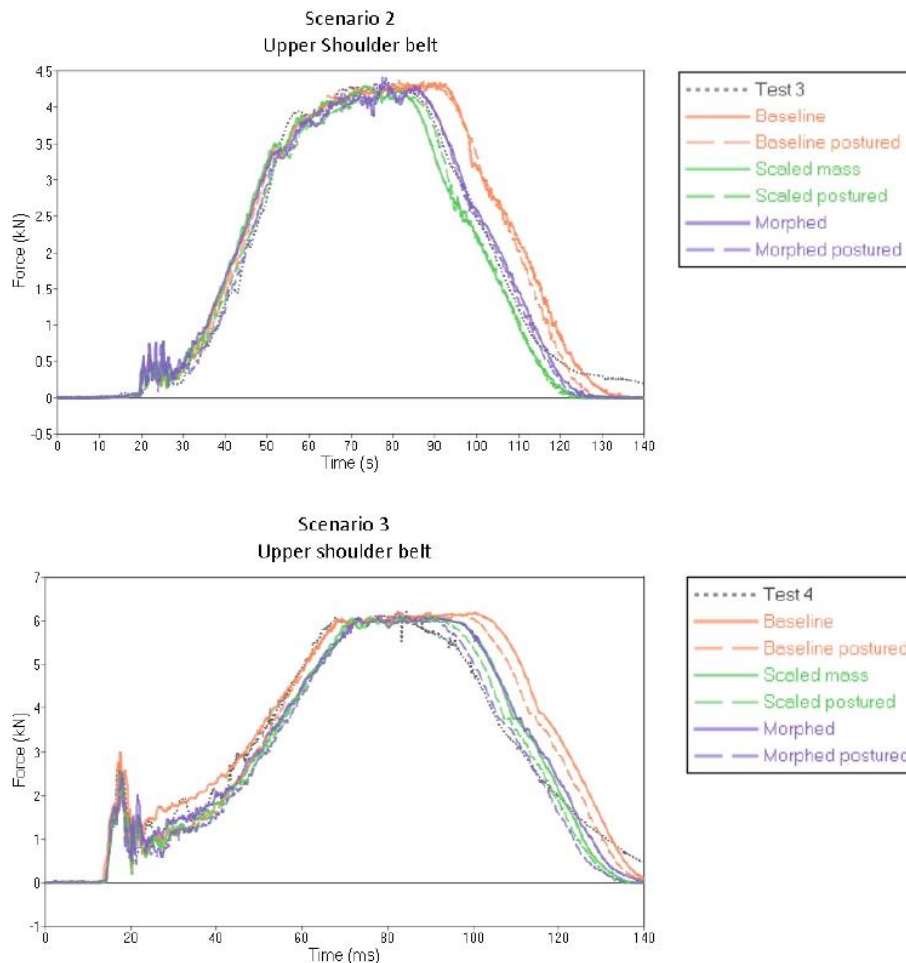


Fig. 3: Upper shoulder belt forces (kN) for the three scenarios.

### ***Nearside Oblique Impacts***

In these load cases, the PMHSs A, B and C were exposed to a nearside oblique impact at  $30^\circ$ . Due to the impact conditions, a significant lateral displacement was obtained.

A good biofidelity (CORA score  $>0.8$  according to the rating stipulated in ISO/TR 18571) was observed for the head displacement of the most personalised versions (0.733 and 0.847 for the morphed postured model version in both Scenarios 1 and 2, respectively), which decreased progressively along the spine until the H-Point, in which poor CORA score ( $\leq 0.58$ ) with the physical tests was found (0.387 and 0.495 for the morphed postured version).

The predicted displacement of T1 in Z-direction differed from the measured Z-displacement in the physical tests. In all simulations T1 moved downwards, while PMHS T1 moved slightly upwards in two of the three PMHS tests, only in one of the tests carried out in the Scenario 1, T1 follows the same tendency predicted by simulation. Consequently, a poor correlation for the T1 Z displacement was obtained, which decreased as the level of personalisation increased.

Similar patterns were obtained for the T8 behaviour. The occupants T8 tended to move upwards or keep a constant Z-coordinate during the PMHS tests. Thus, in all versions of the model, THUMS T8 moved below the Z-coordinate measured in the physical tests.

The highest CORA score for the H-Point was obtained for the morphed non-postured model in both Scenarios 1 and 2. Due to one of the retroreflective markers located on the H-Point was covered by the restrain system at 65 ms in the Scenario 2, H-Point displacement and CORA score were computed only until that time (see Fig. 2(A)).



### **Full frontal impact**

The third load case consisted of a full frontal impact with a restraint system composed by two separated sections of seatbelt. The diagonal portion and the lap portions of the belt were separated at the buckle. In this case, the analysis was carried out in the sagittal plane only, since there was no available information about the lateral kinematics. Unlike the previous tests, the landmarks studied were left EAM, shoulder and knee, instead of Head CoG, T1, T8 and H-Point, as indicators of the head, upper spine and pelvis displacement respectively.

As with the two previous scenarios, the CORA score for the head displacement was between 0.78 (for the baseline version) and 0.941 (for the morphed postured version). The shoulder moved upwards during the PMHS test, in the same way as in the oblique impacts, whereas the THUMS model predicted downward movement. Finally, poor CORA scores were obtained for the knee displacements (0.407 in the case of the baseline model version and 0.534 for the most personalised version of the model, which is the morphed version), similar to the values obtained for the H-Point in the oblique tests.

## **IV. DISCUSSION**

All personification techniques improved the predicted kinematics of the model, but to a different extent depending on the evaluated landmarks and the reference axis. For all scenarios, the highest CORA score was obtained for the morphed and postured model. Generally, the CORA score for the head was higher than for T1, T8, knee and pelvis. One explanation can be that the human body model in previous validation efforts was correlated and validated mainly for head displacement. The reason for that can be that there is less PMHS validation data available for T1, T8 and pelvis than for the head, therefore less validation efforts were put in to validate the prediction of T1, T8, and pelvis kinematics [1]. This fact highlights the need of continued efforts to generate more PMHS data for model validation.

The influence of personification techniques was greater in those cases in which the subject characteristics differ the most from the baseline THUMS model. For instance, this fact can be seen in the CORA score of Scenario 2 in which morphing shows a greater improvement in predicted kinematics than posturing compared to the baseline version. However, the morphed postured version (which involves all personification strategies) shows an improved rating compared to the corresponding PMHS test, as happened in all three scenarios. In the case of Scenario 1, the THUMS weight and shape most closely resembled the occupant's characteristics, but the pre-impact posture of the PMHS differed the most from the baseline model, as can be seen in Fig. 2 and Table II. Due to that, posturing has a greater influence on the kinematic response than the other strategies (mass scaling and morphing).

Nevertheless, personification of the THUMS model increased the agreement (higher CORA score) between the predicted and measured displacements more for the full frontal load cases than for the oblique load case. This despite the fact that the weight, shape and posture of the baseline THUMS model was more similar to the PMHSs in the full frontal load case. This fact can be explained looking into the CORA analysis of the three axis separately, available in Table I(A), Table II(A) and Table III(A) (see Appendix). In general, the personification techniques barely improved the lateral kinematics, which is consistent with the findings by [5]. Only in the Scenario 1, an improvement of the T8 and H-Point correlation was observed when the mass was adjusted to that of the PMHS. Regarding the X-axis, posturing and mass scaling lead to similar improvements in terms of the head kinematics, while the pelvis forward displacement was only sensitive to the mass scaling. The lowest similarity of results was observed for the pelvic vertical displacement which was little influenced when morphing. This effect can be due to the fact that one of the parameters used during the morphing of the models was the buttock circumference and the volume of flesh was significantly reduced with this strategy, hence, the pelvis displacement was more restricted because the contact between the pelvic bone and the lap belt was less cushioned by the soft tissues in the morphed versions.

In any case, poor agreement between predicted and measured pelvis displacement (lowest CORA score) was obtained. This fact can be due to several factors. One of these factors can be due to the modelling. The HBM was positioned onto the seat by means of a pre-simulation with a subsequent export of the node coordinates into the crash simulation without including the initial strains and stresses. This means that the model is not in equilibrium at  $t_0$  and the friction to the seat might be underestimated. Another reason for the poor CORA outcome for the H-point can be due to the HBM's buttock flesh modelling. In the sled tests, the "pelvic bone" information was

approximated as the H-Point marker located bilaterally on the flesh in the same Y-coordinate of the greater trochanter. The node followed during the simulations was selected according to that in all model versions. Either the pelvic bone or the buttock flesh (or both) can be inducing this deviation. A mesh quality check was done to the morphed and baseline models in order to identify potential discrepancies. The results showed that the mesh quality was unaffected by the morphing process.

Best agreement between predicted and measured response was obtained for the most personalised model. Nevertheless, future studies could also include other personalization strategies.

The HBM materials and geometry correspond to an adult male and PMHSs at the time of death were 64±4 year-old for the oblique impact load cases and 39 year-old occupant in the full-frontal impact, thus the material properties of the default HBM can play an important role in the observed discrepancies, since only density has been changed in the scaled mass version. Further, according to the autopsy of the PMHSs done after the sled tests (available in [11-12]), rib and clavicle fractures were observed. This can result in larger deformation of the thorax, which was not represented in the simulations. That can be one of the reasons why the X-displacement (see displacement time history provided in the Appendix) of T1, T8 and shoulder is underpredicted in the more personalised model versions.

Another age related aspect that could be considered in future studies is age related changes in body composition. The Anthropometric Survey of U.S. Army Personnel (ANSUR) anthropometric database used to predict some of the missing anthropometric measurements, is based on younger subjects which are probably more fit than the occupants of these experiments, thus, the muscles/fat/bone volume proportions might differ resulting in a non-accurate morphing of the skeleton. The bones geometry extracted from a seating position CT scan would reveal possible geometrical differences between the HBM and PMHSs.

## V. CONCLUSIONS

For the load cases included in this study, the more personalised the human body model was, greater the agreement between the predicted and measured kinematics. The personification have a grater influence when the HBM characteristics differ the most from the occupants.

Few improvements (only T8 and H-Point in the mass scaled model versions) were related to the lateral displacement of the observed anthropometric landmarks, thus the lateral kinematics were not sensitive to the studied personification strategies.

The lower spine kinematics is not being correctly predicted by the HBM and more effort should be done on the model validation.

This study demonstrates that the combination of the personification techniques improves the accuracy of the prediction of the occupant's kinematic and has the potential to cover a higher percentage of the population, which is not represented by the baseline models.

## VI. ACKNOWLEDGEMENT

The authors thank the donors and their families for their generous act, which was essential for this study. The authors acknowledge Autoliv Research and SAFER (Vehicle and Traffic Safety Centre at Chalmers University) in Sweden for the technical resources and funding which was fundamental for the development of this study. The authors extend their thanks to Ludwig-Maximilians Universität (LMU) in Germany for their technical assistance. This study was partially funded by the Instituto Aragonés de Fomento (IAF) of Gobierno de Aragón in Spain.

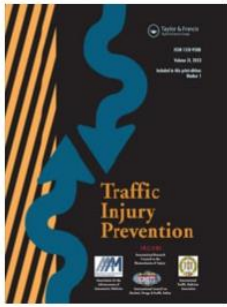
## VII. REFERENCES

- [1] Iwamoto M, Nakahira Y, Tamura A, Kimpara H, Watanabe I, Miki K. Development of Advanced Human Models in THUMS. *6th European LS-DYNA Users' Conference*, 2007, Gothenburg, Sweden.
- [2] Gayzik S, Moreno D, Vavalle N, Rhyne A, Stitzel J. Development of the Global Human Body Models Consortium mid-sized male full body model. *Injury Biomechanics Research*, pp. 39-12.

- [3] Elemance. "Virtual Human Body Models," Internet: [<http://www.elemance.com/virtual-human-body-models/>].
- [4] Beilas P, Berthet F. An investigation of human body model morphing for the assessment of abdomen responses to impact against a population of test subjects. *Traffic Injury Prevention*, 2017, pp. S142-S147.
- [5] Poulard D, Subit D, Donlon J, Lessley D, Kim T, Park G, Kent R. The Contribution of Pre-impact Spine Posture on Human Body Model Response in Whole-body Side Impact. *Stapp Car Crash Journal*, 2014, vol. 58, pp. 385-422.
- [6] Poulard D, Subit D, Nie B, Donlon J, Kent R. The Contribution of Pre-Impact Posture on Restrained Occupant Finite Element Model Response in Frontal Impact. *Traffic Injury Prevention*, 2015, pp. S87-S95.
- [7] Hwang E, Hu J, Chen C, Klein K, Miller C, Reed M, Rupp J, Hallman J. Development, Evaluation, and Sensitivity Analysis of Parametric Finite Element Whole-Body Human Models in Side Impacts. *Stapp Car Crash Journal*, 2016, vol. 60, pp. 473-508.
- [8] PIPER EU project, "piper-project.org" [<http://www.piper-project.org/>], 2017/11/10 [2018/01/11].
- [9] Gehre C, Gades H, Wernicke P. Objective rating of signals using test and simulation responses. *21st International Technical Conference on the Enhanced Safety of Vehicles Conference (ESV)*, 2009, Stuttgart, Germany.
- [10] Iwamoto M, Kisanuki Y, Watanabe I, Furusu K, Miki K. Development of a Finite Element Model of the Total Human Model for Safety (THUMS) and Application to Injury Reconstruction. *Proceedings of IRCOBI Conference*, 2002, Munich, Germany.
- [11] Iraeus J, Davidsson J, Brolin K. Recent HBM activities at Chalmers University. *Presentation at Conference: Human Body Modelling in Automotive Safety*, 2017, Berlin, Germany.
- [12] Afewerki H. Biofidelity Evaluation of Thoracolumbar Spine Model in THUMS. *Chalmers University of Technology*, Gothenburg, Sweden, 2016
- [13] Pipkorn B, López-Valdés F, Juste-Lorente Ó, Insausti R, Lundgren C, Sunnevång C. Assessment of an innovative seat belt with independent control of the shoulder and lap portions using THOR tests, the THUMS model and PMHS tests. *Traffic Injury Prevention*, pp. 124-130, 2016.
- [14] López-Valdés F, Juste-Lorente Ó, Maza-Frechín M, Pipkorn B, Sunnevång C, Lorente A, Aso-Vizan A, Davidsson J. Analysis of occupant kinematics and dynamics in nearside oblique impacts. *Traffic Injury Prevention*, 2016, pp. 86-92.
- [15] Shaw G, Parent D, Purtsezov S. Impact Response of Restrained PMHS in Frontal Sled Tests: Skeletal Deformation Patterns Under Seat Belt Loading. *Stapp Car Crash*, 2009, vol. 53, pp. 1-48.
- [16] López-Valdés F, Lau J, Lamp J. Analysis of Spinal Motion and Loads During Frontal Impacts, Comparison between PMHS and ATD. *Annual Proceedings of the Association of the Advanced of Automotive Medicine (AAAM)*, 2010, p. 2010:54.
- [17] Shaw G, Parent D, Purtsezov S, Lessley D, Crandall J, Kent R, Guillemot H, Ridella SA, Takhounts E, Martin P. Impact response of restrained PMHS in frontal sled tests: skeletal deformation patterns under seat belt loading. *SAE Technical Paper*, 2009 Nov 2.
- [18] Wu G, Siegler S, Allard P, Kirtley C, Leardini A, Rosenbaum D, Whittle M, D'Lima D, Cristofolini L, Witte H, Schmid O. ISB recommendation on definitions of joint coordinate system of various joints for the reporting of human joint motion -- part I: ankle, hip and spine. *Journal of Biomechanics*, 2002, Vols. 35(4):543-8.

**PAPER B**

**Analysis of the Spinal 3D Motion of Post-Mortem Human Surrogates  
in Nearside Oblique Impacts**



## Traffic Injury Prevention



ISSN: (Print) (Online) Journal homepage: <https://www.tandfonline.com/loi/gcpi20>

# Analysis of the spinal 3D motion of postmortem human surrogates in nearside oblique impacts

Ana Piqueras, Bengt Pipkorn, Johan Iraeus, Ana I. Lorente, Óscar Juste-Lorente, Mario Maza & Francisco J. López-Valdés


To cite this article: Ana Piqueras, Bengt Pipkorn, Johan Iraeus, Ana I. Lorente, Óscar Juste-Lorente, Mario Maza & Francisco J. López-Valdés (2023) Analysis of the spinal 3D motion of postmortem human surrogates in nearside oblique impacts, *Traffic Injury Prevention*, 24:1, 69-74, DOI: [10.1080/15389588.2022.2152282](https://doi.org/10.1080/15389588.2022.2152282)

To link to this article: <https://doi.org/10.1080/15389588.2022.2152282>

 View supplementary material 

 Published online: 13 Dec 2022.

 Submit your article to this journal 







 Article views: 154

 View related articles 

 View Crossmark data 



## Analysis of the spinal 3D motion of postmortem human surrogates in nearside oblique impacts

Ana Piqueras<sup>a</sup> , Bengt Pipkorn<sup>b</sup>, Johan Iraeus<sup>c</sup> , Ana I. Lorente<sup>a</sup> , Óscar Juste-Lorente<sup>a</sup> , Mario Maza<sup>a</sup> , and Francisco J. López-Valdés<sup>d</sup> 

<sup>a</sup>Impact Laboratory, Aragon Institute for Engineering Research (I3A), University of Zaragoza, Zaragoza, Spain; <sup>b</sup>Autoliv Research, Vargarda, Sweden; <sup>c</sup>Division of Vehicle Safety, Department of Mechanics and Maritime Sciences, Chalmers University of Technology, Sweden; <sup>d</sup>Instituto de Investigación Tecnológica (IIT), ICAI, Universidad Pontificia Comillas, Madrid, Spain

### ABSTRACT

**Objective:** The objective of this study is to analyze the 6 degrees of freedom (DOF) motion of the spine using the finite helical axis (FHA) in three postmortem human surrogates (PMHS) sled tests.

**Methods:** The sled test configurations corresponded to a 30° nearside oblique impact at 35 km/h. Two different restraint system versions (RSv) were used. RSv1 was used for PMHS A and B while RSv2 was used for PMHS C. The 6 DOF motion of the head and three selected vertebrae have been analyzed using the FHA which describes the 3D motion of a rigid body between two instants of time as a rotation about and a translation along a unit vector. A minimal amount of rotation is necessary to the FHA calculation, thus the FHA components have been calculated based on a pre-defined interval of 8° of rotation.

**Results:** The analysis of the FHA components demonstrated right lateral bending until around 100ms, when the rebound phase was reached and the head and the lower spine undergoes left lateral bending. The three PMHS exhibited, in general, flexion movement of the whole body and torsion to the right side of the occupant. This general motion can be associated to the effect of the seatbelt acting as a fulcrum of the rotational movement of the bony landmarks. The interaction of the PMHS with the retention system can be noted by analyzing the time in which the head and the upper spine initiated the rotation and the sudden changes of rotational direction of the three PMHS's head.

**Conclusions:** The rotational analyses have shown to be more sensitive to experimental events than the trajectory analyses for the studied physical tests. Additionally, the results presented in the present study contributes to the analysis of the body kinematics during an oblique impact and adds new experimental data for Human Body Models (HBM) and Anthropometric Test Devices (ATD) benchmarking.

### ARTICLE HISTORY

Received 23 June 2022  
Accepted 23 November 2022

### KEYWORDS

Finite helical axis (FHA); kinematics; nearside oblique impact; Post Mortem Human Surrogates (PMHS); spine

### Introduction

After severe frontal crashes, oblique and small overlap crashes are the second most common crash type leading to fatal injury (Bean et al. 2009). A recent NASS/CDS study also reported that oblique impact is the most prevalent collision configuration leading to serious injuries (Suarez-del Fuego et al. 2021).

Recognizing this reality, several institutions have proposed testing programs to enhance occupant protection in oblique loading: The Insurance Institute for Highway Safety introduced in 2012 the small overlap configuration in their consumer rating portfolio (IIHS 2012); in the Euro NCAP/ANCAP Moving Progressive Deformable Barrier test, a moving barrier impacts the vehicle with 50% overlap (ANCAP 2020); and in 2015, NHTSA released a request for comment pertaining to including a new oblique test using a moving deformable barrier impacting a stationary vehicle at 15° (NHTSA 2015).

Despite their unquestionable contribution to reduce the number and severity of injuries, Anthropometric Test Devices (ATD) have shown limited capabilities to predict the spinal kinematics compared with Post Mortem Human Surrogate (PMHS) sled tests even in frontal impacts (Lopez-Valdes et al. 2010; Pipkorn, López-Valdés, Juste-Lorente, Insausti, et al. 2016). When lateral bending and axial torsion of the spine are induced by the asymmetric load of the three-point seatbelt, these ATD limitations can lead not only to unrealistic spine and neck loads, but also to errors in the estimation of chest deflections that are evaluated with respect to the spine (Shaw et al. 2013). Therefore, Hwang et al. (2020) suggested the use of Finite Element Human Body Models (HBM) for a detailed assessment of human response in lateral loading.

Experimentally, the occupant spine kinematics during a crash has been frequently analyzed as the 2D trajectories of selected vertebrae both in the sagittal and transverse planes (López-

Valdés et al. 2016; Piqueras et al. 2018; Poulard et al. 2015). However, the 3D rigid body rotation of vertebrae has rarely been addressed in experimental studies, and therefore the validation of the capabilities of ATD and HBM to describe 3D spinal rotations is very limited.

The different methodologies to represent the 3D rotation of anatomical structures have been discussed extensively in the literature (Kinzel et al. 1972; Medendorp et al. 1998; Woltring et al. 1994). Some authors have preferred the finite helical axis (FHA) formulation over other methods, such as Eulerian/Cardanic angles, in 3D rotations to avoid the potential ambiguity caused by the angle sequence dependence (Anderst and Aucie 2017; Kettler et al. 2004; Medendorp et al. 1998; Woltring 1991). An additional difficulty associated to the Euler angles is that successive rotations are calculated with respect to local coordinate systems (LCS) that are oriented based on the previous rotations. These LCS are different from subject to subject and, therefore, the inter-subject comparison is not straightforward. As an alternative, the FHA describes an axis that characterizes the 3D motion of a rigid body between two instants of time as a rotation about and a translation along its unit vector. Since the rotation of the spine is not necessarily aligned with any of the anatomical axes, the FHA allows to report the actual axis of rotation in a global coordinate system that is comparable across different subjects (Kettler et al. 2004). The only previous research that used the FHA to characterize the 3D rotation in frontal impacts, showed correlation between the components of the unit axis of the FHA and the interaction between the seatbelt and the torso of the occupant, also highlighting the capability of the FHA to identify vertebral fractures (Lopez-Valdes et al. 2014).

Thus, the objective of this study is to analyze the 6-DOF motion of the spine using the FHA as the preferred method to report the 3D rotation of the head and vertebrae in three PMHS sled tests. The experiments represented oblique nearside collisions at a 30 degree angle of front seat passengers using contemporary three-point seatbelts (López-Valdés et al. 2016).

## Methods

### PMHS test and experimental setup

Three PMHS were exposed to 30° nearside oblique impact resulting in a nominal change of velocity of 34 km/h as described in López-Valdés et al. (2016). The tests were carried out using the Gold Standard test fixture described in detail in Pipkorn, Lopez-Valdes, Juste-Lorente, Maza, et al. (2016; Figure 1).

The test fixture consisted of a rigid metallic frame and rigid seat approximating the occupant position in a vehicle while permitting visual access to the subject and instrumentation. The seat included a ramp in the posterior/anterior and lateral directions to prevent excessive motion of the occupant's pelvis and mimicking modern seat designs with anti-submarining structures.

The occupant was restrained with a three-point seatbelt in a passenger position in two different Restraint System versions (RSv). Both RSv had a shoulder belt with a 4.5 kN force limiter and a lap belt with a 3.5 kN outboard pretensioner, but, additionally, RSv1 had a shoulder belt pretensioned at 2 kN. Test

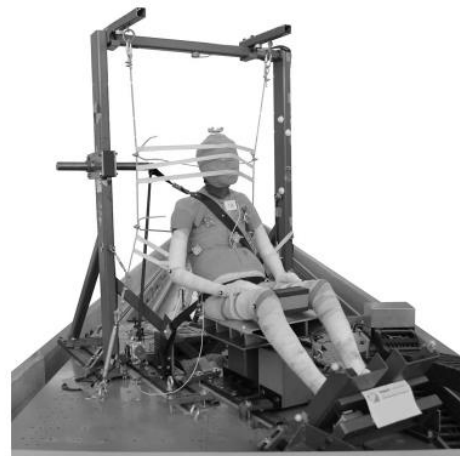


Figure 1. PMHS sled test configuration.

conditions and individual characteristics of the PMHS are summarized in Table A1 and the time history of the sled pulse deceleration is shown in Figure A1 (see supplementary material).

Procurement, handling and testing of the PMHS was done under the approval of the Ethical Commission for Clinical Research of Aragon (CEICA).

### Instrumentation

Kinematic data were collected at 1 kHz using an optoelectric stereo-photogrammetric system consisting of 10 cameras (Vicon, TS series, Oxford, UK). The system captured the position of clusters of four retro-reflective spherical markers within a calibrated 3D volume. Clusters of markers were rigidly attached to the head and to the upper, middle and lower sections of the spine (T1, T8 and L2 vertebrae). Due to the cadaver preparation process, the clusters for the subject C (RSv2), were attached to T4, T7 and L1. The position of the mid hip joint (H-point) was calculated as the average position of markers attached externally to the position of the greater trochanter. The H-point was used as reference for the spinal position. Belt tension was acquired at 10 kHz with four force transducers installed at inner and outer locations on the shoulder and lap belt bands (Figure A2).

### Spine rotation representation (finite helical axis)

The methodology used to report the rotation of the anatomical locations from the Vicon recording, is based on the work described in Kinzel et al. (1972) and discussed extensively by Shaw et al. (2009). The vertebrae LCS origin was placed in the mid-point of the superior and inferior endplate's center obtained from measurements taken from CT scans of each PMHS. The head LCS origin was located in the midpoint between the two External Auditory Meati. In both cases and for the Global Coordinate System (GCS) used as reference, X-axis pointed forward, Y-axis pointed to the right and Z-axis pointed inferiorly according to the SAE J211 recommendations (Society of Automotive Engineers 2014).

The 3D rigid body motion between two positions is characterized using the transformation matrix (T). This matrix is

composed by the rotation matrix ( $R_{3 \times 3}$ ) and the position of a point of the rigid body ( $P_{3 \times 1}$ ) with respect to a reference coordinate system (Eq. (1)). In this study, this matrix was calculated for each anatomical location and expressed with respect to a common coordinate system for the three PMHS.

$$T_{B/G}(t) = \begin{bmatrix} R_{3 \times 3} & P_{3 \times 1} \\ 0_{1 \times 3} & 1 \end{bmatrix} \quad (1)$$

The matrix  $T_{B/G}(t)$  associated to the motion of a particular bone (B) with respect to the GCS (G) cannot be measured directly as there is not visual access to the bone coordinate system. This matrix was obtained as the product of the transformation matrix between the LCS of the bone referred to the LCS created at the markers cluster ( $T_{B/M}$ ) and the transformation matrix between the LCS of the marker cluster and the global coordinate system ( $T_{M/G}(t)$ ), as shown in Eq. (2).  $T_{B/M}$  is constant in time and depends only on the geometry of the assembly connecting the Vicon markers to the bone and  $T_{M/G}(t)$  changes in time and is given from the tracking of the markers.

$$T_{B/G}(t) = T_{B/M} \cdot T_{M/G}(t) \quad (2)$$

Once the transformation matrix  $T_{B/G}(t)$  is obtained with respect to the GCS, the FHA can be calculated according to the equations proposed by Spoor and Veldpaus (1980). The FHA describes the 3D motion of a rigid body between two instants of time as a rotation about and a translation along a unit vector. It is called *finite* because it discretizes the continuous motion of the rigid body in time and, therefore, approximates the definition of the instantaneous helical axis (Woltring 1994). If R is the rotation matrix within the calculated  $T_{B/G}(t)$  of one of the selected bones with elements  $R_{ij}$  ( $i, j = 1, 2, 3$ ), the angle rotated about the FHA ( $\varphi$ ) can be calculated from Eq. (3):

$$\sin(\varphi) = \frac{1}{2} \sqrt{(R_{21} - R_{12})^2 + (R_{32} - R_{23})^2 + (R_{13} - R_{31})^2} \quad (3)$$

The components of the unit vector  $\bar{u}$  are given by Eq. (4):

$$\bar{u} = \begin{bmatrix} ux \\ uy \\ uz \end{bmatrix} = \frac{1}{2\sin(\varphi)} \begin{bmatrix} R_{32} - R_{23} \\ R_{13} - R_{31} \\ R_{21} - R_{12} \end{bmatrix} \quad (4)$$

When the rotation of the rigid body is aligned with a coordinate axis, the corresponding component of the FHA will be equal to 1 or -1. The sign of the component indicates whether the rotation occurs around the positive or the negative axis orientation following the right-hand rule. For instance, if the head rotates around the Y-axis in flexion (toward the chest) between two instants of time,  $ux$ ,  $uy$  and  $uz$  components of the FHA would be equal to 0, -1 and 0 respectively, according to the SAE J211 convention.

As the FHA is used to model the motion between two positions, the closer these two positions are, the more accurate the motion description given by the FHA is. However, small values of the rotation angle  $\varphi$  can produce indeterminate results (Eq. (4)) (Medendorp et al. 1998; Woltring 1994). To avoid this, it was decided to calculate the transformation matrix for positions (p) separated by a  $8^\circ$  rotation ( $T_{B(p)/B(p-8^\circ)}$ ) (Eq. (5)).

$$T_{B(p)/B(p-8^\circ)} = [T_{B(p-8^\circ)/G}]^{-1} \cdot T_{B(p)/G} \quad (5)$$

The components of the unit vector of the FHA every  $8^\circ$  can be obtained from Eq. (4). The calculation of the FHA from the bone transformation matrix ( $T_{B/G}(t)$ ) was carried out using Matlab and the scripts used for this calculation are available in Appendix B.

## Results

### Head and vertebrae displacement

The displacements of the head and selected vertebrae of the occupant in the sagittal and transverse planes are shown in Figures C1–C3. After reaching maximum displacement in the X and Y-axes, the three tested subjects started to rebound between 80 and 100 ms.

A downward displacement of the head from the beginning of the deceleration was observable in subjects restrained with RSv1. Additionally, the distance between the traces on the sagittal plane (XZ) indicate a smaller forward displacement of the bony landmarks before the rebound phase compared with the RSv2, suggesting that the seatbelt provided an earlier engagement with the occupants. However, in the subject in RSv2 (without seatbelt shoulder pretensioner), the traces that represent spine alignment remained almost parallel for the first 60 ms of the deceleration in both sagittal and transverse planes.

Table 1 summarizes the maximum displacements for the PMHS' selected landmarks. For the condition RSv1, the forward displacements (X) presented smaller values than those obtained on RSv2 for all spine levels and the head. On the contrary, the RSv2 condition showed smaller values of maximum lateral displacement (Y) for the head than those exhibited by the RSv1 subjects. However, the lower spine and the H-point presented higher lateral displacements than those observed for RSv1. This can be also identified in Figures C1–C3. Note that the values in the table have been normalized by the peak displacement in each axis among the three subjects to facilitate the comparison between them.

Regarding the vertical displacement (Z), the upper spine exhibited positive maximum values for the condition RSv1, which means downwards displacement, while the same spinal segment in RSv2 exhibited the opposite behavior.

### Global rotation of the head and spine

The results herein included correspond to the FHA unit vector of each bony landmark relating the initial position of the bone ( $t = 0$ ms) with the position at  $t = 140$ ms, regardless of the intermediate positions and attitudes of the rigid bodies. Table 2 shows the FHA components ( $ux$ ,  $uy$  and  $uz$ ) of each landmark referred to the GCS and the angle ( $\varphi$ ) of the landmark rotated about the FHA. While this global motion does not describe the time history of the bones rotation, it provides a visual description of the overall PMHS kinematics.

In the three PMHS experiments, the head rotated ( $\varphi$ ) between  $124$  and  $161^\circ$  around an axis that was primarily aligned with the negative Y-axis which corresponds anatomically with a flexion motion of the head. The total angle rotated by the



**Table 1.** Three-axial maximum displacement (disp) in millimeters and normalized (Norm) by maximum displacement in each axis.

		RSv1				RSv2	
		PMHS A		PMHS B		PMHS C	
		disp (mm)	Norm	Disp (mm)	Norm	disp (mm)	Norm
X	Head	220	0.73	210	0.70	301	1.00
	Upper spine	144	0.48	151	0.50	220	0.73
	Middle spine	105	0.35	110	0.36	190	0.63
	Lower spine	49	0.16	60	0.20	111	0.37
	H-point	21	0.07	24	0.08	57	0.19
Y	Head	251	0.85	297	1.00	230	0.78
	Upper spine	122	0.41	190	0.64	131	0.44
	Middle spine	97	0.33	117	0.40	118	0.40
	Lower spine	84	0.28	47	0.16	115	0.39
	H-point	32	0.11	41	0.14	58	0.20
Z	Head	296	0.96	307	1.00	295	0.96
	Upper spine	34	0.11	76	0.25	-44	-0.14
	Middle spine	-25	-0.08	-19	-0.06	-38	-0.12
	Lower spine	-29	-0.10	43	0.14	-36	-0.12
	H-point	-20	-0.06	-15	-0.05	-19	-0.06

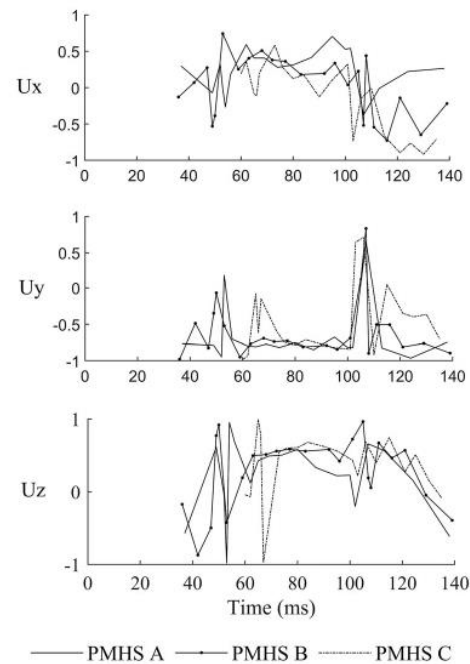
**Table 2.** Components of the unit vector and angle (deg) of rotation about the axis of rotation connecting the initial and the position at  $t = 140$ ms of the subjects' landmarks.

		RSv1		RSv2
		PMHS A	PMHS B	PMHS C
Head	ux	0.304	-0.019	-0.233
	uy	-0.880	-0.924	-0.939
	uz	0.365	0.383	0.251
	$\varphi$	123.88	161.27	138.74
Upper spine	ux	0.215	0.746	0.482
	uy	-0.573	-0.627	-0.789
	uz	0.791	0.224	0.380
	$\varphi$	60.28	76.12	53.62
Middle spine	ux	0.242	0.72	0.311
	uy	-0.688	-0.514	-0.804
	uz	0.684	0.467	0.507
	$\varphi$	41.93	46.30	53.84
Lower spine	ux	0.115	0.589	0.461
	uy	-0.683	-0.678	-0.782
	uz	0.721	0.440	0.420
	$\varphi$	26.98	34.79	34.97

vertebrae was smaller than that of the head (between  $29^\circ$  and  $76^\circ$ ) and it was observed to decrease along the spine from upper to lower sections. Regarding the differences between both restraint conditions, for the RSv2, the FHA components revealed that the rotation of the vertebrae was also primarily aligned with the negative Y-axis, but to a lower extent than the head. Nevertheless, under condition RSv1 the rotation occurs around an axis that cannot be considered aligned with any of the axes of the LCS and the predominant FHA component was the Z-axis for PMHS A and X-axis for PMHS B, except the middle and lower spine respectively where the Y-axis was the predominant component.

### Detailed rotation of the head and spine

The calculation of the components of the FHA unit axis was performed every  $8^\circ$  of rotation intervals for each bone, so that the time evolution of the actual motion could be provided. Figure 2 shows the FHA components of the head and the complete

**Figure 2.** Time history plots of the components of the unit vector of the FHA ( $u_x$ ,  $u_y$  and  $u_z$ ) of the head calculated every  $8^\circ$  for all bony landmarks of the three subjects.

analysis for all bony landmarks can be seen at Figure C4 (see supplementary material).

**X-axis:** All four landmarks exhibited, in general, near-zero or positive  $u_x$  values until around 100 ms when the arm contacted the head and changed the rotation direction. This indicates that the bony landmarks tended to turn clockwise around the X axis toward the right side of the occupant, consistent with the whole spinal motion observed in Figures C1–C3. The lower spine reached negative rotation values around the X axis after 80 ms while the head and the upper spine changed the sign of the rotation after 100 ms.

**Y-axis:** For the three PMHS, the head  $u_y$  FHA component exhibited, in general, values near to  $-1$ , indicating a pure flexion. Regarding the vertebrae, the  $u_y$  component of the FHA showed, mainly, negative values. However, the rotation occurs around an axis that cannot be considered aligned with any of the axes of the LCS for most of the duration of the tests. The primary axis of rotation (that component with the highest value) varies during the time-history of the FHA components.

**Z-axis:** The near-zero and positive values exhibited by the  $u_z$  component reveal a clockwise rotation around the Z axis toward the right side of the occupant. While the head and upper spine showed positive rotation, the middle and lower spine exhibited near-zero values until around 80 ms when the  $u_z$  becomes positive.

Concerning the differences between both restraint conditions, the traces of the unit vector components of the head, and therefore, the rotation, started at  $t = 37$ ms for PMHS A and  $t = 36$ ms for PMHS B, while it is not until  $t = 60$ ms that a rotation greater than  $8^\circ$  occurs in PMHS C. This shows how the pretensioner involved on RSv1 causes the seatbelt to interact earlier with the occupant inducing the spinal vertebrae to rotate.

## Discussion

The 6-DOF motion of the head and selected vertebrae has been analyzed using the FHA method to describe the rotational behavior of the bones, allowing inter-subject comparisons of the rotations with respect to the same coordinate system. The rotational analyses have shown to be more sensitive to experimental events than the trajectory analyses for the three tests analyzed within this study. To the authors knowledge this is the first study reporting the in-situ 6-DOF motion of the head and spine during oblique impacts and adds new experimental data for HBM and ATD benchmarking. In this regard, the present work complements the results included in Piqueras et al. (2018) that focused on the comparison of the displacements of selected bony landmarks between test subjects and HBM.

Other studies have reported the analysis of spinal segments rotations using the FHA for in vitro analysis of spinal segments (Kettler et al. 2004; Medendorp et al. 1998; Woltring et al. 1994). Prior to the current study, Lopez-Valdes et al. (2014) was the only author that characterized the head and spine 6-DOF motion during a sudden deceleration of the human body.

### FHA calculation

The FHA components have been calculated based on a pre-defined interval of rotation instead of using a time interval, because a minimal amount of rotation movement is necessary to the FHA calculation. It has been shown that the accuracy of the results, are related to the length of this interval (Panjabi 1979; Spoor 1984; Woltring et al. 1985). For the tests within this study, the 8° interval has been found to be long enough to avoid indeterminate results without losing information about variations attributed to physical events. Sudden changes of rotational direction of the three PMHS's head were observed for the same intervals in which trajectory discontinuities were found. Between 100 and 110 ms, the right arm contacted the head during the experiments, which affected the three components of the heads' FHA. Fluctuations at the beginning of the rotations observed for some landmarks in Figures 2 and C4 might be an effect of the shoulder belt forces (Figure A2).

### Comparison between RS conditions

The effect of the pretensioner can be noted by analyzing the time in which the head and the upper spine undergo more than 8 degrees of rotation. This implies that the seatbelt started the interaction with the body earlier in RSv1 leading to lower values of maximum forward excursion. The effect of the pretensioner firing caused that, for the very first instant of the body movement, the upper and middle spine presented Y positive rotations indicating an initial extension of the spine, which was not visible for the RSv2 condition. Additionally, the subjects under condition RSv1 exhibited a downward displacement, different to RSv2 and the typically observed movement in PMHS, volunteer and ATD frontal impacts (Arbogast et al. 2009; Lopez-Valdes et al. 2010, 2014).

Some of these results could have been influenced by the difference in the Vicon clusters location (T1, T8 and L2 for RSv1

and T4, T7 and L1 for RSv2), however most of them are referred to the head or are consistent for all vertebrae, such as the predominant axis of rotation and the distance between displacement traces. Due to the foregoing, it was considered that the dissimilarities between RS conditions were most likely attributed to the pretensioner activation. Only in the maximum displacement analysis (Table 1) the similar results obtained for the upper spine lateral displacement can be attributed to the instrumentation.

### FHA components analysis

The three PMHS exhibited, in general, negative uy values indicating flexion movement of the whole body. The ux positive values demonstrated right lateral bending until around 100 ms, when the rebound phase started and the head and the lower spine showed ux values from 0 to -1. Despite the differences in the restraint system used and in the impact direction, these movements are comparable to those published by Lopez-Valdes et al. (2014) except for the uz. The mentioned study consisted of three 40 km/h PMHS sled tests in driver position exposed to frontal impact using a non-pretensioned and non-force-limited 3-point seatbelt where the pelvic motion was restricted with a knee bolster. For the present study, the four bony landmarks uz component of the FHA presented, in general, positive values corresponding to torsion to the right side, while Lopez-Valdes et al. (2014) found negative values due to the driver seatbelt configuration (which was opposite to the one used in this study). The mentioned author addressed that this general motion can be associated to the effect of the seatbelt acting as a fulcrum of the rotational movement of the bony landmarks.

Table D2 shows the analysis of the rotation until the time of maximum x-displacement of the bony landmarks (see Table D1) to be compared with the results obtained by Lopez-Valdes et al. (2014) in frontal impacts. The head angle magnitudes for the current work under oblique impacts (82°, 80° and 74°) showed higher values than those obtained by Lopez-Valdes et al. (2014; 68°, 71° and 69°), despite the lower  $\Delta v$  and the retention system. In contrast, the vertebrae of the subjects under oblique impact presented smaller values of  $\varphi$  (31.11°±10.36°) than those exposed to frontal impacts (54.45°±11.35°).

The oscillations observed on Figure 2 were attributed to the seatbelt interaction and the arm contact with the head can be also noted in Figures C1–C3 in the 2 D analysis of PMHS B and C. However, the trajectory traces of PMHS A (Figure C1) do not show such oscillations. This means that some experimental events acquired with the 6-DOF analysis can remain unnoticed by means of the trajectory analysis.

### Limitations

Belt markers were covered by the PMHS body during the motion of the occupant, limiting the reconstruction of the belt path and avoiding the evaluation of the belt as a fulcrum. It should be noted that the attachment of the marker cluster to the bony landmarks required the perforation of the vertebrae pedicle compromising the integrity of the bone. However, this methodology initially proposed in Shaw et al. (2009) is, to our

knowledge, the only available method to measure the in situ 3 D kinematics of the spine during an impact. During the PMHS preparation process, one of the goals was to avoid disturbing the soft tissue to the extent possible. The specific anthropometry of PMHS C made particularly challenging the correct identification of the vertebral levels without removing a large amount of muscular tissue. This caused the spine clusters location at T4, T7 and L2, differing from the location in PMHS A and B (T1, T8 and L2). However, as mentioned in the discussion section, the dissimilarities between RSv were not attributed to the instrumentation differences since they are referred to the head or are consistent for all vertebrae.

This study was carried out with a small sample of individuals and only one subject was studied under the RSv2. Thus, more experimental data are required, covering different impact angles, subject ages, sex and anthropometrical characteristics, to fully understand the 6 DOF motion of the spine during sudden deceleration of the human body.

### Acknowledgements

The authors thank the donors and their families because without their generous act this study would have never existed.

### Disclosure statement

The authors have no known conflict of interest related to this paper.

### Funding

The author(s) reported there is no funding associated with the work featured in this article.

### ORCID

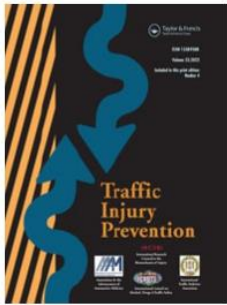
Ana Piqueras  <http://orcid.org/0000-0002-0019-4103>  
 Johan Iraeus  <http://orcid.org/0000-0001-9360-0707>  
 Ana I. Lorente  <http://orcid.org/0000-0001-8292-6613>  
 Óscar Juste-Lorente  <http://orcid.org/0000-0002-3398-067X>  
 Mario Maza  <http://orcid.org/0000-0003-1261-8847>  
 Francisco J. López-Valdés  <http://orcid.org/0000-0003-3167-5732>

### References

- ANCAP. 2020. ANCAP test protocol. Mobile Progressive Deformable Barrier.
- Anderst WJ, Aucie Y. 2017. Three-dimensional intervertebral range of motion in the cervical spine: does the method of calculation matter? *Med Eng Phys*. 41:109–115.
- Arbogast KB, Balasubramanian S, Seacrist T, Maltese MR, Garcia-Espana JF, Hopely T, Constans E, Lopez-Valdes FJ, Kent RW, Tanji H, et al. 2009. Comparison of kinematic responses of the head and spine for children and adults in low-speed frontal sled tests. *Stapp Car Crash J*. 53:329–372.
- Bean JD, Kahane CJ, Mynatt M, Rudd RW, Rush CJ, Wiacek C. 2009. Fatalities in frontal crashes despite seat belts and air bags. *National Highway Traffic Safety Administration (NHTSA)*. p. 88.
- Hwang E, Hu J, Reed MP. 2020. Validating diverse human body models against side impact tests with post-mortem human subjects. *J Biomech*. 98:109444.
- IIHS. 2012. Small overlap frontal crashworthiness evaluation crash test protocol (version I). p. 25.
- Kettler A, Marin F, Sattelmayer G, Mohr M, Mannel H, Dürselen L, Claes L, Wilke HJ. 2004. Finite helical axes of motion are a useful tool to describe the three-dimensional in vitro kinematics of the intact, injured and stabilised spine. *Eur Spine J*. 13(6):553–559.
- Kinzel GL, Hall AS, Hillberry BM. 1972. Measurement of the total motion between two body segments-I. Analytical development. *J Biomech*. 5(1):93–105.
- López-Valdés FJ, Juste-Lorente Ó, Maza-Frechín M, Pipkorn B, Sunnevang C, Lorente A, Aso-Vizan A, Davidsson J. 2016. Analysis of occupant kinematics and dynamics in nearside oblique impacts. *Traffic Inj. Prev*. 17(sup1):86–92.
- Lopez-Valdes FJ, Lau A, Lamp J, Riley P, Lessley DJ, Damon A, Kindig M, Kent R, Balasubramanian S, Seacrist T, et al. 2010. Analysis of spinal motion and loads during frontal impacts. Comparison between PMHS and ATD. In: *Annals of Advances in Automotive Medicine - 54th Annual Scientific Conference*. p. 61–77.
- Lopez-Valdes FJ, Riley PO, Lessley DJ, Arbogast KB, Seacrist T, Balasubramanian S, Maltese M, Kent R. 2014. The six degrees of freedom motion of the human head, spine, and pelvis in a frontal impact. *Traffic Inj. Prev*. 15(3):294–301.
- Medendorp WP, Melis BJ, Gielen CC, Gisbergen JA. 1998. Off-centric rotation axes in natural head movements: Implications for vestibular reafference and kinematic redundancy. *J Neurophysiol*. 79(4):2025–2039.
- NHTSA. 2015. New car assessment program. *National Highway Traffic Safety Administration (NHTSA)*. p. 56928–56935.
- Panjabi MM. 1979. Centers and angles of rotation of body joints: A study of errors and optimization. *J Biomech*. 12(12):911–920.
- Pipkorn B, López-Valdés FJ, Juste-Lorente O, Insausti R, Lundgren C, Sunnevang C. 2016. Assessment of an innovative seat belt with independent control of the shoulder and lap portions using THOR tests, the THUMS model, and PMHS tests. *Traffic Inj. Prev*. 17(sup1):124–130.
- /tcgqzPipkorn B, Lopez-Valdes FJ, Juste-Lorente O, Maza M, Sunnevang C. 2016. Study of the kinematics of the THOR dummy in nearside oblique impacts. In: *Proceedings of IRCOBI Conference*. Vol. 2016. p. 637–648.
- Piqueras A, Iraeus J, Lorente AI, López-Valdés FJ, Juste-Lorente Ó, Maza-Frechín M, Pipkorn B. 2018. Kinematic assessment of subject personification of human body models (THUMS). In: *Proceedings of IRCOBI Conference*. Vol. 2018. p. 191–206.
- /tcgqzPoulard D, Subit D, Nie B, Donlon JP, Kent RW. 2015. The contribution of pre-impact posture on restrained occupant finite element model response in frontal impact. *Traffic Inj. Prev*. 16(sup2):S87–S95.
- Shaw G, Lessley D, Ash J, Crandall J, Parent D. 2013. Response comparison for the hybrid III, THOR mod kit with SD-3 shoulder, and PMHS in a simulated frontal crash. In: *23rd ESV Conference*. p. 1–19.
- Shaw G, Parent D, Purtsezov S, Lessley D, Crandall J, Kent R, Guillemot H, Ridella S a, Takhounts E, Martin P. 2009. Impact response of restrained PMHS in frontal sled tests: skeletal deformation patterns under seat belt loading. *Stapp Car Crash J*. 53:1–48.
- Society of Automotive Engineers. 2014. *Instrumentation for impact test*. Warrendale (PA): Society of Automotive Engineers: SAE J211.
- Spoor CW, Veldpaus FE. 1980. Rigid body motion calculated from spatial co-ordinates of markers. *J Biomech*. 13(4):391–393.
- Spoor CW. 1984. Explanation, verification and application of helical-axis error propagation formulas. *Hum Mov Sci*. 3(1–2):95–117.
- Suarez-del Fueyo R, Junge M, Lopez-Valdes F, Gabler HC, Woerner L, Hiermaier S. 2021. Cluster analysis of seriously injured occupants in motor vehicle crashes. *Accid Anal Prev*. 151:1–12.
- Woltring HJ, Huiskes R, de Lange A, Veldpaus FE. 1985. Finite centroid and helical axis estimation from noisy landmark measurements in the study of human joint kinematics. *J Biomech*. 18(5):379–389.
- Woltring HJ, Long K, Osterbauer PJ, Fuhr AW. 1994. Instantaneous helical axis estimation from 3-D video data in neck kinematics for whiplash diagnostics. *J Biomech*. 27(12):1415–1432.
- Woltring HJ. 1991. Representation and calculation of 3-D joint movement. *Hum Mov Sci*. 10(5):603–616.
- Woltring HJ. 1994. 3-D attitude representation of human joints: a standardization proposal. *J Biomech*. 27(12):1399–1414.

**PAPER C**

**Assessment of in Situ Chest Deflection of Post Mortem Human  
Subjects (PMHS) and Personalized Human Body Models (HBM) in  
Nearside Oblique Impacts.**



## Traffic Injury Prevention



ISSN: (Print) (Online) Journal homepage: <https://www.tandfonline.com/loi/gcpi20>


# Assessment of in situ chest deflection of post mortem human subjects (PMHS) and personalized human body models (HBM) in nearside oblique impacts

Ana Piqueras, Bengt Pipkorn, Johan Iraeus, Mario Maza-Frechín & Francisco J. López-Valdés


To cite this article: Ana Piqueras, Bengt Pipkorn, Johan Iraeus, Mario Maza-Frechín & Francisco J. López-Valdés (2022) Assessment of in situ chest deflection of post mortem human subjects (PMHS) and personalized human body models (HBM) in nearside oblique impacts, Traffic Injury Prevention, 23:4, 181-186, DOI: [10.1080/15389588.2022.2036731](https://doi.org/10.1080/15389588.2022.2036731)

To link to this article: <https://doi.org/10.1080/15389588.2022.2036731>

 View supplementary material 

 Published online: 24 Feb 2022.

 Submit your article to this journal 

 Article views: 291

 View related articles 

 View Crossmark data 

 Citing articles: 2 View citing articles 



## Assessment of in situ chest deflection of post mortem human subjects (PMHS) and personalized human body models (HBM) in nearside oblique impacts

Ana Piqueras<sup>a</sup> , Bengt Pipkorn<sup>b</sup>, Johan Iraeus<sup>c</sup> , Mario Maza-Frechín<sup>a</sup> , and Francisco J. López-Valdés<sup>d</sup> 

<sup>a</sup>Impact Laboratory, Institute of Engineering Research of Aragon (I3A), University of Zaragoza, Zaragoza, Spain; <sup>b</sup>Autoliv Research, Vargarda, Sweden; <sup>c</sup>Division of Vehicle Safety, Department of Mechanics and Maritime Sciences, Chalmers University of Technology, Gothenburg, Sweden; <sup>d</sup>Instituto de Investigación Tecnológica (IIT), ICAI, Universidad Pontificia Comillas, Madrid, Spain

### ABSTRACT

**Objective:** The present study has three objectives: First, to analyze the chest deflection measured in nearside oblique tests performed with three post mortem human subjects (PMHS). Second, to assess the capability of a HBM to predict the chest deflection sustained by the PMHS. Third to evaluate the influence on chest deflection prediction of subject-specific HBM.

**Methods:** Three dimensional chest deformation of five anterior chest landmarks was extracted from three PMHS (A-C) in three sled tests. The sled test configurations corresponded to a 30 degree nearside oblique impact at 35 km/h. Two different restraint system versions (RSv) were used. RSv1 was used for PMHS A and B while RSv2 was used for PMHS C. The capability of the SAFER HBM (called baseline model) to predict PMHS chest deflection was benchmarked by means of the PMHS test results. In a second step, the anthropometry, mass and pre-impact posture of the baseline HBM were modified to the PMHS-specific characteristics to develop a model to assess the influence of personalization techniques in the capability of the human body model to predict PMHS chest deflection.

**Results:** In the sled tests, the measured sternum compression relative to the eighth thoracic vertebra in the PMHS tests was 49, 54 and 55 millimeters respectively. The HBM baseline model predicted 48%, 43% and 34% of the deflections measured in the PMHS tests, while the personalized version predicted 38%, 34% and 28%. When chest deflection was analyzed in x-, y- and z-direction for the five chest landmarks it was found that neither the baseline HBM nor the personalized model predicted x, y and z axis deflections.

**Conclusions:** The PMHS in situ chest deflection was found to be sensitive to the variation in restraint system and the three PMHS exhibited greater values of lower right chest deflection compared to what was found in available literature. The baseline HBM underpredicted peak chest deflection obtained in the PMHS test. The personalized model was not capable of predicting the chest deflection sustained by the PMHS. Hence, further biofidelity investigations have to be carried out on the human body thorax model for oblique loading.

### ARTICLE HISTORY

Received 21 July 2021  
Accepted 28 January 2022

### KEYWORDS



Chest deflection; human body model (HBM); nearside; oblique impact; post mortem human subjects (PMHS)


### Introduction

Oblique impacts are the most prevalent collision configuration leading to serious injuries (Suarez-del Fuego et al. 2021). Despite major improvements in restraint systems over the last decades, thoracic injuries are still the most frequent severe injuries in frontal and lateral crashes. These injuries, particularly rib fractures, are especially relevant in elderly occupants (Forman et al. 2019).

To enhance occupant protection in frontal crashes, the Insurance Institute for Highway Safety introduced the small overlap load case in their rating portfolio, using the Hybrid III in the driver position and limiting chest deflection to 50 mm, but considering also a maximum value for the acceleration ( $a_{3ms} < 60g$ ), the viscous criterion ( $VC < 0.8$  m/s)

and the deflection rate ( $< 6.6$  m/s). The Euro NCAP/ANCAP MPDB (Moving Progressive Deformable Barrier) frontal impact consists of a 50% overlap frontal test with the THOR 50<sup>th</sup> percentile and requires that the maximum resultant deflection of the thorax of the dummy  $R_{max}$  is below 35 mm. In 2015, the NHTSA released a request for comment pertaining to including a new oblique test using a moving deformable barrier impacting a stationary vehicle at 90 km/h at a 15-degree angle. Two THOR dummies were proposed to occupy the front row, but no specific injury thresholds were published at the time. The differences in these testing procedures suggest a lack of agreement in which injury criterion/criteria should be used to assess thoracic injuries in oblique impacts, which resembles the paucity of detailed in situ experimental data.

**CONTACT** Ana Piqueras  [apiquera@unizar.es](mailto:apiquera@unizar.es)  Impact Laboratory, Institute of Engineering Research of Aragon (I3A), University of Zaragoza, Zaragoza, Spain  
Associate Editor Jason Stammen oversaw the review of this article.

 Supplemental data for this article is available online at <https://doi.org/10.1080/15389588.2022.2036731>.

© 2022 Taylor & Francis Group, LLC

Finite Element (FE) Human Body Models (HBM) have been shown to be more sensitive to the loading conditions than ATD (Lopez-Valdes et al. 2018). Previous research has demonstrated that modifying the pre-impact posture of the HBM (Poulard et al. 2015), as well as morphing the models to adapt standard HBM sizes to the anthropometry of specific occupants (Hu et al. 2017), could contribute to improve the prediction of the overall (external) occupant kinematics in side and oblique impacts (Larsson et al. 2019; Piqueras et al. 2018).

Thoracic injury criteria proposed to be used with the THOR dummy rely on the 3D measurement of chest deflection, considered to be the best predictor of thoracic injury (Davidsson et al. 2014; Kemper et al. 2011; Poplin et al. 2017). Whether HBM are used to benchmark the biofidelity of the THOR dummy under specific restraint conditions or to propose an injury mechanism, HBM need to show a reliable prediction of the human chest deformation in 3D. This is also a requirement if HBM are used in strain-based rib fracture prediction (Forman et al. 2012).

Thus, the present study has three objectives: First, to analyze the 3D in situ chest deformation measured in nearside oblique tests. Second, to assess the capability of a baseline (not modified) HBM to predict chest deflection. Third to evaluate the influence on chest deflection prediction by geometrical modifications of the HBM (personalized HBM).

## Methods

### PMHS sled tests

Three PMHS sled tests were performed at the Impact Laboratory (University of Zaragoza) in a 30° nearside oblique impact configuration (López-Valdés et al. 2016). The physical tests were carried out using a modified version of the Gold Standard fixture (Pipkorn et al. 2016) that consisted of a rigid metallic frame that approximated the seating position of a car occupant, allowing visual access to the subject. The SAFER seat (Pipkorn et al. 2016) was used, which consists of angled steel pieces in the posterior/anterior and lateral directions that prevented excessive motion of the occupant's pelvis. The occupants were restrained with two different versions of passenger side three-point seatbelt. In restraint system version 1 (RSv1), the shoulder belt was pretensioned at 2 kN and force-limited to 4.5 kN, while the lap belt was equipped with a 3.5 kN pretensioner. In RSv2, the same restraint system was used but the shoulder pretensioner was not activated. Table A1, on the Supplementary material, summarizes the PMHS tests set-up and subject characteristics.

Procurement, handling, and testing of the PMHS was done under the approval of the Ethical Commission for Clinical Research of Aragón (Spain).

### Instrumentation

A motion capture system Vicon® was used to record the 3D kinematics of retro-reflective markers (1 kHz). Arrays of four non-collinear markers were rigidly attached to the body

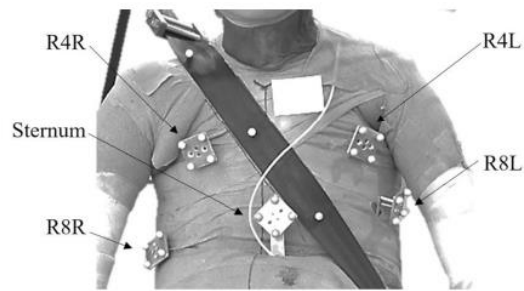


Figure 1. PMHS's anterior chest landmarks.

of the sternum, and to the 4<sup>th</sup> (R4) and 8<sup>th</sup> (R8) ribs bilaterally (L: left; R: right) of each PMHS (see Figure 1). The T8 vertebra motion, used as Local Coordinate System (LCS) for the chest deflection, was also acquired using marker clusters screwed to the vertebral body.

The belt system was also equipped with three markers along the shoulder portion to follow the belt path during the crash test. Belt tension was measured by four force transducers at 10 kHz. Tests were recorded by a lateral and a frontal high-speed cameras at 1 kHz.

### Human body model

The physical PMHS test results were compared to the SAFER HBM v8 model predictions. The SAFER HBM v8 was based on the commercial THUMS v3 that included some modifications, such as a remodeled ribcage (Larsson et al. 2019) and an updated lumbar spine (Afewerki 2016). In this study, the SAFER HBM v8 model was further modified to mimic closely the PMHS experiments. First, the model anthropometry and mass were modified to reflect the characteristics of the PMHS using the Kriging interpolation module included in the PIPER software v1.0.0. The anthropometric dimensions (lengths and contours of the body parts) used as targets for morphing, were extracted from the seated anthropometry measurements taken before the tests (Supplementary material, Table A2). Second, the spine alignment of the model was adapted to the PMHS posture at  $t=0$  ms (see Tables A3 and A4 on the Supplementary material) using a pre-simulation, to conform to the angles between spinal landmarks measured in the PMHS.

Thus, these modifications resulted in three different versions of the model:

1. Baseline: the SAFER HBM v8 model as described above, representing a 50th percentile male occupant, to be compared with the results obtained from, both RSv1 and RSv2, PMHS sled tests.
2. Personalized RSv1: The geometry, posture and body mass were modified to develop a personalized model for RSv1 (Supplementary material, Table A1), as an average of the PMHS A and B.
3. Personalized RSv2: The geometry, posture and body mass were modified to develop personalized a model for RSv2 based on the characteristics of PMHS C.

### Boundary conditions and environment model

The physical sled acceleration pulses were applied to the sled FE models to match the mechanical sled loading conditions. The pretensioner and force limiter triggering times and loading curves were adjusted to represent the time-history seat-belt forces acquired from the physical tests. Additionally, the belt routing over the HBM chest was done using the acquired position of the Vicon belt markers at  $t = 0$  ms.

### 3D chest deflection

Chest deflection for the PMHS was computed based on the kinematics of the sternum and the 4th and 8th ribs bilaterally (R4L, R4R, R8L and R8R). The methodology used to reconstruct and describe the motion of the bones is based on the method proposed by Shaw et al. (2009). The transformation matrix ( $T_{B/G}$ ) that characterizes the 6-dof motion of the bone with respect to a Global Coordinate System (GCS) was obtained as the product of the transformation matrix from the marker cluster to the bone ( $T_{B/M}$ , obtained from the combination of computed tomography images and the geometry of the mount) and the transformation matrix from the marker cluster to the global coordinate systems ( $T_{M/G}$ , measured by Vicon), as shown in Equation (1).

$$T_{B/G} = T_{B/M} \cdot T_{M/G} \quad (1)$$

The deflection was calculated as the change in length of a vector joining the location of a local coordinate system (LCS) rigidly attached to the bones mentioned above and the origin of a LCS attached to the eighth thoracic vertebra (T8). The T8 LCS origin was in the mid-point of the superior and inferior endplate's center, obtained from measurements taken from the CT of each subject taken before test. For both LCS, X-axis pointed forward, the Y-axis pointed to the right and the Z-axis pointed inferiorly according to the SAE J211 recommendations (Engineers Society of Automotive 2014).

A similar procedure was followed for calculating the chest deflection for the human body models. The relative distances of the marker clusters from the sternum along each rib, shown in Table 1, were used to select analogous points on the different versions of the SAFER HBM. Thus, the analyzed chest landmark for each PMHS were compared to homologous points in the corresponding simulation.

The change in chord length between the anterior chest locations and the T8 LCS (Poplin et al. 2017) was calculated for the PMHS and the corresponding HBM.

The accuracy of the HBM chest deflection predictions were evaluated in terms of deflection trends and peak values. The PMHS chest deflection time-history signal was considered predicted when the analyzed landmark on the HBM

**Table 1.** Relative distances of the marker clusters from the sternum along each rib for the three subjects.

Subject Aspect	PMHS A		PMHS B		PMHS C	
	Right	Left	Right	Left	Right	Left
4th rib	32.6%	15.5%	24.2%	26.4%	25.7%	31.4%
8th rib	39.5%	42.3%	38.5%	41.9%	40.5%	39.5%

presented the same trend (i.e., expansion or compression) than that showed by the PMHS and peak deflection values did not differ more than  $\pm 8$  millimeters than the PMHS peak values. This value has been established as the maximum standard deviation of the PMHS sternum X-deflection values.

## Results

### Chest kinematics in the PMHS tests

Figure 2 illustrates the complex deformation exhibited by the rib cage structures in the PMHS B test (RSv1). It shows the time-history plot of the three-axial deformation of the sternum and four rib locations with respect to the T8 vertebra LCS. Regarding to the X-axis, the sternum presented the highest value of compression (X negative) while the adjacent locations, R4L and R4R, showed minor displacements (grey lines without markers on Figure 2a). The lower right chest exhibited X positive deflection, which means expansion.

As for the lateral movement (Figure 2b), the upper chest exhibited higher displacement magnitudes compared with the lower chest landmarks (circle markers). The upper chest, R4L moved to the right (Y positive) while R4R moved to the left. This means that both lateral aspects of the upper chest were

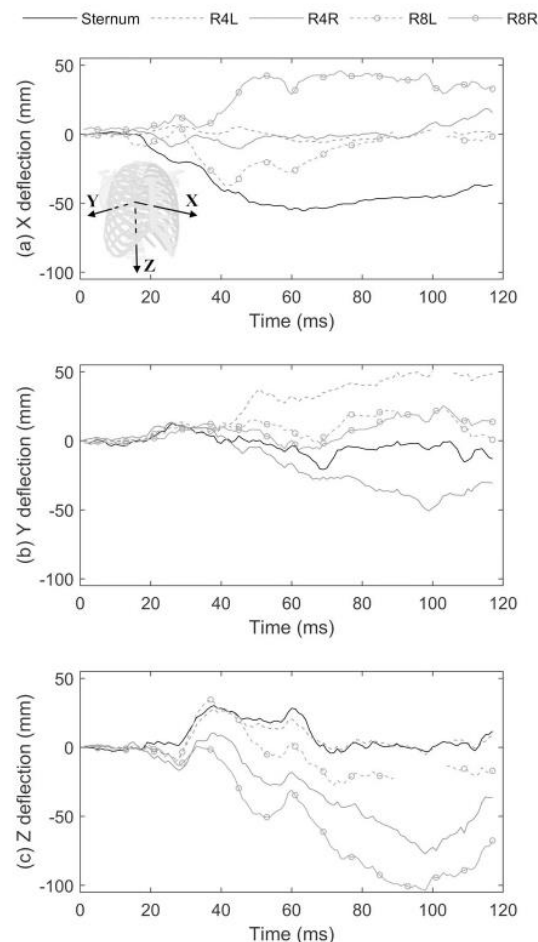


**Figure 2.** Chest deformation referred to T8 vertebra on PMHS B (RSv1). X deflection on top (a), Y deflection in the middle (b) and Z deflection on the bottom (c).



displaced toward the medial ribcage. Attending to the vertical displacement (Figure 2c), the right aspect (solid lines) exhibited upward displacement (Z negative).

There were some common trends observed in the three subjects. The complete time-histories of the anterior chest for the three PMHS are shown in Appendix B (Supplementary material). Regarding the deformation in the X-axis (Supplementary material, Figure B1), the lower right chest of the three PMHS exhibited a positive X-deformation (forward excursion). Figure B2 (Supplementary material) (Y-axis deformation) shows a displacement of the upper chest lateral aspects toward the center of the thorax. Last, Figure B3 (Supplementary material) (Z-axis deformation) shows a general tendency of the chest to move upwards, where the right aspect presented higher values of displacement than the left aspect of the chest.

As for the differences observed between the two restraint system versions, the most relevant ones referred to the X-deflections, since similar trends and peak values were observed on Y and Z-axis. For the occupants A and B (RSv1), the sternum exhibited X-negative deflection (compression) at the beginning of the tests. On the contrary, on the subject C (RSv2), all five chest locations, including the sternum, exhibited positive X deflection (expansion) at the beginning of the tests. For this last subject, after 45 milliseconds, rib landmarks continued moving forward while the sternum was being compressed, undergoing a X-negative deflection (see Figure B1 on the Supplementary material).

Table A1 (Supplementary material) summarizes the injury outcome of the three subjects found during the autopsies carried out after the physical tests.

### Chest kinematics in the HBM versions

Table 2 shows the peak chord deflection, as defined on Poplin et al. (2017), measured in the PMHS experiments and the corresponding predictions obtained with the HBM versions. Both model versions underpredicted the deformation values obtained in the PMHS experiments. The baseline model predicted 48%, 43%, and 34% of the sternum compression magnitude measured in the corresponding PMHS A, B, and C test. The personalized HBM versions predicted even less chest deflection (38%, 34%, and 28%) compared to the corresponding actual PMHS's chest compression.

X-axis: For the RSv 1 (PMHS A and B) both HBM versions consistently predicted similar X deformation trends as the PMHS tests, but underpredicted the magnitudes

(Supplementary material, Figures B4–B8). However, for RSv2, the HBM versions predicted negative-X deformation (rearward motion) for R4L and R4R, while PMHS C indicated positive-X deflection (forward motion) of both ribs. The positive-X deflection of the sternum at the beginning of the tests, was not predicted by any of the HBM versions.

Y-axis: While the lateral rib movement was predicted for the R4L and lower chest locations for the three subjects (Supplementary material, Figures B4, B6, and B7), neither HBM versions predicted the R4R and sternum Y motion of the experiments, as shown in Figures B5 and B8 (Supplementary material).

Z-axis: Regardless of the restraint system, PMHS' anterior chest showed larger deflections along the Z-axis than the ones predicted by the HBM versions, although the personalized version improved the prediction over the baseline.

### Discussion

To the knowledge of the authors, this is the first study reporting on the 3D kinematics of bony rib landmarks of PMHS in nearside oblique impacts. This study adds new oblique impact experimental data to the field that are only comparable in the detailed description of the kinematics to the results reported by Shaw et al. (2009) in frontal impacts.

The displacement of the PMHS' anterior chest was sensitive to the restraint system used regarding the X and Z-axis deflections, but not to the Y-axis deflection that was similar between the two restraints. This may indicate that the use of the pretensioner in PMHS A and B prevented the positive deflection and afterwards sudden compression observed in the upper chest of PMHS C (R4L, R4R and sternum at the beginning of the test), which is likely related to the observed PMHS C's sternum fractures (see Supplementary material, Table A1).

For the three PMHS, deformations on the X-axis showed that the sternum has higher values of deflection (negative-X) relative to T8, than the ribs, especially in PMHS C where the four rib landmarks moved forward (positive-X) with respect to T8. As aforementioned, this can be the reason for the sternum fracture sustained by the mentioned subject. Concerning to the Y-axis, the upper chest landmarks moved toward the medial ribcage and caused a hinge effect of the torso around the seatbelt, increasing the local deformation of the upper chest. The difference between left and right aspects along Z-displacement, revealed a rotation of the chest around the T8' X-axis, which can be only captured by measuring the 3D kinematics of the chest structure.

**Table 2.** Maximum chord deflection values (mm) for the five landmarks on PMHS and simulations.

			Sternum	R4L	R4R	R8L	R8R
RS version 1	PMHS A	PMHS	-48.97	-31.53	-12.62	-22.86	11.86
		Baseline HBM	-23.84	-24.84	7.92	2.69	13.43
		Personalized HBM	-18.68	-23.41	5.79	-3.13	8.50
	PMHS B	PMHS	-54.46	-27.93	-16.28	-26.61	10.87
		Baseline HBM	-23.84	-19.36	-8.90	2.69	13.64
		Personalized HBM	-18.68	-18.12	-6.78	-3.13	8.63
RS version 2	PMHS C	PMHS	-55.39	11.31	38.86	-18.38	-21.75
		Baseline HBM	-18.80	-23.85	11.05	-3.14	12.92
		Personalized HBM	-15.88	-16.68	5.47	-4.13	7.09

Both HBM versions underpredicted the rib cage deformation magnitudes observed in the PMHS experiments, with the baseline models providing a closer estimation to the experimental values. The results in this paper are also supported by those reported in Larsson et al. (2019). It was found that personalized models underpredicted the chest deflection measured using chestbands in side impacts. In the mentioned study, it was demonstrated that modifying the torso flesh materials to a softer viscoelastic response, the HBM predicted higher chest deflection magnitudes compared with the reference model. Future work should investigate the effect of the torso flesh materials on the 3D chest deformation predictions.

Previous studies suggest that the ribcage internal geometry can influence the chest deflection (Kent et al. 2005; Kemper et al. 2007; Shi et al. 2014). The SAFER HBM v8 was developed including the rib cortical thickness and the cross sectional area based on subjects with an average age of 71 years (Iraeus and Pipkorn 2019). Given the age of the subjects within this study ( $64 \pm 4$  y.o.), it was considered that both parameters were represented by the HBM used. Rib material properties of the used HBM models were based on data from an 18-81 age group ( $55 \pm 17$  y.o.) (Kemper et al. 2005, 2007) being a reasonable representation of the subjects within this study ( $64 \pm 4$  y.o.). The relative volume of porous and bone space have been also demonstrated to be negative correlated with the bone material properties (Kang et al. 2017; McCalden et al. 1993). Unfortunately, the resolution of the CT scans taken from the PMHS did not allow to compare these parameters between the HBM and the PMHS.

The HBM model only included the mid-substance material properties for the costal cartilage characterization, even if the perichondrium has been demonstrated to play an important role on the thoracic stiffness (Forman et al. 2010). Additionally, other studies have suggested that the presence of calcifications can be associated with increased structural stiffness of the ribcage and an increment of the number of rib fractures (Forman and Kent 2011). Modeling of calcification areas was not included in the HBM versions and could have contributed to the large amount of fractures sustained by the three PMHS (see Supplementary material, Table A1).

Additionally, all three PMHS sustained right clavicle fractures, which impacted how the chest was loaded by the seatbelt in the experiments. For PMHS C, an instantaneous force drop was visible at 78 ms on the load cell located on the upper shoulder belt that indicates the time of the clavicle fracture, consistently with Poulard et al. (2015) that found clavicle fractures after 80 milliseconds in frontal impacts. Unfortunately, it was difficult to determine the fracture time of the clavicle from the other two PMHS tests from the shoulder belt load cell.

The analysis of the PMHS 3D chest deflections reveals a positive deflection on the lower right chest that was confirmed by the high-speed videos (see Supplementary material, Appendix C). This phenomenon was also reported by Rouhana et al. (2003), and Shaw et al. (2009) confirmed this so-called “bulge-out” effect suggesting that the internal organs and ribs inertia under the effect of the asymmetric

loading can produce the positive displacement of the unrestricted chest areas. Within the present study, PMHS presented larger bulge-out values than those obtained by Shaw et al. (2009). This can be due to the nearside oblique impact configuration, which might have increased the inertial effects to the right aspect of the ribcage. Computational models used within this study only predicted up to 38% of the PMHS chest expansion values observed in the tests. Internal organs individually are not modeled in the SAFER HBM v8 and are lumped into few abdomen parts. Hence, the influence of heavy organs inertia individually was not considered. In addition, a crushable foam material model is used for these abdominal parts. This material model does not accurately model the incompressibility of the solid organs.

A potential cause of these additional bulge-out values found on the PMHS tests was hypothesized to be the belt behavior. During the cadaveric tests, the shoulder belt portion remained almost fixed over the sternum due to the forward movement of the surrounding tissues, while the computational models allowed lateral sliding of the upper seatbelt over the chest. This can be attributed to modeling issues, such as contacts between the belt and the skin tissues or the lack of constraints of the soft tissues over the sternum, which were developed and validated for frontal configurations but not for oblique impacts. To understand the influence of this discrepancy, an additional simulation was carried out in which the lateral belt displacement over the sternum of the baseline model was constrained. Results showed only 3.72 millimeters more of R8R expansion (5% of the experimental value) than the corresponding baseline model. Therefore, it was concluded that the soft tissues behavior, added to the higher compression of the sternum compared with R4L and R4R, produced a “hinge” effect over the seatbelt impeding lateral movements across the chest of the PMHS, although additional work should be done to reflect correctly its effect on the outcome.

### Limitations

Some of the thoracic and belt markers were covered by the PMHS body during the motion of the occupant, limiting the visibility of the markers and therefore the calculation of the chest deformation at those instants. It should be noted that the attachment of the rib markers to the ribs required the perforation of the pleura. The methodology used here was initially proposed in Shaw et al. (2009) and, to our knowledge, there is no other available method to measure the in situ 3D kinematics of the ribs during an impact.

In terms of methodology, the morphing personification technique was implemented attending to the external anthropometry, thus internal subject specific geometry was not personalized. Since the scope of this study was to evaluate the influence of the subject specific posture, mass and anthropometry, soft and hard tissues material properties remained unmodified from the SAFER HBM.

It should be noted that the anthropometry of PMHS A and PMHS B was averaged to develop a single personalized HBM. This was decided due to the large similarities in anthropometry

(see Supplementary material, Table A2) and initial posture (see Supplementary material, Table A3) of the two subjects that would have resulted in minimal differences in the corresponding HBM. Therefore, the results included here are considered representative of the response of both subjects.

## Acknowledgments

The authors thank the donors and their families because without their generous act this study would have never existed.

## Disclosure statement

The Authors declare that there is no conflict of interest.

## Funding

The study was partially funded by the Instituto Aragonés de Fomento of Gobierno de Aragón via the “Collaborative Agreement to Foster Research on Impact Biomechanics,” signed on February 11, 2015. The simulation work and its comparison with the PMHS tests was carried out at SAFER, Vehicle and Traffic Safety Center at Chalmers University of Technology, Gothenburg, Sweden, which is funded by FFI-Strategic Vehicle Research and Innovation, by Vinnova, the Swedish Energy Agency, the Swedish Transport Administration and the Swedish vehicle industry. The simulations were performed on resources at Chalmers Center for Computational Science and Engineering (C3SE) provided by the Swedish National Infrastructure for Computing (SNIC).

## ORCID

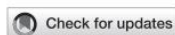
Ana Piqueras  <http://orcid.org/0000-0002-0019-4103>  
 Johan Iraeus  <http://orcid.org/0000-0001-9360-0707>  
 Mario Maza-Frechín  <http://orcid.org/0000-0003-1261-8847>  
 Francisco J. López-Valdés  <http://orcid.org/0000-0003-3167-5732>

## References

- Afewerki H. 2016. Biofidelity evaluation of thoracolumbar spine model in THUMS. Gothenburg, Sweden: Chalmers University of Technology.
- Davidsson J, Carroll J, Hynd D, Lecuyer E, Song E, Trosseille X, Eggers A, Sunnevang C, Praxl N, Martinez L, et al. 2014. Development of injury risk functions for use with the THORAX demonstrator; an updated THOR. In: Proceedings of IRCOBI Conference, Berlin, Germany; 2014; p. 359–376.
- Engineers Society of Automotive. 2014. Instrumentation for impact test. Warrendale (PA): Society of Automotive Engineers: SAE J211.
- Forman J, Poplin GS, Shaw CG, McMurry TL, Schmidt K, Ash J, Sunnevang C. 2019. Automobile injury trends in the contemporary fleet: belted occupants in frontal collisions. *Traffic Inj Prev.* 20(6):607–612.
- Forman JL, Del Pozo De Dios E, Dalmasas CA, Kent RW. 2010. The contribution of the perichondrium to the structural mechanical behavior of the costal-cartilage. *J Biomech Eng.* 132(9):094501.
- Forman JL, Kent RW. 2011. Modeling costal cartilage using local material properties with consideration for gross heterogeneities. *J Biomech.* 44(5):910–916.
- Forman JL, Kent RW, Mroz K, Pipkorn B, Bostrom O, Segui-Gomez M. 2012. Predicting rib fracture risk with whole-body finite element models: development and preliminary evaluation of a probabilistic analytical framework. *Ann Adv Automot Med.* 56:109–124.
- Hu J, Zhang KS, Fanta A, Hwang E, Reed MP. 2017. Effects of male stature and body shape on thoracic impact response using parametric finite element human modeling. In: 25th ESV Conference. Detroit (MI): EEUU; p. 1–11.
- Iraeus J, Pipkorn B. 2019. Development and validation of a generic finite element ribcage to be used for strain-based fracture prediction. In: Proceedings of IRCOBI Conference 2019, Florence (Italy); p. 193–210.
- Kang YS, Agnew AM, Hong CB, Icke K, Bolte JH. 2017. Elderly PMHS thoracic responses and injuries in frontal impacts. In: Proceedings of IRCOBI Conference 2017, Antwerp (Belgium); p. 539–557.
- Kemper AR, Kennedy EA, McNally C, Manoogian SJ, Stitzel JD, Duma SM. 2011. Reducing chest injuries in automobile collisions: rib fracture timing and implications for thoracic injury criteria. *Ann Biomed Eng.* 39(8):2141–2151.
- Kemper AR, McNally C, Clayton AP, Freeman LJ, Duma SM, Rouhana SW. 2007. The biomechanics of human ribs: material and structural properties from dynamic tension and bending tests. *Stapp Car Crash J.* 51:235–273.
- Kemper AR, McNally C, Kennedy EA, Manoogian SJ, Rath AL, Ng TP, Stitzel JD, Smith EP, Duma SM, Matsuoka F. 2005. Material properties of human rib cortical bone from dynamic tension coupon testing. *SAE Tech Pap.* 2005(November):199–230.
- Kent R, Lee SH, Darvish K, Wang S, Poster CS, Lange AW, Brede C, Lange D, Matsuoka F. 2005. Structural and material changes in the aging thorax and their role in crash protection for older occupants. *Stapp Car Crash J.* 2005;2005-Novem(November):231–249.
- Larsson KJ, Pipkorn B, Iraeus J, Bolte JH, Agnew AM, Hu J, Reed MP, Sunnevang C. 2019. Evaluation of the benefits of parametric human body model morphing for prediction of injury to elderly occupants in side impact. In: Conference proceedings International Research Council on the Biomechanics of Injury, IRCOBI. Florence, Italy; p. 150–174.
- López-Valdés FJ, Juste-Lorente Ó, Maza-Frechín M, Pipkorn B, Sunnevang C, Lorente A, Aso-Vizan A, Davidsson J. 2016. Analysis of occupant kinematics and dynamics in nearside oblique impacts. *Traffic Inj Prev.* 17(sup1):86–92. doi:10.1080/15389588.2016.1189077
- Lopez-Valdes FJ, Mroz K, Eggers A, Pipkorn B, Muehlbauer J, Schick S, Peldschus S. 2018. Chest injuries of elderly postmortem human surrogates (PMHSs) under seat belt and airbag loading in frontal sled impacts: comparison to matching THOR tests. *Traffic Inj Prev.* 19(sup2):S55–S63. doi:10.1080/15389588.2018.1542139
- McCalden RW, McGeough JA, Barker MB, Court-Brown CM. 1993. Age related changes in the tensile properties of cortical bone. *J Bone Jt Surg.* 75-A(8):1193–1205.
- Pipkorn B, Lopez-Valdes FJ, Juste-Lorente O, Maza M, Sunnevang C. 2016. Study of the kinematics of the THOR dummy in nearside oblique impacts. In: Proceedings of IRCOBI Conference 2016, Malaga (Spain); p. 637–648.
- Piqueras A, Iraeus J, Lorente AI, López-Valdés FJ, Juste-Lorente Ó, Maza-Frechín M, Pipkorn B. 2018. Kinematic assessment of subject personification of human body models (THUMS). In: Proceedings of IRCOBI Conference 2018, Athens (Greece); p. 191–206.
- Poplin GS, McMurry TL, Forman JL, Ash J, Parent DP, Craig MJ, Song E, Kent R, Shaw G, Crandall J. 2017. Development of thoracic injury risk functions for the THOR ATD. *Accid Anal Prev.* 106(December 2015):122–130. doi:10.1016/j.aap.2017.05.007
- Poulard D, Subit D, Nie B, Donlon JP, Kent RW. 2015. The contribution of pre-impact posture on restrained occupant finite element model response in frontal impact. *Traffic Inj Prev.* 16(September 2016):87–95.
- Rouhana SW, Kankanala SV, Prasad P, Rupp JD, Jeffreys TA, Schneider LW. 2003. Biomechanics of 4-point seat belt systems in frontal impacts. *SAE Tech Pap.* 47:367–399.
- Shaw G, Parent D, Purtsezov S, Lessley D, Crandall J, Kent R, Guillemot H, Ridella S. a, Takhounts E, Martin P. 2009. Impact response of restrained PMHS in frontal sled tests: skeletal deformation patterns under seat belt loading. *Stapp Car Crash J.* 53(November):1–48.
- Shi X, Cao L, Reed MP, Rupp JD, Hoff CN, Hu J. 2014. A statistical human rib cage geometry model accounting for variations by age, sex, stature and body mass index. *J Biomech.* 47(10):2277–2285. doi: 10.1016/j.jbiomech.2014.04.045
- Suarez-del Fuego R, Junge M, Lopez-Valdes F, Gabler HC, Woerner L, Hierzmaier S. 2021. Cluster analysis of seriously injured occupants in real-world crashes. *Accid Anal Prev.* 151:105787.

**PAPER D**

**Assessment of the Sensitivity of Thoracic Injury Criteria to Subject-Specific Characteristics Using Human Body Models**



## OPEN ACCESS

EDITED BY  
 Joel Douglas Stitzel,  
 Wake Forest University, United States

REVIEWED BY  
 Xiaogai Li,  
 Royal Institute of Technology, Sweden  
 Peter Theobald,  
 Cardiff University, United Kingdom

\*CORRESPONDENCE  
 Ana Piqueras,  
 ✉ [apiquera@unizar.es](mailto:apiquera@unizar.es)

SPECIALTY SECTION  
 This article was submitted to  
 Biomechanics, a section of  
 the journal Frontiers in  
 Bioengineering and Biotechnology

RECEIVED 23 November 2022  
 ACCEPTED 25 January 2023  
 PUBLISHED 13 February 2023

CITATION  
 Piqueras A, Iraeus J, Pipkorn B and  
 López-Valdés FJ (2023), Assessment of the  
 sensitivity of thoracic injury criteria to  
 subject-specific characteristics using  
 human body models.  
*Front. Bioeng. Biotechnol.* 11:1106554.  
 doi: 10.3389/fbioe.2023.1106554

COPYRIGHT  
 © 2023 Piqueras, Iraeus, Pipkorn and  
 López-Valdés. This is an open-access  
 article distributed under the terms of the  
 Creative Commons Attribution License  
 (CC BY). The use, distribution or  
 reproduction in other forums is permitted,  
 provided the original author(s) and the  
 copyright owner(s) are credited and that  
 the original publication in this journal is  
 cited, in accordance with accepted  
 academic practice. No use, distribution or  
 reproduction is permitted which does not  
 comply with these terms.

# Assessment of the sensitivity of thoracic injury criteria to subject-specific characteristics using human body models

Ana Piqueras<sup>1\*</sup>, Johan Iraeus<sup>2</sup>, Bengt Pipkorn<sup>3</sup> and Francisco J. López-Valdés<sup>4</sup>

<sup>1</sup>Department of Mechanical Engineering, EINA, University of Zaragoza, Zaragoza, Spain, <sup>2</sup>Division of Vehicle Safety, Department of Mechanics and Maritime Sciences, Chalmers University of Technology, Gothenburg, Sweden, <sup>3</sup>Autoliv Research, Vargarda, Sweden, <sup>4</sup>Instituto de Investigación Tecnológica (IIT), Department of Mechanical Engineering, ICAI, Universidad Pontificia Comillas, Madrid, Spain

**Introduction:** Chest deformation has been proposed as the best predictor of thoracic injury risk in frontal impacts. Finite Element Human Body Models (FE-HBM) can enhance the results obtained in physical crash tests with Anthropometric Test Devices (ATD) since they can be exposed to omnidirectional impacts and their geometry can be modified to reflect specific population groups. This study aims to assess the sensitivity of two thoracic injury risk criteria (PC Score and Cmax) to several personalization techniques of FE-HBMs.

**Methods:** Three 30° nearside oblique sled tests were reproduced using the SAFER HBM v8 and three personalization techniques were applied to this model to evaluate the influence on the risk of thoracic injuries. First, the overall mass of the model was adjusted to represent the weight of the subjects. Second, the model anthropometry and mass were modified to represent the characteristics of the post-mortem human subjects (PMHS). Finally, the spine alignment of the model was adapted to the PMHS posture at  $t = 0$  ms, to conform to the angles between spinal landmarks measured in the PMHS. The following two metrics were used to predict three or more fractured ribs (AIS3+) of the SAFER HBM v8 and the effect of personalization techniques: the maximum posterior displacement of any studied chest point (Cmax), and the sum of the upper and lower deformation of selected rib points (PC score).

**Results:** Despite having led to statistically significant differences in the probability of AIS3+ calculations, the mass-scaled and morphed version provided, in general, lower values for injury risk than the baseline model and the postured version being the latter, which exhibited the better approximation to the PMHS tests in terms of probability of injury. Additionally, this study found that the prediction of AIS3+ chest injuries based on PC Score resulted in higher probability values than the prediction based on Cmax for the loading conditions and personalization techniques analyzed within this study.

**Discussion:** This study could demonstrate that the personalization techniques do not lead to linear trends when they are used in combination. Furthermore, the results included here suggest that these two criteria will result in significantly different predictions if the chest is loaded more asymmetrically.

## KEYWORDS

human body model (HBM), injury metrics, nearside, oblique impact, thoracic injury risk, personification

## 1 Introduction

Anthropometric Test Devices (ATD), also known as crash test dummies, are commonly used in regulatory procedures and consumer testing programs in the assessment of the potential injury risks of car occupants (IIHS 2012; NHTSA 2015; EuroNCAP 2018; ANCAP 2020). This assessment is based on the use of injury criteria, which relate the value of a measured physical magnitude (such as force or deformation) with a certain probability ( $p$ ) of sustaining an injury. In the case of the thorax, several injury criteria have been used historically to predict the probability of chest injuries (Kroell et al., 1974; Lau and Viano 1986; Kleinberger et al., 1998). Contemporary research associated with the development of the Test Device for Human Occupant Restraint (THOR) ATD has proposed injury criteria based on the 3D measurement of chest deformation as the best predictor of the risk of thoracic injuries in frontal impacts (Davidsson et al., 2014; Poplin et al., 2017).

Poplin et al. (2017) developed a multipoint chest deformation injury criterion based on an accelerated failure time model from experimental data obtained from a set of 45 post-mortem human subjects (PMHS) exposed to 13 different impact conditions using age as a covariant. After reproducing the same impact conditions with the THOR ATD, Poplin et al. (2017) proposed the total and differential chest deformations (PC Score) and  $C_{max}$  as the most reliable injury criteria to predict the probability of thoracic injuries in frontal impacts. The authors observed that the predicted probability of AIS3+ (three or more fractured ribs (AAAM 2015)) thoracic injuries obtained by either injury criteria was very similar. The same observation was reported in Lopez-Valdes et al. (2018), which used both injury criteria with the THOR dummy to predict the thoracic injuries of three elderly male PMHS in sled frontal impacts. This study also highlighted that both criteria had underestimated the actual risk of thoracic injury observed in the PMHS tests.

Studies focusing on oblique impacts have suggested that oblique loading can cause larger chest deformations than frontal loading (Acosta et al., 2016; Piqueras et al., 2022). However, current ATD were developed for evaluation of either frontal impacts (Hybrid III, THOR) or side impacts (EuroSID, WorSID) and, thus, the response under oblique impact may not be biofidelic. The use of detailed Finite Element Human Body Models (FE-HBM) can enhance the information obtained from physical crash tests with crash test dummies as FE-HBM can be exposed to omnidirectional impacts. Additionally, the FE-HBM description of the material properties of the tissue allows, at least theoretically, the calculation of injury risk to be based on strain measurements, a magnitude that is more likely to be related to the actual mechanisms causing the tissue to fail. Accordingly, several studies have proposed injury criteria for FE-HBM based on strain (Laituri et al., 2005; Forman et al., 2012; Iraeus et al., 2020). Two main groups can be distinguished: deterministic and probabilistic criteria. In the former, the strain predicted by the FE-HBM is compared to a previously accepted injury threshold and if the strain exceeds the threshold, an injury is predicted. In the latter, the predicted strain is transformed into the probability of sustaining such strain given the known distribution of strain in the population (that needs to be known/estimated before). Several studies using deterministic methods have shown that these methods are less sensitive to changes in the restraint conditions than other injury criteria not based on strain (Song et al., 2011; Larsson et al., 2019). Forman et al. (2012) was the first study developing a probabilistic injury criteria approach for FE-HBM and Pipkorn et al. (2019) showed that this method was capable of predicting the number of fractured ribs

observed in PMHS sled tests. However, to succeed in injury risk prediction, the FE-HBM had to be developed to accurately predict the actual strain of the tissue. Therefore, the injury risk functions are dependent on model characteristics such as the mesh size of each FE-HBM and have to be developed and validated for each loading scenario (Forman et al., 2022), which is not always feasible.

Thus, in parallel to strain-based thoracic injury criteria, several studies have used HBM chest deformations as a potential predictor of thoracic injuries, similar to what is done with ATD. For instance, Mendoza-Vazquez et al. (2015) developed a set of AIS2+ [two fractured ribs (AAAM 2015)] thoracic injury risk curves using several deformation-based criteria such as  $D_{max}$ ,  $C_{max}$ ,  $VC_{max}$ , and  $DcTHOR$ , the latter a multi-point chest deflection metric proposed by Davidsson et al. (2014). The study concluded that  $DcTHOR$  resulted in the best predictor for the thoracic injury risk, despite being a metric developed to be used with ATD. In addition, Mendoza-Vazquez et al. (2015) also found that injury metrics based on multi-point measurements ( $DcTHOR$  and  $C_{max}$ ) were less sensitive to variations in the material properties of the FE-HBM, making these metrics particularly suitable to be used with FE models. Current studies show multiple examples of the application of deformation-based criteria to the prediction of chest injuries using FE-HBM such as Brolin and Wass (2016), which used  $DcTHOR$  and  $D_{max}$  metrics with the THUMS model for the assessment of the injury protection provided by a safety-vest in equestrian riders, or Grébonval et al. (2021), which used the  $C_{max}$  and PC Score to compare the thoracic injury risk predicted by the GHBM HBM and the THOR ATD in frontal impacts in reclined occupant positions.

One of the advantages of FE-HBM is the possibility of modifying the geometry of the model to represent specific groups of people within the population. This possibility has resulted in the development of parametric models capable of reproducing subject-specific characteristics (Shi et al., 2014; Hwang et al., 2016; Hu et al., 2017). Another level of personalization of FE-HBM focused on the possibility of mimicking specific initial postures of occupants (or PMHS if cadaveric tests are being used to benchmark the models). Poulard et al. (2015) found that the HBM pre-impact posture altered the predicted kinematics and rib fracture risk in frontal impacts, even if it had a limited effect on the amplitude of the outputs. However, it is not entirely clear yet how these levels of personalization contribute to the accuracy of FE-HBM thoracic injury risk predictions. Previous research has shown that the modification of the anthropometry and pre-impact posture of FE-HBM contributed to improving the HBM predictions of the external occupant kinematics (Piqueras et al., 2018; Larsson et al., 2019). Despite this improvement, the rib deformation patterns were not correctly captured by the personalized models, and the chest deflection measured in the reference PMHS tests was underpredicted (Piqueras et al., 2022).

Thus, the assessment of the effect of the personalization techniques on the injury risk prediction of FE-HBM requires additional research. This study aims to assess the sensitivity of two multi-point deflection metrics commonly used with FE-HBM to estimate the risk of thoracic injuries (i.e.,  $C_{max}$  and PC Score) to several personalization techniques in nearside oblique impacts.

## 2 Materials and methods

### 2.1 Reference physical tests

In order to assess the sensitivity of the PC Score and  $C_{max}$  metrics under oblique loading, three 30° nearside oblique PMHS sled tests (A,

TABLE 1 Test setup and PMHS information including injury outcome.

PMHS	Restraint system v1		Restraint system v2
	PMHS A	PMHS B	PMHS C
Impact angle (deg)		30	
Velocity (km/h)		35	
Seatbelt		3-point	
Pretensioner		Shoulder (2 kN) Lap belt 3.5 kN	Lap belt 3.5 kN
Force Limiter		Shoulder belt 4.5 kN	
Configuration		Passenger	
Age	66	68	60
Sex	Male	Male	Male
Stature (cm)	175	169	170.5
Weight (kg)	47	53	57
Fractured ribs (total number of fractures)	15 (22)	5 (7)	10 (11)

B, and C, see Table 1) were chosen as reference data for the subject-specific characteristics applied on the HBM modifications (López-Valdés et al., 2016). These PMHS tests have been described in detail in several other publications and are used here only as the physical reference case to build the environment and initial conditions of the different FE models under study (López-Valdés et al., 2016; Piqueras et al., 2018; Piqueras et al., 2022). In the physical tests, the occupants were restrained with two different versions of a passenger-side three-point seatbelt. In restraint system version 1 (RSv1, used with PMHS A and B), the shoulder belt was pre-tensioned at 2 kN and included a force-limiter at 4.5 kN, and the lap belt was equipped with a 3.5 kN pre-tensioner. In RSv2 (used PMHS C), the same restraint system was used but the shoulder pre-tensioner was not activated in the test. The physical tests were carried out using a modified version of the Gold Standard fixture which was fully described in Pipkorn et al. (2016). The three subjects, A, B, and C, sustained AIS3 thoracic injuries.

The sled acceleration pulse, obtained from the physical tests, was applied to the sled FE models to mimic the mechanical sled loading conditions. The pre-tensioner and force limiter triggering times and loading curves were adjusted to accurately represent the time-history seat-belt forces acquired from the physical tests. The sled fixture and belt models used for this study were validated in Pipkorn et al. (2016). The coordinates for the D-ring, footrest, buckle, and attachments, were adjusted in the simulation environment taking as reference the location used during the physical tests (López-Valdés et al., 2016). Additionally, the belt was routed over the HBM chest using the acquired position of the belt positioning markers at  $t = 0$  ms.

## 2.2 Human body model and personalization techniques

The SAFER HBM v8, which is based on the commercial THUMS v3 (Iwamoto et al., 2002), was used for this study. The modifications of

SAFER HBM v8 included an updated ribcage (Iraeus et al., 2017) and a new definition of the lumbar spine mechanical properties (Aferwerki 2016). The trabecular bone of the sternum and ribs was modeled with hexahedral elements as well as the mid-substance of the costal cartilage. Cortical bone and the perichondrium layer were modeled using quadratic shell elements. A piecewise linear plasticity material was used in the formulation of the material properties of the chest elements. Rib material properties were based on experimental data obtained from rib coupon tests in a sample including individuals between 18 and 81 years old (Kemper et al., 2005; Kemper et al., 2007).

The personalization of the SAFER HBM v8 model to the PMHS exposed to the oblique impacts was carried out in three steps.

1. First, the overall mass of the model was adjusted to represent the weight of the subjects preserving the external shape and size of the baseline model. The density of the fat and flesh parts was modified to accomplish the PMHS mass from the THUMS original weight (see Table 2).
2. Second, the model anthropometry and mass of the baseline model were modified to represent the characteristics of the PMHS used in the tests described in López-Valdés et al. (2016) by means of the Kriging interpolation module included in the PIPER software v1.0.0. The anthropometric dimensions (lengths and contours of the body parts) used as targets for morphing, were extracted from the seated anthropometry measurements taken before the tests (see Supplementary Table 1-1).
3. Finally, the influence of the initial posture in the prediction of chest injuries was analyzed by aligning the spine curvature of the FE-HBM to the actual spine curvature of the PMHS measured at  $t = 0$  ms (see Figure 1). This was performed using an independent pre-simulation where a prescribed motion was applied to the head, T1, T8, L2, and H-Point, to conform to the relative angles between landmarks measured on the PMHS (see Supplementary Tables 1-2, 1-3). Due to the specifics of the PMHS preparation process, the clusters for subject C (RSv2), were attached to T4, T7, and L1, thus, the spine alignment was done using these landmarks in this case.

TABLE 2 Mass modification of the mass-scaled models' flesh and fat parts.

Restraint system v1					
	PMHS A	PMHS B	Unscaled SAFER HBM v8 model	Density scale factor	Mass-scaled models
Fixed mass parts (skeleton, internal organs, etc.) (kg)	—	—	25.3	1	25.3
Fat and flesh parts (kg)	—	—	52.29	0.472	24.7
Total mass (kg)	47	53	77.59	—	50
Restraint system v2					
	PMHS C	Unscaled SAFER HBM v8 model	Density scale factor	Mass-scaled models	
Fixed mass parts (skeleton, internal organs, etc.) (kg)	—	25.3	1	25.3	
Fat and flesh parts (kg)	—	52.29	0.606	31.7	
Total mass (kg)	57	77.59	—	57	

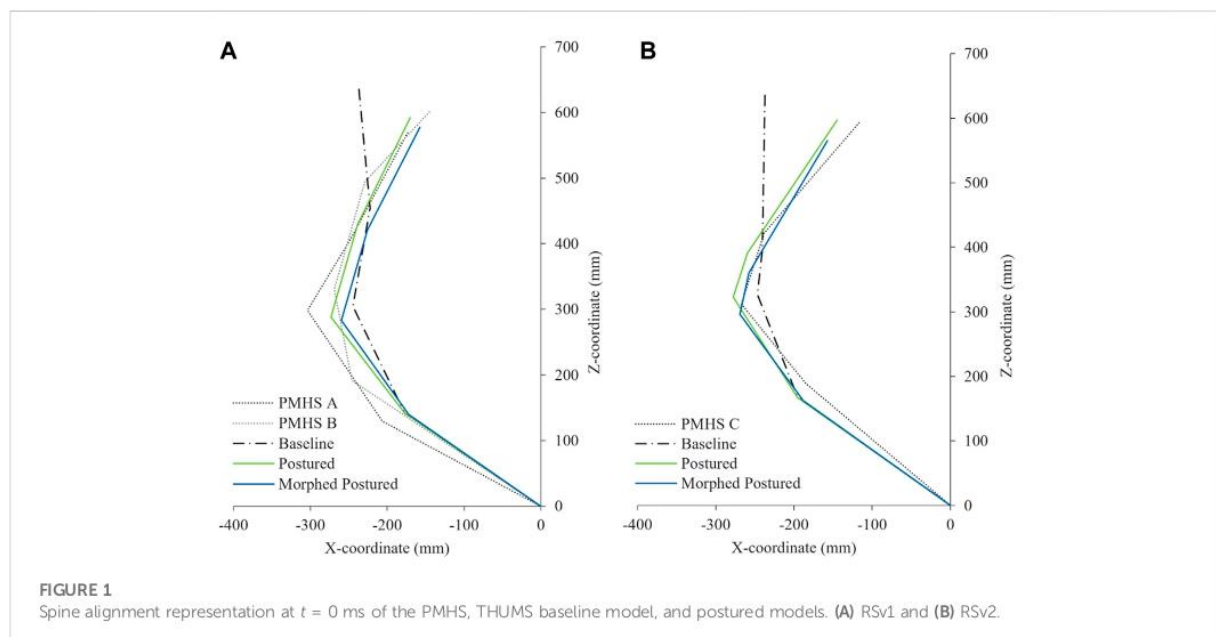


FIGURE 1 Spine alignment representation at  $t = 0$  ms of the PMHS, THUMS baseline model, and postured models. (A) RSv1 and (B) RSv2.

These three modifications were applied in different combinations to the baseline FE-HBM model resulting in six different versions of the HBM for each restrain configuration.

- (1) Baseline model: the SAFER HBM v8 model remains unmodified representing a 50th percentile male occupant.
- (2) Baseline postured model: The spine alignment of the baseline model was adjusted to the PMHS initial position.
- (3) Scaled mass model: The density of the outer flesh parts was adjusted until the full model mass reached the overall weight of the subject.
- (4) Scaled mass postured model: In this version, the spine of the scaled mass model was adapted to the initial posture of the PMHS.
- (5) Morphed model: The geometry and the mass of the baseline SAFER HBM v8 model were modified to represent the PMHS anthropometry using the PIPER software.

- (6) Morphed postured model: The mass, the geometry, and the posture were modified to represent the characteristics of the subject.

The targeted mass, anthropometry, and spine alignment have been calculated considering the subjects tested with each RSv. The anthropometry of PMHS A and PMHS B was averaged to develop a single personalized HBM. This was decided due to the large similarities in anthropometry (see Supplementary Table 1-1) and initial posture (see Supplementary Tables 1-2, 1-3) of the two subjects that would have resulted in minimal differences in the corresponding HBM. Separately, data from PMHS C was used to develop the HBM versions for the RSv2. Thus, a total of 12 simulations have been carried out, corresponding to the six mentioned versions for each of the two RSv (see Table 3).



TABLE 3 Model versions and modifications applied.

Model Number	Model name	Mass scaling	Morphing	Posturing
(1)	Baseline			
(2)	Baseline postured			Yes
(3)	Scaled mass	Yes		
(4)	Scaled mass postured	Yes		Yes
(5)	Morphed	Yes	Yes	
(6)	Morphed postured	Yes	Yes	Yes

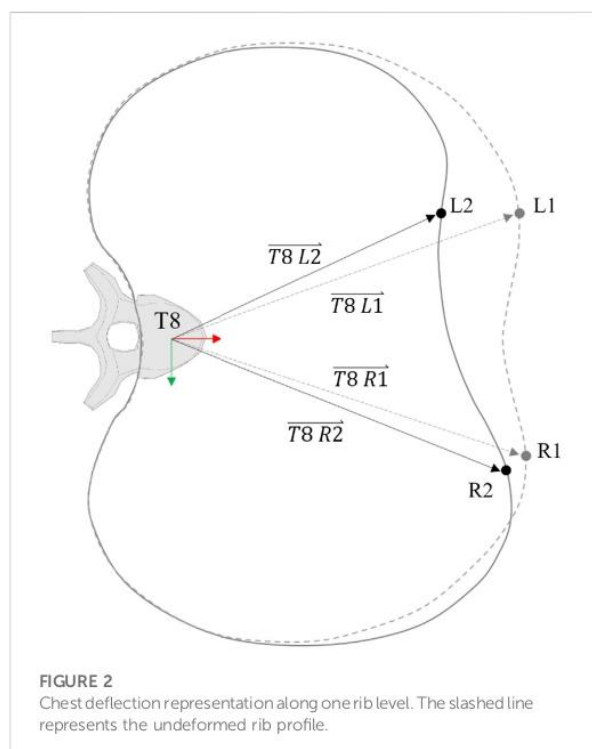


FIGURE 2  
Chest deflection representation along one rib level. The slashed line represents the undeformed rib profile.

### 2.3 Chest deflection measurement

Chest deflection was calculated at the 4<sup>th</sup> and 8<sup>th</sup> ribs bilaterally (UL, UR, LL, and LR). The deflection was calculated as the change in length of a vector joining the location of a marker cluster that was used to define a local coordinate system (LCS) rigidly attached to the rib points mentioned above and the origin of an LCS attached to the eighth thoracic vertebra (T8) ( $|\overline{T8L1}| - |\overline{T8L1}|$ , see Figure 2) (Piqueras et al., 2022). The relative distances of the marker clusters from the sternum along each rib (see Table 4) were used to select analogous points on the different versions of the SAFER HBM so that the calculation of the deflection would be consistent across models.

The differences in the position of the upper chest landmarks between PMHS A and B in the experiments were large. To avoid influencing the results by averaging the position of the clusters, the chest deflection of the Rsv1 model versions was analyzed regarding both landmark locations (PMHS A and B) resulting in 18 comparisons (models A, B, and C and versions 1 to 6).

TABLE 4 Relative position of the nodes used for chest deflection measurement from the sternum along each rib for the three subjects.

Subject	PMHS A		PMHS B		PMHS C	
	Right	Left	Right	Left	Right	Left
4th rib	32.6%	15.5%	24.2%	26.4%	25.7%	31.4%
8th rib	39.5%	42.3%	38.5%	41.9%	40.5%	39.5%

### 2.4 Injury predictors

Two main predictors based on multi-point chest deformation measurements were considered: Cmax and PC Score. Cmax computes the maximum posterior resultant displacement of any studied rib point of the chest, independently of the displacement of the rest of the rib points. For instance, as shown in Figure 2, Cmax will compute the deflection of the left point (L), regardless of the right point (R) deflection. PC Score computes the sum of the maximum deformation measured at the upper and lower chest (UPtot and LOWtot) and the maximum differential deformation of the upper and lower rib measurement points (UPdif and LOWdif) (Poplin et al., 2017). Returning to the example, PC Score will compute, not only the maximum deformation that occurred at L and R points but also the differential deformation between these two points for the upper and lower chest.

In order to consistently compare the results obtained from both injury criteria, the probability of sustaining an AIS3+ injury to the chest (AAAM 2015) was calculated according to the injury risk functions developed by Poplin et al. (2017). This formulation uses age as the co-variant for the calculation, thus, the age of the three subjects at the time of death was considered (66, 68, and 60 y. o. for models A, B, and C respectively).

### 2.5 Statistical analysis

First, the equivalence of using Cmax or PC Score for the p (AIS3+) calculation was assessed. Due to the reduced number of samples, a non-normal distribution has been assumed. Thus, a non-parametric Wilcoxon signed-rank test for paired samples was carried out for the analysis. The results of p (AIS3+) calculated based on Cmax for all the model versions were compared with those calculated based on PC Score, establishing equal medians as a null hypothesis (H).

Second, the influence of the three personalization techniques (mass scaling, morphing, and posturing) on the p (AIS3+) was analyzed by comparing the results of the different model versions.

The simulation results were separated into two groups for each personalization technique: Group one (reference group), in which the model did not include the monitored personalization technique, and group two, with the models that had been modified including that technique (see columns in Table 3). The grouping for the analysis of each modification is shown in Table 5.

Then, the results of  $p$  (AIS3+) were compared using a non-parametric Mann-Whitney  $U$  test for non-paired samples, assuming equal means as a null hypothesis. This comparison was done separately for the PC Score-based calculation and the Cmax-based calculation resulting in a total of six analyses (3personalization techniques  $\times$  2 metrics).

In both analyses, the significance level of the statistical tests was established at a  $p$ -value of  $<0.05$ .

### 3 Results

The maximum deflection results from the PMHS tests were extracted from Piqueras et al. (2022) and are summarized in Supplementary Figures 1-1. Maximum deflection values for the four rib landmarks obtained from the model versions are exposed in Supplementary Figures 1-2-1-4; Supplementary Table 1-4.

#### 3.1 Injury risk by Cmax and PC score

The results of  $p$  (AIS3+) computed using Cmax and PC Score obtained for each HBM version are shown in Table 6.

According to the data observed in Table 6, the postured HBM version (2) obtained, in general, the highest values of injury risk with either PC Score-based or Cmax-based calculations, while the morphed postured version (6) exhibited the lowest probability of injury risk.

#### 3.2 Analysis of the influence on the use of Cmax and PC score

According to the data, the  $p$  (AIS3+) calculated based on the PC Score resulted in higher probability values than those based on the Cmax metric, as can be seen in Figure 3.

This hypothesis was confirmed by the Wilcoxon test, obtaining a  $p$ -value of 0.0007, and even when each RS was analyzed separately, obtaining a  $p$ -value of 0.005 for Rsv1 and a  $p$ -value of 0.03 for Rsv2. However, these differences were found to be higher for the Rsv1 than for the Rsv2.

#### 3.3 Analysis of the influence of the personalization techniques

In order to evaluate the effect of each technique, the results shown in Table 6 were separated into two groups according to what has been shown in Table 5. The resulting  $p$ -values for the Mann-Whitney  $U$  tests are shown in Table 7.

This analysis revealed that the mass scaling and morphing of the HBM significantly influenced the prediction of AIS3+ while the posturing did not show statistically significant differences in the results, regardless of the injury metric used.

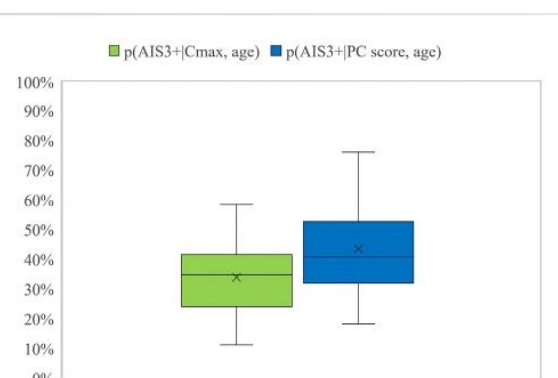


**FIGURE 3**  
Box plot for the probability of AIS3+ calculated using Cmax and PC Score.

**TABLE 5** Model versions groups for the analysis of the influence of the three personalization techniques.

Personalization technique	Group 1	Group 2
Mass scaling	(1) Baseline (2) Baseline postured	(3) Scaled mass (4) Scaled mass postured (5) Morphed (6) Morphed postured
Morphing	(1) Baseline (2) Baseline postured (3) Scaled mass (4) Scaled mass postured	(5) Morphed (6) Morphed postured
Posturing	(1) Baseline (3) Scaled mass (5) Morphed	(2) Baseline postured (4) Scaled mass postured (6) Morphed postured

TABLE 6 Probability of AIS3+ for the different model versions based on the Cmax and PC Score metrics.

Model	p(AIS3+ Cmax, age)			p(AIS3+ PC score, age)		
	RSv1		RSv2	RSv1		RSv2
	A (%)	B (%)	C (%)	A (%)	B (%)	C (%)
(1) Baseline	43.00	38.48	35.64	66.83	56.99	51.39
(2) Postured	51.99	58.48	38.08	76.08	62.55	50.96
(3) Mass scaled	47.70	33.93	41.08	45.97	37.07	41.25
(4) Mass scaled postured	26.55	30.60	29.92	39.16	29.68	40.17
(5) Morphed	40.79	24.91	18.09	45.59	32.77	18.93
(6) Morphed postured	21.61	18.48	11.23	40.15	28.80	18.24

TABLE 7 Summary of the *p*-value of the *p* (AIS3+) discretized by personalization technique and injury metric ( $\alpha = 0.05$ ).

	Mass scaling	Morphing	Posturing
<i>p</i> -value based on <i>p</i> (AIS3+ Cmax, age)	0.016	0.007	0.354
<i>p</i> -value based on <i>p</i> (AIS3+ PC Score, age)	0.001	0.011	0.566

## 4 Discussion

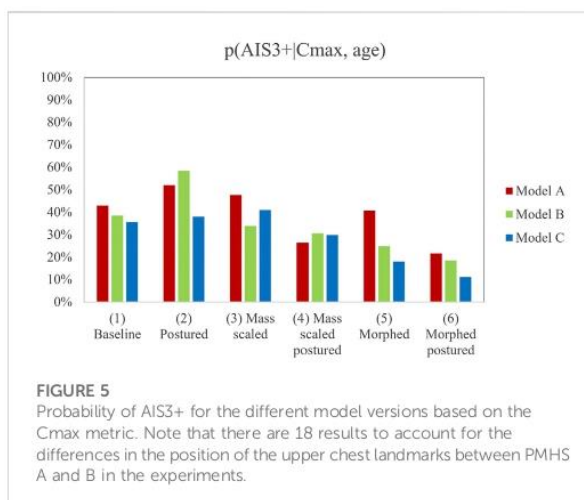
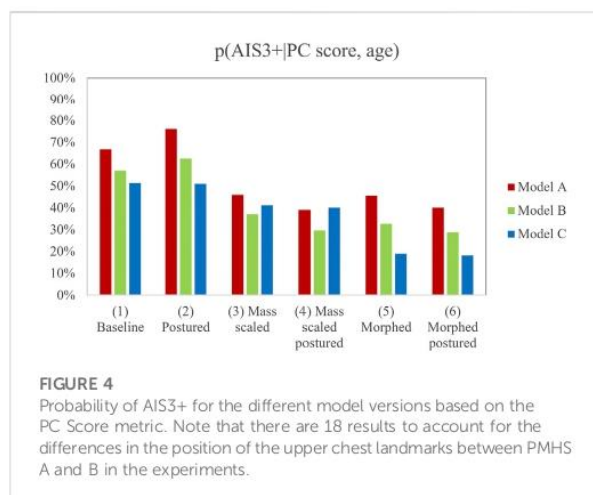
In the present work, the ATD deformation-based criteria, PC Score and Cmax, have been applied to the SAFER HBM v8 under nearside oblique impacts to evaluate the influence of several proposed personalization techniques.

Poplin et al. (2017) developed the formulation of the injury risk functions associated with the PC Score and Cmax based on a set of 45 PMHS tests under 13 different test conditions, considering the age of the subject as a covariant of the injury risk calculation. The results of that study showed that both deformation-based criteria produced similar results in terms of injury prediction. A later study assessing the prediction capability of thoracic injuries of the THOR ATD found the same similarities between the two injury criteria (Lopez-Valdes et al., 2018). These two studies were focused on frontal impact configurations, and similar results can be possibly explained because the study by Poplin et al. (2017) included only one oblique impact in the formulation of the injury risk functions. On the contrary, the present study found differences between the two criteria, revealing that the calculated probability of sustaining three or more rib fractures based on the PC Score showed significantly higher values ( $p < 0.05$ ) than those based on the Cmax metric. These results suggest that these two formulations can result in a different risk estimation in impact configurations that cause a more asymmetric deformation of the chest, such as in the case of the oblique impacts considered here. The formulation of the PC Score includes weighting coefficients assigned to the terms in the formula (UPtot, LOWtot, UPdif, and LOWdif). The UPdif and LOWdif components resulted in the highest weighting coefficients in the formulation. Thus, the more influential parameters on the PC Score calculation are strongly related to the differential deformations as a relevant injury mechanism. Oblique loading has been shown to produce larger chest deformations than frontal impacts (Acosta et al., 2016; Piqueras et al., 2022), leading to more asymmetric chest deformations and, thus, to higher values of the

LOWdif and UPdif components. Since Cmax does not consider the differential deformations, the probability of injury calculated based on this criterion showed lower values of injury risk under the oblique impact configuration. This can also be observed for the nearside oblique test condition, in particular, analyzed by Poplin et al. (2017) in which the *p* (AIS3+) for the nearside oblique configuration was found to be 6.05 percent points higher when the PC Score was applied compared with the same calculation based on Cmax, consistent with the findings of this work. The summary of results including the deflection values at each thoracic landmark and the values of the injury metrics are available in Supplementary Table 1-4.

In a previous study of the THOR injury prediction capability using the same PMHS sled tests as was used in the present study as a reference, the calculations based on the ATD thorax deformation showed a 31% of probability of sustaining three or more rib fractures using Cmax as deformation-based criteria for a 65-year-old occupant (Pipkorn et al., 2016). This value is lower than the prediction obtained with the baseline HBM in this study using the same deformation metric ( $39.04\% \pm 3.71$ ) and, therefore, also lower than the values obtained using PC Score-based calculation ( $58.4\% \pm 7.82$ ). These differences can be attributed to the lack of X-deflection (positive) of the lower right chest of the THOR ATD, something that occurred in the corresponding PMHS sled tests (please see Supplementary Figures 1-1-1-4) (Piqueras et al., 2022).

As mentioned in the introduction, a potential advantage of the use of HBMs is that they allow the study of strain-based injury criteria. In these methods, the strain at any point of the ribcage can be computed and related to the number and location of the fractures when compared to PMHS tests. However, these methods are dependent not only on the HBM biofidelity but also on model construction characteristics such as mesh size. This means that to obtain comparable results, the local strain injury risk functions have to be developed and validated for



each specific loading scenario across diverse HBMs (Forman et al., 2022). For this reason, strain-based criteria were not used for the present study.

The influence of the personalization of the model on the deformation criteria has been assessed for the diverse modifications of the HBM. Figure 4 and Figure 5 show the results obtained for the calculation of the probability of AIS3+ for the six model versions for each RS condition (PMHS A and B on RSv1 and PMHS C on RSv2). The summary of the results can be consulted in Supplementary Table 1-4.

In light of the results, the mass scaling and morphing of the HBM demonstrated a statistically significant influence on the prediction of AIS3+. However, mass-scaled and morphed models provided, in general, lower values of injury risk than the postured version (2), this last version being close to the reference PMHS sled tests that sustained 15, 5, and 10 fractured ribs respectively. Posturing did not show any statistically significant influence on injury prediction and showed a lower  $p$  (AIS3+) when it was combined with the other personalization techniques (versions 4 and 6). This could demonstrate that the separate personalization techniques do not lead to linear trends when they are used in combination. Additionally, those models in which the posturing was performed (2, 4, and 6) successfully predicted that the lower right chest landmark suffered the maximum deformation, while the non-postured model predicted that this deformation would happen at the upper left landmark (see Supplementary Figures 1-1-1-4).

It has to be noted that the results from the PMHS tests were used so that the HBM could be simulated under realistic impact conditions. It would be reasonable to expect that increased levels of personalization would result in improved predictions of risk. However, it is difficult to establish a direct comparison between the risk predicted by the HBM and the risk observed in the PMHS tests. First, even if the three experimental tests resulted in AIS3+ injuries, an exact calculation of the risk of AIS3+ injuries in the experimental loading conditions is not feasible with such a limited sample of PMHS tests. In addition, the definition of the AIS level based on rib fractures encompasses very different injury patterns (i.e. different numbers of rib fractures would result in the same AIS3 score depending on their location in the rib cage). This is why this study does not intend to highlight which personalization technique results in more

biofidelic predictions, but rather how sensitive the injury criteria used with HBM are to the personalization of the models. From a more general perspective, if a criterion is not sensitive enough to change when the model is personalized, then there is not really a reason for not using the normalized, standard HBM.

This study is subject to some limitations. First, only three PMHS sled tests were taken as a reference for the comparison with the different model versions of the thoracic injury risk under oblique impact. Thus, more experimental data are required covering different impact angles, subject ages, sex, and anthropometrical characteristics for supporting the conclusions of this study. In terms of methodology, the morphing personalization technique was implemented attending to the external anthropometry, thus internal subject-specific geometry was not personalized. Since the scope of this study was to evaluate the influence of the subject-specific posture, mass, and anthropometry only, soft and hard tissue material properties remained unmodified in the SAFER HBM model. It should be noted that the anthropometry of PMHS A and PMHS B was averaged to develop a single personalized HBM. This was decided due to the large similarities in anthropometry and initial posture of the two subjects that would have resulted in minimal differences in the corresponding HBM.

## 5 Conclusion

This study analyzed the influence of different personalization techniques on the probability of chest injury predictions of HBM. Despite having led to statistically significant differences in the probability of AIS3+ calculations, mass-scaled and morphed model versions provided, in general, lower values of injury risk than the baseline model and the postured version (1 and 2). The postured model version (2) exhibited the highest values of probability of injury and resulted in predictions that closer resembled the injuries observed in the reference PMHS tests. Furthermore, the models in which the posturing was performed (2, 4, and 6) successfully predicted that the lower right chest landmark suffered the maximum deformation as occurred in the PMHS tests. Additionally, this study found that PC Score-based prediction showed higher values of  $p$  (AIS3+) than the prediction based on Cmax for the loading conditions and personalization techniques analyzed. Previous studies have suggested

only minor differences between the two criteria, but the results included here suggest that these two criteria will result in significantly different predictions if the chest is loaded more asymmetrically.

## Data availability statement

The original contributions presented in the study are included in the article/Supplementary Material, further inquiries can be directed to the corresponding authors.

## Author contributions

AP: First authorship. This author carried out the simulations and calculations, analysed in detail the results and wrote the manuscript. JI: Second authorship. This author supervised the simulations, revised the manuscript and contributed to the discussion of the results. BP: Third authorship. This author revised the manuscript and contributed to the discussion of the results FJL-V: Senior authorship. This author revised the manuscript and contributed to the discussion of the results as well as to the conception of the work.

## References

- AAAM (2015). *The abbreviated injury scale 2008, update 2015*. IL: Des Plaines.
- Acosta, S. M., Ash, J. H., Lessley, D. J., Shaw, C. G., Heltzel, S. B., and Crandall, J. R. Comparison of whole body response in oblique and full frontal sled tests. In 2016 IRCOBI Conf. Proc. - Int. Res. Counc. Biomech. Inj. USA, 21 January 2016. 2016, 740–754.
- Afwerki, H. (2016). *Biofidelity evaluation of thoracolumbar spine model in THUMS*. Berlin, Germany: Springer.
- ANCAP (2020). *Test protocol. Mobile progressive deformable barrier*. Berlin, Germany: Springer.
- Brolin, K., and Wass, J. (2016). Explicit finite element methods for equestrian applications. *Procedia Eng.* 147, 275–280. doi:10.1016/j.proeng.2016.06.277
- Davidsson, J., Carroll, J., Hynd, D., Lecuyer, E., Song, E., Trosseille, X., et al. (2014). "Development of injury risk functions for use with the THORAX Demonstrator; an updated THOR," in Proceedings of IRCOBI Conference 2014, Berlin, Germany, 12–15 July 2014, 359–376.
- EuroNCAP (2018). *European new car assessment programme (Euro NCAP) Full width frontal impact testing protocol*. Berlin, Germany: Springer, 52.
- Forman, J., Kulkarni, S., Rapela, D. P., Mukherjee, S., Panzer, M., and Hallman, J. (2022). "A method for thoracic injury risk function development for human body models," in IRCOBI Conference. Porto, Portugal, 12–15 June 2022.
- Forman, J. L., Kent, R. W., Mroz, K., Pipkorn, B., Bostrom, O., and Segui-Gomez, M. (2012). Predicting rib fracture risk with whole-body finite element models: Development and preliminary evaluation of a probabilistic analytical framework. *Am. Adv. Automot. Med.* 56, 109–124.
- Grébonval, C., Trosseille, X., Petit, P., Wang, X., and Beillas, P. (2021). Effects of seat pan and pelvis angles on the occupant response in a reclined position during a frontal crash. *PLoS One* 16, 1–18. doi:10.1371/journal.pone.0257292
- Hu, J., Zhang, K. S., Fanta, A., Hwang, E., and Reed, M. P. Effects of male stature and body shape on thoracic impact response using parametric finite element human modeling. In: 25th ESV Conference. Berlin, Germany, 12–15 June 2017, 2017:1–11.
- Hwang, E., Hu, J., Chen, C., Klein, K. F., Miller, C. S., Reed, M. P., et al. (2016). Development, evaluation, and sensitivity analysis of parametric finite element whole-body human models in side impacts. *Stapp Car Crash J.* 60, 473–508. doi:10.4271/2016-22-0014
- IIHS (2012). *Small overlap frontal crashworthiness evaluation crash test protocol*. Berlin, Germany: Springer, 25.
- Iraeus, J., Brolin, K., and Pipkorn, B. (2020). Generic finite element models of human ribs, developed and validated for stiffness and strain prediction – to be used in rib fracture risk evaluation for the human population in vehicle crashes. *J. Mech. Behav. Biomed. Mat.* 106, 103742. doi:10.1016/j.jmbm.2020.103742
- Iraeus, J., Davidsson, J., and Brolin, K. (2017). "Recent HBM activities at chalmers university," in Presentation at Conference Human Body Modelling in Automotive Safety, Berlin, Germany, 12–15 June 2017, 1–10.

## Conflict of interest

The authors declare that the research was conducted in the absence of any commercial or financial relationships that could be construed as a potential conflict of interest.

## Publisher's note

All claims expressed in this article are solely those of the authors and do not necessarily represent those of their affiliated organizations, or those of the publisher, the editors and the reviewers. Any product that may be evaluated in this article, or claim that may be made by its manufacturer, is not guaranteed or endorsed by the publisher.

## Supplementary material

The Supplementary Material for this article can be found online at: <https://www.frontiersin.org/articles/10.3389/fbioe.2023.1106554/full#supplementary-material>

- Iwamoto, M., Kisanuki, Y., Watanabe, I., Furusu, K., Miki, K., and Rouhana, S. W. (2002). Development of a finite element model of the total human model for safety (THUMS) and application to injury reconstruction. *Ircobi* 1 (2), 102.
- Kemper, A. R., McNally, C., Clayton, A. P., Freeman, L. J., Duma, S. M., and Rouhana, S. W. (2007). The biomechanics of human ribs: Material and structural properties from dynamic tension and bending tests. *Stapp Car Crash Journal* 51, 235–273. doi:10.4271/2007-22-0011
- Kemper, A. R., McNally, C., Kennedy, E. A., Manoogian, S. J., Rath, A. L., Ng, T. P., et al. (2005). Material properties of human rib cortical bone from dynamic tension coupon testing. *SAE Tech. Pap.* 2005, 199–230. doi:10.4271/2005-22-0010
- Kleinberger, M., Sun, E., Eppinger, R., Kuppa, S., and Saul, R. (1998). *Development of improved injury criteria for the assessment of advanced automotive restraint systems*. United States: National Highway Traffic Safety Administration.
- Kroell, C. K., Schneider, D. C., and Nahum, A. M. (1974). Impact tolerance and response of the human thorax II. *SAE Tech. Pap.* 12, 741187. doi:10.4271/741187
- Laituri, T. R., Prasad, P., Sullivan, K., Frankstein, M., and Thomas, R. S. (2005). Derivation and evaluation of a provisional, age-dependent, AIS3+ Thoracic risk curve for belted adults in frontal impacts. *SAE Tech. Pap.* 2005, 0297. doi:10.4271/2005-01-0297
- Larsson, K. J., Pipkorn, B., Iraeus, J., Bolte, J. H., Agnew, A. M., Hu, J., et al. (2019). "Evaluation of the benefits of parametric human body model morphing for prediction of injury to elderly occupants in side impact," in Conference proceedings International Research Council on the Biomechanics of Injury, IRCOBI, Florence, Italy, 21 september 2019, 150–174.
- Lau, I. V., and Viano, D. C. (1986). The viscous criterion - bases and applications of an injury severity index for soft tissues. *SAE Tech. Pap.* 95, 672–691.
- López-Valdés, F. J., Juste-Lorente, O., Maza-Frechin, M., Pipkorn, B., Sunnevång, C., Lorente, A., et al. (2016). Analysis of occupant kinematics and dynamics in nearside oblique impacts. *Traffic Inj. Prev.* 17, 86–92. doi:10.1080/15389588.2016.1189077
- López-Valdés, F. J., Mroz, K., Eggers, A., Pipkorn, B., Muehlbauer, J., Schick, S., et al. (2018). Chest injuries of elderly postmortem human surrogates (PMHS) under seat belt and airbag loading in frontal sled impacts: Comparison to matching THOR tests. *Traffic Inj. Prev.* 19 (2), S55–S63. doi:10.1080/15389588.2018.1542139
- Mendoza-Vazquez, M., Davidsson, J., and Brolin, K. (2015). Construction and evaluation of thoracic injury risk curves for a finite element human body model in frontal car crashes. *Accid. Anal. Prev.* 85, 73–82. doi:10.1016/j.aap.2015.08.003
- NHTSA (2015). *New car assessment program*. Berlin, Germany: Springer, 56928–56935.
- Pipkorn, B., Iraeus, J., Björklund, M., Bunketorp, O., and Jakobsson, I. (2019). "Multi-scale validation of a rib fracture prediction method for human body models," in Conf. Proc. Int. Res. Counc. Biomech. Inj. IRCOBI, Gothenburg, Sweden, 18–20 september 2019, 175–192.
- Pipkorn, B., López-Valdés, F. J., Juste-Lorente, O., Maza, M., and Sunnevång, C. Study of the kinematics of the THOR dummy in nearside oblique impacts. In: Proceedings of IRCOBI Conference 2016. Malaga, Spain, 14–16 September 2016, 2016:637–648.

Piqueras, A., Iraeus, J., Lorente, A. I., López-Valdés, F. J., Juste-Lorente, Ó., Maza-Frechín, M., et al. (2018). "Kinematic assessment of subject personification of human body models (THUMS)," in Proceedings of IRCOBI Conference 2018, Gothenberg, Sweden, 18-20 september 2018, 191–206.

Piqueras, A., Pipkorn, B., Iraeus, J., Maza-Frechín, M., and Lopez-Valdes, F. J. (2022). Assessment of *in situ* chest deflection of post mortem human subjects (PMHS) and personalized human body models (HBM) in nearside oblique impacts. *Traffic Inj. Prev.* 10, 181–186. doi:10.1080/15389588.2022.2036731

Poplin, G. S., McMurry, T. L., Forman, J. L., Ash, J., Parent, D. P., Craig, M. J., et al. (2017). Development of thoracic injury risk functions for the THOR ATD. *Accid. Anal. Prev.* 106, 122–130. doi:10.1016/j.aap.2017.05.007

Poulard, D., Subit, D., Nie, B., Donlon, J. P., and Kent, R. W. (2015). The contribution of pre-impact posture on restrained occupant finite element model response in frontal impact. *Traffic Inj. Prev.* 16, 87–95. doi:10.1080/15389588.2015.1064529

Shi, X., Cao, L., Reed, M. P., Rupp, J. D., Hoff, C. N., and Hu, J. (2014). A statistical human rib cage geometry model accounting for variations by age, sex, stature and body mass index. *J. Biomech.* 47 (10), 2277–2285. doi:10.1016/j.jbiomech.2014.04.045

Song, E., Lecuyer, E., and Trosseille, X. (2011). "Development of injury criteria for frontal impact using a human body FE model," in International Technical Conference on the Enhanced Safety of Vehicles, Washington, DC, 13-16 June 2011, 1–15.

## **Appendices**

### **APPENDICES**

**Appendix A:** Ethical Approval

**Appendix B:** Methods Extended

**Appendix C:** Model Versions Mesh Quality Analysis

**Appendix D:** MatLab Code for FHA Calculation

**Appendix E:** Chest deflection plots

## Appendix A: Ethical Approval



**Informe Dictamen Favorable  
Proyecto Investigación Biomédica**

C.P. - C.I. PI15/0257

14 de octubre de 2015

Dña. María González Hinjos, Secretaria del CEIC Aragón (CEICA)

### CERTIFICA

1º. Que el CEIC Aragón (CEICA) en su reunión del día 14/10/2015, Acta Nº 16/2015 ha evaluado la propuesta del investigador referida al estudio:

**Título: Nearside Oblique Impacts.**

**Investigador Principal: Mario Maza. Universidad de Zaragoza**

**Versión protocolo: octubre/2015**

**Versión formulario donaciones, personas y familiares: octubre/2015**

2º. Considera que

- El proyecto se plantea siguiendo los requisitos de la Ley 14/2007, de 3 de julio, de Investigación Biomédica y su realización es pertinente.
- Se cumplen los requisitos necesarios de idoneidad del protocolo en relación con los objetivos del estudio y están justificados los riesgos y molestias previsibles para el sujeto.
- Son adecuados tanto el procedimiento para obtener el consentimiento informado como la compensación prevista para los sujetos por daños que pudieran derivarse de su participación en el estudio.
- El alcance de las compensaciones económicas previstas no interfiere con el respeto a los postulados éticos.
- La capacidad de los Investigadores y los medios disponibles son apropiados para llevar a cabo el estudio.

3º. Por lo que este CEIC emite **DICTAMEN FAVORABLE a la realización del proyecto.**

Lo que firmo en Zaragoza, a 14 de octubre de 2015

Fdo:

Dña. María González Hinjos  
Secretaria del CEIC Aragón (CEICA)



## Appendix B: Methods Extended

Table B-1: Subjects and baseline THUMS anthropometry expressed in mm. All dimensions were measured as specified in the NHTSA Data Reference Guide, Version 5, Volume II: Biomechanical Tests (May 2001).

ANTHROPOMETRIC MEASUREMENT	RSV 1		RSV 2
	PMHS A	PMHS B	PMHS C
Seated Height-top of head to bottom of feet	963	1038	1040
<b>Seated Head to Buttock</b>	753	802	832
Seated Hip to Knee length	392	364	387
<b>Seated Chest Breadth</b>	4 <sup>th</sup> Rib	256	277
	8 <sup>th</sup> Rib	260	270
<b>Seated Chest Depth</b>	4 <sup>th</sup> Rib	240	202
	8 <sup>th</sup> Rib	250	202
<b>Seated Chest Circumference</b>	4 <sup>th</sup> Rib	858	865
	8 <sup>th</sup> Rib	870	815
<b>Interscye</b>		297	293
Top of Head to T1	201	202	273
<b>Waist Depth-Umbilicus</b>		170	135
<b>Waist Breadth</b>		263	257
<b>Shoulder Breadth (Biacromial)</b>		331	357
<b>Hip Breadth</b>		292	292
<b>Buttock Depth</b>		167	155
<b>Shoulder to Elbow</b>		319	305
<b>Forearm to Hand</b>		248	235
<b>Foot Breadth</b>		70	68
<b>Foot Length</b>		247	215
<b>Head Length</b>		202	197
<b>Head Breadth</b>		140	147
<b>Head Height</b>		208	195
<b>Head Circumference</b>		553	553
<b>Neck Circumference</b>		334	360
<b>Waist Circumference (Umbilicus)</b>		702	706
<b>Buttock Circumference</b>		776	722
<b>Thigh Circumference</b>		321	355
<b>Lower Thigh Circumference</b>		259	322
<b>Knee Circumference</b>		342	340
<b>Calf Circumference</b>		240	244
<b>Ankle Circumference</b>		242	212
<b>Scye (Armpit) Circumference</b>		235	253
<b>Bicep Circumference</b>		195	218
<b>Elbow Circumference</b>		222	233
<b>Forearm Circumference</b>		150	207
<b>Wrist Circumference</b>		159	159
<b>Weight (kg)</b>		47	53

Table B-2: Angle formed with the horizontal of the selected landmarks in the spine for RSV1 (degree).

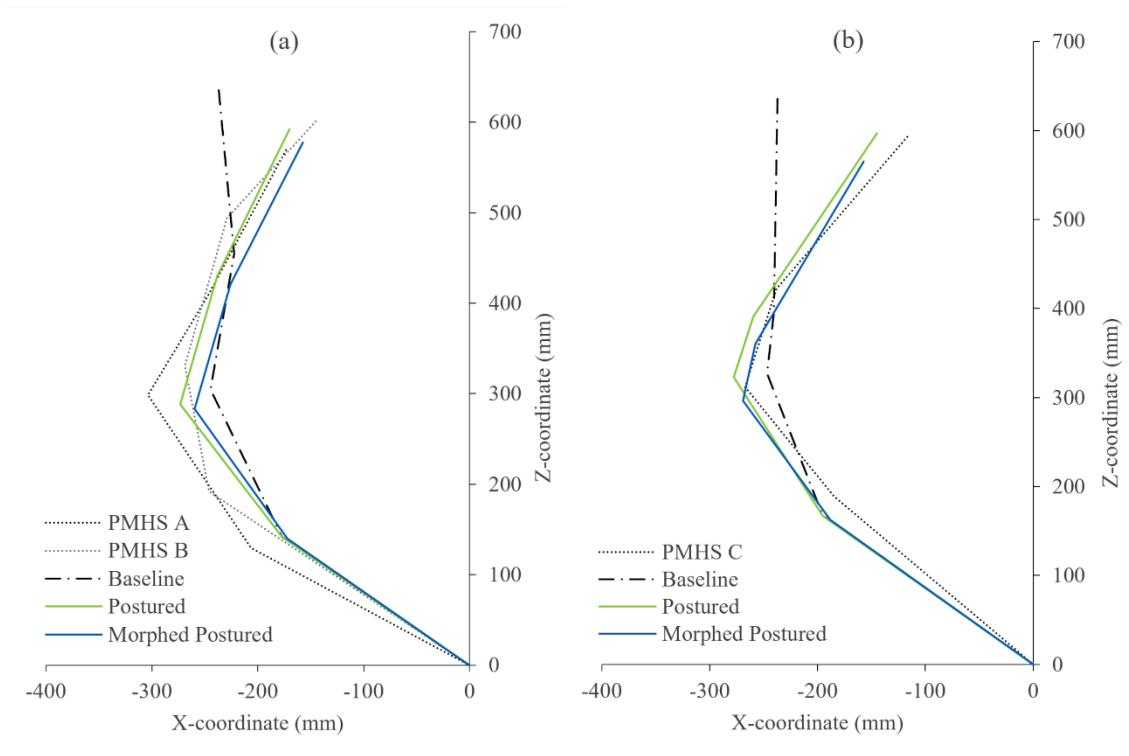
SUBJECT	PMHS A	PMHS B	BASELINE	PERSONALIS ED
$\alpha_{Head-T1}$	66	52	95	66
$\alpha_{T1-T8}$	63	76	81	76
$\alpha_{T8-L2}$	120	99	112	120

$\alpha$ L2-H-Point	147	142	141	140
---------------------	-----	-----	-----	-----

Table B-3: Angle formed with the horizontal of the selected landmarks in the spine for RSv2 (degree).

SUBJECT	PMHS C	BASELINE	PERSONALIS ED
$\alpha$ Head-T4	54	89	63
$\alpha$ T4-T7	76	85	79
$\alpha$ T7-L1	124	107	121
$\alpha$ L1-H-Point	135	139	139

Figure B-1: Spine alignment representation at  $t=0ms$  of the PMHS, THUMS baseline model and postured models. (a) RSv1 and (b) RSv2.



## Appendix C: Model Versions Mesh Quality Analysis

Table C-1: Results of quality checks for RSv 1. Number of elements that violate thresholds, percentage over the total number of elements in parentheses.

<b>2D QUALITY CHECKS</b>	<b>BASELINE</b>	<b>POSTURED</b>	<b>MORPHED</b>	<b>MORPHED POSTURED</b>
<b>Warp angle</b>	13402 (11.45%)	+362 (+0.31%)	+48 (+0.04%)	+434 (+0.37%)
<b>Aspect ratio</b>	303 (0.26%)	+29 (+0.02%)	+26 (+0.02%)	+63 (+0.05%)
<b>Jacobian</b>	1949 (1.66%)	+130 (+0.11%)	+74 (+0.06%)	+217 (+0.19%)
<b>Angle quads</b>	3216 (2.75%)	+141 (+0.12%)	+299 (+0.26%)	+482 (+0.41%)
<b>Angle trias</b>	285 (0.24%)	+9 (+0.01%)	-4 (-0.003%)	+3 (+0.003%)
<b>3D QUALITY CHECKS</b>				
<b>Aspect ratio</b>	5351 (5.48%)	-25 (-0.03%)	+492 (+0.5%)	+466 (+0.48%)
<b>Jacobian</b>	18491 (18.92%)	+55 (+0.06%)	+39 (+0.04%)	+115 (+0.12%)
<b>Angle quads</b>	32178 (32.93%)	+72 (+0.07%)	+1497 (+1.53%)	+1708 (+1.75%)

Table C-2: Results of quality checks for RSv 2. Number of elements that violate thresholds, percentage over the total number of elements in parentheses.

<b>2D QUALITY CHECKS</b>	<b>BASELINE</b>	<b>POSTURED</b>	<b>MORPHED</b>	<b>MORPHED POSTURED</b>
<b>Warp angle</b>	13402 (11.45%)	+220 (+0.19%)	+19 (+0.02%)	+554 (+0.47%)
<b>Aspect ratio</b>	303 (0.26%)	+88 (+0.08%)	+23 (+0.02%)	+64 (+0.05%)
<b>Jacobian</b>	1949 (1.66%)	+241 (+0.21%)	+79 (+0.07%)	+242 (+0.21%)
<b>Angle quads</b>	3216 (2.75%)	+248 (+0.21%)	+426 (+0.36%)	+641 (+0.55%)
<b>Angle trias</b>	285 (0.24%)	+46 (+0.04%)	+27 (+0.02%)	+41 (+0.04%)
<b>3D QUALITY CHECKS</b>				
<b>Aspect ratio</b>	5351 (5.48%)	+38 (+0.04%)	+772 (+0.79%)	+716 (+0.73%)
<b>Jacobian</b>	18491 (18.92%)	+100 (+0.10%)	+64 (+0.07%)	+222 (+0.23%)
<b>Angle quads</b>	32178 (32.93%)	+731 (+0.75%)	+1863 (+1.91%)	+2264 (+2.32%)

## Appendix D: MatLab Code for FHA Calculation

This appendix provide the Matlab code used for the calculation of the FHA from the matrix  $T_{B/G}(t)$ . The code has been developed as a function (Script 2) that has to be called for every landmark and subject to be analysed by means of the mentioned matrix (Script 1).

This code can be applied also to calculate the FHA for HBM for a straightforward comparison with the PMHS results.

The components of the rotation matrix (R) can be extracted from the rigid body simulation results file. For instance, dircos\_ij components from the rbdout for LS-DYNA or activating the function RBODY\_INIT form the PRCTRL card for VPS.

Script 1: The script below shows the code to call the function and the variables needed for the calculation:

```

%%%%%%%%%%%%%%%%%%%%%%%%%%%%%%%%%%%%%%%%%%%%%%%%%%%%%%%%%%%%%%%%%%%%%%%%
%                               FHA calculation                               %
%                                                                           %
%                                                                           %
%                                                                           %
%-----%
% VARIABLES                                                                %
% s = Subject identifier (from 1 to 3 for this example)                    %
% b = bone identifier (from 1 to 4 for this example)                      %
% delta = delta angle for FHA discretization                             %
% ti = initial time for the analysis                                     %
% tf = final time for the analysis                                       %
% PMHS(s,b).Tb_g = T_B/G transformation matrix for each landmark         %
% PMHS(s,b).Time = corresponding time for the matrix T_B/G analysed     %
%%%%%%%%%%%%%%%%%%%%%%%%%%%%%%%%%%%%%%%%%%%%%%%%%%%%%%%%%%%%%%%%%%%%%%%%

delta=8;
ti=1;
tf=140;

%% Call FHA calculation function
for s=1:3
    for b=1:4
        % call function every loop
        [U_global,PHI,U_delta,time_delta]...
            =FHA(delta,ti,tf,PMHS(s,b).Tb_g,PMHS(s,b).Time);

        % variables storage into "rot" structure
        rot(s,b).U_global=U_global;
        rot(s,b).PHI=PHI;

        rot(s,b).U_delta=U_delta;
        rot(s,b).time_delta=time_delta;

    end
end

clear U_global PHI U_delta time_delta

```

After running this code, all variables will be stored into a structured saved as “rot” in the workspace where the columns are referred to the bone (b) and the rows are referred to the subject (s).

Script 2: The following script gives the function to calculate the FHA for every landmark and every subject called on the previous script. For a proper functioning, this script must be named as “*FHA.m*”, otherwise line 20 in this script and line 26 in Script 1 must be modified to refer the name of this file:

```

%%%%%%%%%%%%%%%%%%%%%%%%%%%%%%%%%%%%%%%%%%%%%%%%%%%%%%%%%%%%%%%%%%%%%%%%
%                               FHA calculation function                               %
%%%%%%%%%%%%%%%%%%%%%%%%%%%%%%%%%%%%%%%%%%%%%%%%%%%%%%%%%%%%%%%%%%%%%%%%
%
%
%
%-----%
% INPUT VARIABLES
% delta = delta angle for FHA discretization
% ti = initial time for the analysis
% tf = final time for the analysis
% TransMat = Transformation matrix to be analysed (T_B/G{t})
% Time = Time vector corresponding to T_B/G{t}
%-----%
% OUTPUT VARIABLES
% U_global = FHA components for global analysis between ti and tf (Table 3)
% PHI = Angle rotated around the FHA for global analysis (Table 3)
% U_delta = FHA components every degree interval (delta) (Figure 6)
% time_delta = time vector in which the rotation (delta) was reached
%%%%%%%%%%%%%%%%%%%%%%%%%%%%%%%%%%%%%%%%%%%%%%%%%%%%%%%%%%%%%%%%%%%%%%%%

function [U_global,PHI,U_delta,time_delta]=FHA(delta,ti,tf,TransMat,Time)

%% Calculation of the FHA between the initial time to the end time (Table 3)
for t=ti:tf
    % Extraction of the R components of the transformation matrix T_B/G(t) (Eq.
1)
    RotMat{t,1}=TransMat{t,1}(1:3,1:3);
    % Relative rotation matrix between tf and ti (Similar to Eq. 5)
    globmat=((RotMat{1,1})^-1)*RotMat{t,1};
    % Phi calculation (Eq. 3)
    PHI(t,1)=acos((globmat(1,1)+globmat(2,2)+globmat(3,3)-1)/2);
end

    %FHA components calculation (Eq. 4)
    a=1/(2*sin(PHI(tf,1)));

    u1=a*(globmat(3,2)-globmat(2,3));
    u2=a*(globmat(1,3)-globmat(3,1));
    u3=a*(globmat(2,1)-globmat(1,2));

    % Vector normalization
    nor=sqrt((u1)^2+(u2)^2+(u3)^2);
    Ux=u1/nor;
    Uy=u2/nor;
    Uz=u3/nor;

    %Storage FHA components
    U_global(1,1)=Ux;
    U_global(1,2)=Uy;
    U_global(1,3)=Uz;
    clear u1 u2 u3 Ux Uy Uz nor a globmat

%% FHA calculation every degree interval (delta)

k=1;
for t=ti:tf
    % Extraction of the R components of the transformation matrix T_B/G(t)
(Eq. 1)
    RotMat{k,1}=TransMat{t,1}(1:3,1:3);
    k=k+1;
end

time=Time(ti:tf);

```

```

% Auxiliar time counter
initial=1;
% Auxiliar counter when the condition phi>delta is accomplished
k=0;

for t=initial:tf

    %Rotation matrix between two instants (Relative Matrix) (Eq. 5)
    rm=((RotMat{initial,1})^-1)*RotMat{t,1};
    %Calculation of phi between two instants (Relative phi) (Eq. 3)
    phi=acos((rm(1,1)+rm(2,2)+rm(3,3)-1)/2);

    %Condition of phi >= delta
    if phi>(delta*pi/180)
        %Counter initialization
        k=k+1;
        %Storage of phi
        phik(k,1)=phi;

        % Calculation of FHA components (Eq. 4)
        a=1/(2*sin(phik(k,1)));

        u1=a*(rm(3,2)-rm(2,3));
        u2=a*(rm(1,3)-rm(3,1));
        u3=a*(rm(2,1)-rm(1,2));

        % Vector normalization
        nor=sqrt((u1)^2+(u2)^2+(u3)^2);
        ux(k,1)=u1/nor;
        uy(k,1)=u2/nor;
        uz(k,1)=u3/nor;

        %Storage of the unit vector components
        U_delta(k,1)=ux(k,1);
        U_delta(k,2)=uy(k,1);
        U_delta(k,3)=uz(k,1);

        %Storage of the time
        time_delta(k,1)=time(t,1);

        initial=t; % Counter reset
    end
    clear u1 u2 u3 ux uy uz nor a phi
end

clear RotMat time inital k

```

## Appendix E: Chest deflection plots

Figure E-1: PMHS and HBM time-histories of the 3D upper left chest displacements (R4L) relative to T8 vertebra LCS

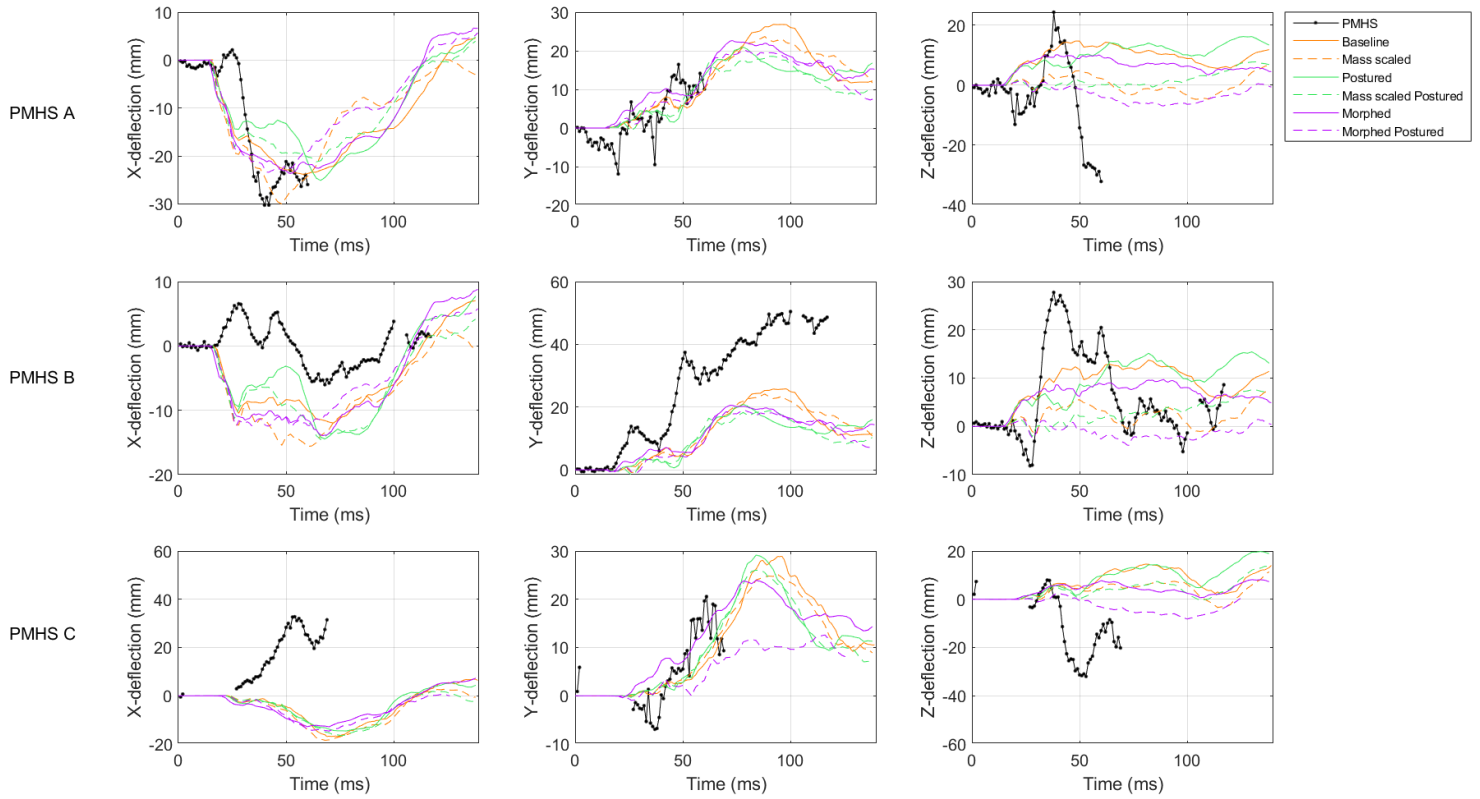


Figure E-2: PMHS and HBM time-histories of the 3D upper right chest displacements (R4R) relative to T8 vertebra LCS.

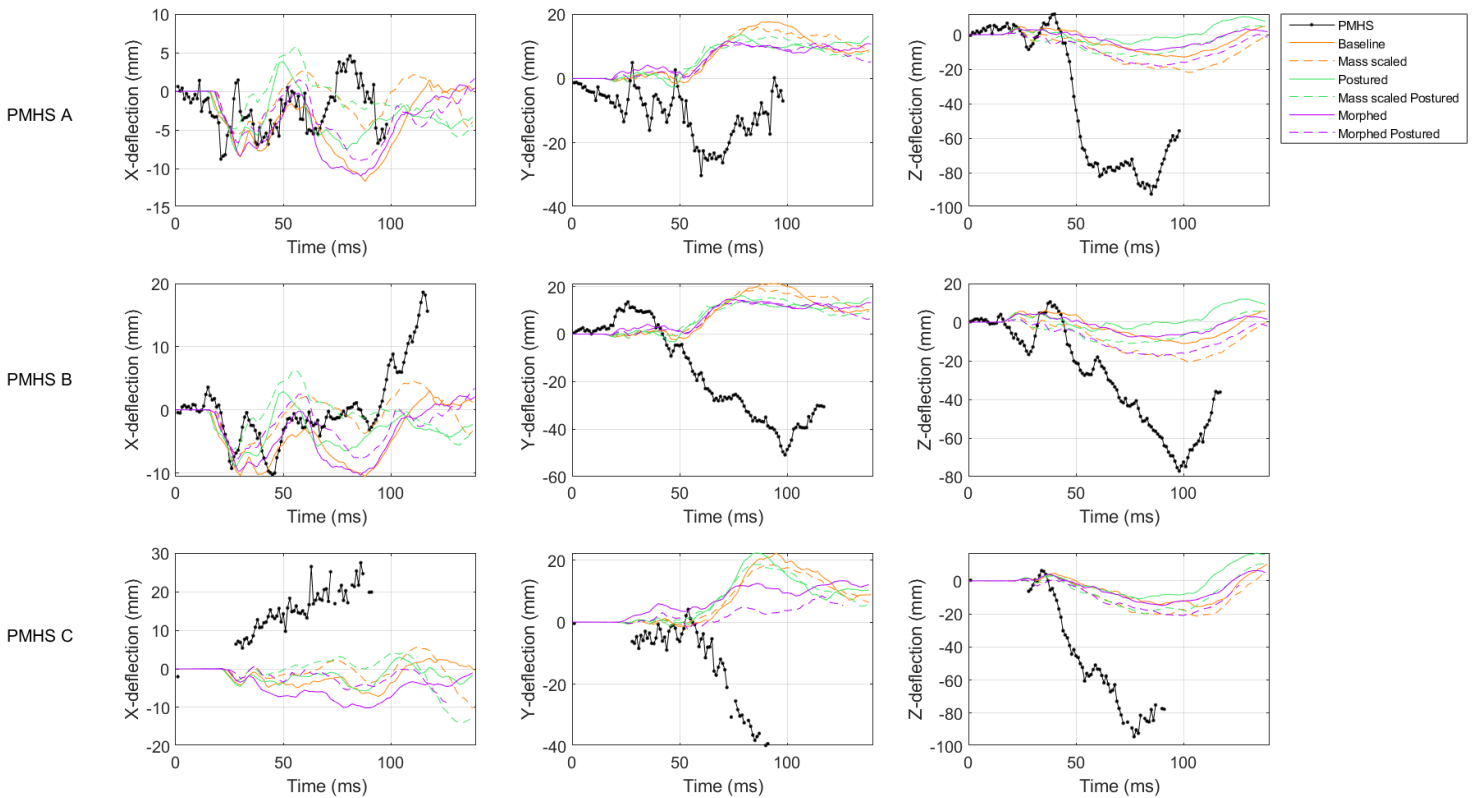


Figure E-3: PMHS and HBM time-histories of the 3D lower left chest displacements (R8L) relative to T8 vertebra LCS

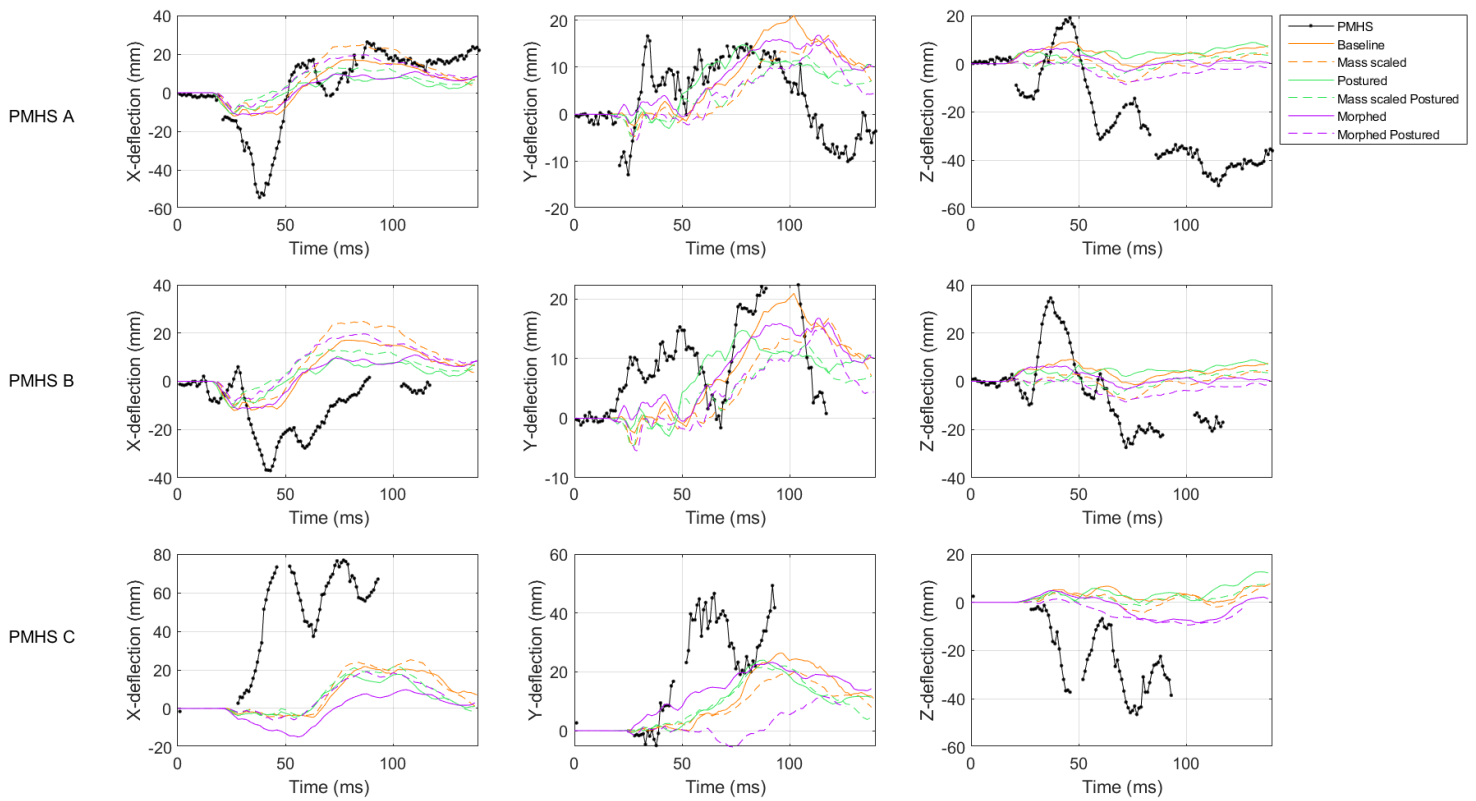
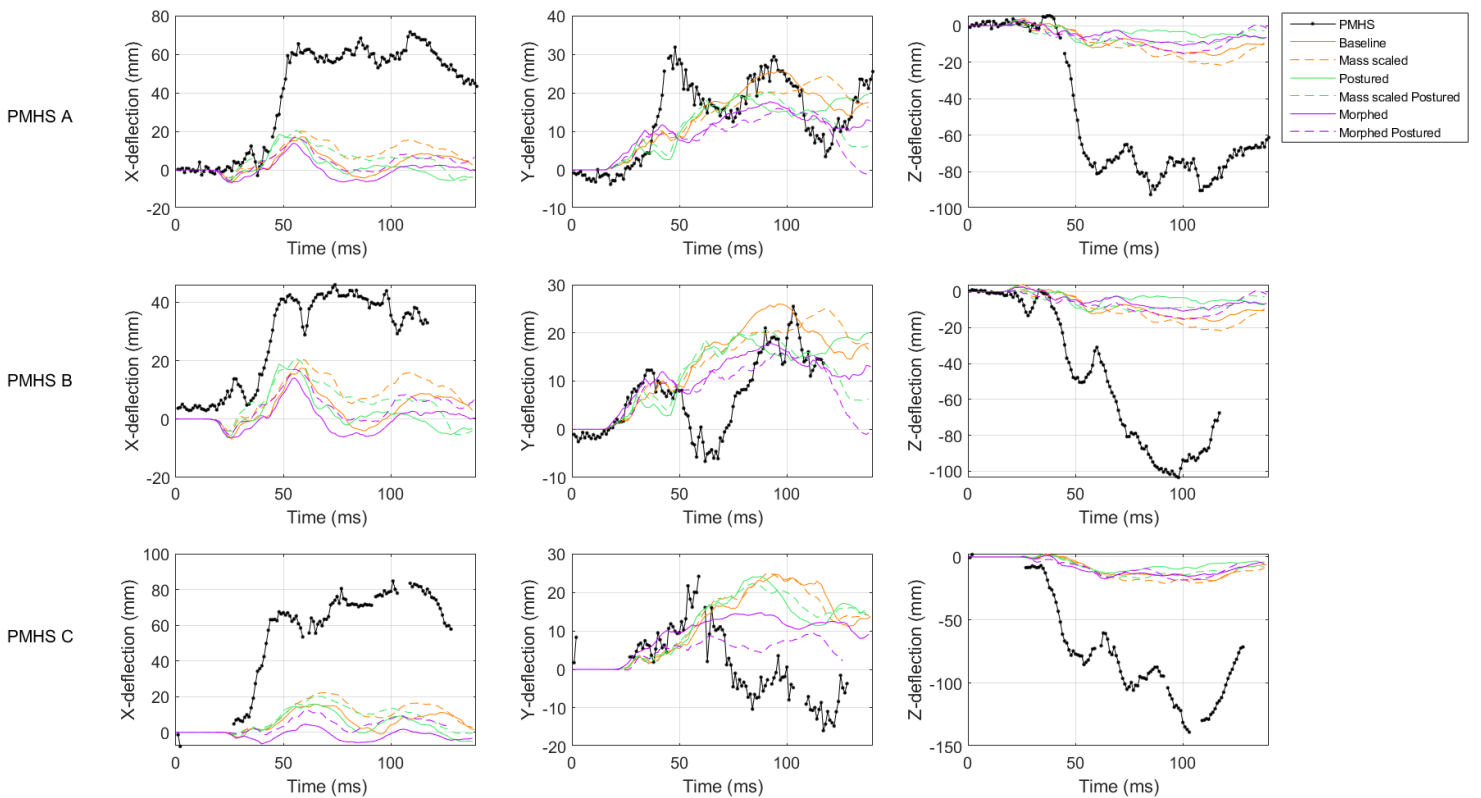


Figure E-4: PMHS and HBM time-histories of the 3D lower right chest displacements (R8R) relative to T8 vertebra LCS



— PMHS — Baseline - - Mass scaled — Postured - - Mass scaled Postured — Morphed - - Morphed Postured



Figure E-5: PMHS and HBM time-histories of the 3D sternum displacements (STERNUM) relative to T8 vertebra LCS

